University of Nottingham

UK | CHINA | MALAYSIA

Development and Application of Mathematical Models in Gait Characterisation after Stroke

Tan Ming Gui, B.Eng (Hons)

Thesis Submitted to the University of Nottingham Malaysia

for the Degree of Doctor of Philosophy

October 2018

Abstract

The number of stroke has increased every years according to American Heart Association (AHA), World Health Organization (WHO) and National Stroke Association of Malaysia (NASAM). These numbers have raised concerns among medical and rehabilitation professionals who manage this neurological disorder. For this project, we aim to develop a sophisticated gait analysis system to help the recovery of stroke patients. This proposed gait analysis system can help clinicians to assess the gait pattern and plan a suitable rehabilitation treatment for stroke patients systematically. It started with the development of gait sensor system. In this study, we are interested to study about the kinematics and kinesiology parameters of stroke patients. Therefore, we developed a low-cost inertial based sensor system and employed commercial ShimmerSensing sEMG sensors. A 3D high-speed camera was used to validate the inertial based sensor system. The parameters obtained from the sensor system were further analysed to extract valuable features for gait characterisation and gait classification.

Two new gait analysis methods, kinesiology and kinematic based gait analysis were proposed to study the characteristic of the stroke patient's gait. For kinesiology based gait analysis, the surface EMG (sEMG) signal was being collected and analysed. We applied sliding window Higuchi Fractal Dimension (HFD) on sEMG signal and computed a new fractal based index, named Kinetic Index (K.I.). This K.I. was further correlated to the Timed Up and Go Test (TUG test). The results showed that K.I. is highly correlated to the TUG test. Besides that, K.I. can also classify stroke patients into three homogeneous subgroups by using Hierarchical Cluster Analysis.

For kinematic based gait analysis, we proposed a new variant of the Symmetry Region of Deviation (SROD) method to quantify gait asymmetry. This new method, named as Cyclogram SROD (CSROD), applies a bilateral cyclogram of both left and right lower limbs gait data to compute the gait deviation from perfect symmetry. Compared to SROD, CSROD does not require a baseline gait database

of normal healthy subjects for comparison purposes. Instead, it uses a 45° symmetry line in the cyclogram to indicate perfect gait symmetry. The validation results showed that the proposed method were similar to those obtained from the SROD method according to Welch t-test analysis. With proper gait alignment technique such as Dynamic Time Warping (DTW), the CSROD results showed the accurate timing and magnitude of the peaks where asymmetry occurred.

Both the K.I. and CSROD provide valuable information regarding the kinesiology and kinematic status of the stroke patients. However, it cannot describe the difference of gait pattern between stroke patients and healthy subjects. Therefore, two new gait functionality indices, G_Funct_{GT} and G_Funct_{TD} were presented. These two indices detect the gait trajectory deviation and time delay between stroke and healthy.

The features extracted for gait characterisation (K.I., CSROD, G_Funct_{GT} and G_Funct_{TD}) were used to develop two recovery prediction models. The first model used stroke patients baseline (stage 1) gait data to predict their third month (stage 2) and sixth month (stage 3) of gait indices. The second model was based on the recovery trajectory from baseline (stage 1) to third month (stage 2) to predict the final state of gait indices (stage 3). The results showed high accuracy among stroke patients. The sEMG signal on each stage of the stroke recovery period were further decomposed using Ensemble Empirical Mode Decomposition (EEMD) method. This was to study the muscle status changes across the recovery period on stroke patients. It is to ensure the recovery in joint motions associates with the recovery of muscles, and not due to muscle compensation.

List of Publications

Journals/Technical paper:

1. M.G. Tan, C.B. Leong, J.H. Ho, H.T. Goh and H.K. Ng, A compact low cost wearable sensor system for quantitative gait measurement Applied Mechanics and Materials: Advanced Development in Industry and Applied Mechanics. 627 (2014), 212-216

2. M.G. Tan, Y.C. Tea, J.H. Ho, H.T. Goh, H.K. Ng and I. Kong, A motion sensor network for quantitative gait measurement. World Journal of Engineering. 12(2015), 619-626

3. M.G. Tan, J.H. Ho, H.T. Goh, H.K. Ng, L.A. Latif, M. Mazlan. A new fractal-based kinetic index to characterize gait deficits with application in stroke survivor functional mobility assessment. Biomed Signal Process Control (accepted in October 2018).

4. M.G. Tan, K.S. Tan, J.H. Ho, H.K. Ng, Cyclogram based symmetry region of deviation approach to quantify gait asymmetry. Gait Posture (submitted and under review).

Acknowledgement

At various stages in doing my PhD, a number of people have given me invaluable supports. In this regard, I owe a depth of gratitude to my supervisor, Dr Ho Jee Hou, who have cultivated devotion and determination in me and have been a helping hand at every moment to support and motivate me. Dr Ho had spent so much time to supervise me. My research would have deviated in the wrong direction if not the guidance from Dr Ho. In addition, I would also like to deeply thank Dr Goh Hui Ting, my co-supervisor in University of Malaya Medical Centre, who helped me in conducting human experiments. Her advices on biomechanical field has helped me to progress forward.

I would like to say thank you to Dr Lydia Abdul Latif and Dr Mazlina Mazlan, for helping me to work in UMMC. Besides that, I would like to show my gratitude to the physiotherapists in UMMC, for helping me to recruit stroke patients and do the experiments with me. I am also thankful to all of the academic staffs, administrative staffs as well as the technical staffs at the Faculty of Engineering at UNMC for their continuous guidance and support.

Finally, I would like to convey my truthful appreciation to all my family members, especially my parents and my wife, for all the unconditional support, endless guidance and encouragement throughout my PhD journey. I would also like to take the opportunity to say thank you to both of my wonderful kids, for being with me.

List of Figures

Lists of Tables

Abbreviation

ADL	Activities of Daily Living
NASAM	National Stroke Association of Malaysia
SEMG	Surface Electromyography
TUG	Timed Up and Go
MEMS	Micro-electro-mechanical systems
IMU	Inertial Measurement Unit
K.I.	Kinetic Index
CSROD	Cyclogram Symmetry Region of Deviation
EEMD	Ensemble Empirical Mode Decomposition
MUAP	Motor Unit Action Potential
HFD	Higuchi Fractal Dimension
SROD	Symmetry Region of Deviation
RLA	Rancho Los Amigos
COM	Center of mass
FSR	Force Sensitive Resistors
SNR	Signal to noise ratio
IROD	Individual region of devation
AHA	American Heart Association
WHO	World Healthy Organization
CNS	Central nervous system
TIA	Transient ischemic attact
TM	Treadmill training
OG	Overground training
BWS	Body weight support
UST	Unilateral step training
AFO	Ankle foot orthosis
FES	Functional electrical simulation
TA	Tibialis anterior
GM	Gluteus medius
NP	Non-Paretic leg
P	Paretic leg
FAC	Functional ambulation categoris
SENIAM	Surface EMG for non invasive assessment of muscle
RMS	Root mean square
ZC	Zero crossing
MDF	Median frequency
MNF	Mean frequency
RP	Recurrance plot

RQA	Recurrence quantification analysis
RR	Recurrence rate
DET	Determinism
FD	Fractal dimension
DFA	Detrended fluctuation analysis
MU	Motor unit
EEG	Electroencephalography
EMD	Empirical Mode Decomposition
SCL	Serial Clock
SDA	Serial Data
SPI	Serial peripheral interface
SS	Slave select
MOSI	Master output slave input
MISO	Master input slave output
SCK	Serial Clock
IGS	IMU based gait sensor system
GL	Gastrocnemius lateral
DI	Direct integration
RM	Resetting mechanism
RMSE	Root mean square error
DPN	Dynamic peak normalisation
CI	Confident interval
SL	Stride length
HC	Heel clearance
GC	Gait cycle time
ST	Stance time
SW	Swing time
AD	Ankle dorsiflexion at mid-stance
AP	Ankle plantarflexion at toe-off
GV	Gait velocity
LLN	Linear length normalisation
PLLN	Piecewise linear length normalisation
POI	Points of interest
DTW	Dynamic Time Warping
PDTW	Piecewise Dynamic Time Warping
IMF	Intrinsic mode functions
UE	Upper envelope
LE	Lower envelope
FFT	Fast fourier transform

Nomenclature

$Accel_{convert}$	Converted readable accelerometer data
$Gyro_{convert}$	Converted readable gyroscope data
$Accel_{Raw}$	Raw accelerometer data
$Gyro_{Raw}$	Raw gyroscope data
g	Gravitational force
$Sens_{Accel}$	Sensitivity scale factor for accelerometer
$Sens_{Gyro}$	Sensitivity scale factor for gyroscope
$Sens_{sEMG}$	Sensitivity scale factor for sEMG
$Gain$	Gain amplifier
$sEMG_{raw}$	Raw ADC output sEMG signal
HS	Heel-strike
TO	Toe-off
θ_{stand}	Pitch inclination angle during standing
ϕ_{stand}	Roll inclination angle during standing
$\mathbf{V}$	3-axis acceleration/gyroscope vector after rotation
$\mathbf{R_B^I}$	Rotation matrix from sensor frame to inertia frame
$\mathbf{R_X}$	Rotation matrix for roll
$\mathbf{R_Z}$	Rotation matrix for pitch
A_X	Acceleration at X-axis
A_Y	Acceleration at Y-axis
A_Z	Acceleration at Z-axis
$\mathbf{D}$	Transformation matrix to convert angular velocities from sensor frame to inertia frame
$\dot{\phi}$	Roll angular velocity at inertia frame
$\dot{\varphi}$	Yaw angular velocity at inertia frame
$\dot{\theta}$	Pitch angular velocity at inertia frame
U	Integrated gait data result before reset
$\widetilde{U}_{T1}$	Segmented Integrated gait data result before reset with *T1* samples
$\widetilde{U}_{T2}$	Segmented Integrated gait data result before reset with *T2* samples
N	Total number of samples
$\widehat{U}_{T2}^{1}$	Intermediate corrected gait data result
$\widehat{U}_{T2}^{2}$	Final corrected gait data result
$\tilde{\theta}$	Inclination pitch angle before reset
θ_{ini}	Initial inclination pitch angle
$\hat{\theta}$	Corrected inclination pitch angle

$A_{X,inertia}$	Acceleration at inertia frame at X-axis
$A_{Y,inertia}$	Acceleration at inertia frame at Y-axis
$A_{Z,inertia}$	Acceleration at inertia frame at Z-axis
Vel_j	Velocity before reset
Vel_j	Initial velocity
$\widehat{Vel}_j$	Corrected velocity
D_j	Displacement before reset
D_{Ini}	Initial displacement
$\breve{D}_X$	Horizontal displacement at ankle
$\breve{D}_Y$	Vertical displacement at ankle
x_m^k	New time series with *m* represent initial time and *k* the interval time
L_m	The length of the curve x_m^k
σ_i	Fractal properties of sEMG
AP	Area of peaks
NP	Number of peaks
F	Sliding window HFD time series
S	Average local minima
PN	Prominence of peak
PH	Peak height
$PM_{norm,t}$	Normalised peak magnitude of CSROD
PM_t	Peak magnitude on CSROD at time *t*
GD_un	Gait data from unaffected limb
W	Time warping path
ED_1	First Euclidean distance between the first point of gait trajectory from healthy and stroke
ED(N)	Time series form by *N* points of ED_1
G_Funct_{GT}	Gait functionality index based on gait trajectoryh
A_{ED}	Area under the curve for *ED(N)*
$A_{GT,h}$	Area under the curve for healthy gait trajectory
TD(i)	Time delay function
G_s	Gait event vector for stroke
G_h	Gait event vector for healthy
G_Funct_{TD}	Gait functionality index based on time delay
A_{TD}	Area under the curve for *TD(i)*
y	True dependent variable
β_c	Random regression intercept
x_p	Independent variables with *p* variables
β_p	Regression coefficient for independent variables
$\hat{y}^{(i)}$	Predicted dependent variables at different stage i

$\beta_{c,Approach1}$	Random intercept for model approach 1
$\hat{\boldsymbol{y}}$	Dependent variable *n* x 1 matrix
$\boldsymbol{\beta}$	Regression coefficient (*p*+1) x 1 matrix
$\boldsymbol{X}$	Independent variable *n* x (*p*+1) matrix
RSS	Sum of squared residuals
$\hat{z}$	Recovery trajectory from stage 1 to stage 3
$\beta_{c,Approach2}$	Random intercept for model approach 2
$\hat{\boldsymbol{z}}$	Dependent variable *n* x 1 matrix
c_j	Intrinsic mode function component *j*
r_n	Residue of the data
ε_n	Final standard deviation error

Contents

Chapter 1 Introduction

1.1 Research background

Stroke is the third largest leading causes to death and approximately 40,000 patients suffer such disease in Malaysia every year according to National Stroke Association of Malaysia, NASAM [1]. Poor coordination, abnormal posture and hemiplegia are the main side effects of this cerebrovascular disease, which lead to restriction in their activities of daily living (ADLs) and mobility problems. Proper rehabilitation services such as speech, physical, occupational and recreational therapies and group activities [1] are necessary to help stroke patients to promote their independence in ADLs. The goals of rehabilitation are to help the patients to improve their body functions and to gain their independency by retraining their neural system and strengthening muscles. Therefore, recognition of stroke symptoms are very important in order to plan a suitable rehabilitation strategy. In this thesis, we focus on identifying the symptom of abnormal walking pattern of stroke. Early rehabilitation is crucial once patients are diagnosed with stroke as study shown that 95% of the patients will recover their walking ability within the first 11 weeks after stroke [2]. The traditional process of gait rehabilitation starts from quantitative gait analysis, gaits classification and gait rehabilitation treatment. Physiotherapist is unable to assess the condition of stroke patients without quantifying the gait pattern and obtaining the gait parameters. These parameters help the physiotherapist to classify the type of abnormal walking. For stroke patients, their abnormal walking includes asymmetry-walking, lack of balancing control, foot drag, slow gait velocity etc. After identifying these abnormal walking conditions, physiotherapist will arrange a proper rehabilitation treatment for them.

1.1.1 Definition of gait

Gait is a complex cyclic movement that can be described as segments of time that mainly consist of stance and swing periods [3]. The function of gait is to translate human body from one point to another by using repetitive reciprocal limb motions [4,5]. The performance of gait is directed to the accomplishment of four related tasks [6]: maintaining balance of lower limb with the rest of the body, maintaining support of limb segments during stance phase, lifting the foot from the ground during swing phase and supplying enough energy to move the entire body forward. Quantitative gait analysis is the first step of rehabilitation and it must be conducted on the stroke patients to provide information of the patient's condition. Gait analysis are commonly performed in three ways: (i) by visually inspecting a patient's gait performance and qualitatively describing the gait pattern; (ii) by using validated clinical tests, such as 10 meter walk test [7] or Timed Up and Go (TUG) test [8] to quantify gait performance; (iii) by the use of sophisticated systems to quantify the motion of the body segments (e.g. video motion capture system and force plate system). The first method is commonly used because it is easily administered and does not require expensive measuring instruments. However, the observation is prone to human biases and the interpretations are rather subjective. The second method provides an objective quantification of gait performance and often administered with a standard procedure such that biases can be reduced. The drawback of these clinical tests is the lack of detailed analysis of movement. In contrast, the third method is more accurate in the quantification of detailed gait performance. It provides objective measurement of movements that are difficult to detect visually. Despite the mentioned advantages, the operating costs are expensive and they require specialised training and high level of technical skills [9–11]. Given the needs for accurate objective quantification of gait performance and affordable cost, a low cost portable gait sensor system could be an attractive alternative solution. With the emergence of miniaturisation techniques, small-size sensors such as micro-electro-mechanical systems (MEMS) has been integrated to form wearable gait sensors. Many researchers had developed low cost sensor systems for their own research purposes [12–14]. In this project, a portable low cost

sensor system will be developed to acquire the gait trajectory and to distinguish the difference of gait patterns between healthy human and stroke patients.

1.1.2 Gait sensor system and gait spatial-temporal parameters

Inertial Measurement Unit (IMU) is an inertial sensor, which consists of accelerometer and gyroscope to track rotational and translational movements [15]. For gait analysis, the position and orientation of lower limbs can be determined by integrating the acceleration and angular velocity from IMU. However, the performance of inertial sensor is still relatively poor [16]. The low signal to noise ratio (SNR) and sensor drifting lead to estimation error grows unbounded. Cross-axis sensitivity, cross-coupling, misalignment, bias, sensor drifting and noise often occurred in these sensors [17,18]. This issue can be solved by applying frequent measurement updates methods. These methods will correct the position and orientation based on certain definitions. Spatial parameters such as stride length can be obtained from the integrated gait trajectory while the temporal parameters can be acquired by using heel strike and toe off information, which can be detected from ankle gyroscope signal [19]. Temporal parameters such as gait cycle time, swing time and stance time are important to study the performance of stroke patients. These parameters are frequently used as an indication of recovery when certain treatment is introduced [2,20,21] or to show the effects when different treatments are compared [22,23]. These spatial temporal parameters are easy to use and provide valuable information to describe the quality of the gait and they are essential in this study.

1.1.3 Gait classification

Gait classification among stroke is to identify homogeneous subgroups of stroke patients, which could enable physiotherapists to deliver treatments that are more effective during rehabilitation. This is particularly important to those researchers who do not have full access to collect necessary gait data; such a method would also facilitate communication between clinicians [24]. Besides that, proper classification can help to organise and manage large amounts of complex gait data.

These gait data are generated by instrumented gait analysis such as kinematic and EMG data [25]. Many authors have attempted to identify homogeneous subgroup of gait pattern among stroke patients using methods such as cluster analysis [26,27] and artificial neural network [24,28]. However, most of these methods require multiple inputs (gait spatial-temporal parameters), which is very subjective and generally based on the observation by visual inspection from researchers or clinicians [27]. Meanwhile, single category of parameter often yielded functionally heterogeneous results [27]. Therefore, it is worth studying different gait classification approaches and compared them to each other.

1.1.4 Gait asymmetry

The spatial-temporal gait parameters described in Section 1.1.2 will be used to determine the type of abnormal gaits. As mentioned previously, one of the significant abnormal gait observed from hemiparesis stroke patients is gait asymmetry [29]. Symmetry of gait is defined as no difference in gait parameters between left and right leg [30] and the lower limbs are acting in the same motion with the same gait pattern [31]. Symmetrical of gait is an indicator of normal walking and physiotherapists quantify the gait symmetry that serves as a diagnostic tool for rehabilitation plan and strategy. The conventional ways to quantify the gait symmetry are symmetry ratio, symmetry indexes, symmetry angle and statistical approaches (correlation coefficients, principal component analysis, analysis of variance) [32]. Univariate parameters such as stance time, step length, gait speed and joint angle are used to assess any gait deficiency. These conventional methods are easy to apply but they have limitations. According to Sadhegi *et al* [31] the symmetry indexes have low sensitivity, unable to identify the location of asymmetry, and poor selection of parameters. There is no universal rule to select the parameters used for calculation and many researchers had reported different parameters would yield different symmetrical values within the same subject [33–36], which leads to confusion during qualitative assessment. The current symmetry indexes are not capable to understand the complexity of gait cycle and the parameters used to calculate the gait symmetry are often treated as a quantified

value to represent the whole gait cycle instead of certain gait event. Since the severity of stroke is related to the symmetrical of gait, there is a need to clarify the confusion caused by the limitations from conventional methods so that the workload of physiotherapists can be reduced and human error can be minimised.

1.1.5 Surface Electromyography

The surface electromyography (sEMG) signal is elucidated as the electrical activity of skeletal muscles and it contains the information about the function of the muscles, which creates the body movement [37]. SEMG has been widely used by researchers and clinicians to perform gait analysis [38–40]. In Olnet *et al* [6] review, there are four types of muscle behavior among stroke patients; Type I has demonstrated hyperactive stretch reflexes, Type II is characterised by lack of activation during both shortening and lengthening contractions, Type III shows excessive and stereotyped coactivations of several muscle groups and Type IV shows combined components of the above three. These characteristics of the sEMG signal can be quantified by several techniques included time and frequency domains analysis. For example, root mean square value (RMS), zero-crossing rate, median frequency (MDF), mean frequency (MNF), can determine muscle fatigue and muscle energy expenditure. These linear analyses assume sEMG to be random and uncorrelated. However, the sEMG signal is highly nonlinear deterministic. Therefore, it leads to the development of non-linear techniques to analyse sEMG signal. Techniques such as largest lyapunov exponent, Recurrence Quantification Analysis and fractal dimension are being utilised to determine the geometry and fractal properties of the sEMG signal. These techniques are particularly useful to determine the muscle force expenditure and fatigue. Nevertheless, to date, there are only limited studies to show the correlation between sEMG during gait and conventional clinical assessment tools such as TUG test. In this study, one of the non-linear analysis technique is applied to study the correlation between sEMG and TUG score.

1.1.6 Gait recovery

Gait rehabilitation generally shows promising positive recovery among stroke patients [41–43]. Therefore, in order to better assess the recovery rate or the efficiency of certain rehabilitation treatment, many researchers started to emphasise the development of recovery prediction models. Generally, these models use patient's baseline gait parameters as the independent variables to predict the motor function, mobility or activities of daily living function among stroke survivors [44–46]. The independent variables can be time-independent or time dependent variables. Time-independent variables such as age, type of stroke, gender, side of hemiparesis etc. are the variables that will not change with time. Time-dependent variables such as clinical assessment test, activities daily living functions, kinematic and kinesiology parameters are the variables that will change with time. Multivariable linear regression model is the most common algorithm to predict the recovery among stroke [44–48].

1.2 Problem statement and motivation

The motivation of this research is to improve the current rehabilitation procedures. With increasing stroke patients in Malaysia, the healthcare service cost and the physiotherapist workload increase rapidly. Teasell *et al* [49] stated most stroke patients could regain the walking ability with proper rehabilitation in the early stage. However, increasing the workloads of physiotherapists will lead to delay in the stroke patient's recovery progress. Therefore, some stroke patients are unable to regain the walking ability due to the delay.

The first step of gait rehabilitation is gait analysis and it starts with acquiring the gait parameters. Human observation is the easiest method to acquire gait parameters but it is prone to human error. Clinical assessment tools are powerful tool to analyse motion and they are frequently used as an indicator of recovery. However, these assessment tools often provide limited information. Sophisticated sensor system is

available in gait motion lab but the operating cost is too high. This will delay the gait assessment when one is diagnosed with stroke.

Gait parameters acquired from the sensor are further processed to analyse the gait characteristics and gait classification. The selection of the proper gait parameters as the input parameters of gait classification is often confusing. Furthermore, stroke patients often exhibit abnormal gait such as gait asymmetry. There are many limitations in current methods to quantify gait asymmetry; for example, (i) low sensitivity, (ii) lack of time history and (iii) mostly univariate.

The neurological information such as sEMG during gait is not always associate with the spatial-temporal parameters and the results from clinical assessment tools. Moreover, most of the recovery models described now relied heavily on clinical assessment tools such as Rivermead Mobility Index, Functional Ambulation Classification, Timed Up and Go test etc. To our knowledge, there are very limited recovery models, which use kinematics and kinesiology parameters derived from motion sensor and EMG sensor to predict the recovery.

These problems have become the primary motivation of this research and the author contributions to this research are stated in the next section.

1.3 Research contributions

This research attempts to fill the knowledge gap and addresses the issues mentioned in Section 1.2. The principal contributions of this thesis are:

1. We developed a low cost gait sensor system that can accurately measure gait trajectory and temporal parameters. This gait sensor system consists of IMU and they are located at different part of lower limbs such as foot and shank. The reason to implement multiple IMU is to provide more information than single IMU. A new gait trajectory computation algorithm was established to obtain the walking pattern. This algorithm is simple to implement with high accuracy.

2. We performed the conventional methods to analyse and classify gait. The gait characteristics of cross-sectional data from 60 stroke patients are being studied and compared to the healthy subjects. We provided an in-depth study of the correlation of different gait parameters with clinical assessment tool and gait asymmetry index. Gait classification using Hierarchical Cluster Analysis was performed with multiple gait parameters as inputs to classify these large groups of stroke patients into three different homogeneous subgroups.

3. We developed two accurate gait analysis techniques. These analysis models are based on the kinesiology and kinematic parameters of stroke patients. The kinesiology based gait analysis is Kinetic Index (K.I.) and the kinematic based gait analysis is Cyclogram Symmetry Region of Deviation (CSROD).

4. The correlation between K.I. and TUG test was studied. These K.I. values were strongly correlate to TUG score and were able to provide detail information such as the weaker muscle on the paretic lower limb.

5. Gait classification using Hierarchical Cluster Analysis was performed with K.I. as the single input. The classification results showed that this approach could classify the stroke patients into three different homogeneous subgroups. The gait characteristics in these subgroups were similar to the conventional multiple inputs approach.

6. Based on the proposed improved gait analysis methods (K.I. and CSROD), we established two recovery models that could predict the recovery status of stroke patients within their first six months after diagnosed with stroke. The first model was solely based on the baseline parameters while the second model was based on the recovery trajectory between certain periods.

7. The recovery models described earlier merely provided physical information based on the gait trajectory and temporal information. The study of muscle status changes across recovery was also important to avoid unnecessary muscle impairment. Therefore, the sEMG during gait was being decomposed by

Ensemble Empirical Mode Decomposition (EEMD). This information can describe the gait recovery status for all stroke patients.

1.4 Research objective

The main objective of this thesis is to develop a sophisticated gait analysis system to assist the recovery of stroke patients. In order to achieve this objective, there are six main areas needed to focus in this research as shown in the followings:

a. **To develop an accurate low cost portable sensor system.**
b. **To study the limitations of conventional gait analysis.**
c. **To propose new gait analysis tools (Kinesiology and Kinematic based gait analysis).**
d. **To study different approaches of gait classification.**
e. **To establish models to predict the recovery progress of stroke patients.**
f. **To describe the gait recovery status based on their muscle conditions.**

1.5 Project Description

The research sought to create a gait analysis system that provided instrumented and systematic analytic system outside of traditional and inefficient analysis methods (such as human observation). Such a system will help to reduce the workload of clinicians. Clinician can apply this gait analysis system to investigate the gait abnormality symptom and recovery status. This system explores every aspect of stroke patient's walking conditions, from individual recovery performances to comparison to healthy gait.

This research evaluated the system with different type of stroke patients. Gait spatial temporal parameters and sEMG signal were obtained from the developed inertia gait sensor system and commercial EMG sensors. Gait characterisation was performed by extracting valuable information from both IGS and sEMG results. These results provided kinematic and kinesiology aspect on stroke patients gait pattern. Furthermore, these gait parameters also can be used as the input to perform

gait classification. New gait functionality indices was introduced to determine the gait trajectory deviation and time delay between stroke patients and healthy human. All the features and indices derived were further being used to develop recovery prediction models. To ensure the recovery during stroke was not based on compensation of other muscle, sEMG signal was decomposed into different component to study the muscle status changes throughout the recovery period.

As stated, this system provides advance and systematic analysis on stroke patient's gait. It includes development of gait sensor system, gait characterisation, gait classification, gait recovery prediction and gait muscle compensation. Such system will be very effective in clinical setting to help clinician in planning rehabilitation strategy. However, this system has high complexity in term of interpreting the outcome, which clinician may hesitate to adopt it.

1.6 Thesis outline

This thesis is organised in ten chapters.

Chapter 1: Introduction

In Chapter 1, the research background, motivation, contribution and the objectives of this research were explained.

Chapter 2: Literature review

An examination of the literature detailing the history of development of low cost sensor system, computation of gait trajectory, non-linear analysis of sEMG, history of asymmetry study with different approaches and rehabilitation recovery models.

Chapter 3: Methodology

The sensor selection for the development of the gait sensor system was explained. Three sets of experiment were conducted to achieve the research objective. The data processing was explained in this chapter.

Chapter 4: An inertia integration method

A new resetting mechanism algorithm was introduced to obtain the gait trajectory. The resetting algorithm was validated using high speed video camera.

Chapter 5: Conventional gait analysis

The gait characteristics of stroke patients were being studied and compared to healthy human gait. The correlation between spatial-temporal parameters and gait velocity and TUG score were being analysed. Gait classification using Hierarchical Cluster Analysis was performed based on multiple inputs.

Chapter 6: Kinesiology based gait analysis- A new fractal-based kinetic index to characterise gait after stroke

The correlation between kinesiology information (sEMG) with TUG score is not well known. In this chapter, Higuchi Fractal Dimension (HDF) was applied to extract features from sEMG during gait. These features was used to explain the phenomenon in TUG test. A novel algorithm, Kinetic Index (K.I.) was proposed by incorporating the features extracted from HFD. This K.I. was highly correlate to TUG test, which provided information such as risk of fall. Besides that, this K.I. was used as a single input to classify stroke patients into three different homogeneous subgroups.

Chapter 7: Kinematic based gait analysis- Cyclogram Symmetry Region of Deviation

A new Cyclogram Symmetry Region of Deviation (CSROD) was proposed in this chapter to eliminate the issues addressed by conventional asymmetry quantification methods. This CSROD method is similar to original Symmetry Region of Deviation (SROD) method. The main advantage of using CSROD is it replaces the walking data from a large group of healthy subject from SROD with a standard 45° symmetry line.

Chapter 8: Development of mathematical gait prediction models in stroke rehabilitation

Two new gait functionality indices were proposed here to assess the gait performance of stroke patients. These two indices were being used as the dependent variables to the recovery models to predict the walking ability at different time. Two different recovery models were computed. The first model was solely based on patient's baseline gait data and the second model was based on the recovery trajectory from a period.

Chapter 9: Determine the fundamental principles of gait recovery through sEMG decomposition

The two gait functionalities indices introduced in Chapter 8 can only detect the changes of gait performance physically. It is necessary to study the development of lower limb muscles associated with the changes of these two indices. sEMG from stroke patients is decomposed using Ensemble Empirical Mode Decomposition (EEMD). This method can decompose the sEMG to provide a rough estimation of motor unit recruitment and frequency.

Chapter 10: Conclusion and Future Work

This chapter concluded all the experiments and analysis of results in this research. The future work based on the limitation from this research was explained.

Chapter 2 Literature review

2.1 Introduction

This chapter explores some background information necessary to fully understand the present work and its associated goals. Here, the literature review covers the various topics:

1. To introduce the terminology of gait and relevant parameters for gait analysis.
2. To review the history of gait sensor development and computation of gait trajectory.
3. To review the methods of asymmetry index used in previous study and the development of new asymmetry algorithm.
4. To review the current analytical tool to assess the recovery status of stroke patients.
5. To discuss the features extracted using non-linear techniques on surface EMG.
6. To review the history of prediction of recovery model.

Lastly, the key points from the literature review are summarised in Section 2.7.

2.2 Gait terminology

Quantitative gait evaluation is important for early stroke's gait rehabilitation as Teasell *et al* [49] stated approximately 60% of stroke survivors has the ability of limited walking in some manner. To understand more about gait analysis, the gait terminology must be well apprehended.

Gait is a cyclic phenomenon that can be divided by phases and there are two sets of terminology currently in use; traditional terminology and *Rancho Los Amigos* (RLA). According to *Rancho Los Amigos* (RLA) system [50], it describes the gait trajectory in segments of time which mainly consist of two phases, stance and swing

periods. Ideally, a gait cycle is started from *Initial Contact*, or heel strike in conventional terminology. It is defined as the instant of first contact between heel and ground so the limb is positioned to begin stance with heel rocker. Both lower extremities are still in contact with the surface during *Initial Contact* until the *Loading Response* where the other foot is lifted for swing and this outstretched limb absorb the shock caused by the weight transferred from the other leg. This is the beginning of single limb support and this period accounts for 0-10% of the gait cycle. The single limb support period continues as the extended foot is lifted totally from the ground and this is the commencement of *Mid Stance*. The human body weight now is only supported by the foot on ground throughout this interval and it consumes 10-30% of the gait cycle. The stance phase is completed with *Terminal Stance*, where the ipsilateral heel off the ground and the opposite foot starts the *Initial Contact* when it strikes the ground and this takes 30-50% of the gait event. Swing phase occurs right after the end of stance phase and it begins with *Pre-Swing*. This interval is the preparation of toe-off and the limb is positioned such that it is ready for swing. The weight now is transferred to the contralateral limb and this is part of the 50-60% of gait cycle. *Initial Swing* or toe-off takes place where the limb begins to lift from the ground and the interval of gait cycle is 60-73%. *Initial Swing* ends when the swinging foot is opposite the stance foot and this is called the *Mid Swing*. During this phase, the limb advances from its trailing position. This phase is taking place in 73-87% of gait cycle. A complete 100% gait cycle ended with *Terminal Swing.* The limb advancement is accomplished as the tibia is moved ahead the thigh and the knee is extended maximally. This phase is important as this is the deceleration of the swing limb and the preparation for stance. **Fig 2.1** shows a schematic diagram between *Rancho Los Amigos* (RLA) system and conventional terminology for a complete gait cycle.

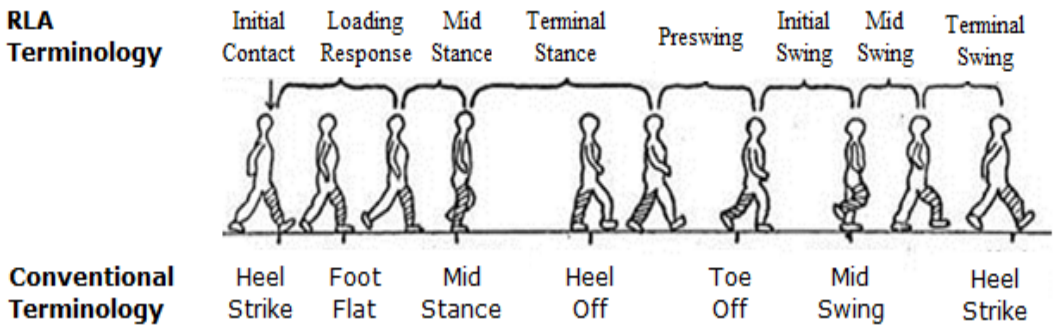

Fig 2.1. Gait Terminology of Conventional and RLA Terminology for Stance and Swing Phase. [51]

Study of locomotion involves the analysis of the magnitudes, directions and rates of three coordinates axes in space [4], therefore there are variety of techniques to present this analysis of the fundamental determinants of gait. Centre of mass (COM) is introduced to simplify the concept of the phenomena of locomotion during a cycle of motion and the entire body weight is concentrated at one point and the limbs are regarded as weightless levers of the body. In the early years 1953, Saunders [4] reported that the displacement pattern of the COM is the summation of all the forces and motions acting upon with the translation of the body from one point to another during a gait cycle. For a normal gait cycle, it can be predicted that the COM fluctuates upward and downward and forms a smooth regular sinusoidal curve in the plane of progression.

Spatial and temporal measures represent distance and time measurement respectively. In gait analysis, spatial-temporal gait parameters are important to define a gait cycle quantitatively. The definitions of these parameters are shown in **Table 2.1**, according to Bugane *et al* [52]. These parameters are normally used to quantify the performance of different stroke patients and a sign of recovery throughout certain treatment.

Table 2.1. Definitions of Spatial Temporal Gait [52]

Gait Parameters	Unit	Definition
Gait Cycle Time	second	Time between two consecutive heel strike of the same foot
Stride length	meter	Distance between two consecutive heel strike of the same foot
Step duration	second	Time between ipsilateral and contralateral heel strikes
Foot symmetry	%	Step duration as percentage of gait cycle
Stance time	second	Duration gait cycle of foot support phase, heel strike to toe off
Swing time	second	Duration of gait cycle of foot swing phase, toe off to heel strike
Double support time	second	Duration of gait cycle of the phase of both limb supported on ground
Single support time	second	Duration of gait cycle of the phase of single limb supported on ground
Gait speed	m/s	Average speed integrated from acceleration within the gait cycle
Cadence	Strides/min	Number of strides in a minute

2.3 Review of gait sensors

Quantitative gait analysis provides physiotherapists an understanding about the condition of patients to select a suitable treatment during rehabilitation process. Intense research works had been done to analyse the gait pattern and try to extract valuable information by using different kind of sensors. Kinetic (ground force and pressure), kinematic (angles, velocities and acceleration) and kinesiology (EMG) analysis have been carried out to evaluate the effects of rehabilitation training. In recent years, there have been increasing amounts of literatures on development of low cost gait sensor systems to reduce the cost and provide quantitative analysis on gait detection during rehabilitation. Multiple body-worn sensors such as accelerometer [52–54], gyroscope [11,55,56], bending sensor [57,58], force sensor [59–61] and electromyography (EMG) sensor [40,62,63] are placed at different body positions to obtain spatial temporal gait parameter.

Back in 1960's, researchers had focused on obtaining foot measurement directly from various pressure sensors [64]. Lereim and Hanssen *et al* [65] used transducer

to record the pressure distribution under the sole of the foot during 1970s. In 1990, Wertsch *et al* [66] developed a system consists of seven pressure sensors which were located at seven high pressure point determined by subjects walking on inked paper. Later in 1994, Hausdorff *et al* [67] introduced a simple "footswitch" system consisted of two Force Sensitive Resistors (FSRs) on an insole that was capable of detecting temporal gait parameters. The results were analysed and compared with commercial force plates and it provided a promising outcome of 3-5% of error. In a recent study, Howell *et al* [68] described the design of a low-cost FSRs sensors insole to evaluate six healthy subjects and four hemiplegic stroke subjects. Besides obtaining temporal parameters, Howell *et al* [68] also determined the ground reaction force and moments corresponding to ankle and knee joints movements. The results showed the system was reliable since the root mean square errors between the designed system and validated results using Motion Analysis Lab were under 10%.

In 2004, Salarian *et al* [55] developed an ambulatory gait analysis method using body attached gyroscope. Six gyroscopes were positioned at left and right forearms, thighs and shanks. In this experiment, a group of Parkinson patients (5 males, 5 females) and a group of normal healthy subjects were recruited. The gait parameters were compared with motion capture system and the outcomes showed insignificant errors. Zdragkas *et al* [54] proposed an algorithm to identify the gait event by using a three-axis accelerometer mounted on foot. After obtaining the *Y* and *Z*-axis accelerometer signals, two new signals, namely energy and product signals, were created to amplify the gait events by narrowing the gait event peaks, which created maximum and minimum extrema in gait events and remove the irrelevant events. Energy signal is the sum of squared *Y* and *Z*-axis acceleration, while product signal is the product of *Y* and *Z* acceleration. Gait events such as initial swing, terminal swing, foot strike, begin stance, toe off and opposite foot stride can be deduced from the two new signals.

Single sensor in a system only provides limited gait information. Hence, recent researches have expanded their interests in sophisticated measurement capabilities

by dealing with more sensors in one platform. In early 2000s, Aminian *et al* [11] had designed an ambulatory system, which included two FSRs in each foot and gyroscopes on each shank for estimation of spatial-temporal parameters during long periods walking for nine young and 11 elderly subjects. Wavelet analysis was implemented to acquire the gait temporal parameters and the accuracy was assessed by using standard foot pressure sensors. The final outcome showed almost identical results for both systems. Similar work had been carried out by Pappas *et al* [69] who integrated three FSRs and a gyroscope. The performance of this device was validated by optical motion analysis system Vicon 370. A gait phase detection algorithm was recommended to distinguish the transition of each gait phase using the device. Experiments were carried out by two different groups; group A contained ten healthy adults and group B contained six adults diagnosed with gait pathologies. The outcomes of the experiments showed high accuracy of the system and the ability to differentiate from non-walking abilities. Lopez *et al* [70] on the other hand adduced an inexpensive and user-friendly methodology to enable clinical application for rehabilitation. One accelerometer was mounted on the heel of the shoes and five FSRs were attached on the insoles. Data collection was performed on a group of sixteen healthy subjects and seven post stroke patients. The estimation error for both societies was in the range of 2.6-18.6%.

Mariani *et al* [71] installed an inertial measurement unit (IMU) consisting of three axis gyroscopes and accelerometers on forefoot and an ambulatory pressure insoles were used as reference to authenticate the IMU. Ten healthy subjects, 12 patients with ankle osteoarthritis, 11 patients treated by total ankle replacement and nine patients treated by ankle arthrodesis were recruited. They were asked to perform 50m walking trials and the comparison of gait events between reference system and IMU system showed valid accuracy and precision. Meanwhile Liu *et al* [72] built a wearable sensor system based on three gyroscopes and a two-axis accelerometer to detect the gait phases and joint angle of ten subjects and the performance of the system was validated through commercial optical motion analysis system Hi-DCam. The correlation coefficient and root mean squared error between two systems proved the good reliability of the system. Frenez *et al* [58] fused three

pressure sensors on an insole and two bending sensors with one on the ankle and one on the insole to form a wireless system and it was tested with seven healthy subjects.

In year 2008, Bamberg *et al* [73] had successful developed a wireless wearable system named "GaitShoe" which integrated three orthogonal accelerometers, three orthogonal gyroscopes, four force sensors, two bidirectional bend sensors, two dynamic pressure sensors and electric field height sensors. To capture the kinematic motion of the foot, accelerometers and gyroscopes were placed at the back of the shoe. Temporal and kinetic parameters were accessed by force sensors and dynamic pressure sensors and the bidirectional bend sensor was used to analyse flexion during gait. To validate this sensor system, 16 volunteers from both healthy and Parkinson's disease subjects were recruited to place the GaitShoe on their own walking shoes. They were underwent simultaneous gait evaluation using the MGH BMLs Selspot II data acquisition system. The outputs had involved the application of standard pattern recognition techniques to discriminate between healthy gait and Parkinsonian gait.

Despite large number of previous research works on developing low cost gait systems, there are still restriction of each individual system. As mentioned previously, single sensor in a system only provides limited information [54,55]. To solve that problem, researchers integrated multi-sensors in a system. Different researchers used different sensors in the system to achieve their project objective and this increases the difficulties in the set-up for stroke patient. Therefore, redesign a sensor system which is easy to wear and comfortable for stroke patients is necessary

Most of these inertial-based sensor system consist of accelerometer and gyroscope to track rotational and translational movements [15]. For gait analysis, the position and orientation of lower limbs can be determined by integrating the acceleration and angular velocity from IMU. However, the performance of inertial sensor is still relatively low [16]. The low SNR and sensor drifting lead to estimation error grow unbounded. Cross-axis sensitivity, cross-coupling, misalignment, bias, sensor

drifting and noise often occurred in these sensors [17,18] This issue can be solved by applying frequent measurement update methods. These methods will correct the position and orientation based on certain definition.

Kalman Filter [74] is one of the most popular method used in this field. Kalman filter is a powerful tool to predict and estimate the state variables based on state model and measurement model. For example, the angle measurement state model from gyroscope can be constructed as a combination of angle and angular velocity bias [75]. The angle measurement model in this study was the angle determined from acceleration and gravity. Cooper *et al* [18] extended the method in [75] to determine the roll and pitch angle during walking. The state model included velocity, acceleration, angular velocity, gyro bias, roll and pitch. To obtain the position and orientation of the sensors, Sabatini [17] corrected the rotation quaternion in the state model by removing the bias from acceleration and magnetism. Similar technique can be seen in [76]. Mazza *et al* [77] state model of the filter was obtained by combining attitude quaternion and gyroscope bias. In this study, the measurement model is the relationship between acceleration and gyroscope. Other approaches use Kalman Filter to remove noises or correct biases including fusion of inertia sensor with GPS [78–80] and fusion of inertia sensor with motion camera [81].

Besides Kalman filter approach, some other researchers used different techniques to obtain position and orientation of the sensors. Stacy *et al* [73] minimised the error by dividing the signals into different gait cycles. The last sample in the signal was adjusted to remove the bias. Another resetting mechanism method proposed by Sabatini *et al* [19] can also be used to remove the drifting and noise in the signals. Other methods such as stick figure model [82] or pendulum model [83] have also been used to acquire the gait trajectory.

2.4 Gait asymmetry

2.4.1 Conventional asymmetry quantification

Symmetry of gait is defined as no difference in gait parameters between left and right legs [30]. Stroke patients often associate with gait asymmetry and this leads to the idea of quantify gait asymmetry. It is believed that gait asymmetry quantification had been introduced since 1970s [84,85] and popularised in the 1980s [86–88]. Gait asymmetry can be assessed in the form of symmetry indices derived from parameters obtained in each side of body, or in the paretic leg and non-paretic leg (as shown in **Table 2.2**). These formulas use discrete values of different gait parameters to quantify the gait symmetry between sides. $X_{unaffected}$ is the gait parameter from the unaffected leg and $X_{affected}$ is the gait parameter from the affected leg. The input parameters X can be any of the spatial-temporal parameters such as gait speed, step length, joint angle, stance time or swing time, depending on the need of study. Theses indices often appear in the form of univariate parameter where the inputs only consist of a single gait parameter.

Symmetry ratio is the simplest form to calculate gait symmetry. It is the ratio of the gait parameter from one side over the other side. Symmetry ratio of 1 indicates a perfect symmetry. A ratio larger than 1 indicates the value on numerator is larger than that of on denominator and ratio smaller than 1 means otherwise. Symmetry index is the difference between legs normalised to the summation of both legs and is expressed in percentage [87]. A value of 0% indicates a perfect symmetry and asymmetry increases as the difference of left and right legs increases. A more recent method, named as log transformation, calculates the logarithm of symmetry ratio multiplied by 100 and expresses it in percentage [89]. The interpretation of the result is similar to the symmetry index where 0% implies a perfect symmetry. Asymmetry increases when the residual of the numerator increases. Finally, symmetry angle is calculated as 45^0 minus arc tangent of symmetry ratio and divided by 90^0 [90]. The value is expressed in percentage. Symmetry angle of 0% indicates perfect symmetry and a greater symmetry angle suggests a greater

asymmetry. Unlike symmetry index and log transformation of symmetry ratio, the symmetry angle does not have a negative value.

On the other hand, statistical approaches such as correlation coefficient, Pearsons coefficient, root-mean-square difference and analysis of variance are attracting attention in gait symmetry quantification as they possess better sensitivity [91–93]. For example, multi-resolution entropy analysis had been applied to study the gait asymmetry in Parkinson disease, Huntington disease and amyotrophic lateral selerosis [94]. Principal component analysis (PCA) is another promising approach as it reduces the dimensions of the data with minimum loss of information [95]. PCA had been applied to correlate the data obtained between joints and muscles in the same and opposite lower limb [32,96–98]. Hong and Polk [99] applied Parelled Factor Analysis (a variation of PCA) to examine the symmetry and interrelationships between joints. Nüesch *et al* [100] applied PCA and linear support vector machine to classify asymmetric osteoarthritis gait patterns. Results showed that there are significant differences in hind foot dorsiflexion angle and vertical ground reaction force between affected leg and non-affected leg.

Table 2.2. Symmetry Indices

Name	Equation
Symmetry Ratio	$SI = \left\lvert \frac{X_{affected}}{X_{unaffected}} \right\rvert$
	$SI = \left\lvert 1 - \frac{X_{affected}}{X_{unaffected}} \right\rvert$
Robinson Index	$SI = \frac{X_{unaffected} - X_{affected}}{X_{unaffected} + X_{affected}} * 100$
Log transformed	$SI = \left\lvert 100 * (\ln\left(\frac{X_{affected}}{X_{Unaffected}}\right)) \right\rvert$
Symmetry angle	$SA = \frac{[45^o - \arctan\left(\frac{X_{affected}}{X_{unaffected}}\right)]}{90} * 100$

$X_{affected}$ is the parameter from paretic leg. $X_{unaffected}$ is the parameter from non-paretic leg. *SI* is symmetry index. *SA* is symmetry angle

2.4.2 Recent development on gait asymmetry analytical techniques

As mentioned, gait asymmetry could be determined through various indices in **Table 2.2**. However these indices have several limitations. For example, (i) they have low sensitivity and provide discrete value only, (ii) they are unable to describe the complexity of gait asymmetry, (iii) they are unable to provide sufficient joint information (such as timing and magnitude of abnormal joint flexion-extension) [31,101,102], and (iv) non-standardisation on selecting the gait symmetry indices and gait parameters. Moreover, the interrelationships between joints on the same lower extremity could not be revealed through these indices. It has stimulated research interest to explore new methodologies to quantify the gait asymmetry.

In 1998, Goswami *et al* [103] introduced a new parameterisation application to characterise human walking patterns. Cyclograms are used to derive quantities from geometrical features of joints. The gait asymmetry was then measured based upon the geometrical properties of bilateral cyclograms [104]. Cyclograms are also known as angle-angle diagrams. They are generated by simultaneously plotting two or more joint variables. This technique was compared and validated with symmetry index to examine the effect of peroneal nerve palsy patients receiving orthosis treatment [105]. Other examples of using bilateral cyclograms to quantify gait symmetry have been reported in relevant literatures [106–109].

On the other hand, phase portrait is a geometrical tool to deduce important characteristics of a dynamical system and it has been used for decades [110–113]. DiBerardino *et al* [114] quantified the phase portrait in terms of inter-cycle variability and complexity. In this case, the variability measurement is based on the consistency of phase portrait location throughout each gait cycle and it can be measured by the fluctuation of the centroid location in the phase diagram. The centroid of each gait cycle is found by the mean of all (x,y) data points. Centroid area and centroid drift are used to assess the inter-cycle variability. Centroid area is the bivariate 95% confidence ellipse area swept out by centroid over gait cycle. Centroid drift is the path length travelled by the centroid over the gait cycle. Meanwhile complexity is defined as the minimum number if harmonics in a

reduced-order fit. This number is used to reduce 99.9% of error between full order fit and zero-order fit of the phase portrait. It can also be described as a quantified of harmonics needed to describe the shape of phase portrait by performing Elliptical Fourier Analysis on every gait cycles for each limb. The maximum error between full and zero-order fit is calculated using sum of squared errors (SSE):

$$SSE_{max} = \sum_{i=1}^{n} \left(\left(x_{full,i} - x_c \right)^2 + \left(y_{full,i} - y_c \right)^2 \right) \quad (2.1)$$

where ($x_{full,i}$, $y_{full,i}$) is the *i*th point in the full fit, (x_c, y_c) is the average centroid and n is the number of data points. Error between reduced-order (*j*-harmonic) fit and full fit is computed by Eq (2.2)

$$SSE_j = \sum_{i=1}^{n} \left(\left(x_{full,i} - x_{j,i} \right)^2 + \left(y_{full,i} - y_{j,i} \right)^2 \right) \quad (2.2)$$

where ($x_{j,i}$, $y_{j,i}$) is the reduced fit of *j*-harmonics. SSE_j is iteratively recomputed until error between full and *j*-harmonic fit is less than 0.1% of maximum error: $SSE_j \leq 0.001 * SSE_{max}$. **Fig 2.2** shows the phase portraits of the braced and unbraced knee joint trajectory [114]. It showed that the braced trajectory is more complex since the centroid area is smaller. Gait symmetry can be determined by looking at the complexity on both legs. Huge difference in complexity among two legs indicates severe gait asymmetry. Furthermore, the centroid is drifting over gait cycle indicates that subjects had different gait patterns. This technique can provide visual display and discrete value of gait symmetry and gait variability throughout the gait cycle. Other studies related to this method can found in [115,116].

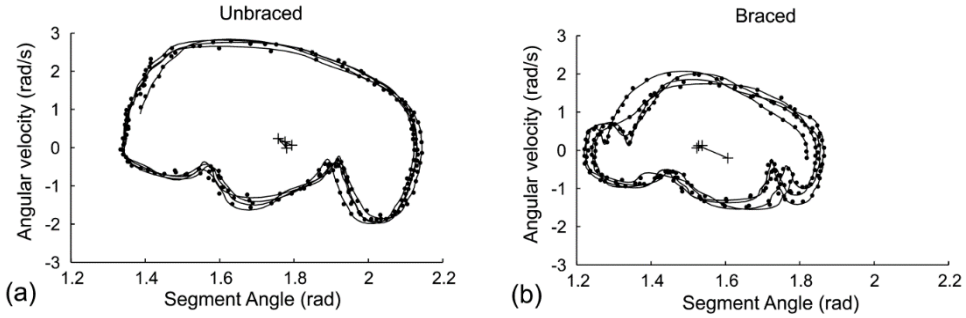

Fig 2.2. Example of result from Phase portrait (a). Unbraced knee joint trajectory (b). Braced knee joint trajectory[114]**.**

In 2003, Manal and Stanhope *et al* [117] revealed the deviation of the gait pattern relative to normative data by colour coding the magnitude and direction of the deviations. The main advantage of this technique is that the time history of several variables can be displayed simultaneously. The deviation of patient data from normative data from healthy human, *d*, at interval *i* is given in

$$d_i = \frac{x_i - Xn_i}{S.D.} \tag{2.3}$$

where *x* is the patients data, *Xn* is the normal value from healthy subject and *S.D.* is standard deviation at *Xn*. Colour codes red and blue indicate negative and positive respectively which is assigned to every value of *d* at point *i* and *d* will be categorised to 4 sub-ranges (i.e., $-3 \leq d < -1$; $-1 \leq d < 0$; $0 < d \leq 1$; $1 < d \leq 3$). This deviation *d* will further process in $f_d' = 3d^2$ which will be substitute in Eq (2.4) and (2.5)

$$C = 85f_d' \quad \{-1 \leq d \leq +1\} \tag{2.4}$$

$$C = 305.7 - 17.596f_d' + 0.2324f_d'^2 \quad \{d < -1; d > +1\} \tag{2.5}$$

C will be converted to an integer based on Table 1 in [117] and then it can be used in Eq (2.6)

$$RGB = (R + G \times 256 + B \times 256^2) \tag{2.6}$$

Fig 2.3 shows the colour coding results of a subject with abnormal walking pattern [117]. The colour bars from top to bottom are: ankle angle, ankle moment, knee angle, knee moment, hip angle and hip moment respectively over one complete gait cycle. This technique allows users to interpret the result by inspecting the colour. Red represents severe asymmetry while green corresponds to better symmetry. This

technique also provides the temporal information. The instant where most severe asymmetry occurred could be detected. This technique was implemented in [118] where one subject with hip flexor muscle weakness was tested and the hip and knee angles were obtained along with 15 healthy subjects. It successfully depicted the joints movement deviation from normal data in a graphical way. Turner *et al* [119] applied this technique on 74 rheumatoid arthritis patients and 54 healthy human to differentiate the foot contact angle, ankle moment, ankle power, navicular height and rear foot motion from these two different populations. Another similar study was conducted by Turner [120].

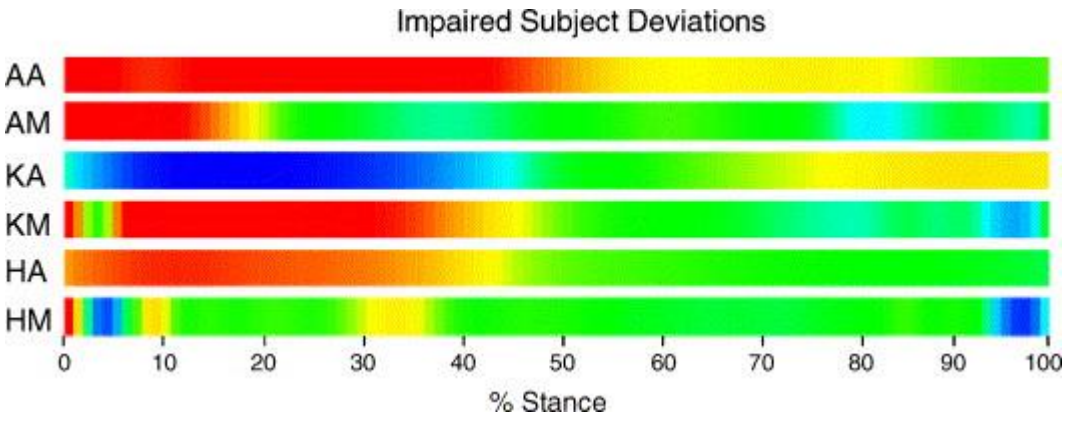

Fig 2.3. Example of Colour Coding Results. The first letter of the two character corresponds to ankle (A), knee (k) and hip (h) joint, and second letter represents A (angle) and M (Moment) [117]**.**

Crenshaw and Richards *et al* [121] proposed a new method to analyse the symmetry and normalcy of gait patterns. There are four measurements proposed: trend symmetry/normalcy, phase shift, range amplitude ratio and range offset. Trend symmetry is measured by utilising eigenvectors. The mean from both right and left legs is calculated and then subtracted by each data point from right and left leg as shown in Eq (2.7)

$$\begin{Bmatrix} X_{Ti} \\ Y_{Ti} \end{Bmatrix} = \begin{Bmatrix} X_i \\ Y_i \end{Bmatrix} - \begin{Bmatrix} X_m \\ Y_m \end{Bmatrix} \tag{2.7}$$

X_i and Y_i are the data point from right and left leg respectively from one data point, X_m and Y_m are the mean value of one gait waveform and X_{Ti} and Y_{Ti} are the translated elements for right and left leg respectively. This translated data points are then form

a matrix *M* where each pair of points is a row, and *M* is multiplied by its transpose M^TM to form a square matrix *S* to extract eigenvector from matrix *S.* This eigenvector is used in the process of rotating each row of *M* between eigenvector and X-axis (θ) in Eq (2.8)

$$\begin{Bmatrix} X_{Ri} \\ Y_{Ri} \end{Bmatrix} = \begin{bmatrix} cos\theta & sin\theta \\ -sin\theta & cos\theta \end{bmatrix} \begin{Bmatrix} X_{Ti} \\ Y_{Ti} \end{Bmatrix} \tag{2.8}$$

where X_{Ri} and Y_{Ri} are the rotated point from right and left leg respectively and θ is the angle formed between eigenvector and the *X*-axis. Variance of the points is then calculated along *X* and *Y*-axes and the trend symmetry value is the ratio of this variability in percentage where 0% indicates perfect symmetry. Meanwhile the second measurement phase shift can be examined by the phase relationship between waveforms. For example, one waveform is phase-shifted 1% increments where sample 1 becomes sample 2, the last sample becomes sample 1, etc and trend symmetry is recalculated for each shift. The purpose of phase shift is to determine the smallest value needed to correct the phase to obtain symmetry. This value can be used as an indicator of symmetry. There are two additional measurements, range offset and range amplitude ratio. The definition of range offset is the measure subtracting average right leg waveform from average left leg waveform. Range amplitude ratio is the ratio of range of motion of left leg to range of motion of right leg. This method was utilised in [122] where the application of trend symmetry, range offset, range amplitude and phase differences were used to compare the treadmill training and overground training for healthy human. The trend symmetry of each hip, knee and ankle moment force between involved and uninvolved limbs for 13 lateral ankle sprain patients and 19 healthy subjects were calculated [123]. This trend symmetry approach is further used in [124] to compare the gait symmetry of active transfemoral amputees while using passive mechanical knee joint or microprocessor controlled knee joint. The concept of phase shift between left and right leg were implemented in [125] to reduce the root mean square difference.

Region of deviation is a relatively new approach to determine the gait asymmetry and it was introduced in year 2007 by Shorter [101]. Region of deviation contains of two derivations; the first is referred as Symmetry region of deviation (SROD) which is a measurement of the bilateral joint asymmetry and the second is called Individual region of deviation (IROD) which is to determine the deviation of individual joint angle for a given limb.

$$SROD(t) = \begin{cases} \langle \Delta\theta_j^i \rangle - \left(\langle \Delta\theta_j^{Norm} \rangle + \langle SD_j^{Norm} \rangle \right), \langle \Delta\theta_j^i \rangle > SNorm^+ \\ \langle \Delta\theta_j^i \rangle - \left(\langle \Delta\theta_j^{Norm} \rangle - \langle SD_j^{Norm} \rangle \right), \langle \Delta\theta_j^i \rangle < SNorm^- \\ 0, SNorm^- \leq \langle \Delta\theta_j^i \rangle \leq SNorm^+ \end{cases} \quad (2.9)$$

Eq (2.9) presents the formula to calculate *SROD* where $\Delta\theta^i_j$ is the difference between left and right leg, $\Delta\theta^i_j = \Delta\theta^i_{j,Affected} - \Delta\theta^i_{j,Unaffected}$; $\Delta\theta_j^{Norm}$ and SD_j^{Norm} are the average and standard deviation of healthy person; $SNorm^+ = \Delta\theta_j^{Norm} + SD_j^{Norm}$ and $SNorm^- = \Delta\theta_j^{Norm} - SD_j^{Norm}$; indices *i* stands for affected or unaffected leg, *j* stands for the joint measurement.

$$IROD(t) = \begin{cases} \langle \theta_j^i \rangle - \left(\langle \theta_j^{Norm} \rangle + \langle SD_j^{Norm} \rangle \right), \langle \theta_j^i \rangle > INorm^+ \\ \langle \theta_j^i \rangle - \left(\langle \theta_j^{Norm} \rangle - \langle SD_j^{Norm} \rangle \right), \langle \theta_j^i \rangle < INorm^- \\ 0, INorm^- \leq \langle \theta_j^i \rangle \leq INorm^+ \end{cases} \quad (2.10)$$

Similarly, *IROD* is computed by Eq (2.10). θ^i_j is the joint angle of specific joint; θ_j^{Norm} and SD_j^{Norm} are the average and standard deviation of healthy person; $INorm^+ = \theta_j^{Norm} + SD_j^{Norm}$ and $INorm^- = \theta_j^{Norm} - SD_j^{Norm}$; indices *i* represents affected and unaffected leg and *j* represents particular joint from right or left leg. **Fig 2.4** represents the result of one subject walking with knee braced [101]. **Fig 2.4** (a) is SROD of hip and **Fig 2.4** (b) is the IROD of hip. Both graphs have four lines; the standard deviation of unbraced/healthy group, the average value of unbraced/healthy group, the standard deviation of unbraced/healthy group and the knee brace subject value from top to bottom. SROD showed the joint deviation from both leg and IROD showed the difference of single joint from normal healthy joint. This technique allows interpreter to distinguish the magnitude and timing of asymmetry by analysing the shaded area. Relevant clinical finding implementing this technique can be found in [126] where the deviation in the shape of mean

vertical position of the centre of mass of the total system COM_{TSYS} on healthy 17 healthy subjects was determined by region of deviation.

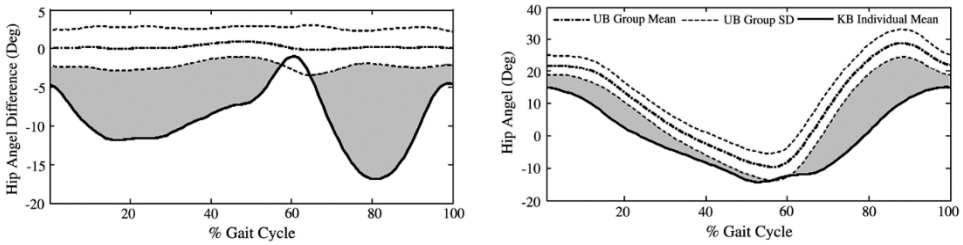

(a) (b)

Fig 2.4. **Example of Region of deviation of hip joint for one individual during knee braced condition, (a) SROD, (b) IROD** [101]**.**

2.5 Stroke

According to American Heart Association (AHA) 2011 report [127], there were 795,000 people suffered from new or recurrent stroke. World Health Organization (WHO) [128] stated that there were around 1,073,569 patients died from cerebrovascular disease in south east asia regions in year 2004. In Malaysia, nearly 40,000 patients suffered from such disease every year according to NASAM [1]. Stroke is a type of cerebrovascular accident which caused by focal injury to the central nervous system (CNS) that causes cerebral infarction [129]. AHA [130] classified stroke based on the causes of the accident:

1. Ischemic stroke - The most common type of stroke caused by focal cerebral, spinal or retinal infaction.
2. Hemorrhage - Two types of hemorrhage, one is caused by intracerebral hemorrhage and the other is caused by subarachnoid hemorrhage. The first hemorrhage is a signs of neurological dysfunction attributed to focal collection of blood within the brain, the second hemorrhage is caused by bleeding into the subarachnoid space which is not caused by trauma.
3. Transient ischemic attact (TIA) - It is also known as mini stroke caused by focal brain, spinal cord or retinal ischemia without acute infaction.

Stroke can causes weakness, or paresis on different part of the body. Extreme cases of paresis can leads to plegia, which refers to complete paralysis. Generally there are four type of weakness observed among stroke; mono (one limb affected), hemi (one side of the body affected), para (both lower limbs affected) and quadri (all limbs and torso affected) [129]. The most common observed condition is hemiparesis, which means one side of the body is paralysed.

2.5.1 Gait impairments in individuals post-stroke

Stroke patients often show several sensorimotor deficits such as poor coordination, abnormal posture and hemiplegia which leads to mobility problems and restrictions in their activities of daily living (ADLs). Early rehabilitation is crucial once patients are diagnosed with stroke as studies have shown that stroke patients could recover their limited walking ability [2,49]. The gait characterisation of stroke is therefore an important role to set appropriate rehabilitation goal.

Chen *et al* [131] reported that stroke patients had inadequate propulsion of the leg during pre-swing, increased swing time and reduced knee flexion at the toe-off and mid-swing in the paratic limb. These phenomenons will lead to slow speed, poor coordination and gait asymmetry [63,132,133] among stroke. Mulroy *et al* [27] classified 52 individuals of stroke into four groups based on their speed. This study concluded that ankle dorsiflexion was inadequate in slowest group, lowest peak thigh extension in terminal stance in second slowest group and least knee and hip hyperextension in fastest group. Lamontagne *et al* [134] reported that maximum plantarflexor moment during stance phase and maximum dorsiflexion during swing phase on paretic sides were lower.

Pizzi *et al* [135] recruited 56 stroke patients and compared their spatial-temporal parameters with 10 healthy subjects. These 56 patients were tested with shoes and without shoes. The results before rehabilitation training showed that these 56 subjects had slower gait velocity, lesser cadence, shorter stride length, longer gait cycle time, longer stance time and swing time on both paretic and non-paretic legs,

longer double support time and greater gait asymmetry than healthy subjects. This result is supported by [136,137].

2.5.2 Recovery after gait rehabilitation in individuals post-stroke

For the past few decades, the most common clinical practices used by the therapist in gait rehabilitation involve treadmill training [2],[31], strength training [138,139], functional electrical stimulation (FES) [140,141], partial and/or full body weight support [2] and electromyography (EMG) biofeedback [49], [142]. Since restoration of gait symmetry is always assumed to be one of the features of gait re-education in stroke patients [143], we are going to study the effect of each rehabilitation methods on stroke patients by using gait asymmetry indices as the indicators.

Several studies showed treadmill training (TM) has significant effect in improving gait symmetry compared to overground training (OG). In Love *et al* study [41], gait asymmetry was determined by the difference between the paretic and non-paretic leg. Temporal parameters such as stance time, single limb support time, and stance/swing ratio of treadmill training showed better gait symmetry than overground training. This result is supported by Khanna *et al* [42] who used Robinson symmetry index to compute the stance symmetry in TM and OG trainings. The results showed subjects who participated in OG had more severe gait asymmetry and subjects who participated in TM were able to walk in a more symmetry manner.

Chen *et al* [43] tested the effect of increasing body weight support (BWS) on six stroke patients. These six stroke patients had improved the swing time symmetry. Similar result was shown in Hesse *et al* study [144].

Robotic assisted devices such as Lokomat is a popular rehabilitation method because physiotherapists can pre-program a normal walking pattern into the device. Westlake and Pattens compared the effect of manual assisted body weight support treadmill training to Lokomat treadmill training [20]. In this study, eight stroke patients were trained by using Lokomat while another eight stroke patients were

allocated to manual-assisted body weight support treadmill training. Absolute step length ratios (SLR_{abs}) of both groups before and after training were collected. Lokomat group exhibited an obvious improvement in SLR_{abs} compared to other group. Geroin *et al* [145] found that the temporal symmetry ratio improved significantly in group of 10 stroke patients who participated in robot assisted training.

Incorporating acoustic pacing during treadmill training has been shown to enhance gait symmetry [146]. During acoustic pacing, the patients need to synchronise the left and right steps to the tones played to the left and right ears respectively. In Roerdink *et al* study [146], the acoustic pacing was found to improve symmetry index of step length and step time in 10 stroke patients. Thaut *et al* [147] also demonstrated that rhythmic auditory stimulation led to a significant enhancement in swing time symmetry ratio compared to the neurodevelopmental therapy. In summary, these findings suggested that gait symmetry could be re-established by providing rhythmic cues.

Muscle strengthening training is a specific physical intervention to regain lower limb functionality. Unilateral step training (UST) is specific training on the paretic lower limb of hemiparesis patient. In Kahn *et al* study [148], the effect of UST on 10 stroke patients was evaluated. In a two-week duration, the step length asymmetry decreased significantly for both normal and fast walking speed. On the other hand, 15 stroke patients practiced trunk exercises and significant improvement of temporal gait symmetry was observed [149].

Pohl *et al* [150] suggested ankle foot orthosis reduced the postural sway and increased the weight-bearing on the paretic leg during stance time. Experiments on 28 stroke patients were conducted. Results showed that subjects with AFO had a better gait symmetry in term of stance duration and deceleration horizontal ground force. This study was supported by Esquenazi *et al* [151].

Meanwhile Swigchen *et al* [152] had tested the effect of FES on a 60 years old stroke patient to compare with the effect of AFO and without FES and AFO. The

results suggested that FES had a superior effect in improving swing time symmetry over AFO and without FES and AFO. Kim *et al* [153] triggered FES on tibialis anterior (TA) and gluteus medius (GM) during swing time to improve the swing/stance ratio symmetry ratio.

Other interventions showed improvement on gait symmetry compared to conventional rehabilitation. For instance, force platform biofeedback [154] illustrated a better gait symmetry than conventional training. Besides that, aerobic cycle ergometry training also presented a significant improvement in gait symmetry during normal speed walking than conventional training. Walking backward training was utilised by Yang *et al* [155] and experimental group who received this additional training had better improvement in gait symmetry than conventional training.

Previous section discussed about the improvement of gait after rehabilitation. However, there are studies reported conflicting results by showing no beneficial effects in rehabilitation treatments. Silver *et al* [156] studied five stroke patients who practiced treadmill training for three months. The gait symmetry ratio changed insignificantly before and after training. Brouwer *et al* [22] computed the gait symmetry by subtracting data from paretic leg and non-paretic leg. This study demonstrated that there was no difference in gait symmetry between overground training and treadmill training. These findings were consistent with other studies where treadmill training showed no or insignificant improvement in gait symmetry [143,157,158].

Furthermore, Stock and Mock [159] investigated the effect of intensive exercise on weight bearing on paretic leg in 12 stroke patients. The patients practiced 6 hours daily intensive exercise for 2 weeks. The spatial-temporal gait symmetry showed no difference pre and post training. Similarly, Pomeroy *et al* [160] examined the effects of weight garments on balance and gait performance of stroke patients. Inconsistency of changes in symmetry index of step length, single support time,

double support time and support base width can be observed before and after the training.

Cyclic training is performed using a cycle-ergometers to improve the muscle power of the lower limbs by altering the torque. In Ferrante *et al* study [161], 153 chronic stroke patients were chosen to perform gait pattern categorisation and three subjects were selected to represent each cluster at baseline. They were asked to complete cyclic training and subject 1 and 3 showed no improvement in gait symmetry before and after this training. Effect of aerobic training on gait symmetry was examined in 13 stroke patients [162]. This study reported that the swing time symmetry showed no significant improvement after training. Meanwhile training gait under a multi-tasking condition is hypothesised to facilitate development of automaticity in walking. Yang [163] tested this hypothesis among 15 community ambulators post-stroke, 15 limited community ambulators post-stroke and 15 age-matched healthy subjects. However, the dual-task gait training led not significant differences in step length and single limb support symmetry indices.

A summary of these studies is tabulated in **Table 2.3**. As discussed earlier, there were contradicting results across studies even with the similar type of intervention (e.g. treadmill training). These findings can possibly be explained by few reasons. First, the inherent variability in stroke gait may play an important role. Different stroke patients exhibit different gait patterns even with the similar diagnoses or severity. For example, some stroke patients present with a longer paretic step length and others have a longer non-paretic step lengths [34,164–166]. Step length is dependent on the plantar flexion propulsion momentum of the ipsilateral leg and the weight bearing capability of contralateral leg. The contralateral leg needs to support body weight (single support) while the ipsilateral leg swings forwards. The ipsilateral plantar flexor needs to generate sufficient propulsion force to move the body forward. Thus, when the affected leg cannot support the body weight during single support time, the non-affected leg will take a shorter step to avoid falls. The patients will present with a relatively longer paretic step length. On the other hand, when the affected leg is weak and cannot generate sufficient propulsion force at the

ankle, the paretic leg will show a shorter step length compared to the non-paretic leg.

Second, the improvement in symmetry may reflect either a true recovery of the affected limb or simply indicates increased dependency on the non-paretic limb [167]. For instance, improvement in stance time symmetry ratio can be the result from an increased stance time of the paretic leg (true recovery) or a decreases stance time of the non-paretic leg (compensation). Therefore, the selection of the computational formula is critical. However, there was a huge variation in the selection of the computational formulas across studies. Further, the inconsistency in the selection of the input parameter for the formula may also contribute to the conflicting results. Some gait parameters might be less sensitive to detect the improvement. For instance, stance time contributes to large percentage during a full gait cycle, the relatively small difference between stance time of paretic and non-paretic leg for stroke patients will cause low sensitivity [31,121,168]. For example, **Fig 2.5** shows a comparison between overground training and treadmill training where the experimental data were extracted from Brouwer *et al* study [22]. **Fig 2.5** (a) is the comparison of two trainings by analysing the stance time and swing time from both non-paretic and paretic leg whereas **Fig 2.5** (b) shows the comparison of both trainings in term of symmetry ratio of stance and swing time. The stance time from both paretic and non-paretic lower limbs had clear difference in both overground and treadmill training where treadmill training possessed shorter stance time. However, this difference cannot be observed from stance asymmetry. This shows that symmetry ratio is very insensitive to detect changes.

Lastly, gait is a very complex movement that involves many variables to achieve a symmetrical rhythmic pattern. Using single parameter to quantify gait symmetry might oversimplify the complexity of gait. Univariate gait symmetry computation may lead to losing other meaningful information on other gait events. For example, gait symmetry could be resulted from the deviations occurred during both stance and swing phases. When using only stance time to measure gait asymmetry one may overlook the important information of the swing phase.

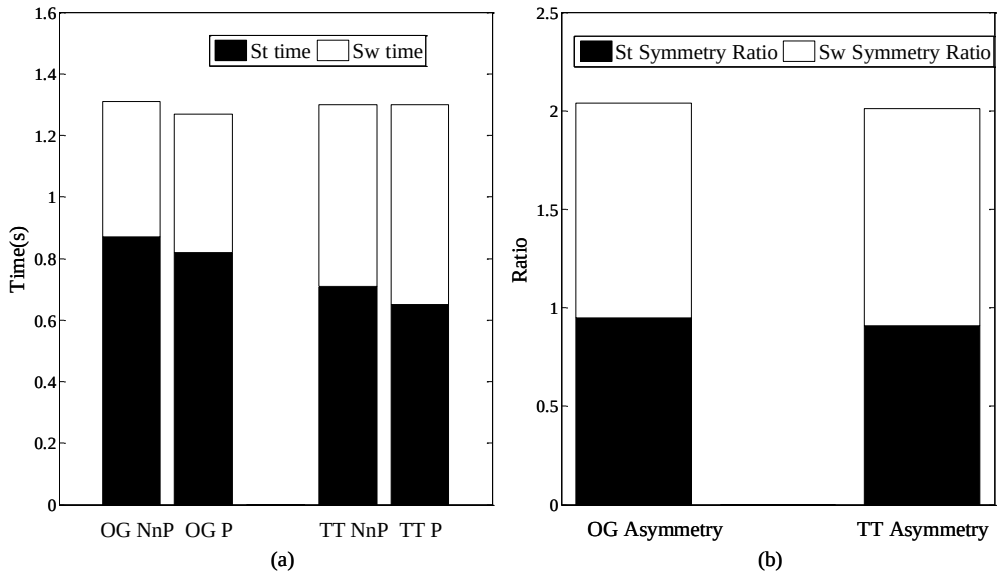

Fig 2.5. Comparison of overground training and treadmill training. (a) Bottom bars are stance (ST) time, top bars are swing (SW) time, (b) bottom bars are stance symmetry, and top bars are swing symmetry. OG=overground, TT=treadmill training, NnP=non-paretic leg, P=paretic leg [22]**.**

Table 2.3. Summary of Previous Studies.

Aurthor	Intervention	Subjects	Inclusive and Exclusive Criteria	Parameters	Result after intervention
[1]**Love *et al* [41]**	Treadmill and overground.	12 males and 6 females stroke patient (11 with left hemiparesis, 7 with right hemiparesis).	**Exclusive criteria:** Unstable angina pectoris, peripheral arterial occlusive disease, dementia, severe aphasia defined as the inability to follow two-step commands, and chronic pain or orthopaedic conditions that might change gait pattern.	Symmetry ratio of stance (SI_{stance_time}), single limb support ($SI_{single\_limb\_support}$), stance/swing ratio ($SI_{stance/swing}$).	Treadmill training - SI_{stance_time}=7.27 $SI_{single\_limb\_support}$=7.25 $SI_{stance/swing}$=0.82 Overground walking-, SI_{stance_time}=14.38 $SI_{single\_limb\_support}$=14.54 $SI_{stance/swing}$=1.76
[1]**Khana *et al* [42]**	Treadmill and overground.	4 males and 6 females chronic stage stroke patient.	**Inclusive criteria:** At least 6 months post stroke with residual hemiparetic gait, able to walk on treadmill, mini mental state exam score>23, able to follow two step commands. **Exclusive criteria:** Unstable angina, congestive heart failure within 3 months, major orthopaedic or chronic pain, poorly controlled hypertension, recent hospitalization for severe disease, severe ankle injure history, severe receptive aphasia.	Symmetry index of stance phase (SI_{stance}).	Treadmill training – SI_{stance}=9.8±9.3% Overground walking – SI_{stance}=22.1±10.7%
[1]**Chen *et al* [43]**	BWS	6 individuals with a single cerebrovascular accident	**Inclusive criteria** A single stroke at least 6 months prior study, able to walk independently overground with use of AFO or assistive device	Symmetry index of swing time.	BWS=20%- SI_{swing}≈30% BWS=50%- SI_{swing}≈20%

			and able to advance the paretic limb independently while walking on treadmill		
[1]**Thaut *et al* [147]**	RAS and NDT.	41 males and 37 females stroke patients	**Inclusive criteria** Stage 4 or early stage 4 on Brunnstrom hemiplegia recovery scale	Symmetry ratio of swing time (SI_{swing}).	RAS – Baseline SI_{swing}=0.42 Post-test SI_{swing}=0.58 NDT- Baseline SI_{swing}=0.40 Post-test SI_{swing}=0.46
[1]**Yavuzer *et al* [154]**	Balance training and conventional training.	25 men, 16 women stroke patients.	**Inclusive criteria:** First time unilateral stroke, ability to understand instructions, able to stand and walk with or without assistance, no medical contraindication to walking. **Exclusive criteria:** History of any other neurological pathology, impaired vision or conscious levels, musculoskeletal conditions.	Symmetry ratio of step length and single support time.	Balance training- Baseline SI_{step_length}=0.64 Baseline $SI_{single\_support\_time}$=0.28 Post-treatment SI_{step_length}=0.44 Post-treatment $SI_{single\_support\_time}$=0.24 Conventional training Baseline SI_{step_length}=0.08 Baseline $SI_{single\_support\_time}$=0.11 Post-treatment SI_{step_length}=0.30 Post-treatment $SI_{single\_support\_time}$=0.14
[1]**Yang *et al* [155]**	Backward walking training and conventional training.	25 stroke patients.	**Inclusive criteria** First cerebrovascular accident, unilateral motor, Brunnstrom motor recovert stage at 3 or 4, ability to walk 11m with or without a walking aid, stable medical condition, ability to understand instructions. **Exclusive criteria**	Symmetry index of single limb support ($SI_{single\_limb\_support}$).	Backward walking training- Baseline $SI_{single\_limb\_support}$=-59.06% Post-test $SI_{single\_limb\_support}$=-14.99% Conventional training- Baseline $SI_{single\_limb\_support}$=-37.84% Post-test $SI_{single\_limb\_support}$=-32.55%

			Have comorbidity or disability other than stroke, uncontrolled health condition, orthopaedic and other gait influencing diseases.		
[1]**Kahn *et al* [148]**	Unilateral Step Training.	18 stroke patients.	**Inclusive criteria** At least 6 months stroke, walk without assistance at speed of less than 1.0m/s, permitted to use assistive device, unimpaired step length at least 20% less than impaired limb during overground walking. **Exclusive criteria** Presence of severe lower-extremity contractures or orthopedic injuries, uncontrolled hypertension, cardiac arrhythmias, uncontrolled diabetes, bilateral, brain-stem or cerebellar stroke, significant cognitive impairment.	Symmetry ratio of step length (SLA).	Baseline SLA≈45% Post-test SLA≈35%
[1]**Pohl *et al* [150]**	With and without AFO.	28 hemiparesis patients.	**Inclusive criteria** Hemiparesis due to traumatic brain injury or stroke, used AFO for less than 1 week, able to stand for 20s without assistant, able to walk 15 m both with and without walking aids. **Exclusive criteria** Obvious ankle contracture, MAS> 2, possess different neurological symtoms.	Symmetry ratio of force (SI_{ground_force}) and stance duration ($SI_{stance\_duration}$).	With AFO- $SI_{stance\_duration}$=2.0 SI_{ground_force}=1.6 Without AFO- $SI_{stance\_duration}$=3.3 SI_{ground_force}=1.9

[1]**Westlake *et al* [20]**	Lokomat and treadmill training.	16 chronic hemiparetic stroke.	**Inclusive criteria** At least 6 months post stroke resulting from a single cortical or subcortical stroke. **Exclusive criteria** Unstable cardiovascular, orthopaedic, neurological conditions, uncontrolled diabetes, significant cognitive impairments.	Symmetry ratio of step length (SLR_{abs}).	Lokomat training- Baseline SLR_{abs}=0.53 Post-test SLR_{abs}=0.37 Treadmill training- Baseline SLR_{abs}=0.39 Post-test SLR_{abs}=0.34
[1]**Bayat *et al* [169]**	Treadmill training and overground training.	10 hemiparesis stroke patients.	**Inclusive criteria** At least 2 weeks post stroke and not longer than 18 weeks, cut off gait speed between 0.15m/s and 1.30m/s, TUG score greather than 20c. **Exclusive criteria** Unstable heart disease, ankle instability, orthopaedic or rheumatologic conditions, severe cognitive deficits, other cerebrovascular accident.	Symmetry ratio of stride length (SLR).	Treadmill training- SLR=0.89 Overground training- SLR=1.0
[2]**Brouwer *et al* [22]**	Treadmill training and overground training.	6 males and 4 females stroke patients.	**Inclusive criteria** Able to walk independently on level surface without aids	Symmetry ratio of stance time (SI_{stance}) and swing time (SI_{swing}).	Treadmill training- SI_{stance}=3.9 SI_{swing}=-3.9 Overground training- SI_{stance}=3.0 SI_{swing}=-3.0
[2]**Fuscaldi *et al* [162]**	Aerobic training.	13 stroke patients.	**Inclusive criteria** At least 9 months post stroke, independently ambulatory with or	Symmetry ratio of swing phase (SI_{swing}).	Aerobic training- Baseline SI_{swing}=1.18 Post-training SI_{swing}=1.20

			without assistive devices for 15 minutes.		
[2]**Pomeroy *et al* [160]**	Weight garments training.	24 stroke patients.	**Inclusive criteria** At least 6 months post stroke, not participating in other physical rehabilitation, able to walk 10 m with or without walking aid, no aphasia, no visual unilateral neglect, able to don and doff garments themselves, no other neurological disorder.	Symmetry index of step length (SI_{step_length}), single support time ($SI_{single\_support\_time}$) and double support time ($SI_{double\_support\_time}$) .	Weight garments training- Baseline SI_{step_length}=-15.03% Baseline $SI_{single\_support\_time}$=-16.88% Baseline $SI_{double\_support\_time}$=-3.98% Post-test SI_{step_length}=-14.94% Post-test $SI_{single\_support\_time}$=-17.78% Post-test $SI_{double\_support\_time}$=-2.59%

[1] indicates improvement after intervention; [2] indicates insignificant or no improvement after intervention; CMSA= Chedoke Mcmaster Stroke Assessment; RAS= Rhythmic Auditory Stimulation; NDT= Neurodevelopmental therapy; AFO= Ankle Foot Orthosis; MAS= Modified Ashworth Scale

2.5.3 Gait prediction model after stroke

In Kollen *et al* [45] paper, the Functional Ambulation Categories (FAC) of stroke patients were predicted using multivariate multilevel regression model. The inputs of this regression model were Fugl-Meyer leg score, motricity index leg score, letter cancellation task, Fugl-Meyer balance and timed balanced test. The regression model showed that time balanced test change scores were the most important factor in predicting improvement of FAC, followed by Fugl-Meyer leg change score and reduction in letter cancellation task omissions and motricity index leg score.

Goodwin and Sunderland [170] applied a logarithmic function to produce recovery curves. In this paper, the dependent variables were speed and range of wrist extension. They concluded that this logarithmic function was a good fit to the patients with no additional physiotherapy, indicating fast early recovery then gradually slowed. Meanwhile patients with additional intervention caused a further acceleration in recovery and did not fit well in this logarithmic function.

Ingrid *et al* [47] developed a prognostic model to predict the mobility outcome one year post-stroke. Univariate and multivariate linear regression models were performed. The independent variables were stroke characteristics, functional status, urinary incontinence, sitting balance, motor and cognitive function. Mobility was measure using the Rivermead Mobility Index.

Meanwhile Masiero *et al* [48] performed a multivariate analysis to predict Functional Ambulation Classification score. The predictive variables were Functional Independence Measure and its motor component, the upper and lower Motricity Index, and the Trunk Control Test. The results showed that age of stroke patients and level of motor and functional impairment measured at baseline were significant variables to predict the Functional Ambulation Classification outcome.

Tilling *et al* [46] used multilevel models to predict the functional recovery, Barthel Index. The independent variables were urinary incontinence, sex, prestrike disability, dysarthria, age, dysphasia and limb deficit. This model was able to predict both recovery and death after stroke accurately.

In Hsieh *et al* [44] report, a multivariable stepwise linear regression analysis was adapted to predict the activities of daily living functions. The result showed that Postural Assessment Scale for Stroke Patients score, age, Fugl-Meyer motor test score and Barthel Index score were the strongest predictors

Most of the recovery models described in this section relied heavily on prediction of clinical assessment scores. To our knowledge, there are only limited models that used kinematics and kinesiology parameters derived from motion sensor and sEMG sensor as the predicted variables. Therefore, it is worth investigating the feasibility of these parameters as the predicted outcomes.

2.6 Electromyography (EMG)

2.6.1 Definition of EMG

The pioneer of EMG is known to be Galvani who published 'De Viribus Electricitatis in Motu Musculari Commentarius' during 1792 stated that electricity could initiate muscle contraction [171]. Later in 1894, Dubois-Reymond discovered that during voluntary muscle contraction, it was possible to record electrical activity. Marey had successful to record this activity and introduced the term 'electromyography' [172].

The muscle contributes to generate EMG signal is the skeletal muscle which is attached to the skeleton and facilities movement and position of the body [37]. The contraction of this skeleton muscle is controlled by electrical impulse, which is known as action potentials. They propagate between the central and peripheral nervous systems and the muscles. These action potentials are transmitted from axons of the motor neurons to muscle fibres through neuromuscular junction. The contraction of the muscle fibre can only be initiated when the neuronal action potentials reach the neuromuscular junction and fire action potentials[37]. Motor unit action potential (MUAP) is then formed from the summation of the spatial temporal of the individual muscle fibre action potential and the result EMG signal

is a compose of different MUAP near the area of recording electrode[37], [173], [174].

EMG signal can be captured by using invasive or non-invasive method. Invasive method is inserting a needle electrode through the skin directly into the muscle. The main advantage of using this method is it provides a high resolution and it only takes the signal from the desired muscle. However, this is relatively painful for the patient and therefore, non-invasive method is introduced [37]. Non-invasive method is placing the surface electrode on the skin overlying the muscle and it reflects the gross activity produced by a large number of motor units. The quality of EMG signal can be hampered by different type of noises and artefacts and the goal is to maximise the SNR to avoid the erroneous interpretation of the signal [175]. There are a number of intrinsic and extrinsic sources of noises and artefacts that can contaminate the EMG signal [175]. Electrode preparation and placement is important when recording EMG signal to ensure high quality of the signal and maximise the SNR. The location and orientation of electrode is crucial since it determines the electrical view of a muscle. De Luca *et al* [176] further explained that the electrode should not place on the tendon of the muscle, on the motor point and at outside edges of the muscle. A detail analysis of literature was presented in a project "Surface EMG for Non Invasive Assessment of Muscle", or in short "SENIAM" [177].

Different muscles contribute to different movements of joint on lower limbs. The lower limbs are connected mainly by four joints, namely hip joint, knee joint, ankle joint and intertarsal joint [178] and they are controlled by specific muscles on leg. Each joint can contribute to the respectively lower limbs movements and they are important in gait analysis. **Fig 2.6** shows the location of each muscle on leg.

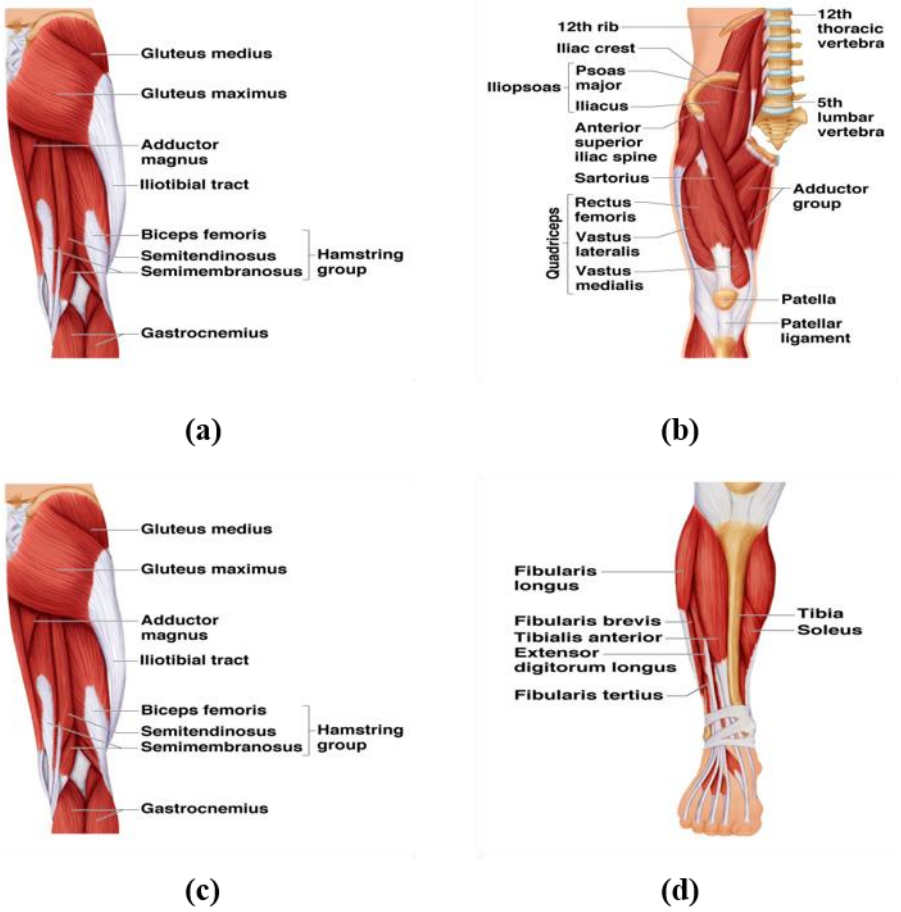

Fig 2.6. Muscle Anatomy; (a) Muscles contribute for Hip movement (back view); (b) Muscles contribute for Hip movement (front view); (c) Muscles contribute for Knee movement ; (c) Muscles contribute for Ankle movement [179]**.**

2.6.2 Processing of EMG

Raw EMG signal is meaningless without proper interpretation and extraction of valuable information. Therefore, after acquire the raw data, this EMG signal is required to perform high and low pass filter to filter the noises and artefacts. **Table 2.4** shows the recapitulate of the different noises and artefacts. A proper signal processing will be executed to suit the user application and the common procedure of signal processing includes pre-processing of the raw data, feature extraction, dimensionality reduction, pattern recognition and online and offline learning [180]. All these processes are best describe as pattern recognition as it is a process to map observed patterns to a set of categories [181]. According to Miller *et al* [180], it is important to determine the onset of the movement to extract the correct part of the

EMG signal to be analysed so that the noise and low-level EMG signals from rest position can be excluded. Staude *et al* [182] explained that there are three basic processing stages needed to perform in order to detect the onset movement and there are signal conditioning, detection unit and post processor. Feature extraction is important in signal processing as it is a way to reduce the dimensionality of a set of signal by elimination redundant features and finds a set of vector best describe the information content of the observation signal in pattern recognition [183]. In pattern recognition, this feature extraction process has the advantage of focusing on salient features that distinguish one class from another [180]. Dimensionality reduction is important to retain information that is important for class discrimination and discard that which is irrelevant [184]. There are generally two approaches to extract features from EMG signal: temporal approach and spectral approach [185], and both of these approaches are classified as non-parametric approaches. After feature extraction, classification of the EMG signal is the next step of signal processing to category this signal into the respective class.

Table 2.4. Description of Noises and Artefacts in EMG Signal.

Name	Description	Reference
Inherent noise in electronics components	All electronic equipment generates noise during detection and recording signal. This noise cannot be eliminated and can only be reduced by using modern electronics technology and appropriate circuit design. Range from 0 to few thousand Hz	[175], [176], [186]
Ambient noise	Source from electromagnetic radiation which generated by any electromagnetic device. Range approximately 50 to60Hz	[176],[186], [187]
Motion artifacts/Transducer Noise	Interface between detection surface of the electrode and skin and relative movement of the cable which is connected to the amplifier. Range from 0 to 20Hz	[37],[175], [176], [186],[187]
Inherent instability of the signal	Frequency between 0 and 20Hz are not stable because they are affected by the quasi-random nature of EMG. This noise can be treated as unwanted noise.	[176],[186]

2.6.3 EMG characteristics in individual post-stroke

It is believed that Hirschberg and Nathanson were one of the earliest to report analysis of EMG in stroke [188] back in 1952. They used sEMG on gluteus medius, adductor longus, semintendinosus, vastus lateralis, medial gastrocnemius and tibialis anterior. They concluded that EMG activation levels decreased on the paretic side of lower limbs. In Shao *et al* [188] study, four stroke patients were recruited and the sEMG of tibialis anterior, medial gastrocnemius, lateral gastrocnemius and soleus muscles were recorded. The results showed that gastrocnemii and soleus were active during initial contact and tibialis anterior had increased in amplitude during mid-stance. This is abnormal phenomenon because gastrocnemii and soleus should be silent during plantarflexors and tibialis anterior should not have high amplitude during stance phase. Mulroy *et al* [27] classified 52 individuals of stroke into four groups based on their speed. This study showed that soleus, tibialis anterior, vastus intermedius, semimembranosus and biceps femoris had greater mean EMG intensity in fastest group; the onset of soleus, vastus intermedius activity was delayed in the slowest group; and the onset of semimenbranous and biceps femoris were earlier in the fastest group.

Otter *et al* [143] recruited 14 individuals of stroke and analysed the muscle activation timing during gait. The muscles biceps femoris, rectus femoris, gastrocnemius medialis and tibialis anterior were tested. Authors observed abnormal long duration of biceps femoris and rectus femoris during single support phase and gastrocnemius medialis during double support phase. Duration of biceps femoris and rectus femoris coactivation was longer on the paretic side lower limb.

Lamontagne *et al* [134] reported low gastrocnemius medial activity led to low peak plantarflexor moment on paretic side. The reduced in this peak plantarflexor moment on non-paretic side was due to excessive coactivation between gastrocnemius medial and tibialis anterior. Buurke *et al* [189] used an objective burst detection algorithm to analyse the timing of erector spinate, gluteus maximus, gluteus medius, rectus femoris, vastus lateralis, semitendinosis, gastrocnemius and

tibialis anterior muscles. Results showed delayed in gluteus medius, gluteus maximus, vastuc lateralis and semitendinosus muscles.

2.6.4 Non-linear analysis of EMG

As mentioned earlier, many researchers treated EMG signal as a linear system. However, EMG is highly non-linear deterministic signal. Information embedded in the EMG signal are rich. Hence, many other researchers performed non-linear techniques on EMG such as fractal dimension [190], lyapunov exponent [191], recurrence plot [192] etc. Rodrick and Karwowski observed positive Lyapunov exponents existed in sEMG of the biceps muscle in some work postures. These suggested chaotic-liked behaviors [193]. Ouyang *et al* [194] revealed the characteristics of sEMG during different hand movements using recurrence plots. Besides that, fractal analysis is another common approach to identify nonlinear characteristics of sEMG signals.

Recurrence Plot (RP) has received attention due to its ability to locate hidden rhythms (the recurring patterns) and non-stationarities (drifts) of a set of experimental data. Recurrence plot was first introduced by Eckmann *et al* [192] to visualise the recurrences of dynamical system in phase space. It transforms multi-dimensional phase space trajectory into a two-dimensional map. Therefore, the inherent recurrence characteristics of the dynamical systems could be revealed and visualised in a two-dimensional plane. A comprehensive review of the theory of recurrence plot and its associated quantification methods was published by Marwan *et al* [195]. The applications of RP method are wide and the focus of this paper is on EMG analysis. In related studies, Morana *et al* [196] applied Recurrence Quantification Analysis (RQA) [197] to analyse and quantify EMG data to detect the state changes. RQA is a quantification method to measure the complexity of recurrence plots. Two common measures of RQA, namely percentage of recurrence or recurrence rate (RR) and percentage of determinism (DET) are often associated with fatigue related changes in EMG signals [198–201]. DET has been shown to be more dominant in detecting the muscle fatigue then spectral analysis [202]. This

is due to RP provides a useful framework for discerning abrupt changes or drifting in dynamics [203].

Meanwhile, fractal dimension (FD) measures self-affine and dominant complexity of a signal [204]. Detrended fluctuation analysis (DFA) [205], correlation dimension, Katz method [206], box counting method, Higuchi fractal dimension (HFD) [207] and bi-phase power spectrum [190] are common methods to estimate FD of a time series. These techniques have been widely applied to correlate the sEMG FD and its interference patterns [190,208]. Besides that, fractal analysis is also commonly applied in sEMG signal classification [209,210] In a recent study, FD of rectus femoris muscle sEMG was strongly correlated to the height of vertical jump [211]. Besides that, FD was used to estimate the contraction force from different muscles [212]. In gait analysis, Beretta-Piccoli *et al* [213] extracted FD from the quadriceps femoris muscle sEMG to scrutinise fatigue. Boccia *et al* [214] correlated the rate of change of FD from vastus lateralis and medialis muscles sEMG to fatigue contraction.

2.6.5 EMG decomposition

As mentioned earlier, EMG signal is composed of the action potentials from groups of muscle fibers organised into functional units called motor units (MUs) [215]. It is desirable to study the information contained in the timing, shapes, interpulse interval, firing rate, synchronisation characteristics and morphology of shapes of amplitudes of the discharges of individual MU [215]. This can be achieved by decomposing the EMG signal. Noted most of the EMG decomposition methods focus on decomposed needle EMG and high-density arrays EMG into MUAP. For surface EMG, it is very challenging to accurately decompose it due to its low spatial selectivity [216]. All the MUAPs from surface EMG tend to look alike and they overlap with each other. Therefore, it is very hard to extract useful information of MUAP from sEMG by using existing EMG decomposition methods.

In 1998, Huang *et al* [217] proposed a new technique for analysing non-linear and non-stationary data and the key part of the method is the Empirical Mode

Decomposition (EMD). EMD can decompose a complicated signal into finite and small number of Intrinsic Mode Functions (IMF). These IMFs yield instantaneous frequencies as functions of time. To date, applications of EMD on biomedical signal such as Electroencephalography (EEG) and EMG are mostly on filtering noises [218], treated as a source separation method when combining with independent component analysis [219] and extracting features from IMFs on surface EMG [220,221]. One of the problem arises in cases of EMD is mode mixing. Mode mixing is defined as single IMF consists of signals of widely disparate scales, or a signal of similar scare residing in different IMF components [222]. This issue can cause failure to decompose the signal accurately. To overcome this issue, Wu and Huang [222] proposed a noise-assisted EMD algorithm called Ensemble Empirical Mode Decomposition (EEMD) in 2005.

As described earlier, the study of IMFs from decomposed sEMG signal mostly on filtering and feature extraction. However, extracting features among stroke patient's gait sEMG is very limited. Therefore, it is worth applying EEMD to obtain IMFs of sEMG from stroke patients to correlate the kinesiology status to kinematic parameters.

2.7 Chapter Summary

The development of sensor system has a long history from single sensor to multiple sensors this day. Different designs of the sensor system has been observed from different researchers to suit their own studies. Computation of gait trajectory from these inertial based sensors is complicated and hard due to the low SNR of the low cost sensor. Therefore, a new inertial based integration algorithm is necessary to provide a better accuracy of the gait trajectory.

Gait rehabilitation is crucial in stroke recovery. The recovery status of stroke patients can be obtained by proper gait analysis. Conventional spatial-temporal gait parameters have been crucial in the quantification of gait analysis. However, these parameters used to assess the recovery status of stroke patient is often confusing. The result from **Fig 2.5** shows inconsistency from interpretation of different results.

This contradict outcomes is due to the different sensitivity among conventional analytical measurements. Therefore, it is necessary to develop new gait assessment quantification methods by studying patient's kinesiology and kinematic parameters.

Analysis of sEMG could be characterised by techniques involving time and frequency domain analysis. These methods reveal specific properties in the linear system context. However, sEMG signal is non-linear in nature. While there are extensive reports on sEMG non-linear analysis, its applications in patients with neurological disorders are relatively limited. This could be attributed to the requirement of analysing long time-series. Furthermore, the correlation between sEMG and clinical assessment scale such as Timed Up and Go test is not well known. Therefore, it is worth investigating the feasibility of applying non-linear analysis such as fractal analysis on sEMG to characterise their gait deficits.

Intense studies show that stroke patients with proper gait rehabilitation tends to have better gait recovery. It leads to the need of modelling a recovery prediction model. We have discussed plenty of recovery models in this chapter, and most of the time-dependent independent variables in these models relied solely on clinical assessment test such as Rivermead Mobility Index, Functional Ambulation Classification, Timed Up and Go test etc. Therefore, a new recovery model based on kinematic and kinesiology parameters is needed.

To our knowledge, there are limited studies that analysed the association of recovery of joints and recovery of muscles. Most of the researchers only focused on either one of the aspect, which may lead to overlook of some of the recovery behaviour of stroke patients. For example, most of the researchers investigated the spatial-temporal parameters as the recovery indicator without looking at the muscles conditions. Recovery in spatial-temporal parameters may be a type of compensation from other muscles. This can causes muscle injury in long term. Therefore, the characteristic of sEMG during recovery period and its association of kinematic behaviour is worth examined.

Chapter 3 Methodology

3.1 Introduction

In this chapter, the methods and procedures to conduct the experiments were described. The project started with the design of a gait sensor system. Based on the discussion in Chapter 2, there is a need to redesign a gait sensor system for this study. This is to ensure the gait sensor system is suitable and comfortable for the recruited subjects. The experiments designed for this project involved recruitment of healthy subjects and different type of stroke patients. Data processing for the sensor system was discussed. The aims of this chapter are:

1. To redesign an IMU based gait sensor system which only have minimal to none effect on participants walking style.
2. To describe the experiment designed for this research included the total number of participants and their demographic.

3.2 Hardware development

The first step in designing this gait sensor system is to select appropriate sensor and build a suitable data logger to store the data, with the goal of creating a highly instrumented system capable of sensing many parameters that characterise gait. In this project, there are few important parameters of gait needed to be extracted to describe the gait characteristics of a human, and there are temporal parameters (gait cycle time, stance time, swing time), spatial parameters (stride length and velocity), joint angle and muscle activity. These motivated us in the selection of the sensors described later in this chapter.

The sensor selected in this project was MPU 6050 (Invensense). To build a data logger, Arduino pro mini was used as the microcontroller board and a micro-SD card slot was connected to the microcontroller board. A lithium battery was used to power up the whole system. The sensor system and data logger were integrated in

a plastic casing to form one gait sensor module. There were four modules positioned on shank and ankle of lower limb of each participant. **Fig 3.1** shows a picture of the integrated IMU based gait sensor (IGS) system.

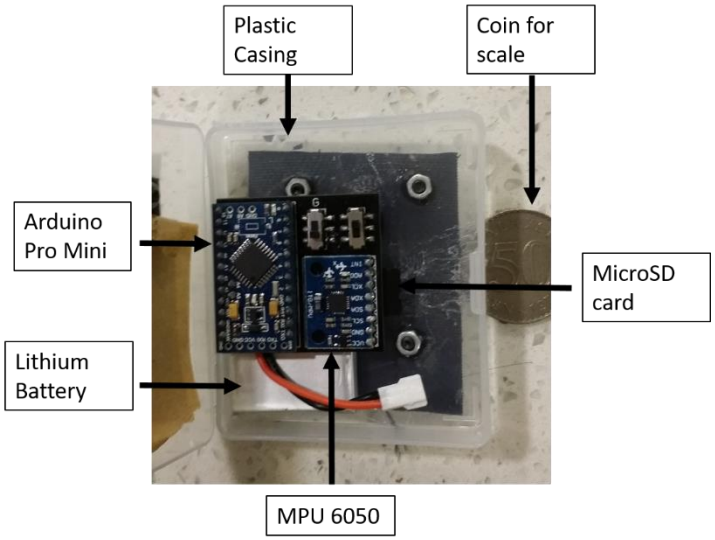

Fig 3.1. An IGS module consisting IMU, Arduino Pro mini, a microSD card slot and a lithium battery in a plastic casing. Coin for scale.

3.2.1 Inertial Measurement Unit

MPU 6050 was the selected IMU sensor. It contains a 3-axis MEMS accelerometer and a 3-axis MEMS gyroscope in a single chip as shown in **Fig 3.2**. It can capture the *x*, *y*, and *z*-axis at the same time using the 16-bits analogue to digital conversion. This sensor uses I2C-bus to communicate with the microcontroller board; in this case, it is an Arduino pro mini. There are just two wires on I2C bus called Serial Clock (SCL) and Serial Data (SDA) lines. SCL is the clock line used to synchronise all data transfers over the I2C bus. On the other hand, SDA is the data line to transfer the data from IMU to microcontroller board.

The VCC pin on this sensor is the voltage pin, which can be used to connect to either 3.3V or 5V of power supply. GND is the ground for this sensor. Meanwhile, the ADO pin is to help the sensor to select the I2C address. If it is connected to ground, the address is 0x68; meanwhile if it is connected to a voltage supply, it is 0x69.

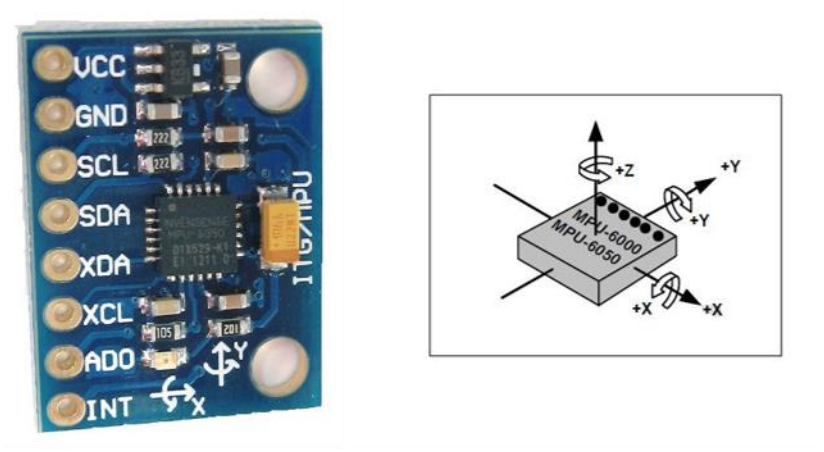

(a) (b)

Fig 3.2. (a) Sketch of MPU-6050 on a breakout board, (b) default coordinate system of MPU-6050.

3.2.2 Microcontroller board

Arduino Pro Mini was used in this project because of its small size (33.3mm x 18.0mm). It is available in both 3.3V and 5V version, and both of them are powered by ATmega328. 3.3V Arduino pro mini is selected which is running at the 8MHz bootloader. This Arduino Pro Mini does not have any USB connector on the board. Therefore, a six-pin header can be connected to an FTDI breakout board to provide USB power and communication to the board. The CP2102 USB-serial converter FTDI board is used to connect Arduino Pro Mini to computer. **Fig 3.3** presents the Arduino Pro Mini and CP2102 USB-series converter diagrams.

(a) (b)

Fig 3.3. (a) Arduino Pro Mini microcontroller board. (b) CP2102 USB-serial converter FTDI breakout board.

3.2.3 Micro SD card module

Micro SD Card slot module uses standard Serial Peripheral Interface (SPI) interface for communication. The four important pins on this SPI module are slave select (SS) pin, Master Output Slave Input (MOSI) pin, Master Input Slave Output (MISO) pin, and Serial Clock (SCK) pin. As suggested by the name, SS pin is to select the slave devices by the master (microcontroller board), MOSI pin is to receive data from slave to master, MISO is to command slave from master and SCK pin is the clock signal from the master to slave. The power supply for this board is 3.3V. The detail of each pins is described in **Fig 3.4**.

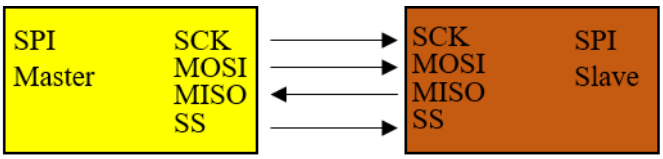

Fig 3.4. Typical SPI communication from master to slave. The arrows indicate the direction of signal flow.

3.2.4 Assembly

Fig 3.5 presents the schematic diagram of the pin connection of one IGS module. **Table 3.1** shows the pin location for both MPU6050 and Micro SD slot module. Two switches were used to control the power input to the board and data logging. The first switch was connected to RAW pin on Arduino to power up the board. The second switch as connected to D6 pin on the microcontroller board. The system will start logging data when the second switch pin was set to high. The sampling rate of this system was set to 100Hz.

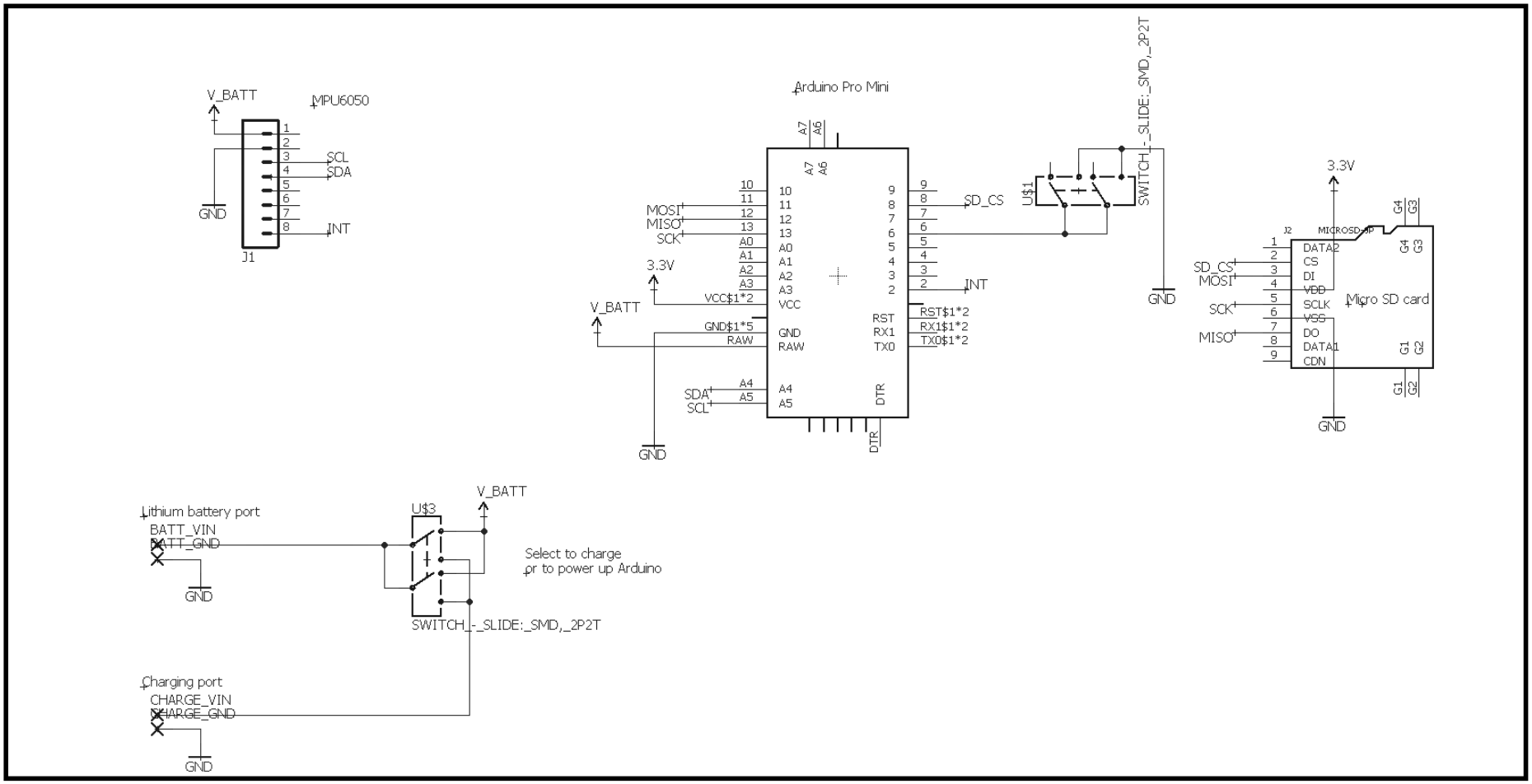

Fig 3.5. Schematic diagram of this gait sensor module.

Table 3.1. Pin connection from MPU6050 and micro SD slot to Arduino Pro Mini.

Arduino Pro Mini	MPU-6050	Micro SD Slot
A4	SDA	-
A5	SCL	-
VCC	VCC	VCC
GND	GND	GND
D2	INT	-
D8	-	SD_CS
D11	-	MOSI
D12	-	MISO
D13	-	SCK

3.2.5 Surface Electromyography (sEMG) system

A Shimmer3 EMG (ShimmerSensing) unit was used for this research. This Shimmer equipped with a MSP430 microcontroller board with two channels of EMG and a reference channel with gain amplifier of one. 24-bit ADC converts the input analogue signals to a digital representation of this signal and store in the SD card. The recommended sampling rate for this equipment is 512Hz to ensure high quality signal. A pair of self-adhesive disc shape surface electrodes (Ag/AgCL; CONTEC) were placed in a bipolar configuration with 2cm inter-electrode-distance over the muscle. **Fig 3.6** shows the diagram of Shimmer3 and the disc shape surface electrodes.

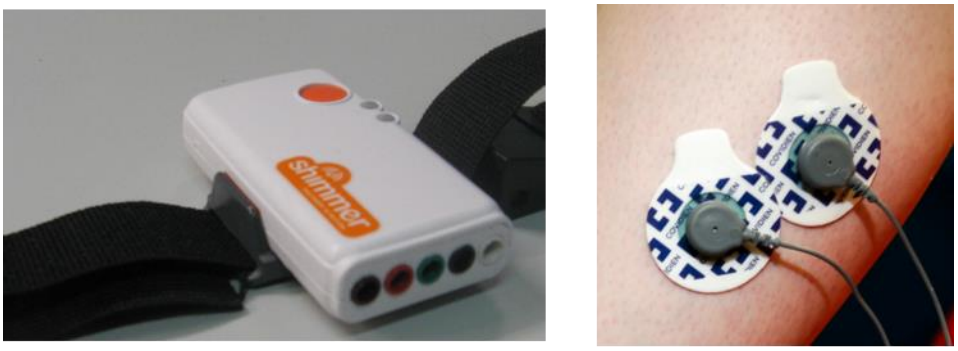

(a) **(b)**

Fig 3.6. (a) Shimmer3 sensor, the brown and red colour on the left side are channel 1 positive and negative respectively, green colour in the middle is the reference channel, black and white colour on the right side are channel 2 positive and negative respectively. (b) A pair of disc shape surface electrode with 2cm inter-electrode-distance.

3.2.6 Integration of IGS and sEMG system on human subject

There were total four embedded IGS modules and two Shimmer Sensing sEMG system located on different parts of lower limbs. **Fig 3.7** shows the exact location of each IGS and sEMG system. These systems were strapped on the participants using Velcro strap. The sEMG electrodes were located at Tibialis Anterior (TA) and Gastrocnemius Lateral (GL) muscles.

The exact location of these electrodes were recommended by SENIAM [177].

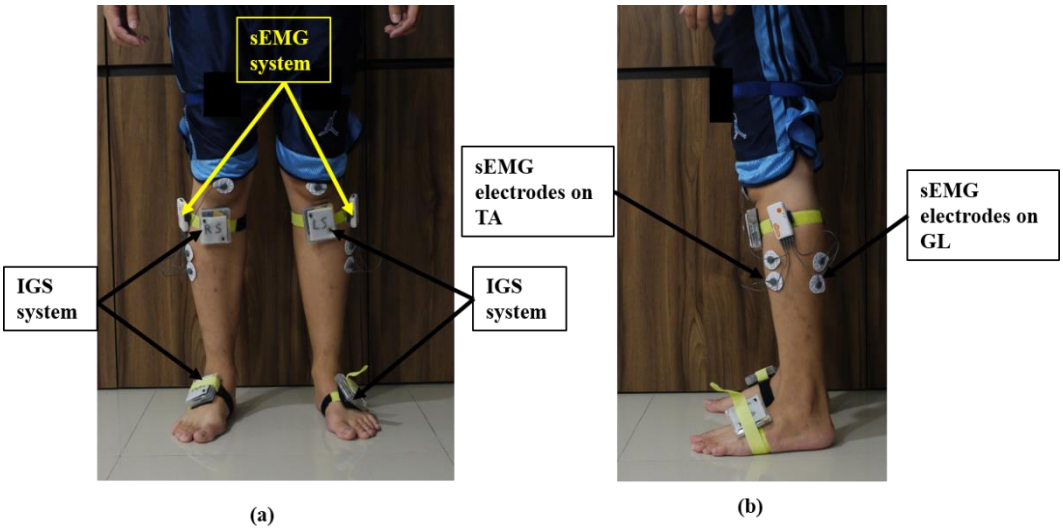

Fig 3.7. (a) Location of IGS and sEMG system on lower limbs, (b) location of sEMG electrodes on Tibialis Anterior (TA) and Gastrocnemius Lateral (GL) muscles.

3.3 Experiment Design

There were three different experiments designed in this research. In this project, the objective is not to prove superiority of the certain rehabilitation treatment, but rather to estimate and model parameters for the recovery of stroke patients [262]. Furthermore, when designing the experiments, there are no prior information upon which to base the sample size. Therefore, we followed the simplest method applied on pilot trial from Whitehead study [262] where sample size of 12 to 30 were enough this study.

The first experiment (Experiment 1) recruited 10 healthy subjects. This experiment was designed for validation purpose. It also served as a standard comparison for the stroke patients walking experiment. These healthy subjects had no history of gait illness. They were instructed to walk on 5-meter walkway with three different conditions; (i) normal walking with self-selected speed, (ii) knee-braced walking and (iii) ankle-braced walking. For validation, red colour LED were put on heel and knee indicating markers on each location. Each walking trail was video recorded by a motion camera simultaneously and the red LED represented the exact position of each lower limb segment. The video images were sampled at a frame rate of 60 frames per second. **Fig 3.8** shows subjects wearing knee and ankle braces.

The second experiment (Experiment 2) was cross-sectional study of stroke patients. 60 stroke patients in their different stages of post-stroke were recruited. This experiment was designed to study the gait characteristics of different kinds of stroke patients. The IGS module and sEMG system were positioned on patient's shank and ankle. They were instructed to walk on a 5-meter walkway. Stroke patients were more responsive to 5-meter walk test than other standard clinical assessment such as 6-meter walking test and 10 meter walking test, as the patient is less apt to fatigue. Among them, 30 stroke patients agreed to participate in TUG test. The remaining 30 stroke patients did not participate in TUG test. This was due to patient fatigue, time consuming and emotional unwilling to take part.

The third experiment (Experiment 3) was a longitudinal study on stroke patients. 15 stroke patients who just diagnosed with stroke and admitted to hospital were recruited. For this experiment, the walking results during the first month (stage 1), third month (stage 2) and sixth month (stage 3) after diagnosed with stroke were taken. This experiment is to study the recovery condition on stroke patients. These 15 stroke patients were instructed to wear IGS and sEMG system and walk on 5-meter walkway.

All participants were taking part in the respectively experiments voluntary and they were allowed to quit the experiment any time without any prior notice. They read the information sheet and signed the consent form prior to participation.

Experiment 1 was conducted in University of Nottingham Malaysia Campus (UNMC), while Experiments 2 and 3 were conducted in University Malaya Medical Center (UMMC). The research protocol and consent form were approved by both UNMC and UMMC research ethic committee. The basic demographics of the participants are shown in **Table 3.2**.

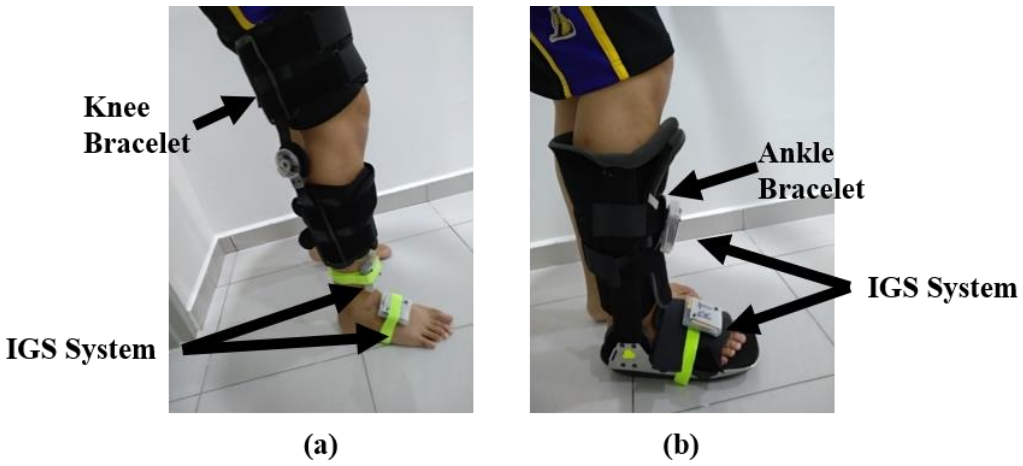

Fig 3.8. A subject wearing knee brace and ankle brace on lower limbs.

Table 3.2. Demographic of all participants from Experiment 1, 2 and 3.

Group	Total
Experiment 1	
***n*[1]**	10
Gender (male/female)	6/4
Age, years (±SD)	22.5 ± 1
Experiment 2	
***n*[2]**	60
Gender (male/female)	39/21
Age, years (±SD)	51 ± 10
Hemiplegia side (left/right)	48/12
Years between stroke onset and assessment (±SD)	5 ± 2
Type of stroke (I/H)	45/45
Experiment 3	
***n*[3]**	15
Gender (male/female)	11/4
Age, years (±SD)	55.4 ± 20.3
Hemiplegia side (left/right)	13/2
Days between stroke onset and first assessment (±SD)	8.5 ± 5.4
Type of stroke (I/H)	10/5

n^1-number of participant for Experiment 1; n^2-number of participant for Experiment 2; n^3-number of participant for Experiment 3; I- ischemic stroke; H- hemorrhagic stroke.

The data acquired from these experiments have a normal distribution by using the Chi-squared test. This test compare the data collected from the experiments to a normal distribution with the same mean and standard deviation. The *p*-value of different set of data from each experiments were found to be greater than 0.05, which indicating these data are normally distributed.

3.4Data Processing

All data from the IGS and EMG systems were processed in Matlab (MathWork) offline. According to the Nyquist sampling theorem, the sampling rate must be at least twice that of the highest intrinsic frequency. The cadence (step per sec) of human walking is around 1.5Hz. Therefore, for IGS module, it was sampled at 100Hz. A 5th order Butterworth low- pass filter with cut-off frequency of 10Hz was used. It is to remove the high frequency noise in the IGS system and retain the low frequency walking data from the participants. Eq (3.1) and (3.2) were used to convert raw accelerometer and gyroscope signal to readable data:

$$Accel_{convert} = Accel_{Raw}\left(\frac{\mathrm{g}}{Sens_{Accel}}\right) \tag{3.1}$$

$$Gyro_{convert} = \left(\frac{Gyro_{Raw}}{Sens_{Gyro}}\right) \tag{3.2}$$

where $Accel_{convert}$ and $Gyro_{convert}$ are the converted readable accelerometer and gyroscope data, $Accel_{Raw}$ and $Gyro_{Raw}$ are the raw accelerometer and gyroscope data, *g* is the gravitational force, $Sens_{Accel}$ and $Sens_{Gyro}$ are the sensitivity scale factor for accelerometer and gyroscope respectively. From the datasheet, the $Sens_{Accel}$ and $Sens_{Gyro}$ are 16384 LSB/g and 131 LSB (^{o}/s).

Meanwhile Shimmer3 EMG system was sampled at 512Hz. A 5th order Butterworth band-pass filter with lower cut-off frequency of 5Hz and a higher cut-off frequency of 250Hz was used to filter sEMG signal. In order to convert the ADC output sEMG signal to mVolts, Eq (3.3) is used:

$$sEMG_{(in\ mv)} = \left(\frac{(sEMG_{Raw} - Zero) \cdot Sens_{sEMG}}{Gain}\right) \quad (3.3)$$

where $sEMG_{(in\ mV)}$ is the sEMG signal in mVolts, $sEMG_{raw}$ is the raw ADC output sEMG signal, *Zero* is the ADC offset value of the electrodes, $Sens_{sEMG}$ is the sensitivity scale factor for sEMG and *Gain* is the gain amplifier value. From the datasheet, the $Sens_{sEMG}$ is $\frac{2420mVolts}{2^{23}-1}$, and we configured the gain amplifier value as 1. The ADC offset value, *Zero* is the mean value when the positive and negative electrodes from same channel were connected together. Since most of the stroke patients recruited in this study did not perform maximum voluntary contraction (MVC), dynamic peak normalisation was used to normalise sEMG signal.

Linear envelope of the sEMG signal can be simply achieved by full wave rectification followed by a low-pass filter. In this study, a low pass 4th order Butterworth filter with a cut-off frequency of 6 Hz was applied. The sEMG processing procedure is summarised in **Fig 3.9**. The onset of muscle activity timing was detected by using a threshold value. According to Ozgunen *et al* [264], 35% of the mean root mean square of sEMG value is the best threshold value for both GL and TA.

All IGS and sEMG system were synchronised using the Unix time available in every system. After synchronised, heel-strike and toe-off events from **Fig 4.1** were used to segment the signals into different gait cycles.

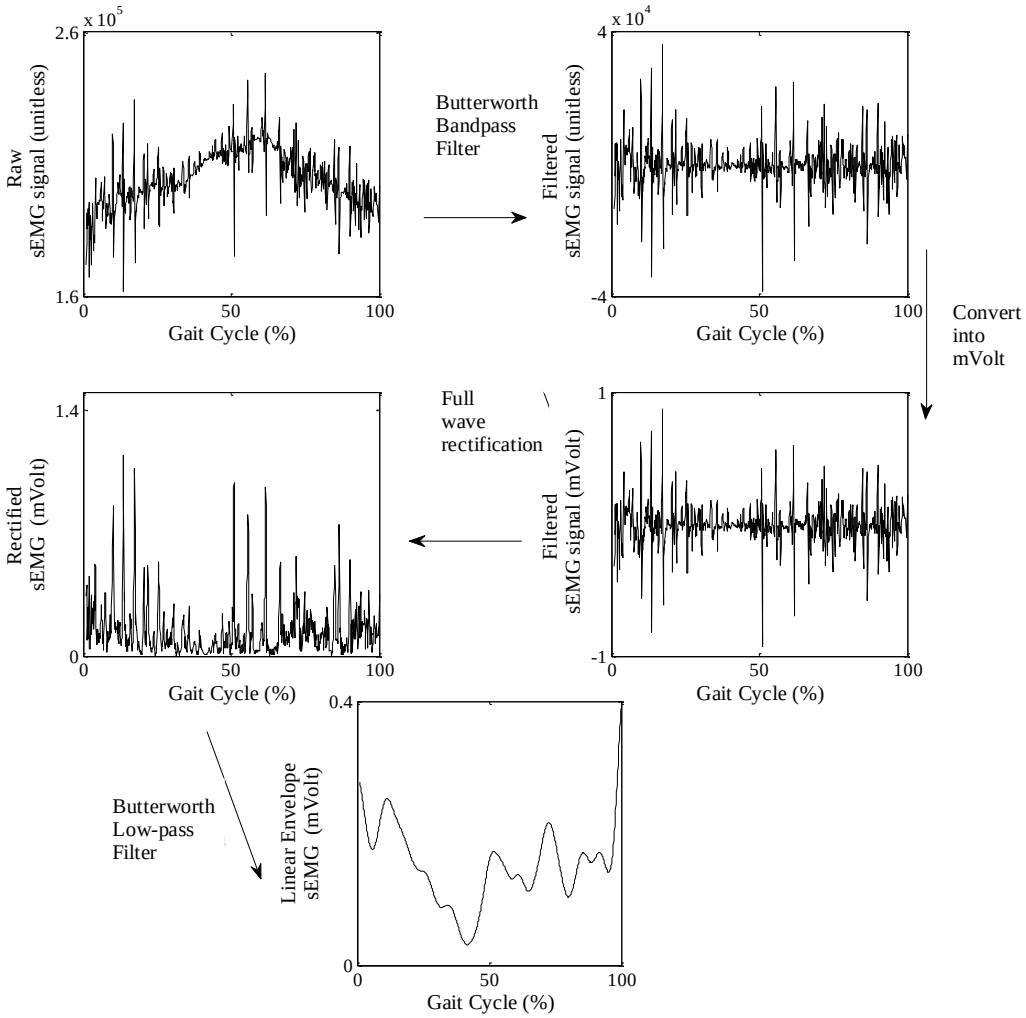

Fig 3.9. Processing of sEMG from raw signal to linear envelope.

3.5 Chapter Summary

In this chapter, the design and requirement to develop an IGS module were well described. MPU-6050, Arduino Pro Mini and a micro SD shield module were embedded to form one IGS system. The properties of Shimmer Sensing sEMG were also discussed in this chapter.

The experiment designs for this research were well explained. There were three different experiments designed to cover the whole scope of the research (Experiment 1, Experiment 2 and Experiment 3). Experiment 1 recruited 10 healthy subjects and their gait data were being used as validation purpose. This gait data can also be served as a standard comparison to the gait performance from stroke in the later chapters. Meanwhile, Experiment 2 was cross-sectional study on 60 stroke patients. This experiment was designed to study the gait characteristic and classify the large group of stroke patients in detail. Lastly, Experiment 3 was a longitudinal study on 15 stroke patients during their first month, third month and sixth month after diagnosed with stroke. The aim of this experiment is to study the recovery trajectory of stroke patients during the early recovery.

Chapter 4 An inertia integration method

4.1 Introduction

In this chapter, a new inertia based integration algorithm was proposed in this chapter to obtain gait trajectory. This algorithm yields gait velocity, gait displacement and joint angle. The aims of this chapter are:

1. To propose a new IMU based integration algorithm, which can accurately yield gait trajectory.
2. To validate the propose new IMU based integration algorithm.

4.2 Inertial based integration algorithm

4.2.1Temporal parameters

Heel-strike and toe-off events are necessary to obtain temporal parameters. This heel-strike and toe-off events can be detected from the gyroscope signal as described earlier which located on ankle [223] as seen from **Fig 4.1**. The temporal parameters interested in this project are stance time, swing time and gait cycle time. These parameters can be determined by using Eq (4.1), (4.2) and (4.3):

$$GCT = HS_{i+1} - HS_i \tag{4.1}$$

$$STT = TO_i - HS_i \tag{4.2}$$

$$SWT = HS_{i+1} - TO_i \tag{4.3}$$

where *GCT*, *STT* and *SWT* are the gait cycle time, stance time and swing time respectively, *HS* and *TO* are the heel-strike and toe-off events respectively and *i* represents the time of *i*th heel-strike (or toe-off).

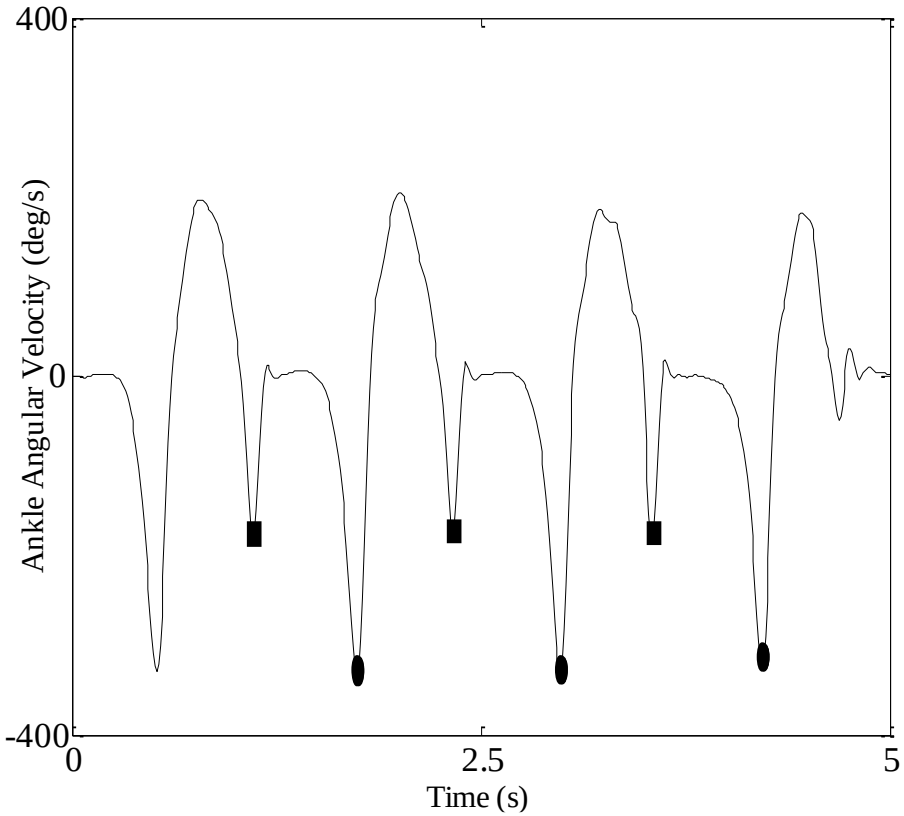

Fig 4.1. **An example of gyroscope output from pitch rotation and the subsequent heel-strike (square box) and toe-off (circle) events.**

4.2.2 Kinematic parameters

The IGS module that contains IMU will provide the angular velocity and linear acceleration from ankle and shank. To obtain kinematic parameters such as joint angle, gait velocity and gait displacement, integration of these angular velocity and linear acceleration must be performed. However, direct linear integration tends to yield high error due to low SNR. Therefore, some sophisticated integration algorithm must be applied.

4.2.2.1 Inertial frame and sensor frame

The first step to obtain these kinematic parameters are to correct the initial orientation of the tilted sensor. The orientation of the IMU on foot is showed in **Fig 4.2**. There are two orientation frames in this figure; the first is defined as the inertia frame (*X*-axis point in horizontal direction (roll,ϕ), *Y*-axis pointing in vertical

direction (yaw, φ) and *Z*-axis pointing out from the paper (pitch, θ)). The second frame is called sensor frame (*X*'-axis and *Y*'-axis). Inertia frame is a fixed frame with *X*-axis always parallel to the horizontal direction, *Y*-axis always parallel to the vertical direction and *Z*-axis always parallel to the direction pointing out from the paper. Meanwhile, the sensor frame is always parallel to the direction of the sensor axes. This sensor frame will rotate during gait with respect to the rotation of foot.

The accelerometer and gyroscope data in the inertia frame can be integrated to yield gait velocity, gait displacement and joint angle. Meanwhile, this sensor frame is changing for different subjects and throughout different gait cycle events. This is because (i) initial orientation of sensor on ankle, which can be different for different subjects, (ii) rotation of lower limb during gait cycle that tilts the IMU. The value d_{S_A} is the distance between the IGS module to exact ankle joint, which is different for each participant. Since the shape of foot is unique for every participant, the initial tilted angles for the sensor frame and d_{S_A} will be different. These issues need to be addressed to get consistent results for every participant. To obtain these kinematic parameters, the IMU data from sensor frame must be converted to the inertia frame.

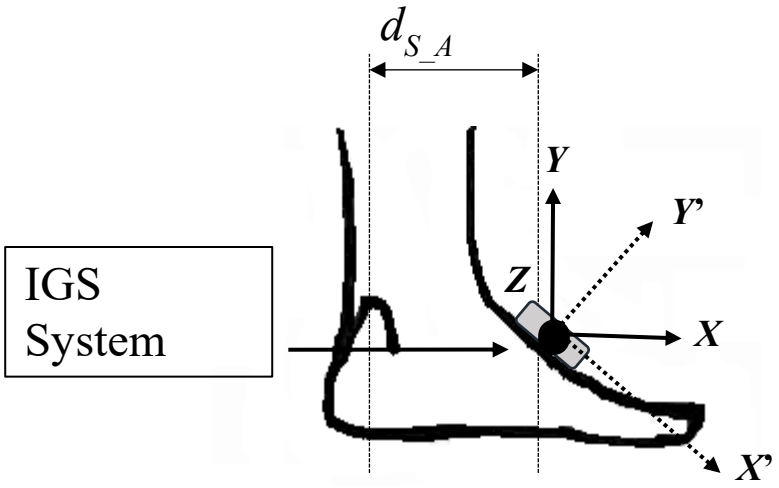

Fig 4.2. IGS system is located on human foot by using Velcro strap. The inclination angle of the sensor to horizontal axis is different for each subject. The inertia frame consist of *X*-, *Y*- and *Z*-axis (roll, yaw and pitch respectively). It is necessary to convert sensor frame (*X*'- and *Y*'-axis) to inertia frame to obtain kinematic parameters. The value d_{S_A} is the distance from sensor to the exact location of ankle joint, which can be different for each participant.

It is necessary to determine the initial inclination angle with respect to the inertia frame. Before the start of experiment, all participants were instructed to stand still for few seconds. The initial pitch and roll inclination angles during standing, θ_{stand} and ϕ_{stand} respectively can therefore be obtained from Eq (4.4) and (4.5).

$$\theta_{stand} = atan\left(\frac{-\bar{A}_{X,stand}}{\bar{A}_{Y,stand}}\right) \tag{4.4}$$

$$\phi_{stand} = atan\left(\frac{-\bar{A}_{Z,stand}}{sqrt\left(\bar{A}_{X,stand}{}^{2} + \bar{A}_{Y,stand}{}^{2}\right)}\right) \tag{4.5}$$

where $\bar{A}_{i,stand}$ are the mean accelerations data measured during standing (i=*X*, *Y* and *Z* axis respectively).

These initial pitch and rolls angles are used to correct the initial tilted angle to obtain the initial inertia frame. Rotation of IMU from sensor frame to inertia frame can be achieved by using simple rotation matrix.

$$\mathbf{V}=\mathbf{R}_{\mathbf{B}}^{\mathbf{I}}\cdot\mathbf{V}' \tag{4.6}$$

where **V** is the 3-axis acceleration vector after rotation ($\mathbf{V} = \begin{bmatrix} A_X \\ A_Y \\ A_Z \end{bmatrix}$), $\mathbf{R}_{\mathbf{B}}^{\mathbf{I}}$ is the Rotation Matrix from sensor frame to inertia frame and **V'** is the 3-axis acceleration vector before rotation. In this study, the initial yaw angle is impossible to obtain based on accelerometer. This is because there is no gravity change with different yaw angle. Therefore, yaw angle is not taking into consideration to form the rotation matrix $\mathbf{R}_{\mathbf{B}}^{\mathbf{I}}$.

$$\mathbf{R}_{\mathbf{B}}^{\mathbf{I}} = \mathbf{R}_{\mathbf{X}}(\phi) \cdot \mathbf{R}_{\mathbf{Z}}(\theta) \tag{4.7}$$

$$\mathbf{R}_{\mathbf{X}}(\emptyset) = \begin{bmatrix} 1 & 0 & 0 \\ 0 & \cos(\phi) & \sin(\phi) \\ 0 & -\sin(\phi) & \cos(\phi) \end{bmatrix} \tag{4.8}$$

$$\mathbf{R}_{\mathbf{Z}}(\theta) = \begin{bmatrix} \cos(\theta) & -\sin(\theta) & 0 \\ \sin(\theta) & \cos(\theta) & 0 \\ 0 & 0 & 1 \end{bmatrix} \tag{4.9}$$

where $\mathbf{R}_{\mathbf{X}}(\phi)$and $\mathbf{R}_{\mathbf{Z}}(\theta)$ are the rotation matrices for roll and pitch respectively. The Rotation Matrix $\mathbf{R}_{\mathbf{B}}^{\mathbf{I}}$ is then being constructed.

$$\mathbf{R}_{\mathbf{B}}^{\mathbf{I}} = \begin{bmatrix} \cos(\theta) & \sin(\theta) \cdot -\cos(\phi) & \sin(\theta) \cdot -\sin(\phi) \\ \sin(\theta) & \cos(\theta) \cdot \cos(\phi) & \cos(\theta) \cdot \sin(\phi) \\ 0 & -\sin(\phi) & \cos(\phi) \end{bmatrix} \tag{4.10}$$

By substituting θ_{stand} and ϕ_{stand} into this rotation matrix $\mathbf{R}_{\mathbf{B}}^{\mathbf{I}}$, the corrected initial 3-axis acceleration vector during standing is therefore shown in:

$$\begin{bmatrix} A_X \\ A_Y \\ A_Z \end{bmatrix} = \begin{bmatrix} \cos(\theta_{stand}) & \sin(\theta_{stand}) \cdot -\cos(\phi_{stand}) & \sin(\theta_{stand}) \cdot -\sin(\phi_{stand}) \\ \sin(\theta_{stand}) & \cos(\theta_{stand}) \cdot \cos(\phi_{stand}) & \cos(\theta_{stand}) \cdot \sin(\phi_{stand}) \\ 0 & -\sin(\phi_{stand}) & \cos(\phi_{stand}) \end{bmatrix} \cdot \begin{bmatrix} A_X' \\ A_Y' \\ A_Z' \end{bmatrix} \tag{4.11}$$

Fig 4.3 shows the example of a corrected acceleration from one subject. As observed in this figure, the acceleration before correction did not align well with the inertia frame. The *X*- and *Z*- axis acceleration did not stay at zero and *Y*- axis

acceleration did not show gravitational acceleration g when the IMU is at rest (standing). This is because all the 3-axis acceleration experience gravitational force when the IMU was tilted. After the correction is performed using rotation matrix $\mathbf{R_B^I}$, *X*- and *Z*- axis acceleration remain at zero and *Y*- axis acceleration roughly equal to 9.81ms^{-2} during standing period.

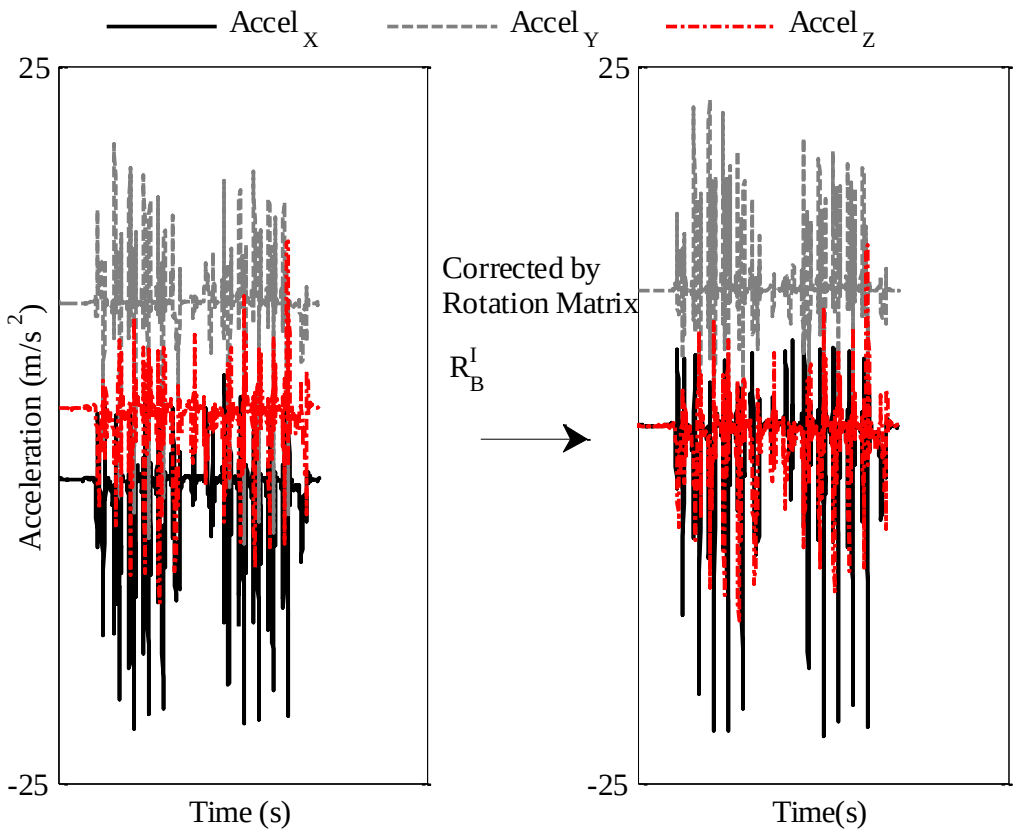

Fig 4.3. Example of 3-axis acceleration being corrected by using the tilted angles determined during standing.

Converting gyroscope data from sensor frame to inertia frame is necessary since the raw gyroscope data is recorded with respect to the sensor frame. According to [224], the transformation matrix for converting the sensor frame angular rates to inertia frame is given Eq (4.12):

$$D(\phi,\theta) = \begin{bmatrix} 1 & \cos(\phi)\cdot\tan(\theta) & \sin(\phi)\cdot\tan(\theta) \\ 0 & \cos(\phi)/\cos(\theta) & \sin(\phi)/\cos(\theta) \\ 0 & -\sin(\phi) & \cos(\phi) \end{bmatrix} \tag{4.12}$$

where matrix *D* is the transformation matrix to convert sensor frame angular velocities to inertia frame angular velocities. The inertia frame angular velocities are therefore:

$$\begin{bmatrix} \dot{\phi} \\ \dot{\varphi} \\ \dot{\theta} \end{bmatrix} = \begin{bmatrix} p + q \cdot \cos(\phi) \cdot \tan(\theta) + r \cdot \sin(\phi) \cdot \tan(\theta) \\ q \cdot \cos(\phi) \,/\, \cos(\theta) + \; r \cdot \sin(\phi)/\cos(\theta) \\ q \cdot \sin(\phi) + r \cdot \cos(\phi) \end{bmatrix} \tag{4.13}$$

where $\dot{\phi}$, $\dot{\varphi}$ and $\dot{\theta}$ are the inertial frame roll, yaw and pitch respectively, *p*, *q* and *r* are the sensor frame angular velocities from *X*-, *Y*- and *Z*- axes gyro output respectively.

4.2.2.2 Boundary conditions and resetting mechanism

The pitch and roll angles, θ and ϕ during walking are needed to rotate the IMU orientation to the inertia frame. They can be obtained by integration of angular velocity from gyroscope. The numerical integration algorithm employed here is similar to Stacy's thesis [64]. The derivation and Matlab code for this integration algorithm is given in Appendix A.

Furthermore, these angles will be used to rotate the acceleration signal to inertia frame to yield gait velocities and displacements. However, direct integration of angular velocity always result in drifting issue. The error would be propagated to the acceleration signal and the error will grow unbounded after double integrating the acceleration signal.

To reduce the error, the heel-strike and toe-off information are needed to segment the gyroscope and accelerometer results into individual gait cycle. One gait cycle is defined as the heel-strike to the next heel-strike.

After the gait phase segmentation, the gyroscope and accelerometer signals can be integrated separately. There is one boundary condition to be imposed to reduce the error:

1. The initial (first heel-strike) and final (next heel-strike) conditions for integration of angular velocities, gait velocities (*X*- and *Y*-axis) and gait vertical displacement (*Y*-axis) are zero at ankle joint (distance d_{S_A} from IGS)

Due to unbounded error and drifting, the final point of integrated results will never be zero after integration. Therefore, a resetting mechanism is introduced to reset the last sample to zero.

$$U = \begin{cases} \widetilde{U}_{T1} & T1(n_{1:toeoff}) = T(1), T(2), \dots, T(toeoff) \\ \widetilde{U}_{T2} & T2(n_{toeoff:end}) = T(toeoff+1), T(toeoff+2), \dots, T(N) \end{cases} \quad (4.14)$$

where U is the integrated result before reset (U = pitch and roll angles, gait horizontal and vertical velocities, gait vertical displacement), $T(N)$=[$T(1)$, $T(2)$, …, $T(toeoff)$,…, $T(N)$], $T(N)$=[$T1(n_{1:toeoff})$, $T1(n_{toeoff:end})$], N is the number of sample in the time series. These results are further segmented into two phases according to Eq (4.14), $\widetilde{U}_{T1}$ and $\widetilde{U}_{T2}$ ($\widetilde{U}_{T1}$ and $\widetilde{U}_{T2}$ have sample size of $n_{1:toeoff}$ and $n_{toeoff:end}$ respectively). To compensate the drifting issue and correct the final sample back to zero, the resetting mechanism shown in Eq (4.15) and (4.16) are used for $\widetilde{U}_{T2}$. This resetting mechanism does not interfere with the segmented result during $T1(n_{1:toeoff})$ (i.e. $\widetilde{U}_{T1}$). It only reset the last sample in $T2(n_{toeoff:end})$ into zero; therefore this resetting mechanism will only apply on $\widetilde{U}_{T2}$.

$$\widehat{U}^1_{T2} = \widetilde{U}_{T2} - \left(\frac{\widetilde{U}_{T2}(N) - \widetilde{U}_{T2}(1)}{T2(N) - T2(1)} \right) \cdot T2(n_{toeoff:end}) \quad (4.15)$$

$$\widehat{U}^2_{T2} = \widehat{U}^1_{T2} - \left(\frac{0 - \widehat{U}^1_{T2}(1)}{T2(N) - T2(1)} \right) \cdot T2(n_{toeoff:end}) \quad (4.16)$$

where $\widehat{U}^1_{T2}$ is the intermediate corrected result, $\widehat{U}^2_{T2}$ is the final corrected result. Since $\widetilde{U}_{T1}$ is remained the same, the new corrected $\widehat{U}^2_{T2}$ will be substituted into Eq (4.14) when it is $T2(n_{toeoff:end})$.

$$U = \begin{cases} \widetilde{U}_{T1} & T1(n_{1:toeoff}) = T(1), T(2), \dots, T(toeoff) \\ \widehat{U}^2_{T2} & T2(n_{toeoff:end}) = T(toeoff+1), T(toeoff+2), \dots, T(N) \end{cases} \quad (4.17)$$

4.2.2.3 Integration of inertia data

After the gyroscope result is rotated from the sensor frame to the inertia frame to remove the initial tilted angle, angular velocities $\dot{\theta}$ and $\dot{\phi}$ are ready to integrate to yield both pitch (θ) and roll (ϕ) angles.

$$\tilde{\theta} = \int_{T_{start}}^{T_{end}} \dot{\theta}(t)dt + \theta_{ini} \tag{4.18}$$

where $\tilde{\theta}$ is the inclination pitch angle before reset, $\dot{\theta}$ is the pitch angular velocity, T_{start} and T_{end} are the current and subsequence heel-strike events respectively, θ_{ini} is the initial condition for integration of angular velocity, which is zero. The drifting problem from this $\tilde{\theta}$ is corrected using the resetting mechanism from Eq (4.14) - (4.17) to form corrected pitch angle $\hat{\theta}$. Similar procedure is used to yield roll angle $\hat{\phi}$.

Once both pitch and roll angles are determined, the acceleration can be rotated back to inertia frame using the rotation matrix

$$\mathbf{A}=\mathbf{R}_{\mathbf{B}}^{\mathbf{I}} \cdot \mathbf{A}'-\mathbf{g} \tag{4.19}$$

$$\begin{bmatrix} A_{X,inertia} \\ A_{Y,inertia} \\ A_{Z,inertia} \end{bmatrix} = \begin{bmatrix} \cos(\hat{\theta}) & \sin(\hat{\theta}) \cdot -\cos(\hat{\emptyset}) & \sin(\hat{\theta}) \cdot -\sin(\hat{\emptyset}) \\ \sin(\hat{\theta}) & \cos(\hat{\theta}) \cdot \cos(\hat{\emptyset}) & \cos(\hat{\theta}) \cdot \sin(\hat{\emptyset}) \\ 0 & -\sin(\hat{\emptyset}) & \cos(\hat{\emptyset}) \end{bmatrix} \cdot \begin{bmatrix} A_X \\ A_Y \\ A_Z \end{bmatrix} - \begin{bmatrix} 0 \\ g \\ 0 \end{bmatrix} \tag{4.20}$$

where $A_{X,\text{inertia}}$, $A_{Y,\text{inertia}}$ and $A_{Z,\text{inertia}}$ are the acceleration at inertia frame, g is the gravitational acceleration (~=9.81ms^{-2}). In this equation, the gravity component from the accelerometer must be removed and this is called gravity compensation. $A_{X,\text{inertia}}$ and $A_{Y,\text{inertia}}$ are integrated to obtain the horizontal and vertical velocities and displacements.

$$Vel_j = \int_{T_{start}}^{T_{end}} A_{j,inertia}(t)dt + Vel_{ini} \tag{4.21}$$

where Vel_j is the velocity after integration, $A_{j,\text{inertia}}$ ($A_{X,\text{inertia}}$ and $A_{Y,\text{inertia}}$) is the acceleration, j=(X and Y-axis) and Vel_{ini} is the initial condition for integration of acceleration, which is zero. Before further integrate the velocity Vel_j to yield displacements, the same resetting mechanism from Eq (4.14) - (4.17) is used to yield $\hat{Vel}_j$. The displacements, D_j are now ready to compute using Eq (4.22).

$$D_j = \int_{T_{start}}^{T_{end}} \widehat{Vel}_j(t)dt + D_{ini} \tag{4.22}$$

where D_{ini} is the initial condition for integration of velocity, which is zero. Following the boundary conditions, only vertical displacement is being corrected using Eq (4.14) - (4.17) to remove the bias to form $\hat{D}_Y$. According to **Fig 4.2**, the location of the sensor on the foot is different from subject to subject, which yields different gait trajectories depending on the distance of the sensor to the ankle, d_{S_A}. Therefore, we will only consider the vertical and horizontal displacements at the ankle and not the sensor.

$$\breve{D}_X = D_X - d_{S\_A} \cdot \cos(\hat{\theta}) \tag{4.23}$$

$$\breve{D}_Y = \hat{D}_Y - d_{S\_A} \cdot \sin(\hat{\theta}) \tag{4.24}$$

where $\breve{D}_X$ and $\breve{D}_Y$ are the horizontal and vertical displacement at ankle. After obtaining the displacement, gait velocity GV can be calculated as follow:

$$GV = \frac{\breve{D}_{X,left}(end) + \breve{D}_{X,right}(end)}{GCT_{left} + GCT_{right}} \tag{4.25}$$

The angle, linear velocity and linear acceleration on shank IMU is determined using the same method. The ankle angle is the difference in pitch angles between two segments (ankle and shank), which the method has been validated in Williamson paper [263]. **Fig 4.4** show the schematic diagram the integration method.

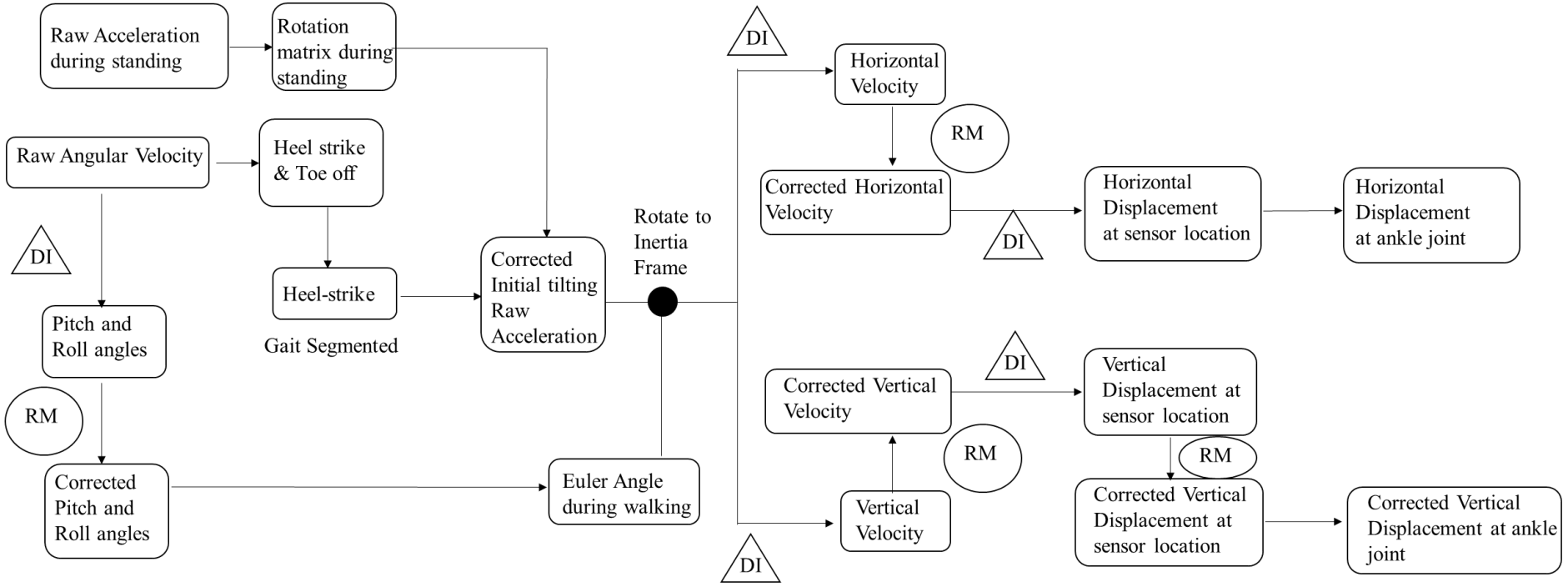

Fig 4.4. Schematic diagram of the proposed inertia integration method. DI indicate direct integration while RM indicate resetting mechanism.

4.3 Validation of inertial based integration algorithm – Experiment 1

For Experiment 1, the mean and standard deviation of all gait trajectories and gait velocities were calculated for both video image results and inertial sensor results. The Root Mean Squared Error (RMSE) was calculated to yield the difference between results obtained from the video footage and the sensor system.

The results from video images were used as a standard comparison to validate the accuracy of the proposed method. As mentioned earlier, red colour LED was put on subject's heel. The process of red colour marker tracking was performed by using an open source Matlab code [263]. This Matlab code is presented in Appendix B. Synchronisation between video and IGS system was based on gait event. The first heel strike event from the video was being synchronised with the first heel strike observed from **Fig 4.1**.

Fig 4.5 to **Fig 4.10** present the average ankle horizontal and vertical displacement for normal walking, ankle braced walking and knee braced walking respectively from 10 subjects. The dotted line was the results from video images; solid line was the results from inertial sensor and the shaded area were the standard deviation from both video images and sensor result. Qualitative analysis on the figures tells that the proposed method was able to capture the amplitude and peak timing. **Table 4.1** shows the root mean square error between the gait trajectory obtained from the proposed method and the video. The relatively low error indicates the reliability of the proposed method. Meanwhile **Table 4.2** illustrates the average horizontal walking speed for 10 subjects and the standard deviation. The average gait velocity from 10 subjects for normal walking was 0.909ms^{-1}, knee braced walking was 0.769 ms^{-1}, and ankle braced walking was 0.539 ms^{-1}. Root mean square error as computed to validate against the video result.

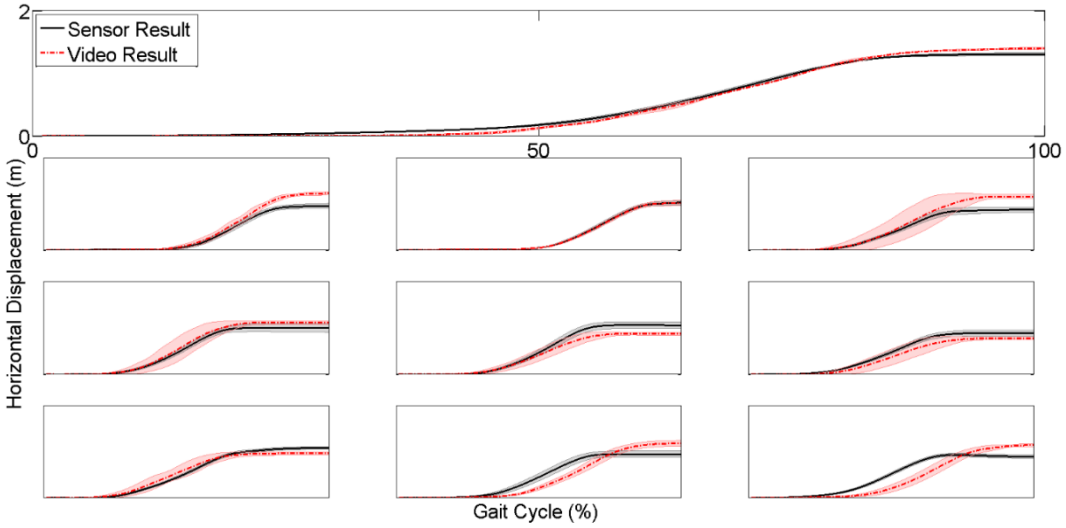

Fig 4.5. Ankle horizontal displacements for during normal walking from 10 subjects. Shaded area indicates standard deviation for each results.

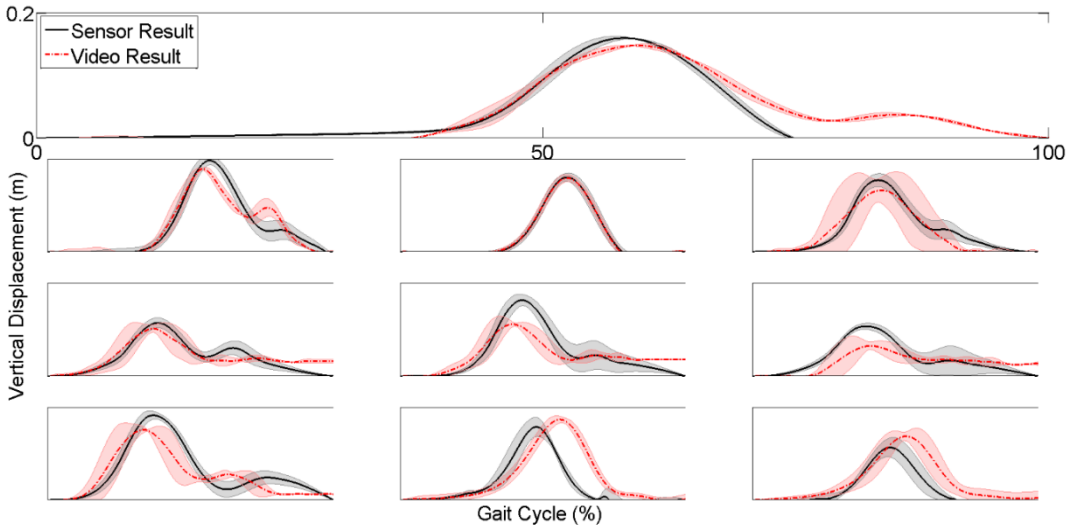

Fig 4.6. Ankle vertical displacements for during normal walking from 10 subjects. Shaded area indicates standard deviation for each results.

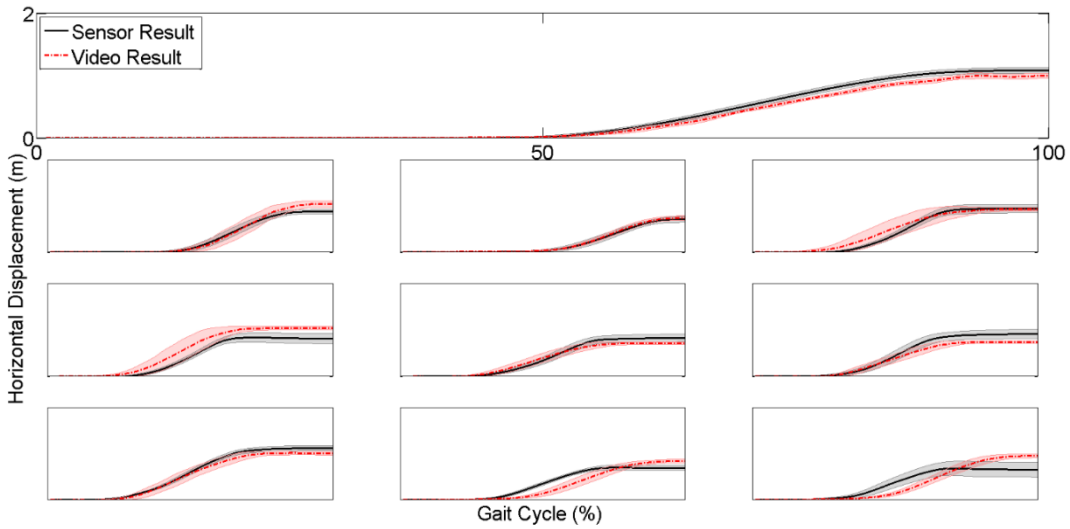

Fig 4.7. Ankle horizontal displacements for during knee braced walking from 10 subjects. Shaded area indicates standard deviation for each results.

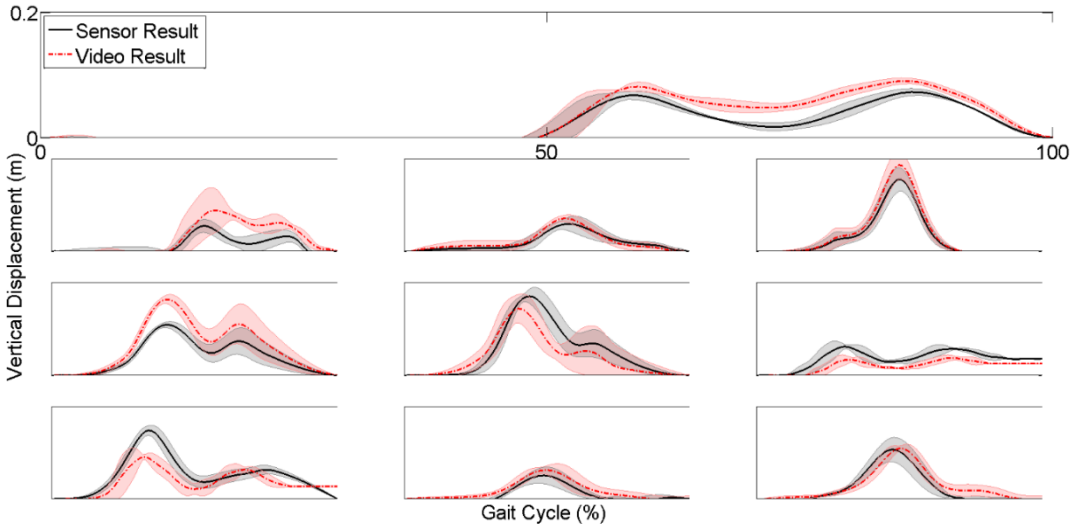

Fig 4.8. Ankle vertical displacements for during knee braced walking from 10 subjects. Shaded area indicates standard deviation for each results.

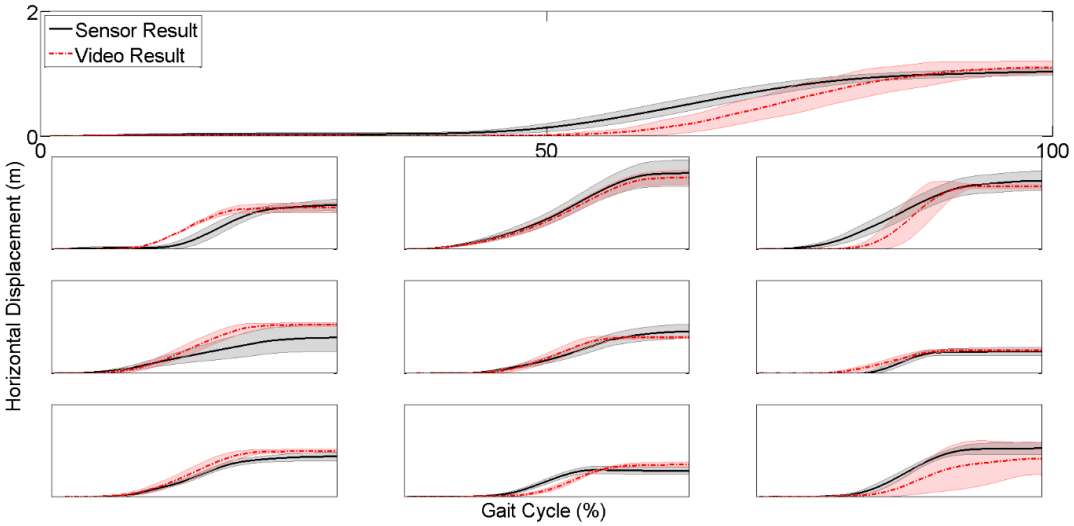

Fig 4.9. Ankle horizontal displacements for during ankle braced walking from 10 subjects. Shaded area indicates standard deviation for each results.

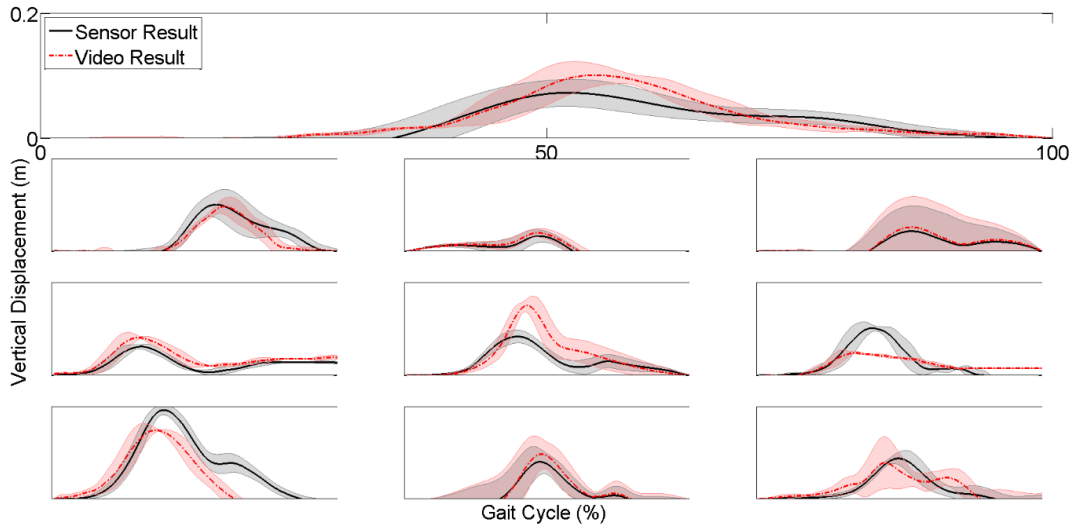

Fig 4.10. Ankle vertical displacements for during ankle braced walking from 10 subjects. Shaded area indicates standard deviation for each results.

Table 4.1. Root mean square error analysis for both horizontal and vertical displacement.

Walking Condition	Orientation	RMSE	
		Displacement	
		Right	Left
Normal walking	Horizontal	0.0159	0.0124
	Vertical	0.0020	0.0030
Knee Braced	Horizontal	0.0124	0.0137
Walking	Vertical	0.0015	0.0021
Ankle Braced	Horizontal	0.0100	0.1090
walking	Vertical	0.0013	0.0020

Table 4.2. The average and standard deviation of horizontal gait speed from sensor for 3 walking conditions. The root mean square error is computed to validate against result from video.

Walking Condition	Mean Gait Speed (ms^{-1})	Standard Deviation	RMSE
Normal walking	0.909	0.12	0.1745
Knee Braced Walking	0.769	0.15	0.1335
Ankle Braced walking	0.539	0.20	0.0782

Based on the result above, the proposed inertia-based integrating algorithm had accurately computed the gait trajectory for different walking conditions. This algorithm adopts the assumption from Zero Velocity Update, ZUPT and reset the velocity and position to zero during heel-strike. This algorithm only considers the gait movement in the sagittal plane.

The initial orientation of IMU on different subjects were always different due to different physical shape of foot. Therefore, the first step of the proposed as iws to re-orientate the tilted IMU. Noted that when the IMU was tilted, pitch and roll angles could be determined from the tilted acceleration. The initial tilted pitch and roll angles were found and corrected to the inertia frame. However, yaw angle cannot be determined due to the rotation around *Y*-axis will not affect the changes in gravitational acceleration. The angular velocity reading from *Y*-axis only provided the rate of change of angle, but it did not suggest the exact nor initial orientation around this axis. Therefore, the rotation matrix for yaw angle as not considered to compute the rotation matrix in Eq (4.7). Since the initial tilted yaw

angle cannot be found, proper alignment of the sensor system around *Y*-axis was needed to minimise the error.

The resetting mechanism used in this study is similar to the one proposed in [19]. In our study, the resetting mechanism considered the drifting as linear and the algorithm removed the bias caused by the straight line from the drifting phenomenon. **Fig 4.11** presents an example of a drifting velocity and corrected velocity after applying the resetting mechanism. In this figure, the segment during swing phase was considered drifted downwards. The gradient of the straight line was found and was subtracted from the signal.

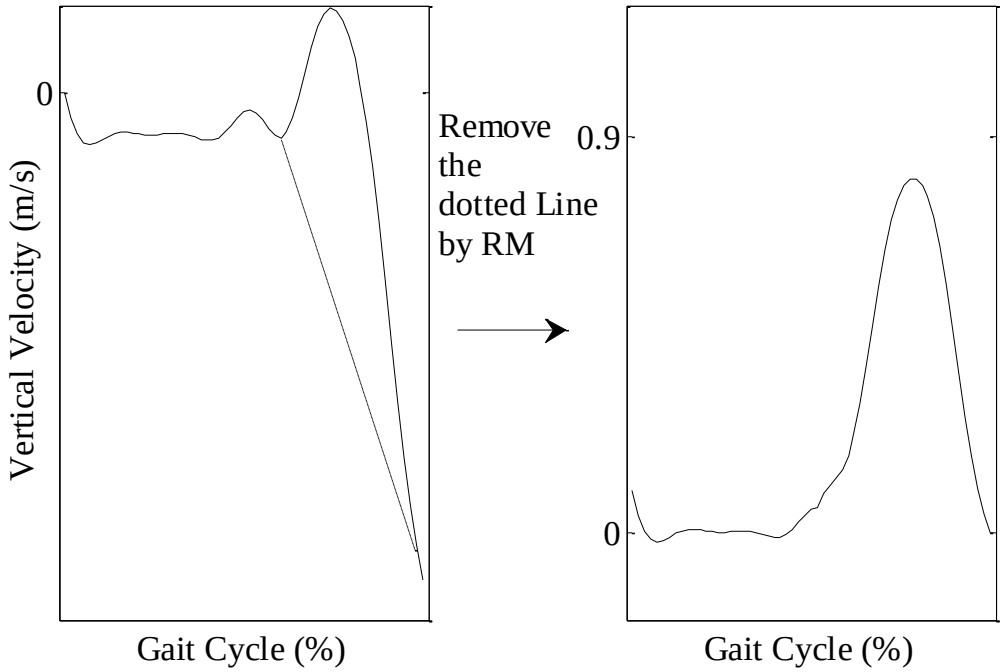

Fig 4.11. **Resetting Mechanism Algorithm remove the straight line in the drifted curve. RM- resetting mechanism**

Overall, the low RMSE **Table 4.1** indicates the algorithm is robust enough to obtain gait trajectory from different walking style. The magnitude and the gait profile from the inertia sensor were very accurate compared to the video results. Furthermore, the comparison in **Table 4.2** only shows a little discrepancy in gait velocity between results yielded from inertia sensors and video. The average gait velocity was highest in normal walking condition, lowest in ankle walking condition and moderate in

knee walking conditions. During walking, ankle propulsion is very important to carry the lower limb forward. With restricted ankle (ankle braced walking), there is no ankle dorsi and plantar flexion and it will reduce the propulsion force. This will either increase the gait cycle time or reduce the step length, depends on different individual. Therefore, gait velocity is lowest in ankle braced walking condition. For both knee and ankle braced walking, most of the participants had lower the foot clearance from the ground. The vertical displacement determines the foot clearance from the ground and it is crucial in maintaining a good walking pattern. Insufficient foot clearance may leads to foot drag and it can prone to fall easily.

4.4 Chapter Summary

In this chapter, a new inertial based integration algorithm is proposed. This algorithm as being validated by high-speed camera. The validation results showed high accuracy regardless walking conditions. The reason to test different walking conditions is to ensure the robustness of the algorithm. The spatial-temporal gait parameters described in this chapter will be used to analyse the gait of stroke in the later chapters. These gait parameters can be used as the input to perform gait classification.

Chapter 5 Conventional gait analysis

5.1 Introduction

It is very important to understand the nature of gait characteristics before physiotherapist can arrange suitable intervention for stroke patients during rehabilitation. As mentioned in Chapter 2, there were many researchers conducted gait analysis on stroke patients to understand the mechanism behind their gait pattern. Due to lack of an accepted general theory of walking [225] and the high variability during interpretation of gait data [226], it is necessary to study the gait characteristics of stroke patients in details. Therefore, gait classification is essential to identify homogeneous subgroups of stroke patients and extract the crucial gait information. In this chapter, the results from 60 stroke patients from Experiment 2 described in Chapter 3 were analysed. The aims of this chapter are:

1. To understand gait terminology using gait data from healthy subjects.
2. To classify and study the gait characteristic among a large group of stroke patients.
3. To find the correlation between spatial-temporal parameters and gait velocity and TUG test.
4. To study the muscle condition among different kind of stroke.

5.2 Data analysis

In this chapter, the gait data from both Experiment 1 (10 healthy) and Experiment 2 (60 cross-section stroke patients) were analysed. **Table 5.1** presents the outcome yielded from these experiments.

All statistical analyses were performed using Matlab. The mean, standard deviation (SD) and 95% confident interval (CI) of all measurements were calculated for stroke and healthy subjects. Unpaired *t*-test were used to compare the stroke populations to healthy populations. One-way ANOVA analysis was used to

compare the differences between each stroke patient's subgroup after classification. A level of $p<0.05$ was considered statically significant.

For stroke patients, Pearson correlation was used to determine the relationship between:

1. Gait parameters and TUG score. Five correlations were performed between the five parameters described in Table 5.1 (Stance, swing, gait cycle times, Stride length, maximum heel clearance) and TUG score.
2. Gait parameters and gait velocity. Five correlations were performed between the five parameters described in Table 5.1 (Stance, swing, gait cycle times, Stride length, maximum heel clearance) and gait velocity.
3. Symmetry Index and TUG score. Five correlations were performed between five symmetry indices (stance, swing, gait cycle times, Stride length, maximum heel clearance symmetry) and TUG score.
4. Symmetry Index and gait velocity. Five correlations were performed between five symmetry indices (stance, swing, gait cycle times, Stride length, maximum heel clearance symmetry) and gait velocity.

Noted that the five parameters from items (1) and (2), i.e. stance, swing, gait cycle times, Stride length, maximum heel clearance and the five parameters from items (3) and (4), i.e. stance, swing, gait cycle times, Stride length, maximum heel clearance symmetry are different parameters. The parameters from first two items illustrate the spatial temporal parameters from individual lower limbs. Meanwhile, the parameters from items (3) and (4) describe the symmetry degree, or the level of similarity between left and right lower limbs using the parameters as input.

Robinson Index was selected over the other symmetry indices presented in **Table 2.2** is because this index is very commonly used in many other researches [87,101]. Other symmetry indices in **Table 2.2** are looking for the ratio between left and right. In contrast, Robinson Index is determining the difference between both left and right legs, and normalised again the summation from both legs. Therefore, Robinson Index was selected in this study.

Table 5.1. The outcomes obtained from the IMU and EMG system described in Chapter 3.

Parameters	Definition
Stance time (%)	Duration of gait cycle of foot support phase, from heel strike to toe off
Swing time (%)	Duration of gait cycle of foot swing phase, from toe off to next heel strike
Gait Cycle time (s)	Time between two consecutive heel strike of the same foot
Stride length (m)	Distance between two consecutive heel strike of the same foot
Maximum Heel clearance (m)	Maximum distance between the heel and the ground during swing time
Ankle angle (º)	The range of motion of ankle joint during gait
-Dorsiflexion at mid-stance	Ankle dorsiflexion angle during mid-stance event
-Plantarflexion at toe-off	Ankle plantarflexion angle during toe-off event
Gait Velocity (m/s)	Average velocity integrated from acceleration within the gait cycle
***Symmetry Indices**	Using Robinson Index as shown in Table 2.2.
- Stance symmetry	Robinson Index with stance time as input
- Swing symmetry	Robinson Index with swing time as input
- Stride length symmetry	Robinson Index with Stride length as input
- Heel clearance symmetry	Robinson Index with Maximum Heel clearance as input
***,[1] TUG**	Clinical assessment where the time taken of a subject to stand up from chair, walk a distance of 3 meters, turn around, walk back to the chair and sit down.
sEMG	Electric signal of muscle contraction and extension during gait

*Only applicable on Stroke patients; [1]Timed Up and Go Test

To obtain the temporal features (onset and duration) of sEMG signal, computation of sEMG signal linear envelopes is necessary. Dynamic peak normalisation (DPN) was used to normalise sEMG signal. The reason DPN was chosen is because it is more favour for stroke patients since they did not require to perform the standard maximum voluntary contraction (MVC) exercise.

Hierarchical Cluster Analysis [26] was used to subgroup homogenous gait patterns of these 60 chronic stroke patients based on spatial temporal parameters and joint kinematic measurement in the sagittal plane. The three variables that were best

determined group placement for cluster analysis were: ankle angle dorsiflexion at mid-stance, stride length and gait velocity at their paretic limb.

The Ward's linkage method and the Squared Euclidean distance measures were the standard clustering routines applied. Agglomeration coefficient was used to determine the number of clusters to be included with the stopping rule. The number of cluster groups was considered appropriate if continued increase in the number of clusters resulted in large percentage change in the agglomeration coefficient.

Once the number of clusters were identified, these 60 stroke subjects were categorised into their subgroups accordingly. Their other parameters such as ankle angle at toe-off, gait cycle time, stance time, swing time and maximum heel clearance were measured respectively.

The classification results from the method described above is regarded as Approach 1. These results will be used as a standard comparison to other approaches, which will be introduced in Chapter 6.

5.3 Healthy gait data

In this section, the gait pattern from healthy subjects were analysed. It is necessary to understand the healthy gait profile before extending the study on abnormal gait from stroke patients.

5.3.1 Gait spatial-temporal data

The gait results of 10 healthy subjects from Experiment 1 were analysed. **Table 5.2** shows the mean, standard deviation and 95% CI of gait spatial-temporal results from left and right lower limb across all healthy subjects. Both left and right lower limbs had very similar results. The average gait velocity from this group of healthy subjects was 1.5441 (0.14) m/s. The gait analysis results from these 10 healthy subjects (**Table 5.2**) were very similar when compared to the results from other researchers [70,227–230].

Table 5.2. Mean, standard deviation and 95% confident interval of spatial-temporal results from all healthy subjects.

	Mean	SD	95% CI	
Gait Velocity (m/s)	1.5441	0.14	1.520	1.570
Left lower limb				
Gait Cycle Time (s)	1.235	0.041	1.2222	1.2478
Step Time (s)	0.598	0.028	0.5911	0.6040
Stance Time (%)	56.60	2.21	55.91	57.29
Swing Time (%)	43.40	2.21	42.71	44.09
Stride Length (m)	0.9234	0.0799	0.8985	0.9483
Max. Heel Clearance (m)	0.1028	0.0096	0.0998	0.1058
Right lower limb				
Gait Cycle Time (s)	1.2333	0.0433	1.2199	1.2468
Step Time	0.596	0.025	0.5899	0.6034
Stance Time (%)	57.44	2.91	56.53	58.34
Swing Time (%)	42.56	2.91	41.66	43.47
Stride Length (m)	1.0145	0.0534	0.9978	1.0311
Max. Heel Clearance (m)	0.1141	0.0153	0.1093	0.1188

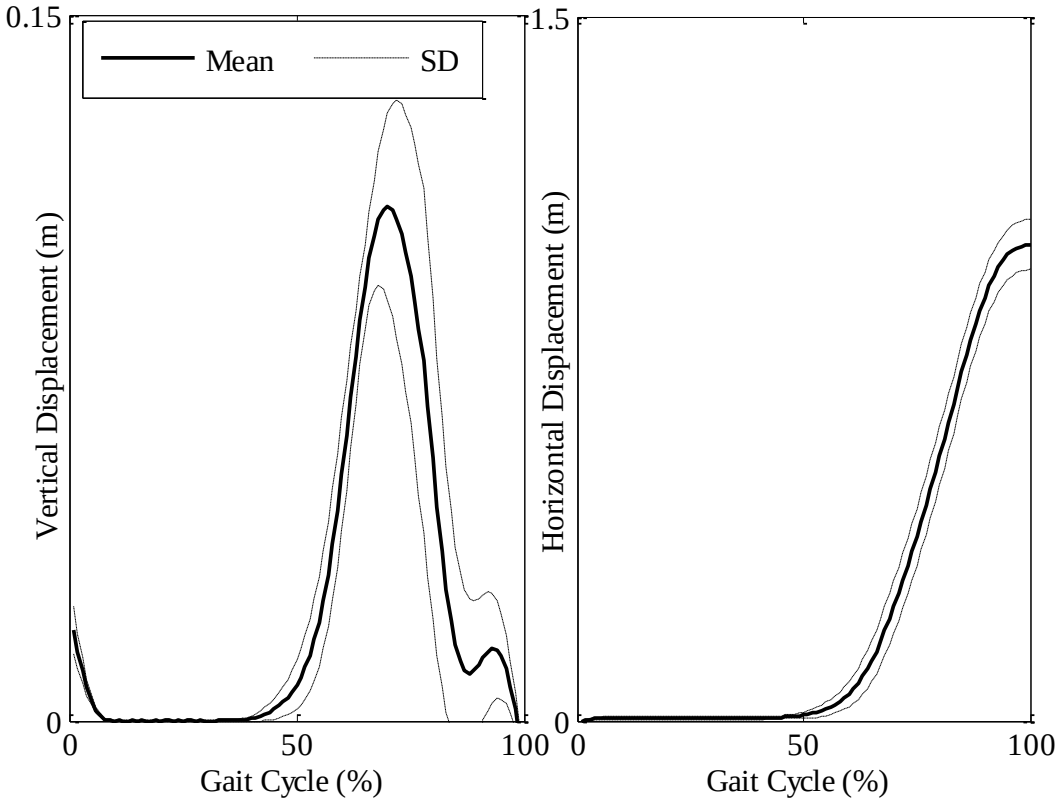

Fig 5.1. Ensemble vertical and horizontal heel displacements over one gait cycle.

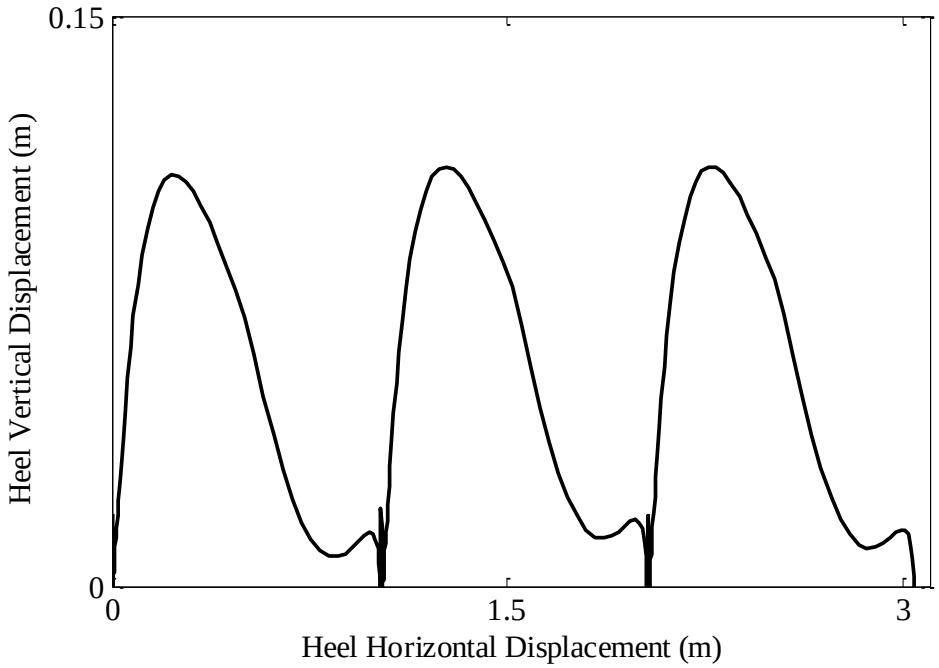

Fig 5.2. Example of heel gait trajectory from one healthy subject over three gait cycles.

Fig 5.1 shows the mean and standard deviation of vertical and horizontal heel displacements from all healthy subjects. Both vertical and horizontal displacements show minimal to no movement during 0-50% of gait cycle time. This is during stance phase where the foot is supporting the upper body. At 50-60% of gait cycle time, the heel starts to leave the ground (heel-off). Vertical heel displacement reached the peak around 70-75% of gait cycle time, where mid-swing happen. This maximum vertical heel displacement is a very important indication to determine foot drop symptom (one of the abnormal gait feature observed in hemiplegia patients). Meanwhile, the maximum horizontal heel displacement yields the stride length during gait cycle. A complete heel gait trajectory can be observed in **Fig 5.2**. This heel gait trajectory is constructed by plotting the vertical heel displacement against the horizontal heel displacement.

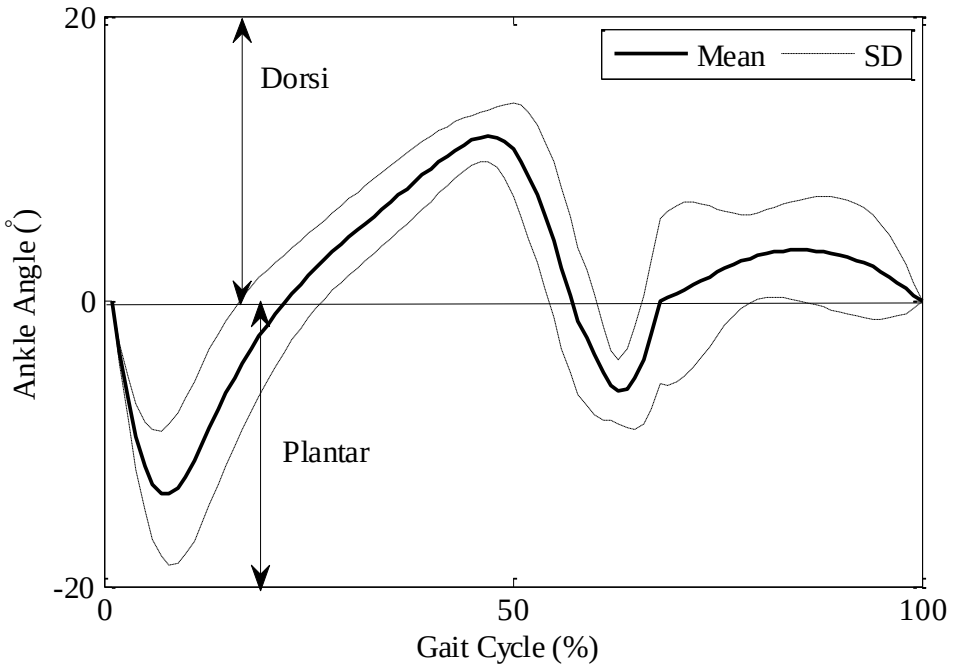

Fig 5.3. Ensemble ankle angle over one gait cycle. Positive value indicates dorsi flexion and negative value indicates plantar flexion.

Fig 5.3 presents the mean and standard deviation of ankle angle over one gait cycle from all healthy subjects. The positive and negative values on this diagram indicate both dorsi- and plantar-flexion respectively. After heel-strike, at 0-10% of gait cycle time, the ankle plantar-flex to prepare the foot to stance phase. During 10-50% of gait cycle time (during stance phase), the foot is trying to propel the body COM forward, which is achieved by the ankle joint dorsi-flexion. Besides that, it can increase contralateral step length [231]. To lift the foot to mid-air for swing phase, the ankle joint plantarflexion occurs around 50-60% of gait cycle time. This plantarflexion at this moment is very crucial as it contributes to the vertical displacement as seen in **Fig 5.1**. The dorsiflexion of ankle continues from 60% to 80% of gait cycle time to lift the toe part of the foot away from the ground and maintain at the neutral ankle position at mid-swing. It is very important to achieve neutral position because at this time, the foot passes the closest to the ground, and ankle stays at neutral position in the gait cycle facilitates limb clearance to prevent the toes from touching the ground, hence decreasing the risk of falling. Lastly, the ankle joint plantarflexion happens to prepare for the next heel-strike.

5.3.2 Gait sEMG data

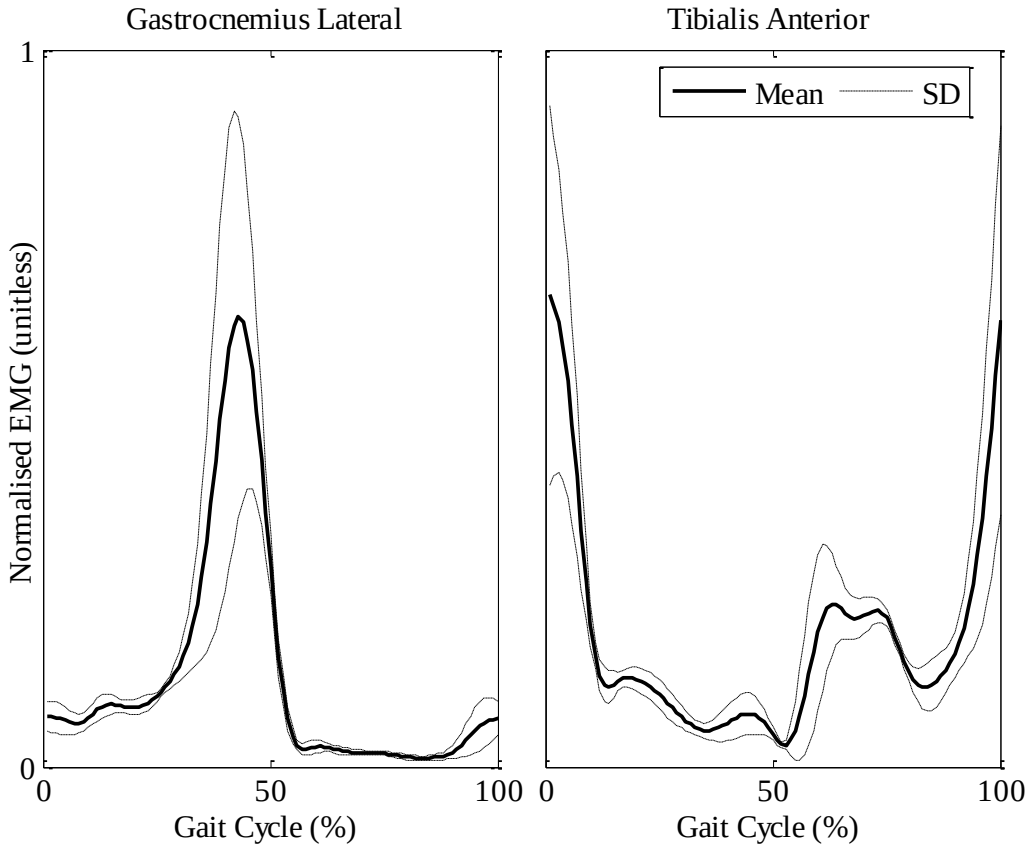

Fig 5.4. Ensemble normalised linear enveloped sEMG of gastrocnemius lateral and tibialis anterior muscles over one gait cycle.

SEMG signal during gait often shows the onset, duration and amplitude of the muscle burst in relation to the gait cycle. In this study, only temporal features such as onset and duration of muscle were analysed. This is because it is very hard to study the amplitude of sEMG inter-subjects using Dynamic Peak Normalisation. This normalisation method only normalised against the peak of the sEMG trial for each different subjects.

Gastrocnemius lateral (GL) and tibialis anterior (TA) muscles are agonist-antagonist muscles. This means that when GL muscle is contracting, TA muscle is relaxing, or vice versa. According to Seniam [177], GL muscle is mainly for plantar-flexion while TA muscle is for dorsi-flexion of ankle joint. **Fig 5.4** shows the ensemble normalised linear enveloped sEMG from these two muscles. For GL

muscle, it only activates approximate 25-55% of gait cycle time, which is during stance time. As mentioned earlier, the dorsiflexion of ankle joint is to propel the upper body forward. This can be achieved by contraction of GL muscle. Similar phenomena can be observed for TA muscle where it only activates during plantarflexion of ankle joint.

5.4 Stroke Gait Data

The gait pattern of 60 stroke patients from Experiment 2 were analysed. The mean and the standard deviation of results from these patients were being compared to the results from healthy subjects. These 60 stroke patients were then further divided into three different subgroups using Hierarchical Cluster Analysis.

5.4.1 Stroke gait spatial-temporal data

One of the temporal features of hemiplegic gait is reduced gait velocity compared to the healthy gait [232]. From **Table 5.3**, the mean gait velocity from 60 stroke subjects was slower than healthy gait velocity (stroke=0.4379m/s; healthy=1.5441m/s). Other studies had reported that the preferred self-selected walking speed of chronic phase stroke patients range from 0.10m/s to 0.76m/s [232,233]. This finding matched the results reported in **Table 5.3**. The decrease of gait velocity have multiple factors, including poor motor recovery, impaired balance, and decrease mucle strength. Decrease in gait velocity has a significant negative effect on a person level of independence.

Besides that, the gait cycle time and stance time were longer than the healthy gait. The swing time was shorter for stroke since they had longer stance. With the paretic limb, less time is spent in stance and more time is spent in swing. This leads to non-paretic limb exhibited a prolonged period of stance and a reduced period of swing. This finding coincided with studies [234,235].

For spatial features, the stride length of stroke patients from both paretic and non-paretic limbs were shorter than healthy (paretic=0.48m, non-paretic=0.48m,

healthy=1.04m). There were many studies with contradic outcomes reported paretic stride length is longer than non-paretic stride length, or vice versa [70]. Studies that stated paretic limb with longer stride length observed that the stroke patients increased propulsion by the non-paretic leg to contribute to an increase in paretic stride length [232] as a type of compensatory strategy. The mean maximum heel clearance had insignificant difference from healthy's result. Maximum heel clearance occurred during mid-swing, which is to prevent foot drag. Foot drag is one of the abnormal gait which will increase the risk of falling among stroke patients.

Table 5.3 Mean, standard deviation and 95% CI of spatial-temporal results from 60 stroke patients. The *p*-value show difference of the results between stroke and healthy subjects.

	Mean	**SD**	**95% CI**		**Comparison with healthy**
Gait Velocity (m/s)	0.4379	0.356	0.393	0.583	p <0.05
	Paretic limb				
Gait Cycle Time (s)	2.13	0.86	1.88	2.37	p <0.05
Stance Time (%)	71.52	10.91	68.39	74.66	p <0.05
Swing Time (%)	28.48	10.91	25.34	31.61	p <0.05
Stride Length (m)	0.48	0.34	0.38	0.57	p <0.05
Max. Heel Clearance (m)	0.11	0.07	0.09	0.13	p =0.9
	Non-Paretic limb				
Gait Cycle Time (s)	2.13	0.87	1.88	2.38	p <0.05
Stance Time (%)	74.52	10.30	71.56	77.48	p <0.05
Swing Time (%)	25.48	10.30	22.52	28.44	p <0.05
Stride Length (m)	0.48	0.40	0.36	0.59	p <0.05
Max. Heel Clearance (m)	0.12	0.08	0.10	0.14	p =0.7

GC= Gait Cycle; ST=Stance; SW=Swing; SL=Step Length; HC= Heel Clearance

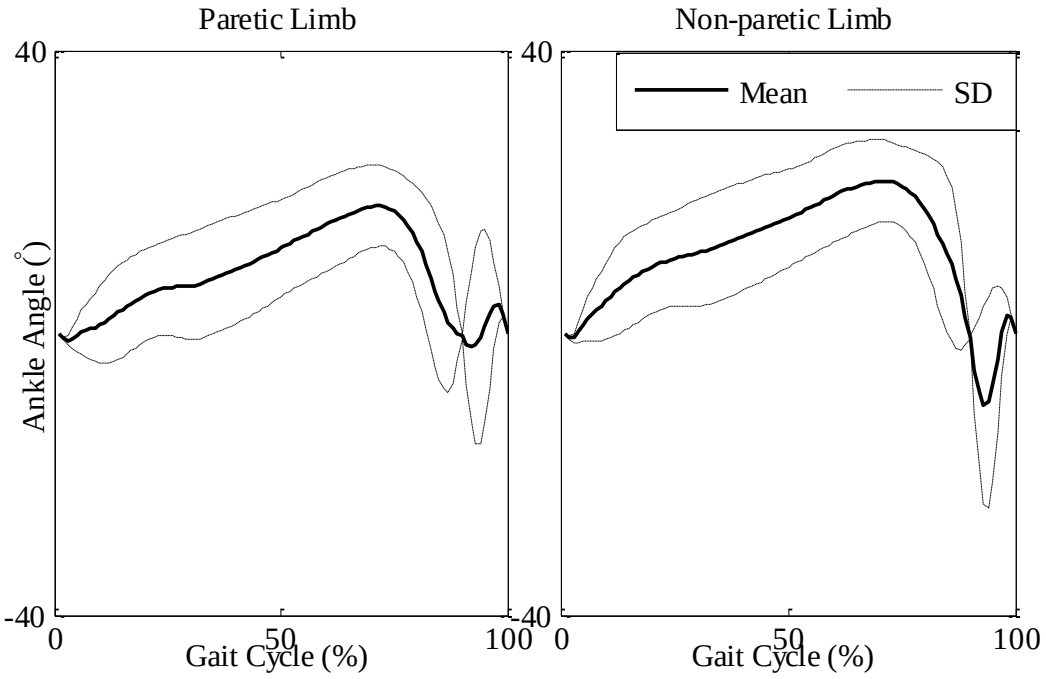

Fig 5.5. Ensemble ankle angle of paretic and non-paretic lower limbs over one gait cycle.

Fig 5.5 shows the mean ankle angle over one gait cycle from 60 stroke patients. The common kinematic disturbances occured during stance phase (heel-strike and toe-off) and swing phase (mid-swing). During stance phase, decreased in plantar flexion can be observed during initial-contact, or heel-strike (0-10% of gait cycle time) and toe-off (70-80% of gait cycle time). Noted the toe-off for these patients was much later compared to the healthy's toe-off. This is due to the prolong stance phase observed among stroke patients. Decreased in plantar flexion at toe-off might be the result of the inability to contract the plantar flexors concentrically with enough tension to overcome the inertia of the remainder of the body [232]. Furthermore, a decrease in the length of plantar flexor muscles after hemiplegic stroke is likely to reduce the ability of the plantar flexor muscles to contract and generate enough force [231]. Moreover, there was decrease in dorsi-flexion from toe-off to mid-swing (80-90% of gait cycle time). This lack of dorsi-flexion at this period leads to ankle joint unable to return to its neutral position, hence foot drop happened.

5.4.2 Gait characteristic of stroke patients in different subgroups

Since the results from **Table 5.3** came from a wide variation of stroke patients with their own preferred self-selected speed, it is necessary to divide these patients into different homogeneous subgroups. This is to ensure a fair comparison with healthy data. To achieve that, these 60 stroke patients were divided into three different subgroups using Hierachical Cluster Analysis. Three cluster of gait patterns were identified and there were shown in **Table 5.5**. In this table, the mean and standard deviation of spatial-temporal results from three differenct subgroups of stroke are presented.

The three identified subgroups can be named based on their most significant features; Group 1 (Fast) had the fastest gait velocity (0.45m/s). Group 2 (Moderate) had moderate gait velocity (0.30m/s) with a motion pattern similar to Group 1 except for greater ankle dorsiflexion during mid-swing. Group 3 (Slow) had the slowest velocity (0.21m/s) and inadequate ankle dorsiflexion during mid-stance (3.50°).

Group 1 subjects had shortest stance phase (65.97%) and longest swing phase (34.03%), which is very similar to healthy gait. The gait pattern of this group is similar to the fast group in previous studies [26, 27]. The greater gait velocity of this group was due to them having the greatest stride length (0.61m) among the three groups. Group 2 subjects had very similar stance and swing phase to Group 1 (66.63 and 33.37% respectively). The gait characteristics of this group were similar to the moderate gait velocity group in [26] and Mulroy *et al* [27]. The slower gait velocity appears to be a result of having shorter stride length (0.47m) despite similar gait cycle time (1.78s) compared to Group 1 subjects (1.71s). This walking group also demonstrated the greatest dorsiflexion angle at swing phase (5.35°), which probably is the compensatory strategy to prevent foot drag and increase heel clearance during swing phase (0.10m). Group 3 subjects appeared to be the most severe stroke subjects as they had the longest stance time and shortest swing time (77.44 and 22.56% respectively). This group had gait pattern characteristics similar to the slowest gait velocity group in Kinsella and Moran [26] and Mulroy *et al* [27].

The main reason they had the slowest gait velocity is due to shortest stride length (0.44m) and longest gait cycle time (2.56s). Furthermore, the lowest ankle dorsiflexion angle during mid stance (3.50°) had limited the forward motion of upper body. This may lead to shorter step length in contralateral limb (non-paretic limb).

Fig 5.6 presents box-and-whisker plot of eight spatial-temporal parameters and joint kinematics at sagittal plane with different stroke patient and healthy subgroups. The median, inter-quartile range and 95% confidence interval are shown in these plots. Unpaired *t*-test showed significant difference between parameters from each subgroup of stroke patients and healthy beside ankle dorsi and plantarflexion during mid-stance and toe-off (see **Table 5.5**). One-way ANOVA analysis shows significant difference between each cluster subgroup for ankle angle dorsiflexion at mid-stance, stride length and gait velocity.

Table 5.4 illustrates that profound overall temporal asymmetry can be found in many stroke patients classified as independent ambulators. Overall, the spatial-temporal asymmetry increased from Group 1 to Group 3. High spatial asymmetry indicates stride length from one lower limb is much longer than the other. This will create an inbalance posture. Patterson *et al* [236] stated that 55.5% of a group of poststroke subjects exchibited high temporal gait asymmetry while only 33.3% of the same group of poststroke subjects had spatial gait asymmetry. Spatial gait asymmetry only appears more likely in stroke patients who exhibit severe temporal asymmetry compared with survivors who fall in the mild asymmetry or normative symmetry groups.

Table 5.4. Mean and standard deviation of Robinson Symmetry Index from three different group of stroke patients.

	Group 1	Group 2	Group 3
SL Symmetry	0.81	6.82	7.32
HC Symmetry	4.35	9.09	5.26
GC Symmetry	1.18	1.14	1.99
ST Symmetry	1.04	2.74	3.18
SW Symmetry	1.81	5.95	9.58

Table 5.5. Mean, standard deviation and 95% CI of spatial-temporal results from three differenct groups of stroke patients. The *p*-value show difference of the results between stroke and healthy subjects.

	Stroke	**Healthy**	***P* value**	**Stroke**	**Healthy**	***P* value**
			Group 1 (Fast) (*n*=31)			
Gait Velocity(m/s) [1]			0.45			
		Paretic limb			Non-Paretic limb	
Stride length (m) [1]	0.61	0.9234	<0.05	0.62	0.9234	<0.05
Max. Heel Clearance (m)	0.12	0.1028	<0.05	0.11	0.1028	<0.05
Gait Cycle Time (s)	1.71	1.235	<0.05	1.67	1.2333	<0.05
Stance Time (%)	65.97	56.60	<0.05	64.61	57.44	<0.05
Swing Time (%)	34.03	43.40	<0.05	35.39	42.56	<0.05
Ankle Dorsiflexion Angle at Mid-stance (°)[1]	13.08	12.33	=0.38	27.78	12.33	<0.05
Ankle Plantarflexion Angle at Toe-off (°)	-0.36	-3.76	=0.12	-1.07	-3.76	=0.22
			Group 2 (Moderate) (*n*=13)			
Gait Velocity (m/s) [1]			0.30			
		Paretic limb			Non-Paretic limb	
Stride length (m) [1]	0.47	0.9234	<0.05	0.41	0.9234	<0.05
Max. Heel Clearance (m)	0.10	0.1028	<0.05	0.12	0.1028	<0.05
Gait Cycle Time (s)	1.78	1.235	<0.05	1.74	1.2333	<0.05
Stance Time (%)	66.63	56.60	<0.05	70.38	57.44	<0.05
Swing Time (%)	33.37	43.40	<0.05	29.62	42.56	<0.05
Ankle Dorsiflexion Angle at Mid-stance (°)[1]	8.51	12.33	<0.05	10.32	12.33	=0.23

Ankle Plantarflexion Angle at Toe-off (°)	-0.37	-3.76	<0.05	-1.32	-3.76	=0.14
	Group 3 (Slow) (*n*=16)					
Gait Velocity (m/s) [1]	0.21					
	Paretic limb			Non-Paretic limb		
Stride length (m) [1]	0.44	0.9234	<0.05	0.38	0.9234	<0.05
Max. Heel Clearance (m)	0.10	0.1028	<0.05	0.09	0.1028	<0.05
Gait Cycle Time (s)	2.56	1.235	<0.05	2.46	1.2333	<0.05
Stance Time (%)	77.44	56.60	<0.05	72.66	57.44	<0.05
Swing Time (%)	22.56	43.40	<0.05	27.34	42.56	<0.05
Ankle Dorsiflexion Angle at Mid-stance (°)[1]	3.50	12.33	<0.05	9.07	12.33	=0.06
Ankle Plantarflexion Angle at Toe-off (°)	-1.34	-3.76	<0.05	-0.50	-3.76	<0.05

[1]Indicates significant difference inter-subgroup (*p*-value<0.05)

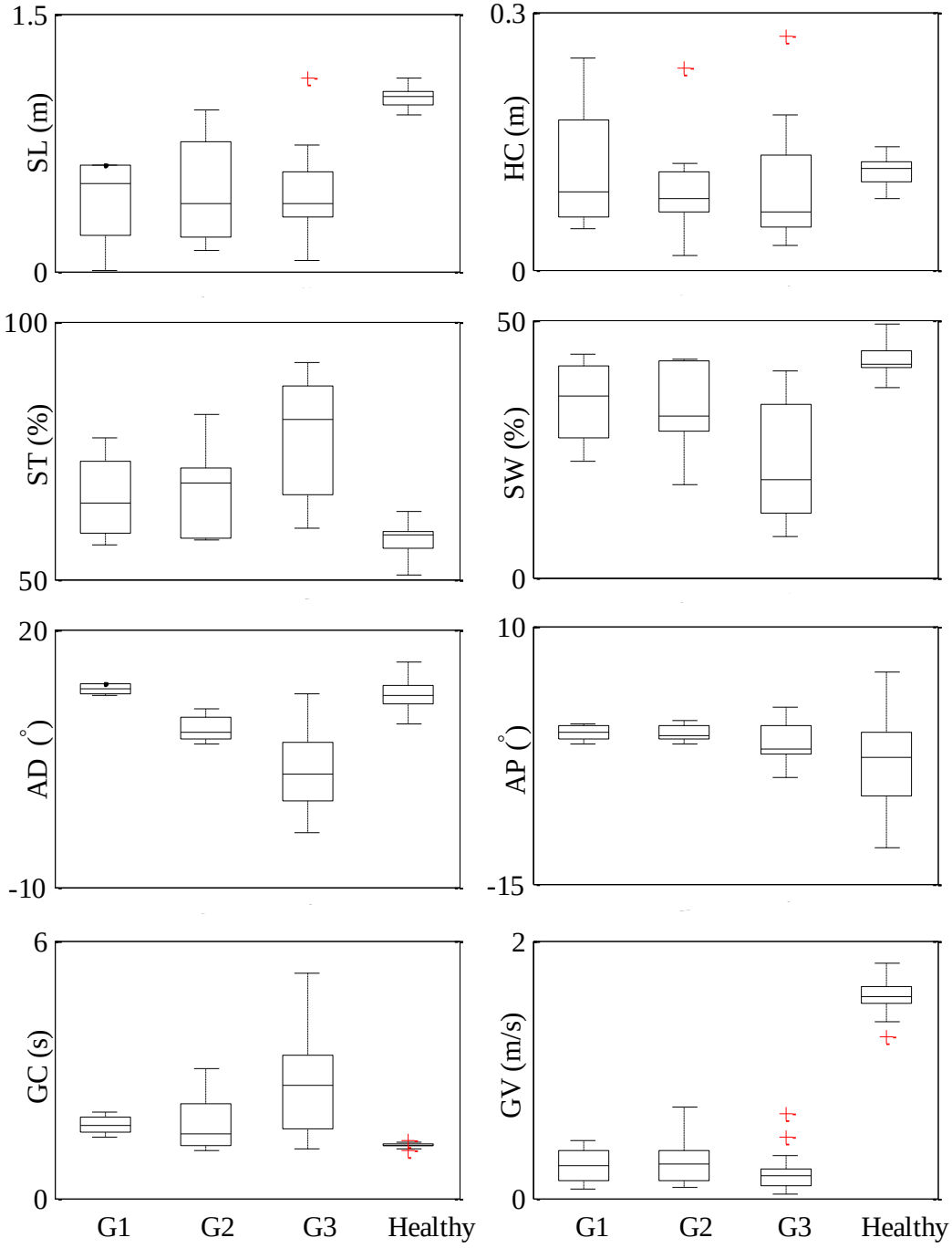

Fig 5.6. Box-and-whisker plots of spatial-temporal parameters and joint kinematics with 95% CI for the median of different cluster subgroups patients and healthy subjects. SL-Stride length, HC-Heel clearance, ST-Stance time, SW-Swing time, AD-Ankle dorsiflexion at mid-stance, AP-Ankle plantarflexion at toe-off, GC-Gait cycle time, GV-Gait velocity.

5.4.3 Stroke gait sEMG data

The phasic patterns of the muscles in GL and TA muscles of stroke patients are significantly different compared to those healthy subjects. The amplitudes in these results are meaningless since they cannot compare inter-subject.

In Olney *et al* [6] review, there were generally 4 types of stroke's gait sEMG pattern (Type I, Type II, Type III and Type IV). **Fig 5.7**, **Fig 5.8** and **Fig 5.9** show GL and TA muscles ensemble sEMG from three different subjects over one gait cycle. These three subjects were randomly selected from the subgroups from cluster analysis. The details of these patients were described as follow.

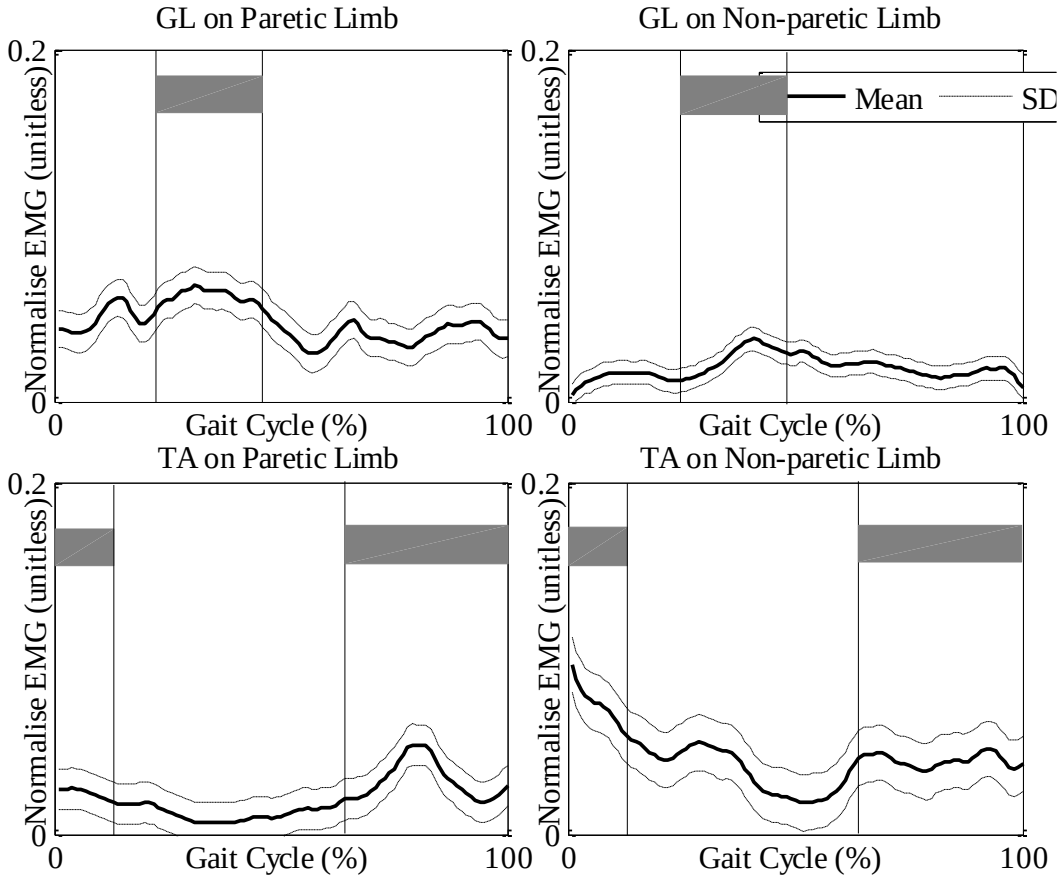

Fig 5.7. **Ensemble normalise linear enveloped sEMG of GL and TA muscles of both paretic and non-paretic lower limbs from one subject demonstrates Type I disorder, over one gait cycle. Grey shaded area indicates the muscle activation timing from healthy subject with respective muscles.**

The patient in **Fig 5.7** was from Group 1, demonstrated typical Type I disorder where the GL muscle on the paretic limb showed hyperactive stretch reflexes, and the premature activation before the healthy onset (25-55% of gait cycle time) and duration.

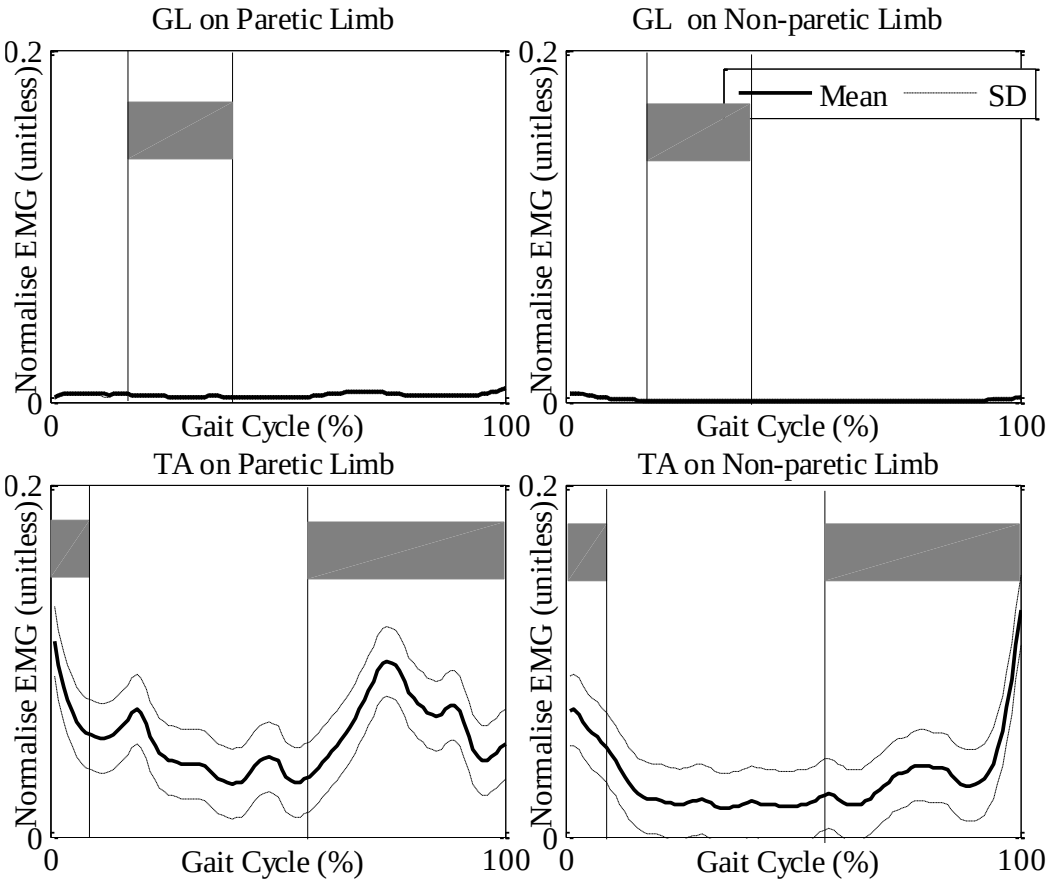

Fig 5.8. Ensemble normalise linear enveloped sEMG of GL and TA muscles of both paretic and non-paretic lower limbs from one subject demonstrates Type II disorder, over one gait cycle. Grey shaded area indicates the muscle activation timing from healthy subject with respective muscles.

Meanwhile, the patient in **Fig 5.8** was from Group 2, showed lack of activation in GL muscles in both paretic and non-paretic limb. Lack of GL muscle contraction leads to lack of plantar-flexion during stance phase, and ankle joint cannot propel the upper body forward. Besides that, it also causes decrease in step length in contralateral limb. This can be compensated by knee hyperextension, providing a stable limb for weight bearing [237].

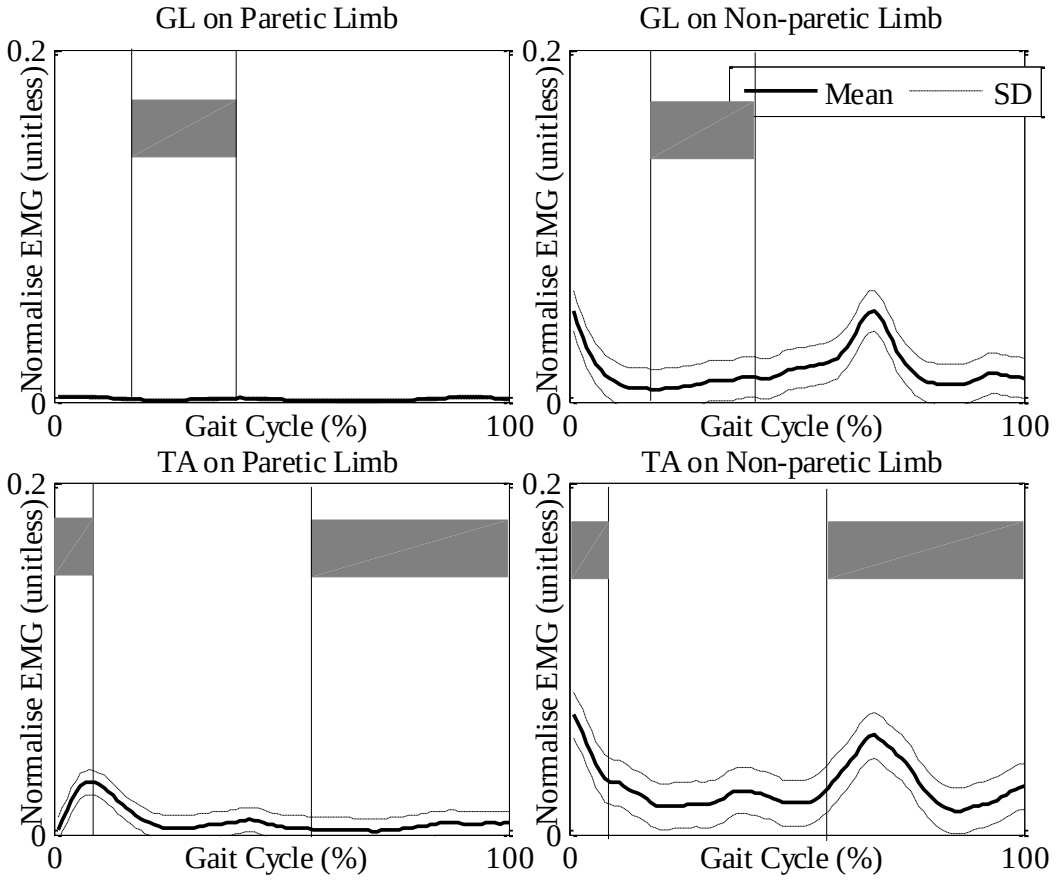

Fig 5.9. Ensemble normalise linear enveloped sEMG of GL and TA muscles of both paretic and non-paretic lower limbs from one subject demonstrates Type IV disorder, over one gait cycle. Grey shaded area indicates the muscle activation timing from healthy subject with respective muscles.

The patient in **Fig 5.9** was from Group 3, presented typical Type IV, where coactivation on non-paretic limb was observed, and lack of activation occurred on GL muscle on paretic limb. A peak was observed around 65% of gait cycle time on both GL and TA muscles, indicating coactivation from both muscles. Coactivation from TA and GL mucsles will leads to counteracting each other, and it will limit the ankle joint range of motion.

5.4.4 Correlation between spatial-temporal data with TUG and Gait Velocity

The correlation between spatial-temporal parameters and gait asymmetry index with TUG score and gait velocity were investigated in this section. Both TUG score and gait velocity are always used as indicators to classify hemiplegia patients into different gait deficiencies [259]. It is important for physiotherapists to understand the gait dysfunction level so that they can arrange suitable rehabilitation.

Fig 5.10 shows scatter plots of different spatial-temporal parameters to TUG score and gait velocity respectively. In this figure, the Pearson Correlation Coefficient shows poor correlation between all parameters and TUG score (r=-0.431, -0.466, 0.541, 0.127 and -0.127 for stride length, heel clearance, gait cycle time, stance time and swing time respectively. However, in contrast, it shows most spatial-temporal parameters were highly correlate to gait velocity (r=0.700, -0.713 and 0.713 for stride length, stance time and swing time respectively) but not for heel clearance and gait cycle time (r=0.374 and -0.321 respectively). The reason most parameters were not highly correlate to TUG score is because these parameters were obtained in just one gait cycle over the sagittal plane only. Meanwhile, TUG score consists of multiple task, which includes standing, walking, turning and sitting. Therefore, it leads to poor correlation. On the other hand, stride length, stance time and swing time were highly correlate to gait velocity but not heel clearance and gait cycle time. Greater stride length indicates greater step length, which is crucial in determining gait velocity. The heel clearance is the vertical distance between heel and ground; therefore, it has less impact on the gait velocity. Meanwhile, the poor correlation between gait cycle time and gait velocity suggested that some stroke patients who had short gait cycle time come with even shorter step length. This is probably a compensatory mechanism to reduce the step length and improve balance during walking to prevent fall.

Fig 5.11 shows scatter plots of different Robinson Index to TUG score and gait velocity respectively. In this figure, the Robinson Index with different inputs show poor correlation to both TUG score and gait velocity. This can be due to several factors, (i) low sensitivity using conventional asymmetry indices (in this case Robinson Index) [31], (ii) univariate asymmetry measurement lack the ability to

capture the complexity of gait cycle [101]. Our results were similar to Patterson *et al* [238] report. Both studies shows poor correlation between asymmetry index and gait velocity. Patterson *et al* [239] explained that gait velocity is more strongly associated with gait phases of the non-paretic limb than paretic limb. This may reflect adaptive behaviours of the non-paretic limb that compensate for the paretic limb [240]. Once the behavioural compensation have been developed, it is possible that stroke patients have varied in gait asymmetry but not gait velocity.

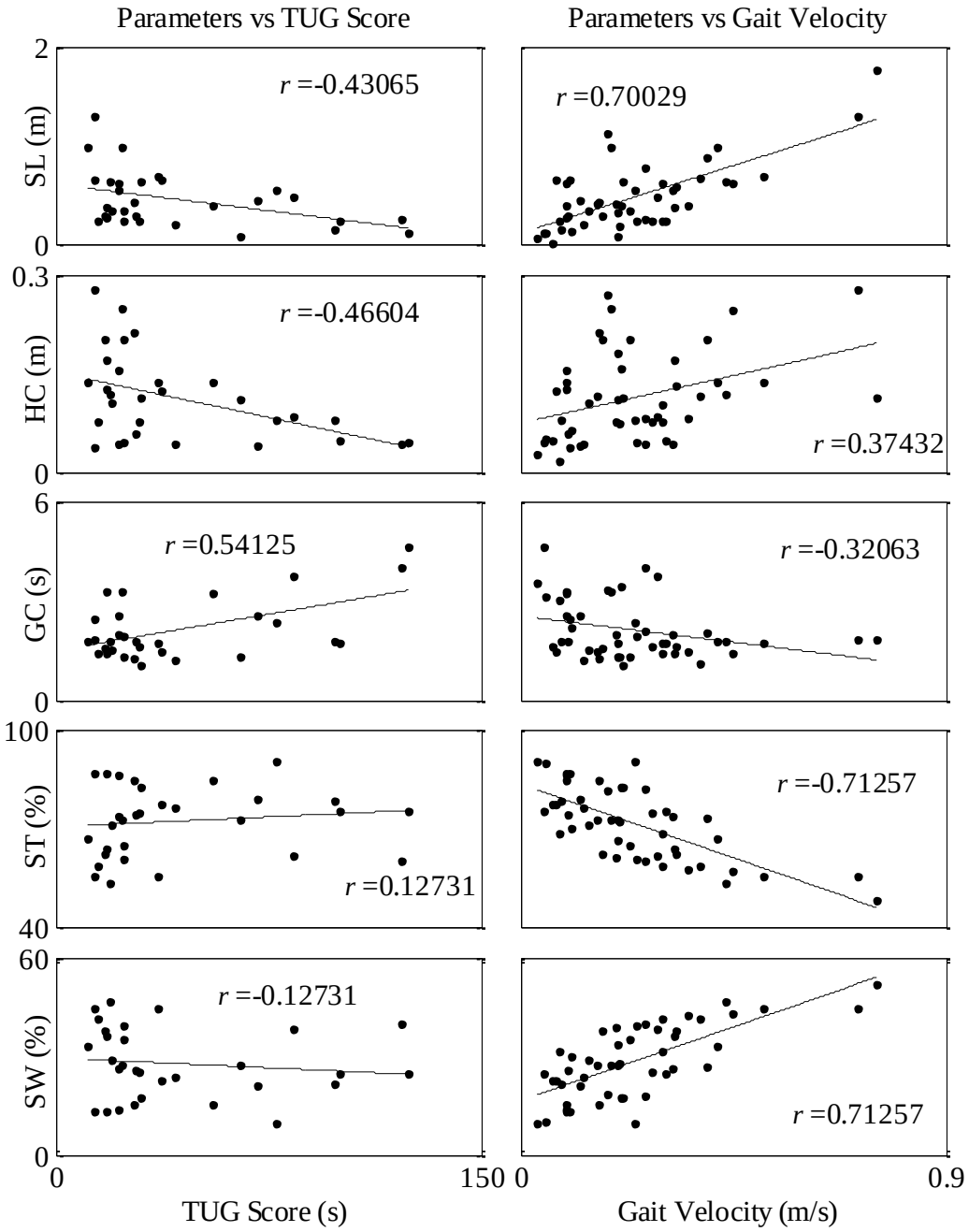

Fig 5.10. Scatter plot of spatial-temporal parameters to TUG score and gait velocity respectively. Pearson correlation were found on each results and a best-fit line was plotted. (SL=stride length; HC=Heel clearance; GC=Gait cycle time; ST=stance time, SW=swing time).

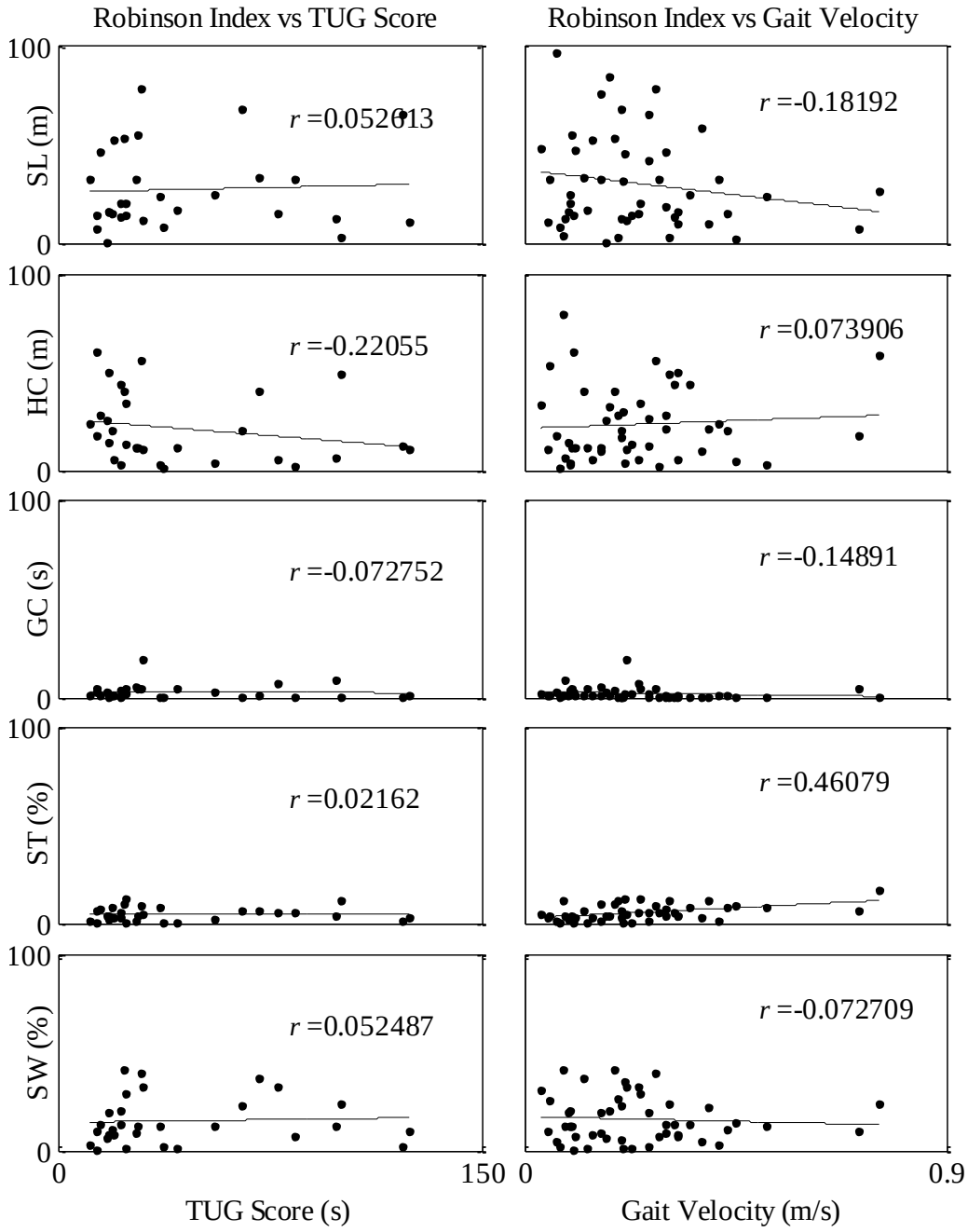

Fig 5.11. Scatter plot of Robinson Index to TUG score and gait velocity respectively. Pearson correlation were found on each results and a best-fit line was plotted. (SL=stride length; HC=Heel clearance; GCT=Gait cycle time; STT=stance time, SWT=swing time).

5.5 Chapter Summary

In this chapter, the conventional gait analysis was performed on both healthy and stroke patients. The healthy normal gait characteristics were discussed in detail. After that, the gait pattern of a large group of stroke patients were classified into three different homogeneous subgroups using Hierarchical Cluster Analysis. One-way ANOVA analysis showed significant difference between each subgroups. Furthermore, the gait patterns of each of these subgroups were compared to healthy one using unpaired *t*-test. Most parameters showed significant difference between stroke patient subgroups and healthy group. Moreover, the muscle impairments on these three subgroups were presented and they were described in term of their temporal information. Meanwhile, only certain spatial-temporal parameters (stride length, stance time and swing time) were highly correlate to gait velocity but not TUG score. Gait asymmetry index using Robinson Index showed poor correlation to TUG score and gait velocity.

This chapter showed some limitations from current conventional gait analysis:

i. Poor correlation between gait parameters and TUG score.
ii. Poor sensitivity of gait asymmetry indices.
iii. The selection of multiple inputs of gait parameters for classification is often subjective.
iv. Linear envelope of sEMG signal provides limited information (temporal information only) without further processing.

Therefore, the following chapters in this thesis will be focusing on improving these limitations. Based on these limitations, new kinesiology and kinematic gait analysis techniques are proposed. Resolving these issues will provide a better insight in gait analysis, which will benefit the study in observing gait recovery in the later chapter.

Chapter 6 Kinesiology based gait analysis- A new fractal-based kinetic index to characterise gait after stroke

6.1 Introduction

SEMG has been widely used by researchers to perform gait analysis. Raw sEMG signal provides minimal to none information without any analytic signal processing techniques. Amplitude and temporal analysis of sEMG often require the computation of the signal's linear envelope. As mentioned in Chapter 4, linear envelope of sEMG provides very limited information (such as onset timing, duration and amplitude) without any further processing. Conventional linear envelope of sEMG signal could be characterised by techniques involving time and frequency domain analysis. These methods reveal specific properties in the linear system context. However, sEMG signal is nonlinear in nature [241]. As mentioned previously, early researchers reported chaotic-liked behavior in sEMG [193, 194]. Among them, fractal analysis is one the common approach to determine non-linear characteristics of sEMG signals.

The application of fractal analysis in stroke patients are relatively limited. This could be attributed to the requirement of analysing long time-series [242,243]. Nevertheless, this technique shows great potential as a quantitative gait assessment tool for neurological pathologies [243]. The correlation between sEMG and clinical assessment tools such as Timed Up and Go score is not well known. We aim to investigate the feasibility of applying fractal analysis on sEMG signals from stroke patients to characterise their gait deficits and to classify the gait deficits based on their TUG score.

In Chapter 5, gait classification is performed by using Hierarchical Cluster Analysis. We adopted multiple gait parameters as the inputs to classify the stroke patients into homogeneous subgroups. However, the selection of inputs can be very

subjective and generally based on observation by visual inspection from researchers or clinicians [27]. Meanwhile, single category of parameter often yielded functionally heterogeneous results [27]. Therefore, it is worth applying this classification method (Hierarchical Cluster Analysis) to classify stroke patients based on the fractal features mentioned earlier and compared it to conventional classification results. The aims of this chapter are:

1. To formulate a new sEMG based index (Kinetic Index) that is highly correlate to TUG score.
2. To classify the gait pattern of stroke subjects into homogeneous subgroups using different approaches.

6.2Theory

6.2.1 Higuchi Fractal Dimension (HFD)

In this study, Higuchi algorithm [207] is used and it is briefly described as follows:

Consider a sEMG time series $x(t) = x(1), x(2), \dots, x(N)$, where N is the total number of samples in the time series. A total of k new time series x_m^k, are constructed and defined as Eq (6.1):

$$x_m^k : x(m), x(m+k), x(m+2k), \dots, x\left(m + \left[\frac{N-m}{k}\right] \cdot k\right) \quad (m = 1,2, \dots, k) \quad (6.1)$$

where m and k are integer numbers which represent the initial time and the interval time respectively, [■] indicates the integer part of the expression. The length of the curve x_m^k is computed as Eq (6.2):

$$L_m(k) = \left\{ \left(\sum_{i=1}^{\left[\frac{N-m}{k}\right]} |x(m+ik) - x(m+(i-1)\cdot k)| \right) \frac{N-1}{\left[\frac{N-m}{k}\right] \cdot k} \right\} \Big/ k \qquad (6.2)$$

Where $\frac{N-1}{\left[\frac{N-m}{k}\right] \cdot k}$ is the normalisation factor for the curve length of the new time series x_m^k.

The length of curve for $x(t)$, $L(k)$ is obtained by averaging all $L_m(k)$, where m =1,2,…,k. If $L(k)$ is proportional to $\frac{1}{k^D}$ then the EMG time series has a fractal dimension of D. This could be done by plotting ln($L(k)$) against ln(1/k), where k =1,2,…k_{max} and the slope would be D.

6.2.2 Sliding window approach on HFD

In Section 6.2.1, HFD is described to compute the whole sEMG time series and only return one value. To obtain the temporal evolution, a sliding window approach on HFD could be computed. This sliding window approach separates the initial signal with N points into w point's windows as described by Eq (6.3):

$$\begin{aligned} &x(1), x(2), \dots, x(w) \\ &x(2), x(3), \dots, x(w+1) \\ &x(3), x(4), \dots, x(w+2) \\ &\vdots \\ &x(N-w+1), x(N-w+2), \dots, x(N) \end{aligned} \tag{6.3}$$

In each sliding window, the HFD could be computed using the procedures described in Section 6.2.1, where the sample size is now the window length w in Eq (6.4) and (6.5):

$$x_m^k : x(m), x(m+k), x(m+2k), \dots, x\left(m + \left[\frac{w-m}{k}\right] \cdot k\right) \quad (m = 1,2,\dots,k) \tag{6.4}$$

$$L_m(k) = \left\{ \left(\sum_{i=1}^{\left[\frac{w-m}{k}\right]} |x(m+ik) - x(m+(i-1)\cdot k)| \right) \frac{w-1}{\left[\frac{w-m}{k}\right] \cdot k} \right\} \Big/ k \tag{6.5}$$

Fig 6.1 describes the sliding window concept in a graphical way. In this study, the HFD of stroke subject's sEMG in a gait cycle is computed using this approach. The k_{max} and w values are 5 and 10 respectively. To determine k_{max}, HFD of the data is computed with a range of k_{max} values. The values of HFD are then plotted against k_{max}, and the point of saturation in the graph is selected as the final k_{max} value [244,245]. For the sliding window w, we selected the lowest possible value to reduce the sample lost in F. The w value lower than 10 will generate false fractal dimension peaks as seen in **Fig 6.2**. On the other hand, high w will lead to smoother

HFD time series, which the correct peaks will not reveal. The rationale of choosing *w* value is similar to other researches [246,247].

6.2.3 Fractal properties in sEMG

To test the practicality of sliding window HFD, a preliminary investigation on the fractal properties of sEMG signal from stroke patients was conducted. A sliding windowed HFD from the Gastrocnemius Lateral (GL) sEMG signal for one gait cycle is computed following the methods described in Section 6.2.2. This is shown in **Fig 6.2**. Results showed that there are higher fluctuations in HFD time histories of stroke subjects as their TUG scores increase (from 15.6 s – 98 s). Nevertheless, the complexity of HFD time histories for subjects with high TUG scores was different from those with low TUG scores. The number of peaks, *NP* is increasing with increase of TUG score. This suggests sliding windowed HFD could be a good indicator. However, the result of HFD on single muscle is not sufficient to differentiate the stroke patients effectively as observed in **Fig 6.3**. The average number of peak computing from single muscle for 30 stroke patients is presented in **Fig 6.3** upper row and the average for different TUG score group is shown **Fig 6.3** bottom row. High correlation coefficient (0.8046) can be observed in the result from **Fig 6.3** upper row. However the correlation coefficient from individual group is relatively low for TUG score group of below 20s, between 20 to 30s and above 30s (0.4403, 0.6919 and 0.7217 respectively). The model should be refined to reveal a better picture.

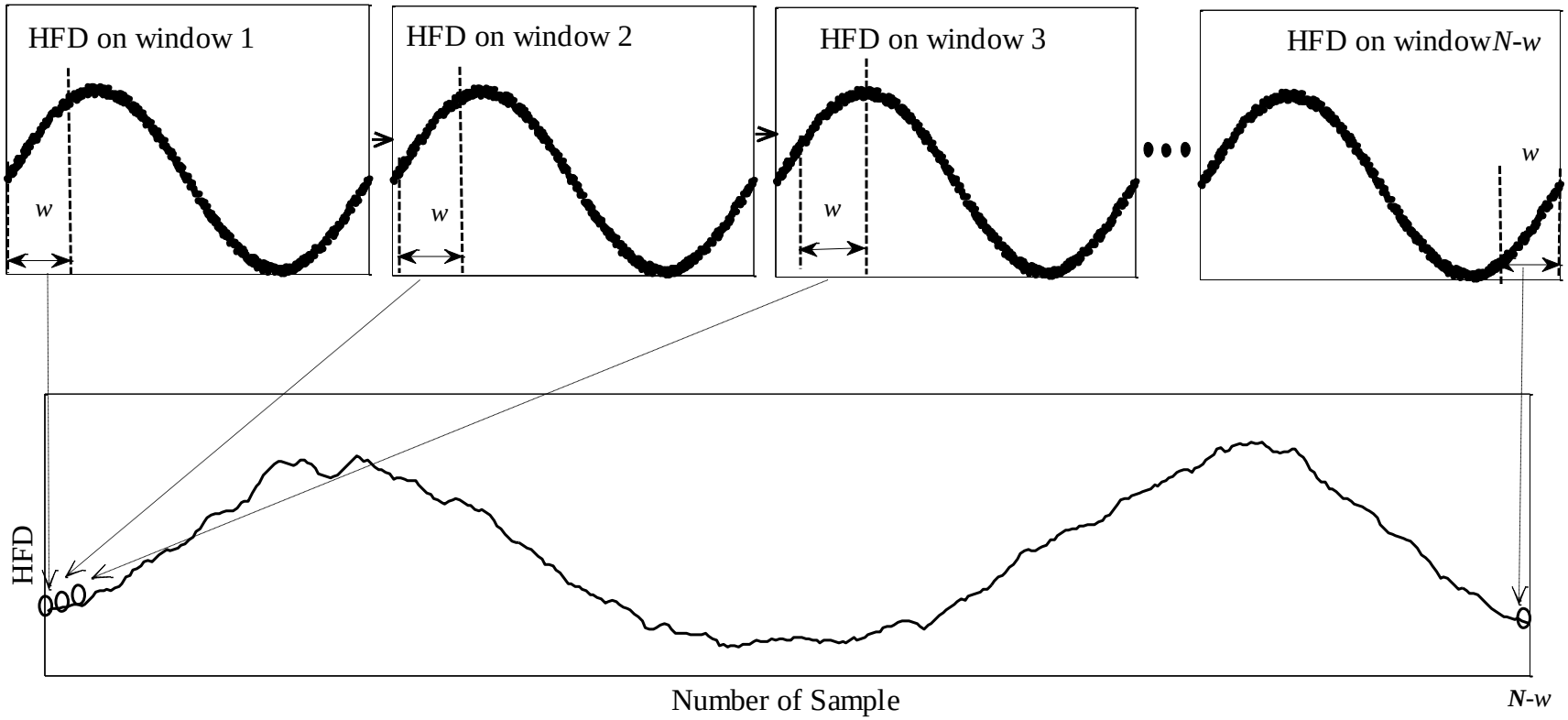

Fig 6.1. Graphical representation of sliding window approach to determine HFD on a signal.

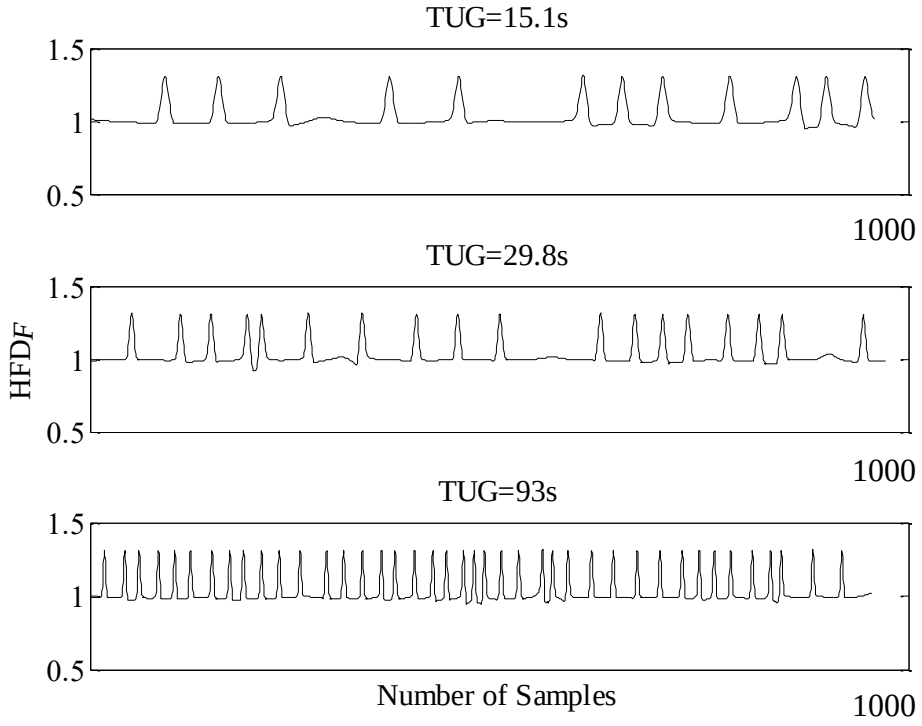

Fig 6.2. Time histories of HFD from GL muscle, acquired from three stroke patients with different TUG scores.

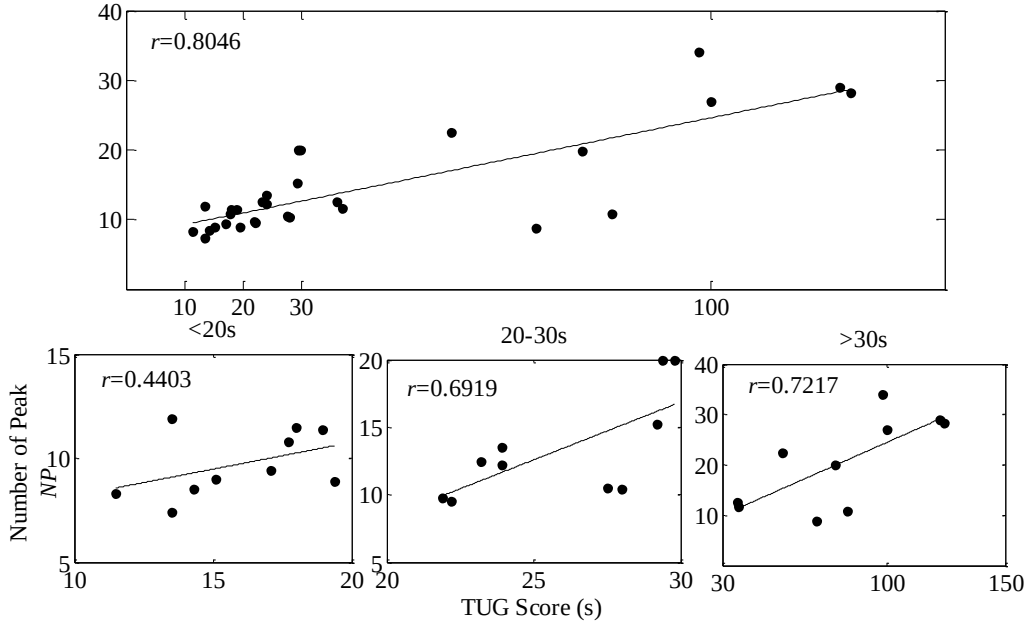

Fig 6.3. Scatter plot of *NP* against TUG score with its best-fit line with correlation coefficient, *r* of 0.8046 on upper row. Scatter plot of *NP* from category of TUG score below then 20s, between 20-30s and above 30s against TUG score with its best-fit line with correlation coefficient of 0.4403, 0.6919 and 0.7217 respectively on bottom row.

6.2.4 Kinetic Index

The issue addressed in Section 6.2.3 suggested that single fractal property (number of peak) on single muscle is not sufficient to draw correlation to TUG score. Therefore, a new kinetic index (K.I.) comprises of multiple fractal properties of sEMG signals is proposed in this study. Both Tibialis Anterior (TA) and Gastrocnemius Lateral (GL) muscle signals are used since these two agonist and antagonist muscles mainly contribute to walking. K.I. consists of the average fractal properties from both TA and GL muscles from both legs.

$$\text{K.I.} = \frac{\sum_{i,j} \sigma_{i,j}}{2n}, (i = \text{TA,GL}), (j = \text{left,right}) \tag{6.6}$$

where *n* is the number of muscles investigates. In our study, *n* is two as TA and GL muscles are studied here.

σ_i in Eq (6.6) is derived from the fractal properties of sEMG during gait. A HFD time series *F* can be computed from the sliding windows of both TA and GL sEMG during gait. The temporal evolution of fractal dimension can then be obtained. Next, two features are extracted from *F* to form σ_i. One feature is number of peaks *NP* and the second feature is the area of peaks *AP* in the time series *F*.

Fig 6.4 illustrates an example of sliding window HFD time series *F* of a sEMG. In this figure, the circle indicating the local maxima and the square indicates the local minima. The first fractal properties feature, number of peaks, *NP* can therefore be obtained by counting the number of local maxima. To acquire the second feature the area of peaks *AP*, the first step is to determine the average of local minima. The area under the graph between the curve and the straight line formed by the average local minima is then computed.

$$AP_{i,j} = \int_{1}^{N-w} F dt - \big(S \cdot (N-1)\big) \tag{6.7}$$

where *S* is the average of local minima. The fractal property $\sigma_{i,j}$ of each muscle is therefore defined as:

$$\sigma_{i,j} = AP_{i,j} + NP_{i,j} \tag{6.8}$$

The prominence and width of the peak are defined as:

$$PN = PH - S \tag{6.9}$$

where *PN* is the prominence, *PH* is the peak height. As observed in **Fig 6.5**, each prominence is different from peak to peak. In this diagram, one peak height is 1.399 and the other peak height is 1.385, which leads to different *AP* in Eq (6.8). Each of this peak contains two local minima and one local maxima as shown in the enlarged diagram in **Fig 6.4** (with square indicating local minima and circle indicating local maxima). The distance from the first local minima (first square) to the next local minima (second square) in this enlarged diagram is equal to the sliding window length *w*. As seen in **Fig 6.5**, both peaks are caused by the sudden change of slope in sEMG signal. When there is no change in the slope of sEMG signal, it results in relatively flat straight line in *F*. The peak HFD value in *F* depends on the variation in slope of sEMG signal.

Fig 6.6 illustrates the flow chart to compute Kinetic Index.

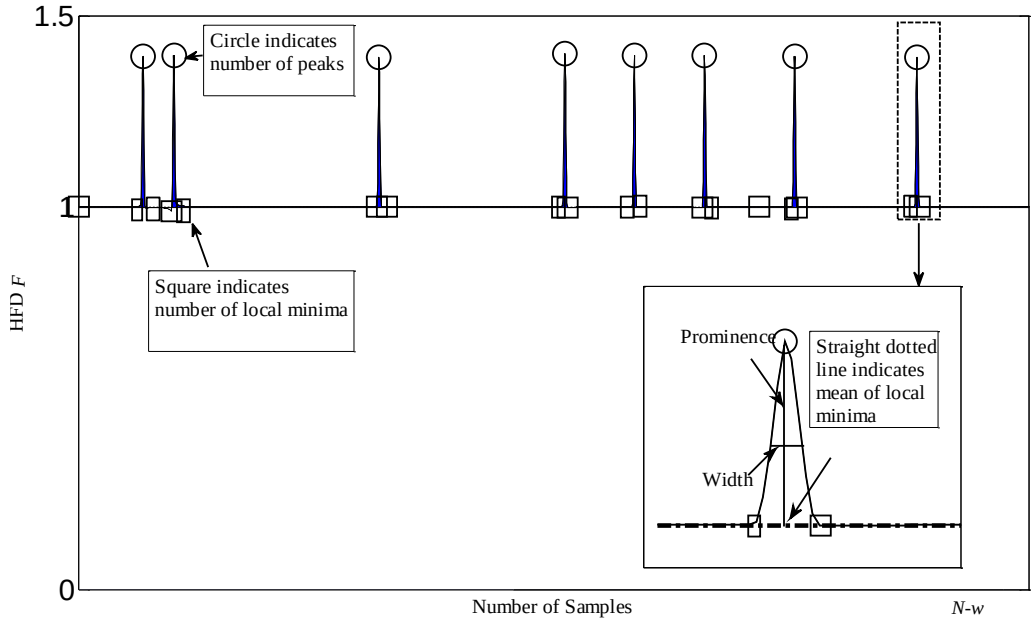

Fig 6.4. Graphical illustration of the computation of fractal properties $\sigma_{i,j}$.

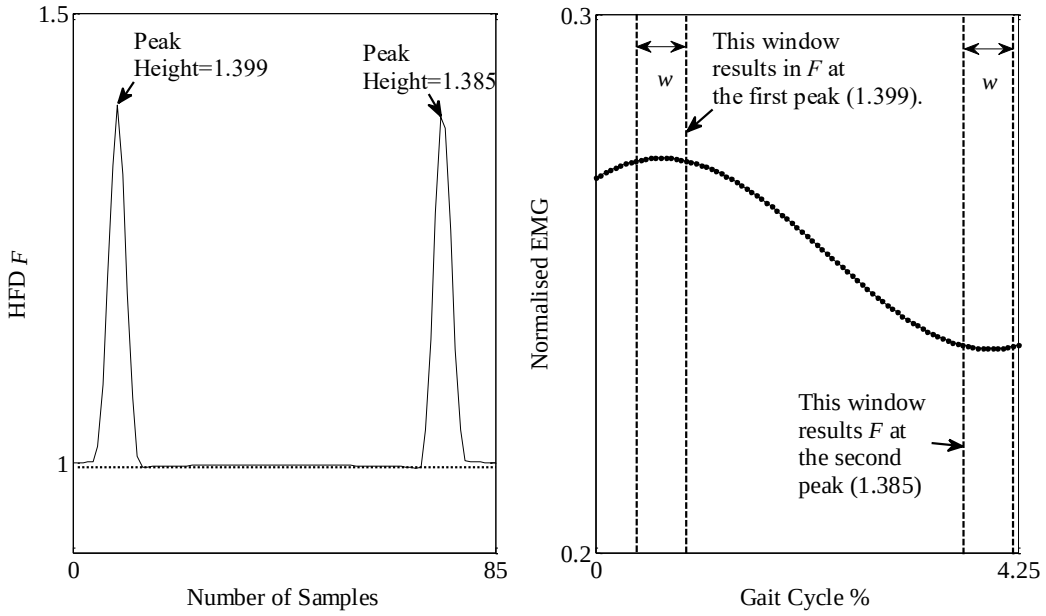

Fig 6.5. An example of a small segment of HFD time series *F* with its corresponding sEMG from GL muscle. 85 samples in *F* corresponds to 4.25% of gait cycle in sEMG signal.

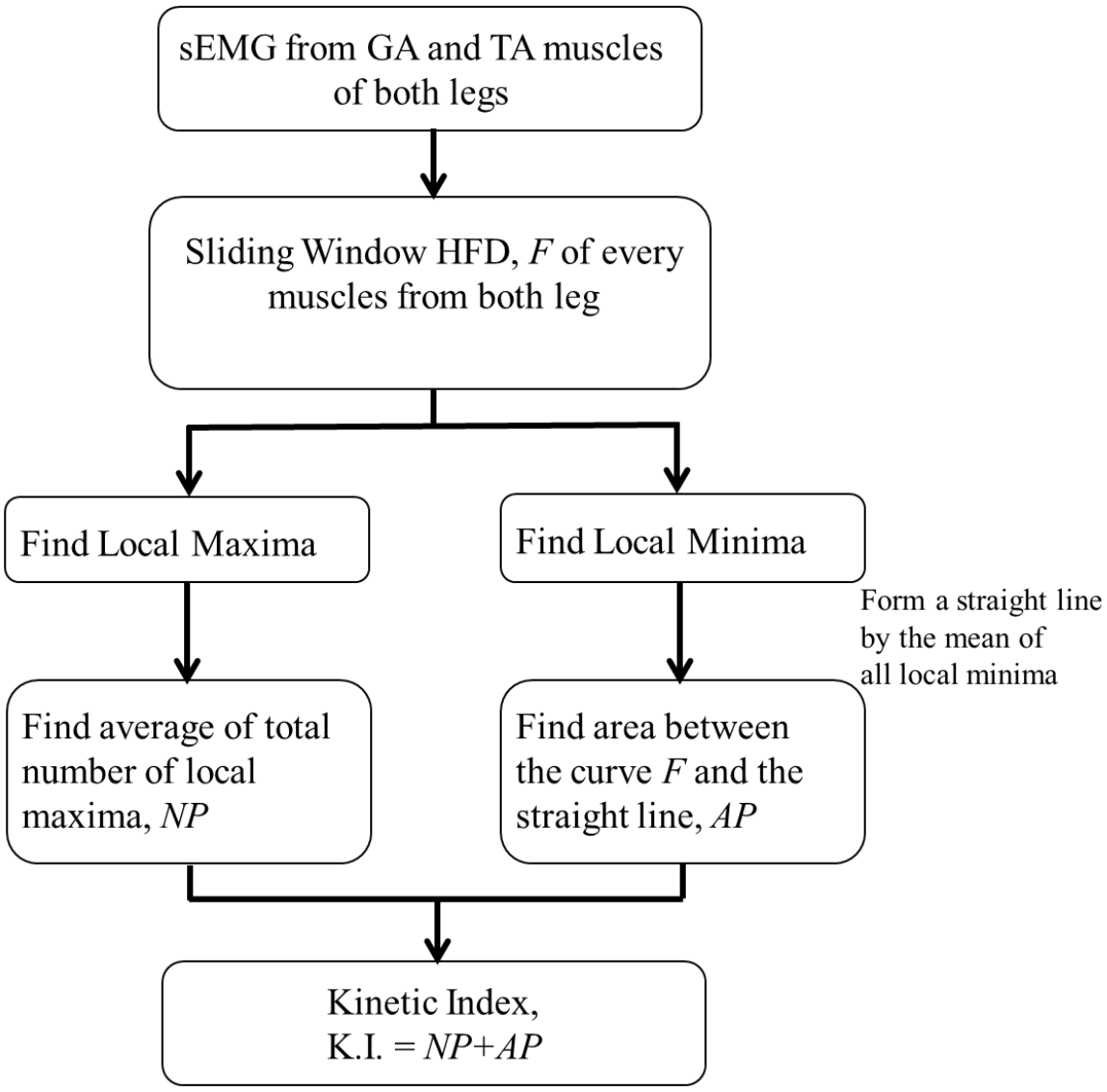

Fig 6.6. Flow chart to determine Kinetic Index K.I. from the raw gait's sEMG.

6.3 Experiment Procedure

The sEMG data from 30 stroke patients from Experiment 2 as mentioned in Chapter 2 were analysed. These 30 stroke patients took part in TUG test. They were further categorised into three different groups according to their TUG scores, with 10 subjects in each group. The first group contained stroke subjects of TUG scores from 10-19s, the second group TUG scores from 20-29s and the third group TUG scores 30s and above (TUG < 20 s, 20 s < TUG < 30 s and TUG > 30 s). The demographic of these 30 stroke patients is shown in Chapter 2.

Linear envelope of sEMG was acquired according to the procedure in Chapter 3. This sEMG envelope was further processed to determine the K.I. as described in Section 5.2. Correlation coefficient *r* was computed to determine the correlation between K.I. and TUG scores. One-way ANOVA analysis was used to compare the differences in the K.I. values across these three groups. A Tukey Post- Hoc analysis was performed to determine which of these three groups were significantly different from each other. SNR of each individual stroke patients is determined by:

$$SNR_{dB} = 20\left(log_{10}\left(\frac{RMS_{Signal}}{RMS_{Noise}}\right)\right) \tag{6.10}$$

where SNR_{dB} is the SNR with unit dB, RMS_{Signal} and RMS_{Noise} are the root mean square of the sEMG signal and noise. The noise is the baseline noise during zero% maximum voluntary contraction, which can be obtained before the walking experiment, while the sEMG signal is the data during gait from one heelstrike to next heelstrike. Higher SNR value indicates better quality of sEMG.

Hierarchical Cluster Analysis described in Chapter 5 was used to perform gait classification with K.I. value as the only gait parameters single input. This classification results were being compared to the Approach 1 results in Chapter 5, which used multiple gait parameters. Gait classification solely based on TUG score was also performed as comparison. The Hierarchical Cluster Analysis classification results using single K.I. value were Approach 2.

6.4 Results

6.4.1 Correlation between K.I. and TUG score

Fig 6.7 shows the correlation between K.I. and TUG scores. The correlation coefficient *r* was 0.9222. The result suggests that K.I. is strongly correlated to TUG scores. **Table 6.1** shows the means, standard deviations (SD) and 95% confidence interval of the K.I. for the three different stroke groups. In particular, stroke patients with TUG scores ranged from 10-19 s had the lowest K.I. value ($\overline{\text{K.I.}}$ =33.1, SD=2.45). Subjects with TUG score of 20-29 s had increased K.I. value ($\overline{\text{K.I.}}$ =45.7, SD=10.5). Meanwhile, subjects with TUG score greater than 30 s had more variable results but generally higher K.I. values ($\overline{\text{K.I.}}$ =74.1, SD=28.1). **Fig 6.8** shows the individual performance from different TUG score group. Compared to the results in **Fig 6.3**, the correlation coefficient for K.I. against TUG is significantly improved from NP against TUG (0.4403, 0.6919 and 0.7217 to 0.9143, 0.8665 and 0.9026 for TUG score below 20, between 20 and 30 and above 30 respectively).

To test whether the differences across the three groups were statistically significant, one-way ANOVA analysis was used. ANOVA analysis returned a *p*-value of 0.0000051378 (<0.05), indicating the mean values of the three groups were different from each other. The Post-Hoc results showed that the means of TUG score group <20s and 20~20s are significantly difference from the mean of TUG score group 30>. Meanwhile, there is no significant difference between the mean between TUG score group <20s and group 20~30s.

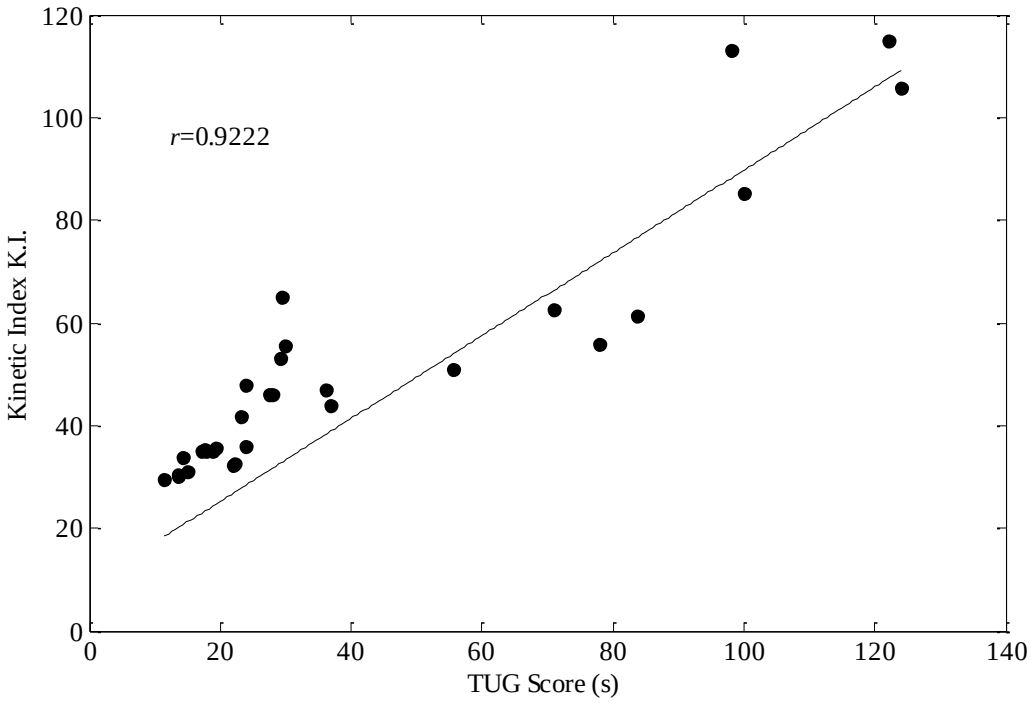

Fig 6.7. Scatter plot of K.I. against TUG score with its best-fit line. Correlation coefficient between them is 0.9222.

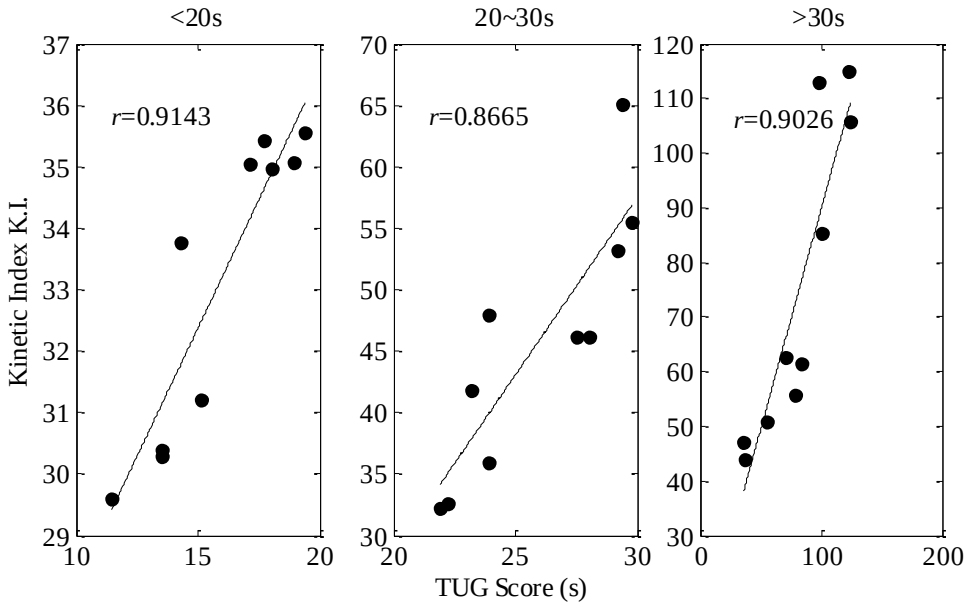

Fig 6.8. Scatter plot of K.I. against TUG score with its best-fit line from category of TUG score below then 20s, between 20 and 30s and above 30s against TUG score with its best-fit line with correlation coefficient of 0.9143, 0.8665 and 0.9026 respectively.

Table 6.1. Mean standard deviation (SD) and 95% CI of K.I.

Population group	Mean K.I.	SD K.I.	95% CI
Stroke subjects with TUG <20s	33.1	2.45	31.4-34.9
Stroke subjects with TUG 20 - 30s	45.7	10.5	38.1-53.2
Stroke subjects with TUG >30s	74.1	28.1	54.0-94.2

6.4.2 Gait classification and assessment

In this section, the results from gait classification described in Section 6.3 are presented.

Table 6.2 shows the gait parameters from Approach 2. Similarly, this approach is able to differentiate three different groups in term of their gait velocity with Group 1 (KI 1) was the fastest group (0.42m/s), Group 2 (KI 2) was the moderate group (0.32m/s) and Group 3 (KI 3) was the slowest group (0.20m/s). Meanwhile, one-way ANOVA analysis showed that K.I., gait velocity, stride length, stance time and swing time had significant difference between three different groups.

Meanwhile, the gait parameters results from **Table 6.3** were classified based on their TUG score. As expected, Group 1 (<20s) had fastest gait velocity (0.42m/s), Group 2 (20-30s) had moderate gait velocity (0.25m/s) and Group 3 (>30s) had the slowest gait velocity (0.22m/s). One-way ANOVA analysis showed that K.I., gait velocity, stride length and ankle dorsiflexion angle at mid-stance had significant difference between three different groups.

Table 6.2. Mean (standard deviation) for K.I., gait velocity, spatial-temporal parameters and ankle joint angle at sagittal plane divided into cluster subgroups based on Approach 2.

	Group 1 (KI 1) *n* = 9	Group 2 (KI 2) *n* = 9	Group 3 (KI 3) *n* = 12	*p*-value
K.I.	38.39 (16.85)	42.65 (11.44)	66.04 (14.06)	<0.05
Gait Velocity (m/s)	0.42 (0.10)	0.32 (0.20)	0.20 (0.06)	<0.05
	Spatial-Temporal Parameters			
Stride length (m)	0.58 (0.22)	0.44 (0.31)	0.22 (0.14)	<0.05
Max. Heel Clearance (m)	0.12 (0.04)	0.10 (0.10)	0.08 (0.05)	0.513
Gait Cycle Time (s)	1.91 (1.19)	2.12 (0.91)	2.94 (0.53)	0.135
Stance Time Percentage (%)	68.13 (11.13)	71.12 (9.80)	83.53 (7.69)	<0.05
Swing Time Percentage (%)	31.87 (11.13)	28.88 (9.80)	16.47 (7.69)	<0.05
	Ankle Angle			
Ankle Dorsiflexion Mid Stance (°)	13.00 (11.24)	13.59 (6.26)	3.30 (8.71)	0.080

Table 6.3. Mean (standard deviation) for K.I., gait velocity, spatial-temporal parameters and ankle joint angle at sagittal plane divided based on their TUG score.

	Group 1 (<20s) *n* = 10	Group 2 (20-30s) *n* = 10	Group 3 (>30s) *n* = 10	*p*-value
K.I.	33.1 (2.45)	45.7 (10.5)	74.1 (28.1)	<0.05
Gait Velocity (m/s)	0.42 (0.20)	0.25 (0.09)	0.22 (0.16)	<0.05
	Spatial-Temporal Parameters			
Stride length (m)	0.57 (0.36)	0.41 (0.27)	0.38 (0.26)	<0.05
Max. Heel Clearance (m)	0.10 (0.08)	0.13 (0.08)	0.10 (0.04)	0.476
Gait Cycle Time (s)	1.55 (1.23)	1.76 (0.63)	2.01 (0.54)	0.152
Stance Time Percentage (%)	66.58 (7.55)	72.84 (12.14)	76.40 (10.04)	0.123
Swing Time Percentage (%)	33.42 (7.55)	27.16 (12.14)	23.60 (10.04)	0.123
	Ankle Angle			
Ankle Dorsiflexion Mid Stance (°)	11.63 (7.91)	5.38 (3.85)	9.78 (5.41)	<0.05

6.5 Discussions

6.5.1 Discussion on methods

To test the quality of sEMG signal, the SNR was determined using Eq (6.10) for stroke survivors from all three categories. The SNR of raw sEMG from the first group (TUG 10-19s) ranges between 24-30dB, the second group (20-29s) ranges between 22-28dB and the third group (30s and above) ranges between 21-26dB. SNR results showed that the third group has lower quality compared to two other categories due to lower level of muscle contraction. However, the difference is not significant.

Fractal analysis on sEMG is a study of signal self-similarity and fractional dimensionality. Many studies indicated that fractal dimension of sEMG are directly proportional to the muscle force [190,208]. This is because fractal dimension algorithm is sensitive to high frequency muscle signals generated from the temporal and spatial motor unit recruitment [190]. For example, high frequency components may exist in the sEMG signal when the muscle force is large. The difference between adjacent sample points in each time series x_m^k may be larger. This results in higher value of L_m in Eq (6.2) and higher fractal dimension. In the sliding window HFD analysis, the temporal evolution of fractal dimension could be observed. As shown in **Fig 6.2**, it reveals that stroke patients with high TUG score had more fluctuated fractal dimensions throughout the whole gait cycle. As seen in **Fig 6.5**, the number of peak in *F* is highly corresponding to the convex and concave part of the sEMG signal. The convex and concave part of the sEMG is caused by the activation of the muscle contraction and therefore it will affect the number of peak in *F*. From Section 6.2.3, the HFD results shows that the number of peak from single muscle has promising correlation to all TUG score patients. However, sliding window HFD analysis of a single muscle did not perform well to distinguish the differences of lower TUG score stroke subjects (see **Fig 6.3**). This means that study the convex and concave part alone in sEMG signal is not sufficient. This

observation suggested that a more sophisticated model is needed to characterise gait deficits in stroke subjects.

The proposed K.I. incorporates the fractal properties of sEMG time series. These fractal properties are average number of peak *NP* and area between *F* and mean of local minima *AP*. Gait profile of different stroke patients will result in different complexity of *F*, and hence different *NP* and *AP*. The local maxima are caused by the fluctuation of sEMG time series. Meanwhile the *AP* is the area of the curve during the occurrence of these local maxima. The prominence of these curves (see **Fig 6.5**) are different from time to time.

According to Seniam [177], GL muscle is mainly attributed to plantar flexion while TA muscle contributes to dorsiflexion. **Fig 6.9** shows an example of GL and TA muscles from Hof *et al* [248]. It is noted that GL muscle activates during mid-stance to toe-off event to move human body forward. Meanwhile TA muscle activates during swing phase to heel-strike (initial loading) to provide the foot clearance. Stroke patients often have different sEMG profile compared to healthy human due to several factors. These include hyperactive stretch reflexes, lack of activation during both shortening and lengthening contractions, excessive and stereotyped coactivations of several muscle groups [6]. As an example, by observing the sEMG from 3 different stroke patients in **Fig 6.10**, it is easy to distinguish the difference between low TUG score (Subject 1) and high TUG score (Subjects 2 and 3). However, it is very difficult to qualitatively differentiate between the two high TUG score stroke patients. Therefore, the advantage of having K.I. is to provide quantitative assessment between different TUG groups with higher sensitivity. While conducting TUG test will still prone to human error due to several factors (time synchronise, different examiners on different days), collecting sEMG during walking is much more reliable.

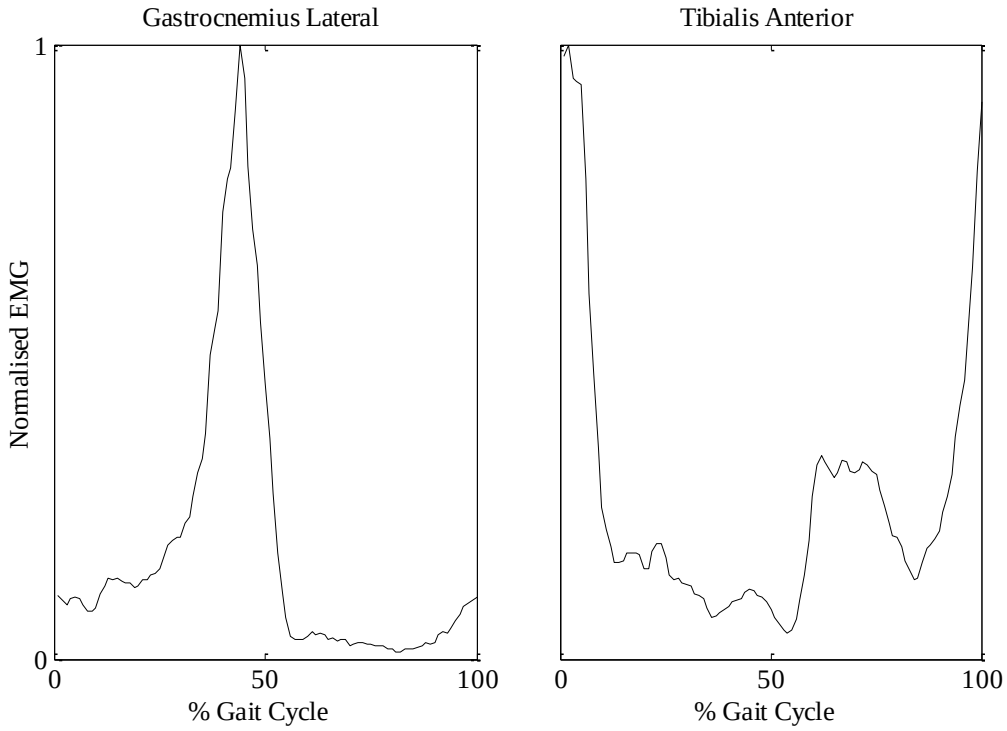

Fig 6.9. Ensemble sEMG from GL and TA muscles from normal healthy subjects. Database taken from Hof *et al* [248].

6.5.2 Discussion on result

6.5.2.1 Correlation between TUG score and K.I. value

Results in Section 6.4.1 shows that the proposed K.I. has a strong correlation with TUG scores. **Fig 6.8** demonstrates strong correlation between K.I. and TUG score in three different TUG score groups (r= 0.9143, 0.8665 and 0.9026 for TUG score group of <20s, 21-30s, >31s respectively). High value of K.I. corresponds to high TUG score. It indicates a severe stroke gait deficits and high risk of fall. One-way ANOVA suggested that gait classification based on their TUG score shows significant difference (p-value <0.05) among three different TUG score groups. It enables researchers and clinicians to study gait deficits at neuromuscular levels such that targeted treatments could be developed based on sEMG information.

6.5.2.2 Gait assessment and classification

1. ***Gait classification based on single input, Approach 2***

Table 6.2 shows the Hierarchical Cluster Analysis Approach 2. This approach can classify stroke patients into three different homogeneous subgroups based on their gait velocity as well. (Group 1 (KI 1) 0.42m/s; Group 2 (KI 2) 0.32m/s; Group 3 (KI 3) 0.20m/s). Group 1 (KI 1) had very similar gait characteristic to healthy gait. They had the shortest stance phase (68.13%) and longest swing phase (31.87%). Group 2 (KI 2) and Group 3 had longer stance phase (71.12 and 83.53% respectively) and shorter swing phase (28.88 and 16.47% respectively), which increased their gait cycle time (2.12 and 2.94s respectively). While Group 3 (KI 3) had the lowest ankle dorsiflexion angle at mid-stance, Group 2 (KI 2) had higher angle than Group 1 (KI 1). This may lead to longer step length in the contralateral limb (unaffected limb).

2. Gait classification based on TUG score

Table 6.3 shows the gait parameters from classification solely based on TUG score. Group 1 (<20s) had fastest gait velocity (0.42m/s) with longest stance phase (66.58%) and shortest swing phase (33.42). Besides that, the ankle dorsiflexion angle at mid-stance was the highest among three groups (11.63°). The gait velocity decreased from Group 2 (20-30s) to Group 3 (>30s) (0.25 and 0.22m/s respectively), with increasing stance phase (72.84 and 76.40% respectively) and decreasing swing phase (27.16 and 23.60% respectively). However, the ankle dorsiflexion angle at mid-stance was higher in Group 3 than Group 2. This may due to the complexity of TUG test. It involves multiple tasks besides walking in sagittal plane such as standing, turning and sitting. Some stroke subjects may performed better in walking in straight line (sagittal plane) but not other tasks.

3. Comparison of different classification approaches (Approach 1 & 2, TUG classification)

Generally, all Groups 1 were fast gait velocity, Groups 2 were moderate gait velocity and Groups 3 were slow gait velocity. The one-way ANOVA analysis suggested both Approach 1 and Approach 2 had similar gait parameters, which were significant difference between each subgroup (stride length, stance and swing time percentage), except for K.I. and ankle dorsiflexion angle at mid-stance showed

insignificant difference from Approach 1 and Approach 2 respectively, but not vice-versa. Meanwhile, classification based solely on TUG score illustrats significant difference in K.I., gait velocity, stride length and ankle dorsiflexion angle at mid-stance. However, this classification method is not able to classify stroke patients into different subgroups based on their temporal parameters, which indicates each subgroups were heterogeneous in term of their gait timing information. Since patients in homogenous subgroups should have independent correlation between each subgroups in term of both spatial and temporal parameters, it can be concluded that classification method based solely on TUG score produced three heterogeneous subgroups compared to Hierarchical Cluster Analysis.

For Hierarchical Cluster Analysis, Approach 1 requires one to obtain multiple spatial-temporal parameters as inputs, which is very subjective and generally based on personal observation [27]. Meanwhile, cluster analysis with single category of parameter often yielded functionally heterogeneous subgroups [27]. Furthermore, classification based on EMG patterns (amplitude, onset and duration) resulted in large variability in kinematic patterns and stride characteristics within subgroups [27]. Therefore, the introduction of K.I. method addressed these limitations. Hierarchical cluster analysis with K.I. value as a single parameter input had very similar subgroups compared to the Approach 1 according to the One-way ANOVA analysis. This shows that K.I. method is a good indicator to assess the severity of gait among stroke patients as it is highly correlate to TUG score and could classify stroke into homogeneous subgroups using Hierarchical Cluster Analysis.

6.5.3 Implications on clinical assessment

TUG score is a typical clinical assessment tool to assess balance, mobility and locomotor skill of disabled persons. It involves individual performing various tasks such as standing, walking and turning. Successful completion of these tasks requires appropriate lower extremity muscle activations. Stroke patients with higher TUG score are at high risk of falls. A potential cause of falling could be weak power generated by the paretic muscle during gait. K.I. provides information

at the neuromuscular level to identify the weak or abnormal muscle activities during gait. For example, improper contraction of TA would lead to failure in lifting the foot (dorsiflexion) during the swing phase. It would cause foot drop, resulting in insufficient toe clearance and falls. The higher value of K.I. indicates weaker muscle of a stroke subjects.

To illustrate the application of K.I., three stroke subjects in different TUG score populations are included in a case study. **Table 6.4** presents the breakdown of K.I. of three stroke subjects with TUG scores of 14 s, 28 s and 50 s respectively while **Fig 6.10** shows the ensemble sEMG from both GL and TA muscles from the hemiplegia side of the stroke patients. The σ value from hemiparetic leg's muscles could inform the weaker muscle. This can be validated by qualitative comparison with the normal GL and TA muscles sEMG from **Fig 6.9**. For validation purpose, two important elements are being observed; activation magnitude and timing. For Subject 1, on the hemiparetic side, σ value for TA muscle is higher (30.9) compared to GL muscle (21.9). Both GL and TA muscles had same activation timing compared to the normal sEMG with TA lacked activation magnitude during heel-strike event. For Subject 2, σ value for GL muscle is higher (49.1) compared to TA muscle (46.2). GL muscle is weaker due to the earlier activation timing while TA sEMG has same activation timing in this case. The activation timing for GL muscle shifted earlier right after heel-strike event. Both muscles started to show jittering. For subject 3, σ value for TA muscle is higher (86.2) compared to GL muscle (84.0). In this case, both TA and GL are co-activated despite they are agonist antagonist muscles. For TA muscle, the activation timing shifted to stance phase. The prolong activation timing is another sign of abnormal contraction. These entire scenarios tally with the description from Olney *et al* [6] review. For some stroke patients, the non-paretic side has higher σ value for particular muscle than the hemiplegia side. This is due to the increased amount of positive work accomplished by the non-paretic side which cause biomechanical compensation from the non-paretic side to the paretic side [249].

Table 6.4. Kinetic Index and the corresponding breakdown of σ_{TA} and σ_{GL} values from three different stroke patients.

Subject ID	Hemiplegia Side	TUG Score	$\overline{\text{K.I.}}$	Right Leg		Left Leg	
				σ_{TA}	σ_{GL}	σ_{TA}	σ_{GL}
1	Left	14s	25.9	26.3	24.8	30.9	21.9
2	Right	28s	47.2	46.2	49.1	50.2	43.9
3	Right	50s	84.3	86.2	84.0	85.5	81.6

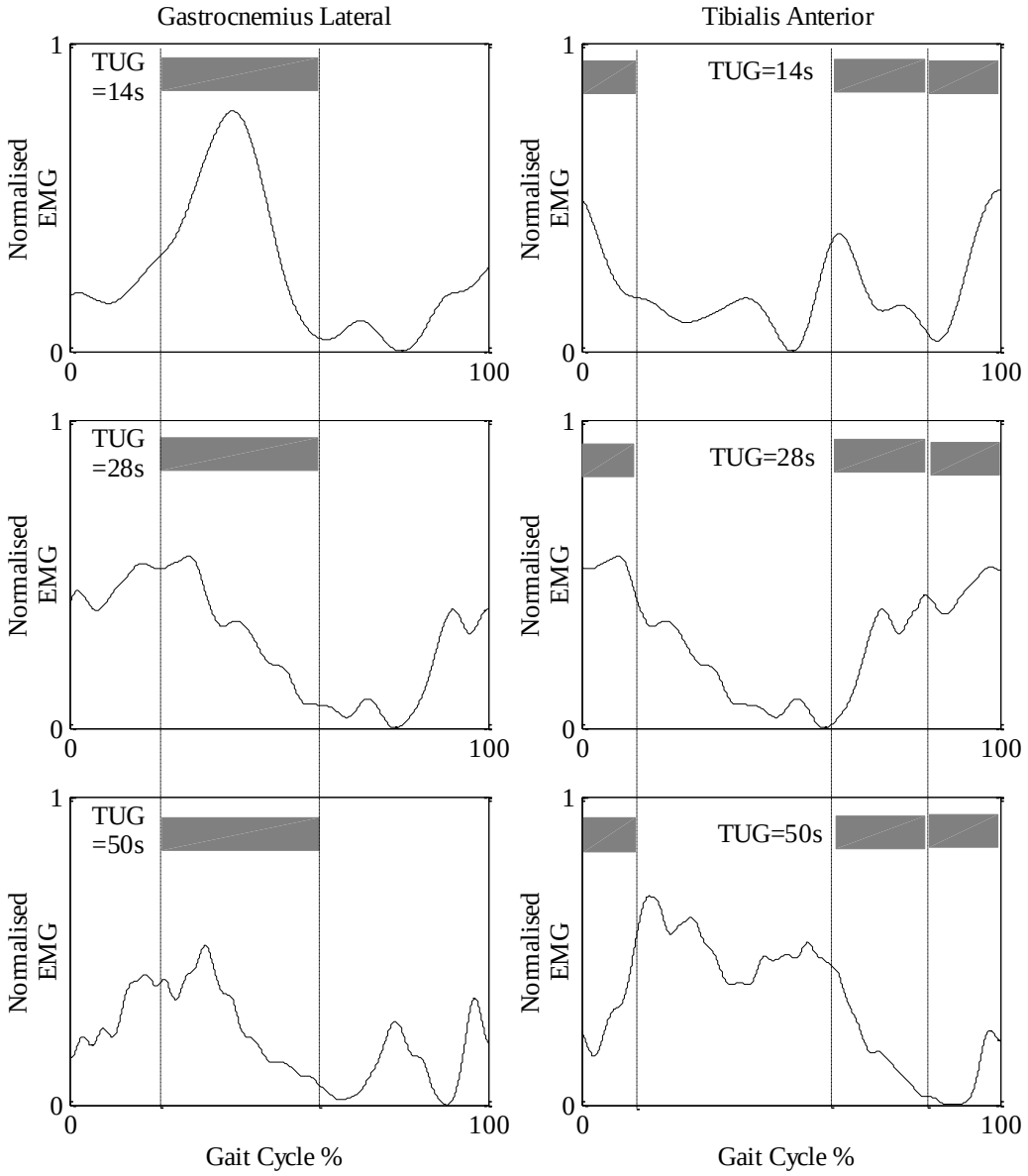

Fig 6.10. Ensemble sEMG of three subjects from their hemiparetic lower limb. Left column are ensemble sEMG for GL muscle and right column are ensemble sEMG for TA muscle. Grey shaded area indicates the muscle activation timing from healthy subject with respective muscles from Fig 6.9.

6.6 Chapter Summary

In this study, a new Kinetic Index K.I. is proposed to characterise stroke patient's gait deficits. 30 stroke patients with different gait deficits were recruited (from Experiment 1 and 2 as described in Chapter 3). Their sEMG from TA and GL muscles were acquired in a 5-meter walk experiment. Results showed that K.I. has strong correlation to the TUG scores ($r = 0.9222$, $p<0.05$). The proposed method allows patients gait deficits to be examined at neuromuscular level.

Hierarchical Cluster Analysis was used to classify these 30 stroke patients into different homogeneous subgroups with single input by using K.I. value (Approach 2). Besides that, classification based on stroke subjects TUG score was also applied. Results show that all Approach 2 was able to classify stroke subjects into proper homogeneous subgroups, similar to Approach 1 in Chapter 5. This results suggested that single input using K.I. was capable to classify stroke survivor as well. This is an advantage using K.I. as multiple parameters were too troublesome to use. Therefore, it can be concluded that K.I. can be served as a powerful gait assessment indicator.

Chapter 7 Kinematic based gait analysis-Cyclogram Symmetry Region of Deviation

7.1 Introduction

In Chapter 2, the limitation of current gait symmetry indices had been described. There are many other researchers proposed new algorithms to solve these limitations and among them, Region of Deviation from Shorter *et al* [101] provided a good gait asymmetry quantification algorithm that provide time history. However, this method requires users to collect healthy walking data as baseline and it may not be user friendly. Moreover, many researchers used linear length normalisation to align gait data from left and right lower limbs. This method removes temporal differences between gait cycles in term of duration, but it does not remove the temporal differences between gait cycles in term of gait events. Therefore, it is necessary to deploy a better alignment method to compare left and right lower limbs. Among them, Dynamic Time Warping is a common and powerful non-linear technique to compress or expand the time axis of tested time series. To date, there are no researchers apply Dynamic Time Warping technique to demonstrate gait asymmetry in left and right legs among strokes.

Therefore, the aims for this chapter are:

1. To develop and validate a new gait asymmetry quantification method based on Cyclogram.
2. To align gait data using Dynamic Time Warping and analyse the results.
3. To observe the asymmetry among stroke using these methods.

7.2 Theory

7.2.1 Cyclogram Symmetry Region of Deviation (CSROD)

Bilateral cyclogram method proposed by Goswami *et al* [103] was adopted and further developed in relation with the time history of a gait cycle. Bilateral cyclogram is a plot of closed trajectories generated by a plotting of a similar joint variable from both sides of lower limbs on the same X-Y Cartesian coordinate system. A 45º straight line, referred as the symmetry line, represents the perfect symmetry gait. This symmetry line is analogues to the joint variables from healthy subject in the original SROD method. Magnitude of deviation was determined by the perpendicular distance between the cyclogram trajectory and symmetry line. These magnitudes of deviation, together with its time stamp information (i.e. percentage of gait cycle, aligned using Linear Length Normalisation (LLN) or Dynamic Time Warping (DTW)), were then plotted in a gait cycle to form the CSROD graph.

The procedure to determine CSROD is as follow:

i. Let $X = [x_1, x_2, x_3, \dots, x_{\mathrm{N}}]$ and $Y = [y_1, y_2, y_3, \dots, y_{\mathrm{M}}]$ be the affected and unaffected lower limb gait data (ankle angle or heel vertical displacement). N and M are the number of samples in affected and unaffected gait data. After alignment (can be LLN or DTW), both *X* and *Y* signals will have same sample size.

ii. Plot *Y* against *X* with a 45^0 straight line. CSROD is therefore determined by:

$$CSROD = \begin{cases} \langle \mathrm{X} - \mathrm{Y} \rangle * \sin(45), & Y < X \\ -\langle \mathrm{Y} - \mathrm{X} \rangle * \sin(45), & X < Y \end{cases} \quad (7.1)$$

The detailed derivation of CSROD can be seen in Appendix C. Negative value of CSROD indicates smaller magnitude of ankle angle from the affected leg. **Fig 7.1** summarises the procedure of this new method.

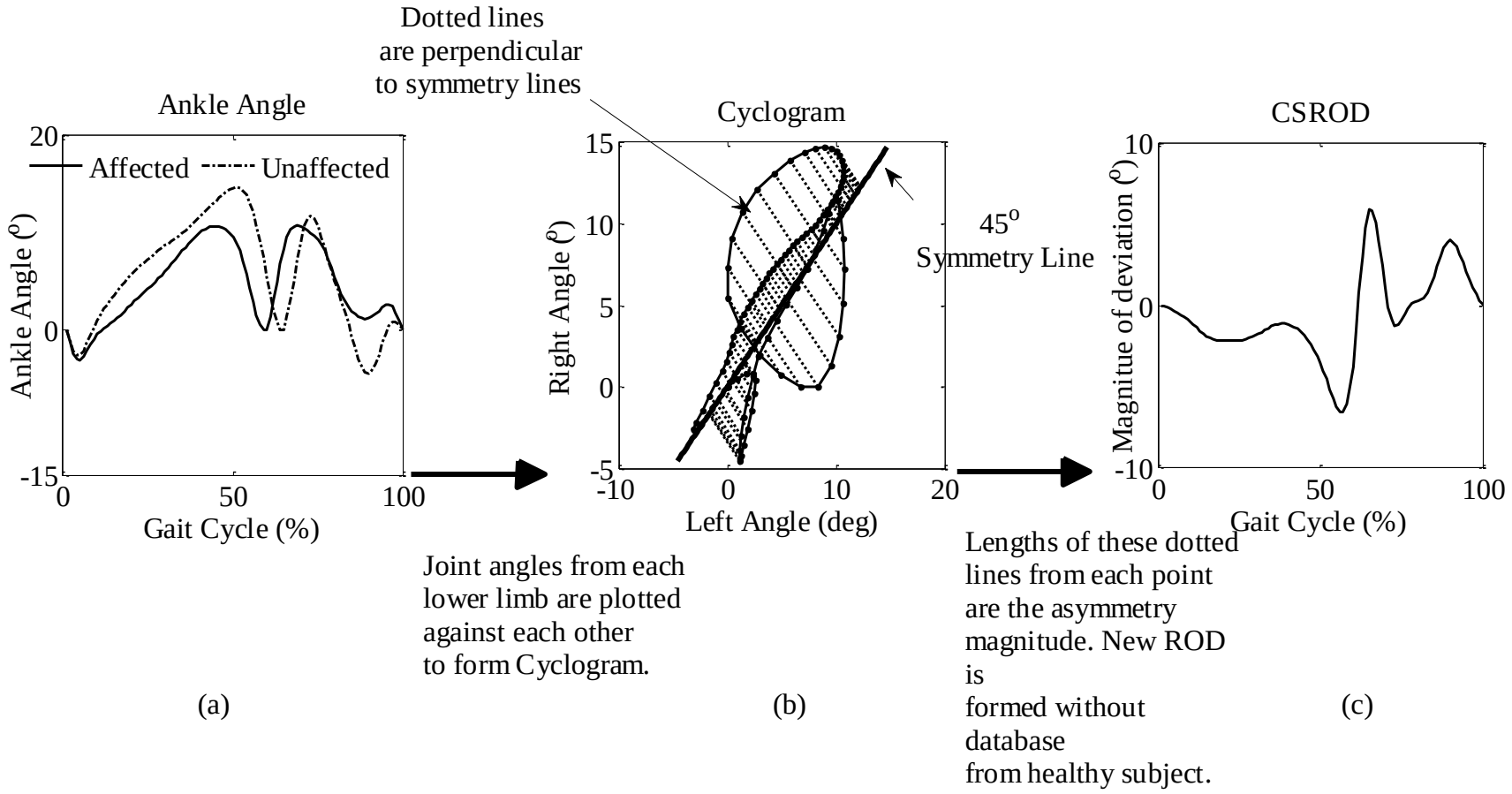

Fig 7.1. Procedure to produce the CSROD from (a) to (c). (a) Ankle angle from left and right lower limbs during walking with right leg knee restricted with braced, (b) Cyclogram diagram plotted by left and right ankle angles, (c) CSROD formed using the distance of the dotted lines in cyclogram.

7.2.2 Experimental protocol

The results from CSROD was validated against SROD using gait data from healthy subjects in Experiment 1 (described in Chapter 3). The SROD method had been explained in Chapter 2. The knee and ankle were restricted by using knee or ankle braced. They were being compared to SROD results using the data from Experiment 1 and the SROD results from original paper [101]. Heel vertical displacement was further applied to test the versatility of the methods. Results using ankle joint angle and heel vertical displacement were referred as Input 1 and Input 2 respectively. Both the joint angle and heel vertical displacement were obtained following the methods from Chapter 3. This CSROD was later being used to study the gait asymmetry characteristic among stroke patient using the data from Experiment 2. The patients from Experiment 2 were further categorised into three different group, according to the Approach 2 from Chapter 6. The mean and standard deviation of peak magnitude and gait cycle timing from all subjects were determined. Three stroke individuals from these three groups were further analysed and their stance time, swing time, gait cycle time and Robinson Index (stance and swing time as variables) were compared to their CSROD results.

7.3 Validation of CSROD (Experiment 1, LLN alignment)

7.3.1 Comparison between CSROD and SROD

Fig 7.2 shows the traditional plots of ankle joint dorsi-plantar flexion, SROD and CSROD respectively from between affected and unaffected sides. SROD is computed by using Eq (2.9). In this figure, the peak magnitude and gait cycle percentage (±SD) are presented using square box (original SROD) and circle (CSROD). **Table 7.1** demonstrates the comparison of results from Shorter paper *et al* [101] ($SROD^1$), SROD applied on the recruited healthy subjects in this paper ($SROD^2$) and the CSROD method using Input 1.

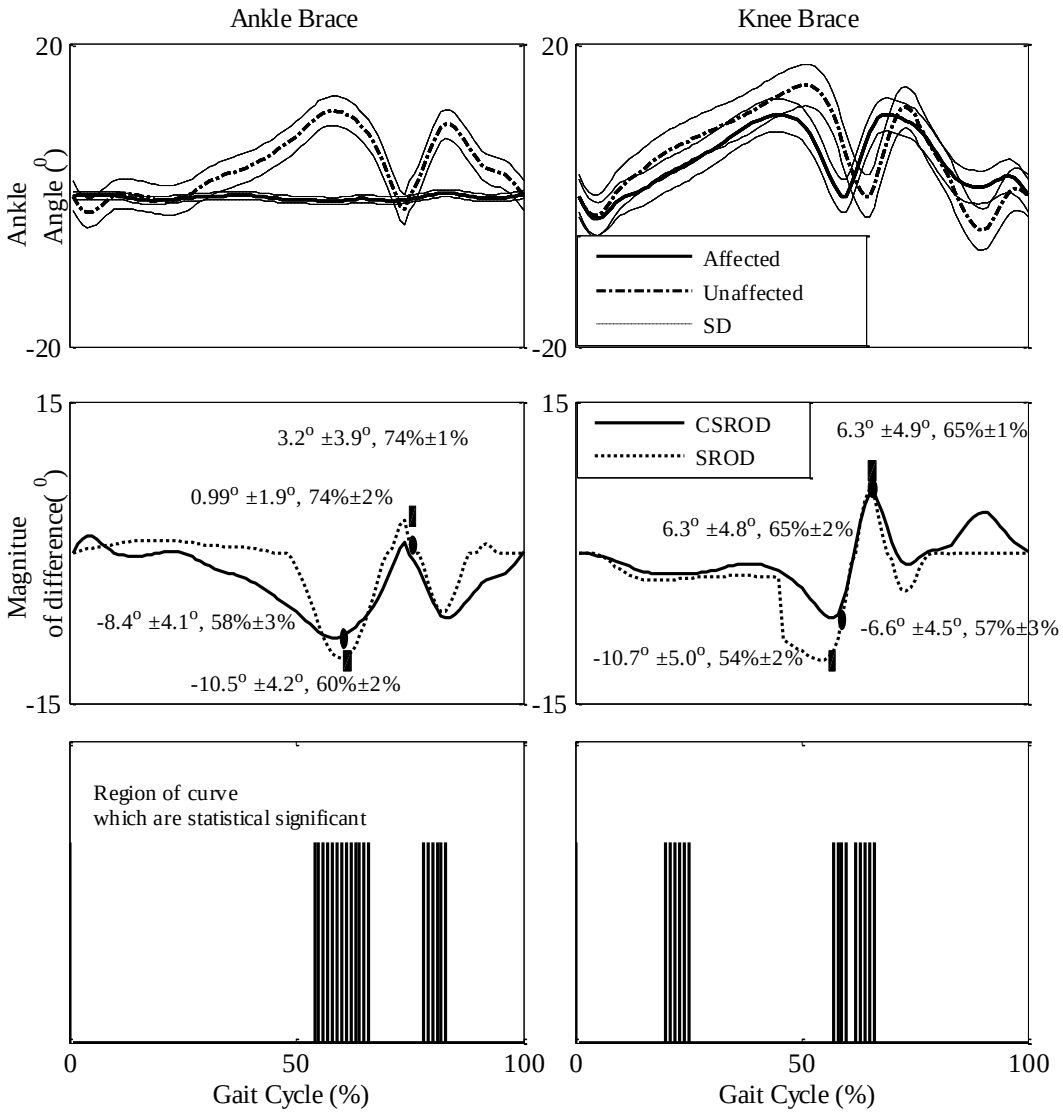

Fig 7.2. (Top) Ankle angle from affected and unaffected lower limb, (Left) Results from ankle brace walking experiment, (Right) Results from knee brace walking experiment. (Middle) Comparison of SROD and CSROD, square box and circle are the peak magnitude and gait cycle timing for both SROD and CSROD respectively (average from 10 subjects ± SD). A negative value indicates smaller joint angle from the braces restricted lower limb. (Bottom) Region of curve which are statistical significant between SROD[2] and CSROD.

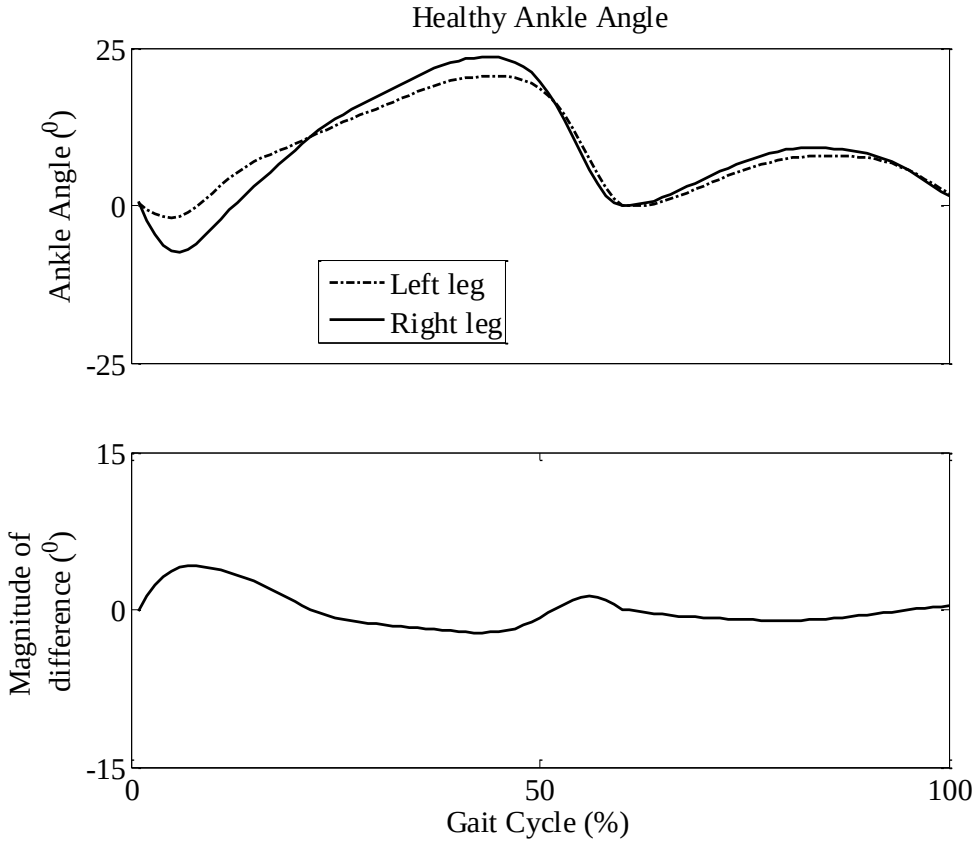

Fig 7.3. (Top) Left and right ankle angles from healthy subject normal walking, (Bottom) Corresponding CSROD result.

In contrast, Fig 7.3 shows the application of CSROD on healthy subject normal walking. It clearly shows that there are no significant peaks, which indicate asymmetry in certain gait event compared to the results from **Fig 7.2**. This outcome illustrates that CSROD is able to distinguish the different between gait pattern from an able body and abnormal walking. The result from Fig 7.3 can be used as a baseline to compare to stroke patients.

Table 7.1. Comparison of validation results using Input 1 from different methods.

			SROD[1]	SROD[2]	CSROD	*p-value*	SROD[1] vs SROD[2]		SROD[1] vs CSROD	
							ε	Z	ε	Z
Ankle	First	Magnitude	-8.2° ± 2.9°	-10.5° ± 4.2°	-8.4° ± 4.1°	0.802	2.3	70.8%	0.2	51.9%
Brace	peak	Timing	52% ± 3%	60% ± 2%	58% ± 3%	0.990	8	99.9%	6	97.7%
	Second	Magnitude	3.5° ± 4.4°	3.2° ± 3.9°	0.99° ± 1.9°	0.903	0.3	50.8%	2.51	77.6%
	Peak	Timing	70% ± 2%	74% ± 1%	74% ± 2%	0.990	8	97.7%	6	74.8%
Knee	First	Magnitude	-5.8° ± 4.2°	-10.7° ± 5.0°	-6.6° ± 4.5°	0.079	4.9	83.7%	0.8	57.1%
Brace	peak	Timing	59% ± 2%	54% ± 2%	57% ± 3%	0.984	5	99.4%	2	74.8%
	Second	Magnitude	12.3° ± 4.5°	6.3° ± 4.9°	6.3° ± 4.8°	0.958	6	88.9%	6	89.4%
	Peak	Timing	71% ± 1%	65% ± 1%	65% ± 2%	0.997	6	99.9%	6	99.8%

[1]SROD results from Shorter *et al* [8]. [2]SROD results from this paper. **ε** absolute mean error. **Z** probability of the normal distribution.

7.3.1.1 SROD results

For ankle bracing, two peaks were observed during gait cycle percentage 58% ± 3% and 74% ± 1%. The peak magnitudes during these events were -8.4^o ± 4.1^o and 3.2^o ± 3.9^o respectively. The first peak was a negative peak, indicated a smaller joint angle on the braced side by 8.4^o and the second peak indicated a smaller joint angle on the unbraced side by 3.2^o. For knee bracing, two peaks were observed and they were -10.7^o ± 5.0^o at 54% ± 2%, and 6.3^o ± 4.9^o at 65% ± 1%. All *p*-values from **Table 7.1** were more than 0.0167, which suggested insignificant difference between two SROD results (in terms of timing and magnitude). However, the probability of the mean peak magnitudes from SROD^2 equals to the mean of peak magnitudes from SROD^1 was lower than the probability of the mean timing information, especially for first and second peaks from ankle braced experiment (70.8% and 50.8% respectively).

7.3.1.2 CSROD results

Similar to the original SROD, the CSROD showed two peaks for both ankle and knee bracing walking experiments. For ankle bracing, the first peak was -8.4^o ± 4.1^o at 58% ± 3%, second peak was 0.99^o ± 1.9^o at 74% ± 2%. For knee bracing, the first peak was -6.6^o ± 4.5^o at 57% ± 3% and second peak was 6.3^o ± 4.8^o at 65% ± 2%. All *p*-values from **Table 7.1** were more than 0.0167, which suggested insignificant difference between SROD^1 and CSROD results (in terms of timing and magnitude). However, the probability of the mean peak magnitudes from CSROD equals to the mean of peak magnitudes from SROD^1 was lower than the probability of the mean timing information, especially for first peaks from both ankle and knee braced experiments (51.9% and 57.1% respectively).

7.3.1.3 Discussion on validation results (Experiment 1, LLN alignment)

In this study, ten healthy subjects were recruited to perform three different walking experiments. The ankle angle from both lower limbs were processed to obtain the SROD and CSROD. The magnitude and timing of each peak in both SROD and

CSROD from these experiments were presented and they were compared to the SROD results from Shorter's paper.

The timing of the peak deviation of SROD from this study and Shorter's paper were very similar in term of Welch t-test analysis (Welch t-test showed that all timing had *p*-value > 0.0167 indicating statistically insignificant difference). However, the probability of the mean peak magnitudes from both $SROD^2$ and CSROD equal to the mean of peak magnitude from $SROD^1$ were lower for certain peaks. Nonetheless, the Welch t-test analysis suggested statistically insignificant between results (*p*-value > 0.0167). This difference can be caused by several factors such as (i) data acquisition system, (ii) data analysis algorithm, (iii) nature of experiment. Shorter used six camera infrared motion analysis system at 120 Hz (Vicon, Oxford, UK; Model 460). The joint angle can be determined directly from the camera results. By comparison, in this study, the experiment used two IMUs strapped on ankle and shank and a further integration algorithm was needed to compute the joint angle. There could be some differences in deriving the joint angle between both studies and hence affected the peak magnitude of SROD graph despite using the same algorithm. This means that the peak difference can be caused by the accumulated errors between the optical system and IMU. For example, Seel *et al* [250] illustrated that there were deviations between the joint angle measurements of the optical and the IMUs from transfemoral amputee. Despise small deviations ($\sigma \approx 1^{\circ}$), the error would still slowly accumulate and lead to variations in SROD and CSROD results from both studies. Moreover, in the original paper, the tested participants walked on a treadmill. In contrast to this original paper, we had the participants walked on the ground. According to Puh and Baer [251], treadmill demonstrated lower cadence and longer step time, stance time and double support time compared to overground walking on stroke patients. This would cause the timing difference between gait events of overground and treadmill walking. Therefore, it is difficult to reproduce the SROD result.

Meanwhile, the CSROD algorithm could improve the reproducibility of the experiment results. This method is easy to use since healthy data is not needed to

perform the algorithm. The healthy data is replaced by introducing a 45º symmetry line in the bilateral cyclogram. The cyclogram is obtained by plotting the affected and unaffected joint angle together. The symmetry line represents the perfect gait symmetry and this is analogous to the normal healthy walking data used in the SROD algorithm. The results from CSROD were compared to SROD in this paper. The timing of peak occurrence from CSROD had good correlation to SROD. This finding shows that using CSROD is capable to detect the asymmetry in any legs from any given time accurately. However, the peak magnitude from the CSROD results were slightly different compared to the SROD method. The peak magnitude indicated the level of deviation between both legs. The main reason peak magnitude is different in both methods is due to the baseline comparison data. The SROD method uses healthy gait data as baseline comparison data. The demographic of healthy subjects from the original Shorter *et al* [101] paper and this study were completely different. This would lead to slightly different SROD magnitude. Therefore, the proposed CSROD method that treats the 45º symmetry line as the perfect gait condition will eliminate this issue. Researchers do not need to collect different demographic groups of healthy subjects to compute CSROD. This will save the research time and cost. This 45º symmetry line is regarded as a "standard" which can be used throughout different studies. However, one of the limitations with this symmetry line is that it assumes normal gait is perfectly symmetric, but this is not the case according to Sadeghi *et al* [31] review. Nonetheless, the difference in the peak magnitude is small for both approaches.

7.4 Limitation of LLN and peak magnitude

The results from Section 7.3 and the original Shorter *et al* paper [101] used LLN to align the gait data from left lower limb to right lower limb. They were temporally aligned by expressing the data in percentages (0-100%) of gait cycle. Despite of LLN is very common technique used by many researchers [101,117]; it cannot align the events between the gait data from left and right lower limbs. Such temporal misalignments will confound any point-by-points comparisons [252]. For

example, **Fig 7.4** shows heel vertical displacements (Top) with different walking condition and their respectively CSROD and SROD results (Bottom). **Table 7.2** displays their peaks magnitude and timing. **Fig 7.4** clearly shows different gait phase from both walking conditions (signal out of phase). Both experiments showed the affected lower limb had shorter stance time and completed the swing time faster than the unaffected lower limb. This leads to two peaks observed in CSROD and SROD results. For both experiments, the first peak was caused by the affected leg vertical heel movement while the second peak was caused by the unaffected leg vertical heel movement. Similar result was observed with Input 1 where the ankle angles for knee restricted walking condition were not in phase, which leads to two peaks on CSROD and SROD results. These peaks are referred as false peaks.

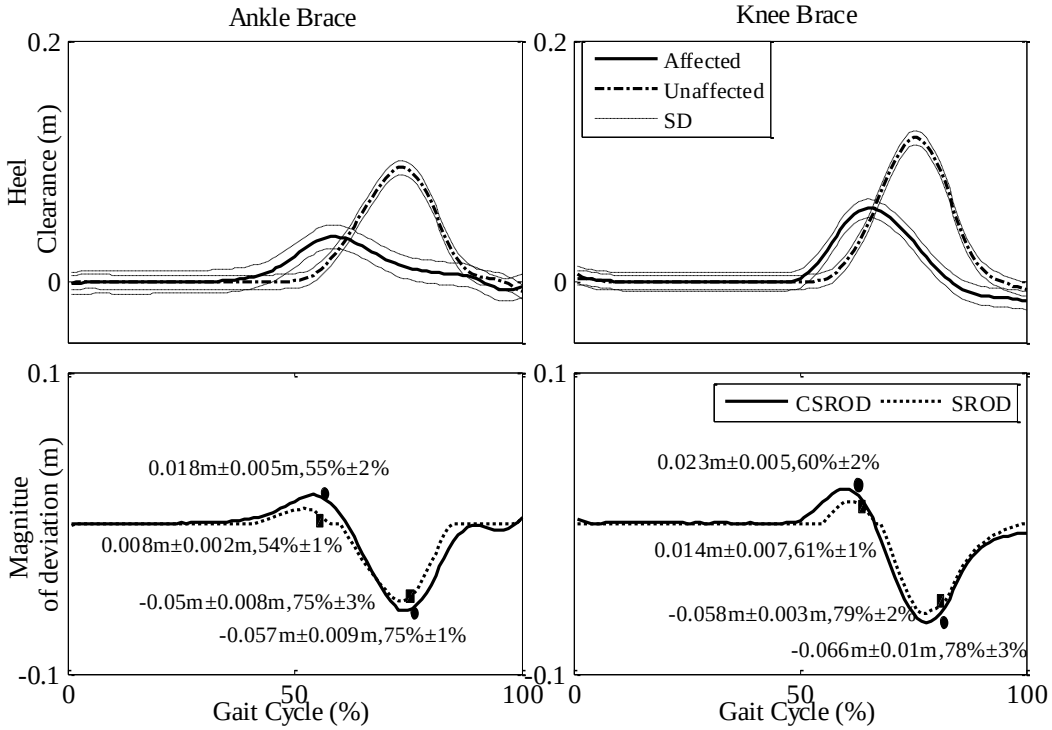

Fig 7.4. (Top) Heel Vertical Displacement from affected and unaffected lower limb, (Left) Results from ankle brace walking experiment, (Right) Results from knee brace walking experiment. (Bottom) Comparison of SROD and CSROD, square box and circle are the peak magnitude and gait cycle timing for both SROD and CSROD respectively (average from 10 subjects ± SD). A negative value indicates smaller joint angle from the braced restricted lower limb.

Table 7.2. Comparison of results using Input 2 from different methods.

			SROD	CSROD
Ankle Brace	First peak	Magnitude (m)	0.008 ± 0.002	0.018 ± 0.005
		Timing (%)	55 ± 2	54 ± 1
	Second Peak	Magnitude (m)	-0.05 ± 0.008	-0.057 ± 0.009
		Timing (%)	75 ± 3	75 ± 1
Knee Brace	First peak	Magnitude (m)	0.014 ± 0.007	0.023 ± 0.005
		Timing (%)	61 ± 1	60 ± 2
	Second Peak	Magnitude (m)	-0.058 ± 0.03	-0.066 ± 0.01
		Timing (%)	79 ± 2	78 ± 3

The CSROD and SROD results of three individual stroke patients from each group were analysed. **Fig 7.5** shows the traditional ankle dorsi-plantar flexion (top) and their respectively CSROD and SROD results (bottom) from each group. **Fig 7.6** shows the heel vertical displacement (top) and their respectively CSROD and SROD results (bottom) from each group. Both CSROD and SROD results from Input 1 and Input 2 suggested individual patients from Group I and II had greater gait asymmetry compared to individual patient from Group III. This is because the affected side of patient from Group III had minimal to none ankle movement, which causes almost flat signal in term of ankle angle and vertical displacement. This lack of movement will reduce the peaks magnitude in CSROD and SROD results. Therefore, peak normalisation is needed to compare the asymmetry among stroke patients.

$$PM_{norm,t} = \frac{PM_t}{|\sigma_t^i|} \tag{7.2}$$

where $PM_{norm,t}$ is the unitless normalised peak magnitude at time *t*, PM_t is the peak magnitude on CSROD at time *t*, σ_t^i is the gait data from unaffected lower limb at time *t*, *i* is the input (*i* = ankle angle or heel vertical displacement), and |.| bracket indicates absolute value. Greater value of $PM_{norm,t}$ indicates greater asymmetry at time *t*.

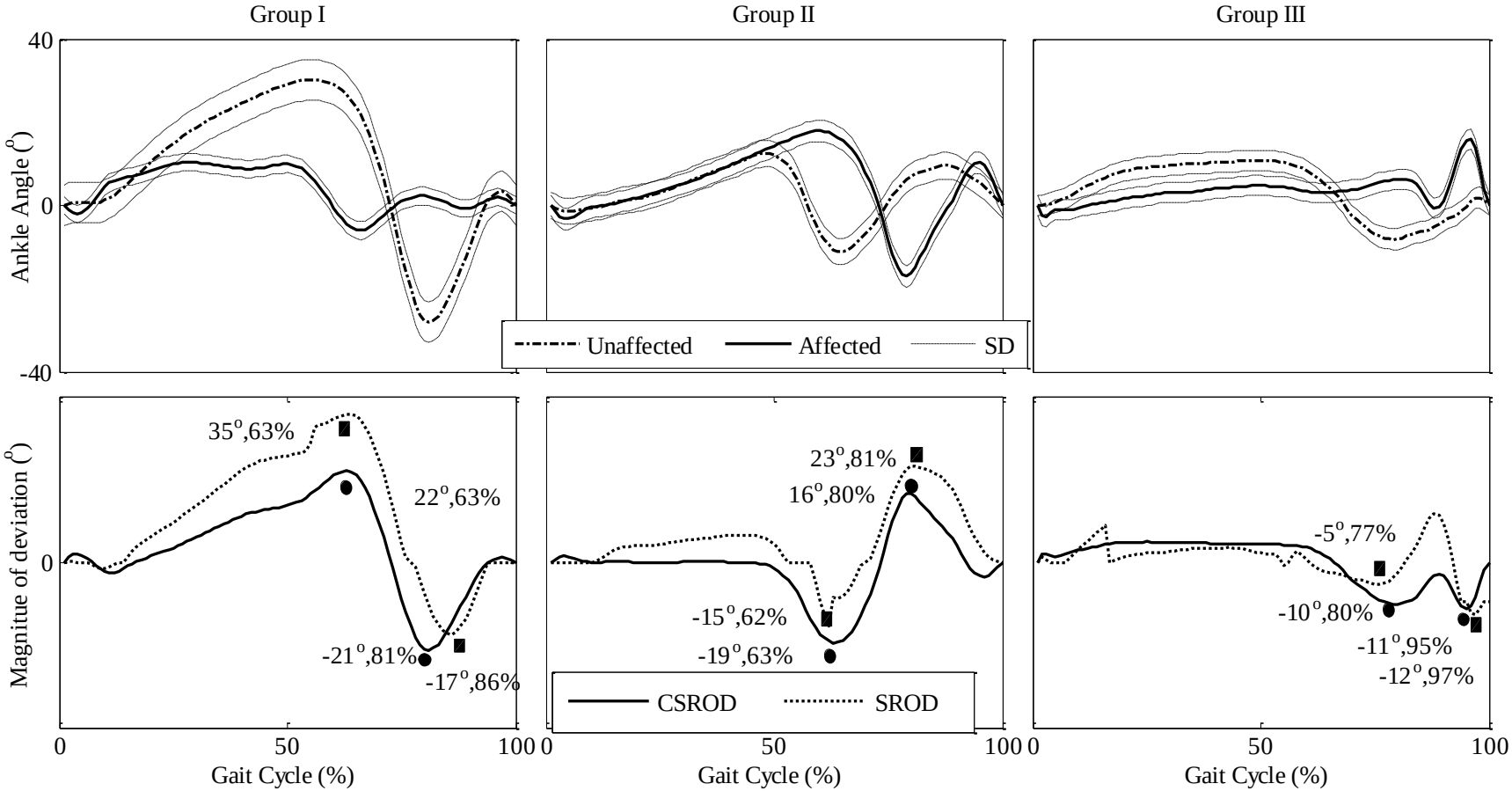

Fig 7.5. (Top) Ankle angle from Group I, II and II respectively; (Bottom) Input 1 CSROD and SROD results from Group I, II and II respectively.

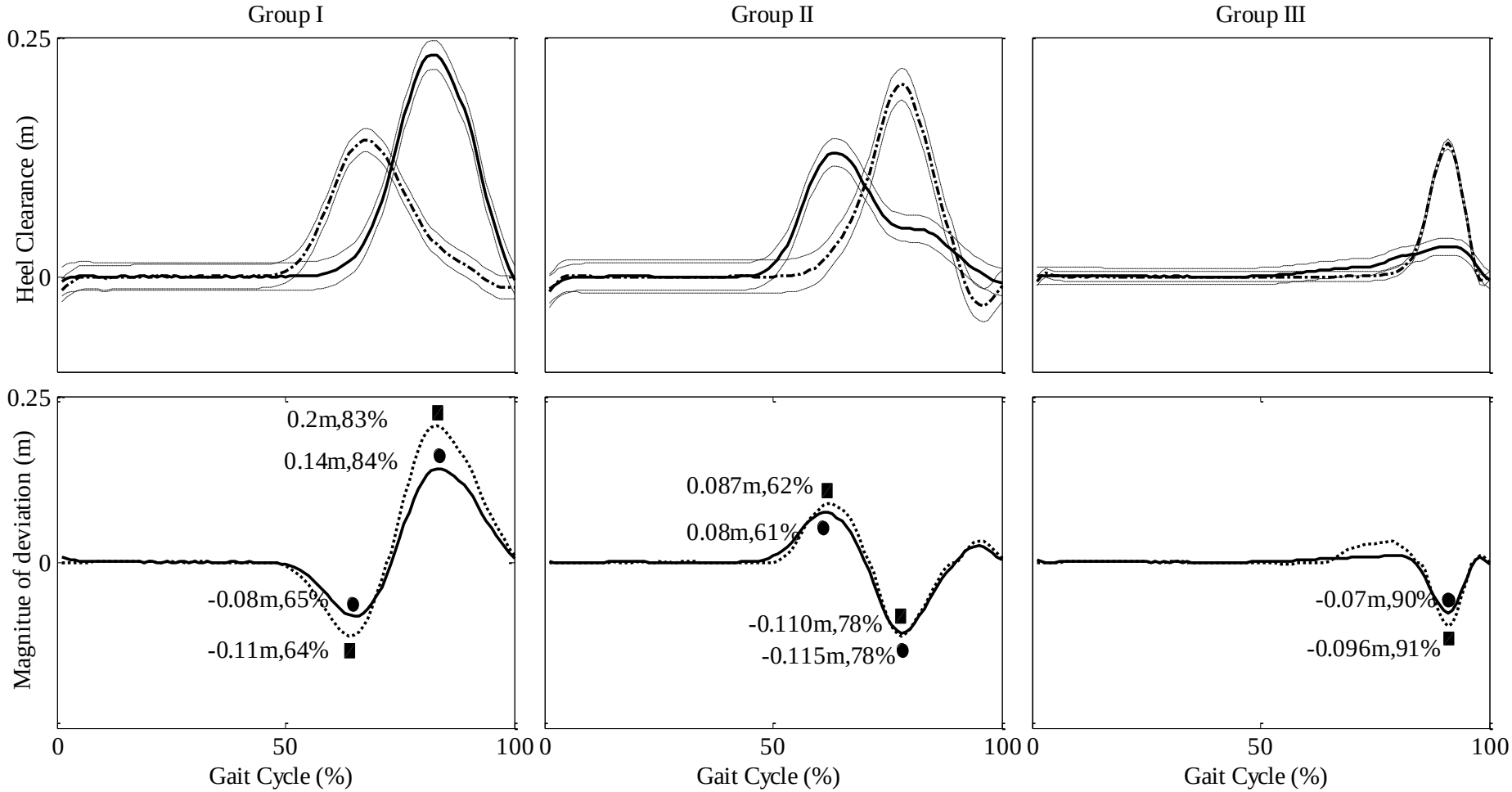

Fig 7.6. (Top) Heel vertical displacement from Group I, II and II respectively; (Bottom) Input 2 CSROD and SROD results from Group I, II and II respectively.

7.5 Gait alignment techniques

7.5.1 Piecewise Linear Length Normalisation (PLLN)

Piecewise Linear Length Normalisation (PLLN) is one of the alignment approach that segments the gait cycle trajectories into subphases at points of interest (POI; user-determined points to align) [252]. This approach utilises LLN in pieacewise manner to align the subphases of gait cycle trajectories according the POI assigned by the user. POI can be any characterising-points of gait cycle features (trajectory shape [253] or gait events such as heel-strike and toe-off [252]). In this study, toe-off event was chosen as POI and the gait cycle trajectories were divided into two segments. The first segment was from heel-strike to toe-off and the second segment started right after toe-off to the next heel-strike. We interpolated the first segment to 60 data points and the second segment to 40 data points. This is because the first segment is stance phase, which normally is 60% of one gait cycle time and the second segment is swing phase, which is 40% of gait cycle time. **Fig 7.7** shows the procedure of PLLN.

7.5.2 Dynamic Time Warping (DTW)

In 1978, Sakoe and Chiba developed Dynamic time warping (DTW) for spoken word recognition [254]. DTW is a nonlinear time normalisation technique to find the temporal alignment that minimises the distance between two time series. To find the similarity between two gait data, DTW looks for the best alignment, which referred to as Warp-Path.

Given $X = [x_1, x_2, x_3, \dots, x_{\mathrm{N}}]$ and $Y = [y_1, y_2, y_3, \dots, y_{\mathrm{M}}]$ as the affected and unaffected lower limb gait data, with *N* and *M* samples respectively. In order to calculate the DTW, a matrix D with *N*x*M* size is constructed. Each cell (*n*,*m*) in this matrix contains a Euclidian distance $d(x_n, y_m)$ between x_n and y_m. The warping path *W*, is a contiguous set of matrix elements that defines a mapping between *X* and *Y*.

$$W = w_{1,}, w_2, \dots, w_k \qquad \max(\mathrm{N}, \mathrm{M}) < \mathrm{k} < \mathrm{N} + \mathrm{M} - 1 \qquad (7.3)$$

$$w_k = (n_k, m_k) \tag{7.4}$$

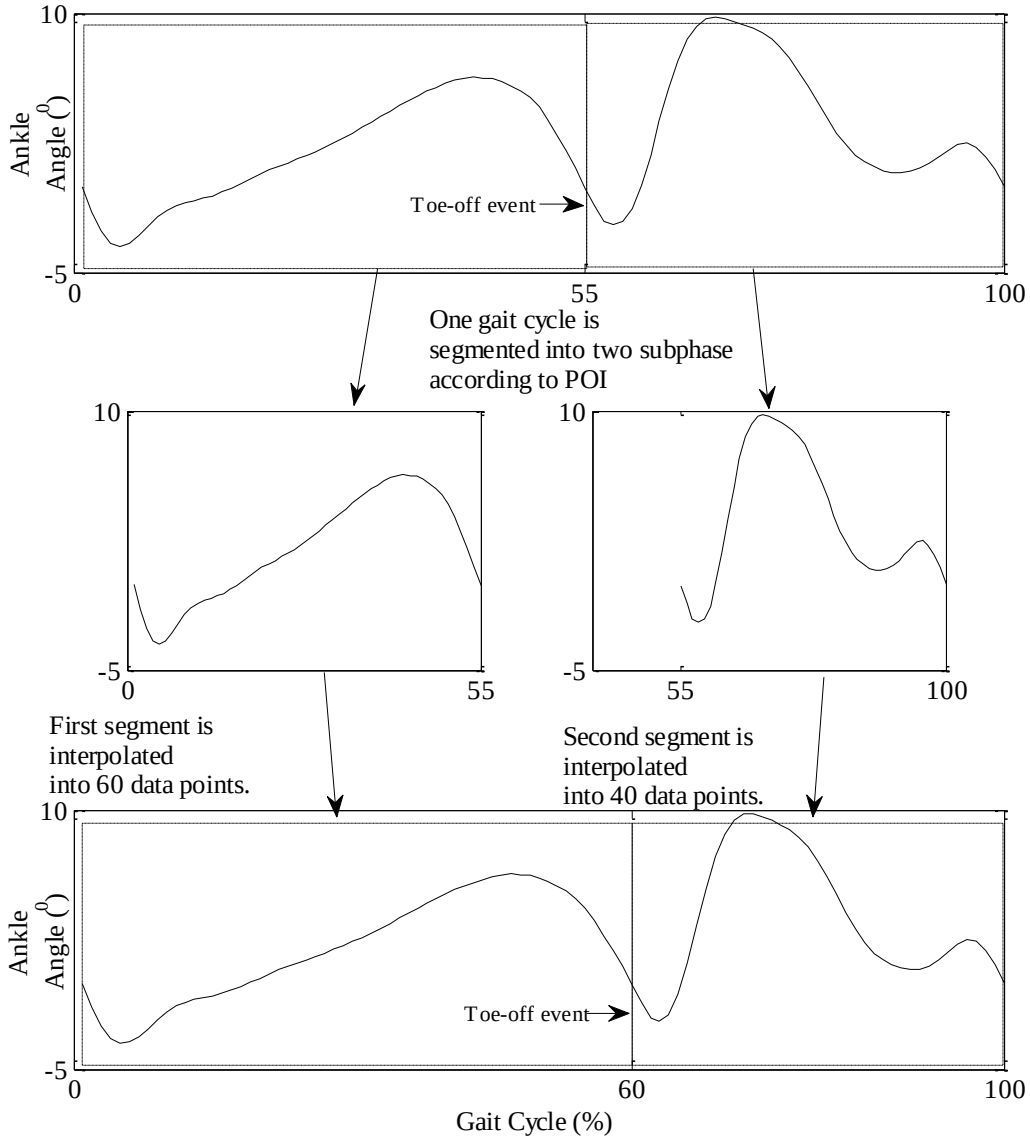

Fig 7.7. Schematic diagram of PLLN procedure.

Each of *W*'s elements is a cell on the matrix D. Generally, this warp path *W* is restricted to the following conditions.

i. Monotonic conditions: $n_{k-1} < n_k$ and $m_{k-1} < m_k$

ii. Continuity conditions: w_k is allowed to connect only with adjacent cells.

iii. Boundary conditions: The warping path *W* must start and finish in diagonally opposite corner cells on the matrix D. $w_1 = (1,1)$ and $w_k = (\mathrm{N}, \mathrm{M})$.

Fig 7.8 presents an example of warping path *W* started with bottom left corner (1,1) to top right corner (*N*,*M*). **Fig 7.9** shows the alignment of two gait data time series using DTW.

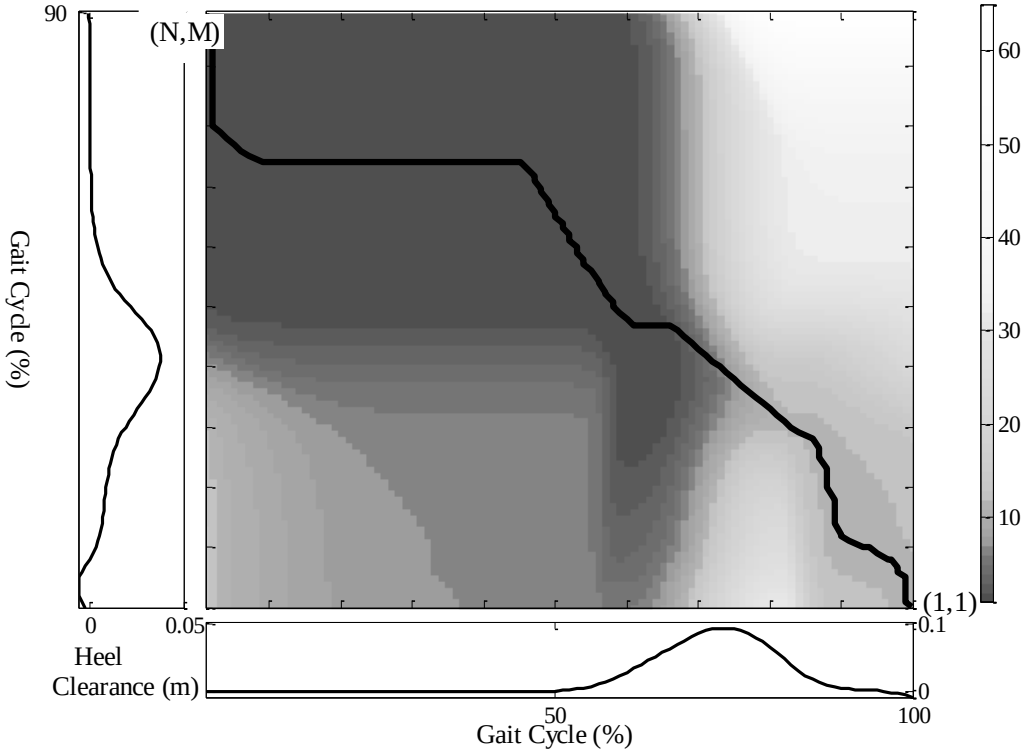

Fig 7.8. **An example of warping path *W* with affected and unaffected heel vertical displacement. The grey square box is the matrix D, and the thick line is *W*. This example started from bottom left (1,1) to top right (*N*,*M*).**

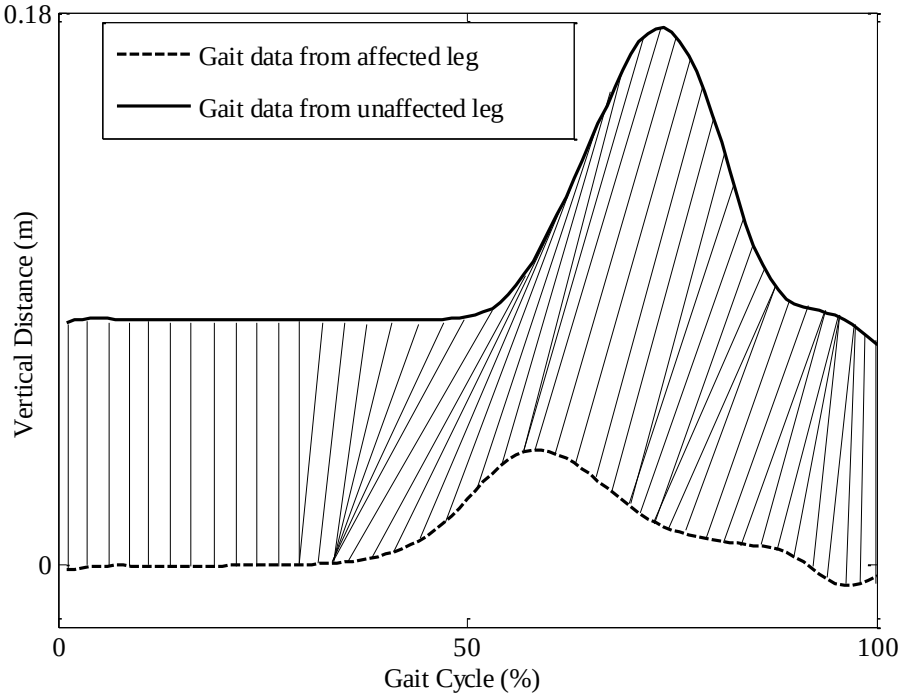

Fig 7.9. **Alignment of two gait time series from affected and unaffected lower limbs.**

7.5.3 Piecewise Dynamic Time Warping (PDTW)

Once the gait cycle is segmented into different subphase according to POI (see Fig 7.7), it is also possible to apply DTW in a piecewise manner to align each subphases of the trajectories. The alignment of each subphase is treated as its own DTW, hence named PDTW.

7.5.4 Comparison between different alignment techniques

Different alignment techniques (DTW, PLLN or PDTW) can lead to different interpretations of the data. Therefore, it is necessary to compare each technique and determine the most suitable for our study. **Fig 7.10** shows the affected and unaffected ankle angle without any alignment **Fig 7.10** (a) and ankle angle after alignment DTW, PLLN and PDTW **Fig 7.10** (b), (c) and (d) respectively. In this figure, the results yielded by DTW and PDTW are very similar. Both results show high shape similarity between affected and unaffected ankle angle. In contrast, PLLN produced less shape similarity. With toe-off as POI, PLLN managed to align

the shape around toe-off event. However, the huge gap between the affected and unaffected ankle angle during stance phase suggested that PLLN is not able to remove the temporal differences between both legs. These results demonstrate that DTW and PDTW produced more desirable alignment results when comparing the left and right lower limbs intra-subjects. Since DTW required less computation time and yet it can produces similar results with PDTW, DTW is selected as the alignment technique to analyse the CSROD of stroke patients.

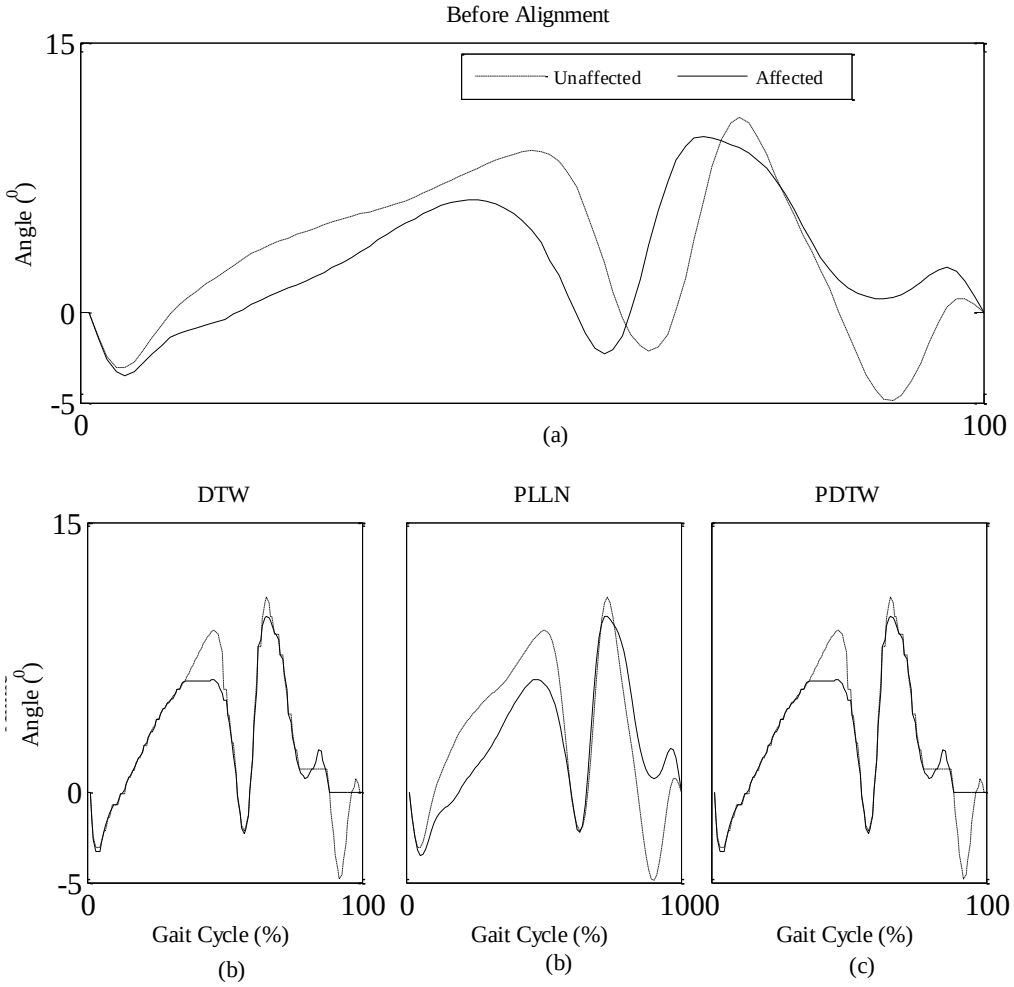

Fig 7.10. Comparison of different alignment normalisation techniques. (a) Affected and Unaffected ankle angle before alignment. (b) Affected and Unaffected ankle angle after alignment using DTW; (c) Affected and Unaffected ankle angle after alignment using PLLN; (d) Affected and Unaffected ankle angle after alignment using PDTW.

7.6 CSROD results (Experiment 1, DTW alignment)

Fig 7.11 and **Fig 7.12** show (Top) the ankle joint angles (Input 1) and heel vertical displacement (Input 2) from affected and unaffected lower limbs after aligned using DTW, and (Bottom) their respectively CSROD results. **Table 7.3** and **Table 7.4** show the comparison of peaks magnitude and timing before and after alignment for Inputs 1 and 2.

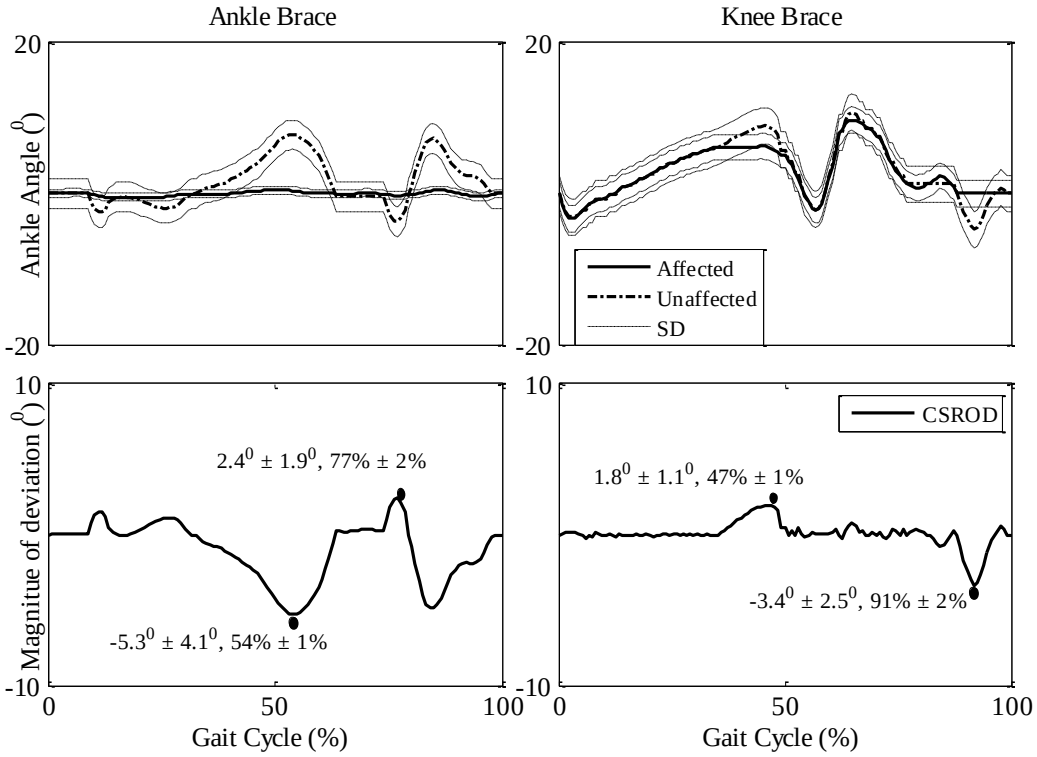

Fig 7.11. (Top) Ankle angle from affected and unaffected lower limb after alignment using DTW, (Left) Results from ankle brace walking experiment, (Right) Results from knee brace walking experiment. (Bottom) CSROD result.

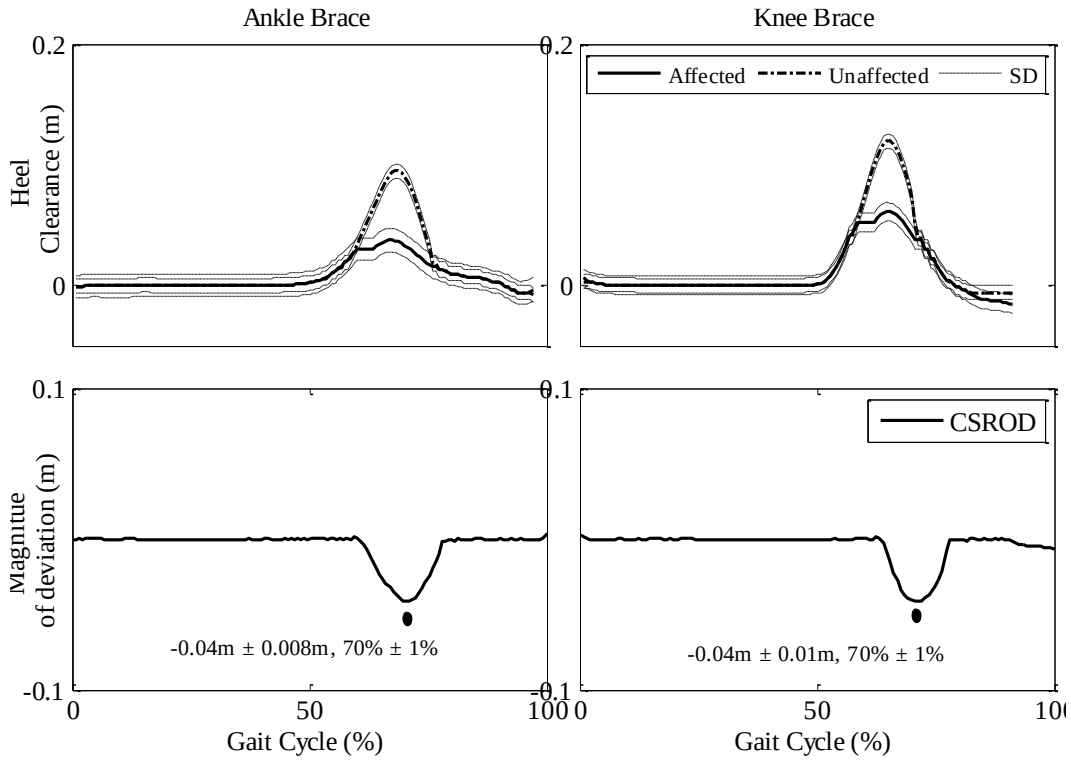

Fig 7.12. (Top) Heel vertical displacement from affected and unaffected lower limb after alignment using DTW, (Left) Results from ankle brace walking experiment, (Right) Results from knee brace walking experiment. (Bottom) CSROD result.

Table 7.3. Comparison of results using Input 1 before and after alignment using DTW.

			Before	After
Ankle Brace	First peak	Magnitude (°)	-8.4 ± 4.1	-5.3 ± 4.1
		Timing (%)	58 ± 3	54 ± 1
	Second Peak	Magnitude (°)	0.99 ± 1.9	2.4 ± 1.9
		Timing (%)	74 ± 2	77 ± 2
Knee Brace	First peak	Magnitude (°)	-6.6 ± 4.5	1.8 ± 1.1
		Timing (%)	57 ± 3	47 ± 1
	Second Peak	Magnitude (°)	6.3 ± 4.8	-3.4 ± 2.5
		Timing (%)	65 ± 2	91 ± 2

Table 7.4. Comparison of results using Input 2 before and after alignment using DTW.

			Before	After
Ankle Brace	First peak	Magnitude (m)	0.018 ± 0.005	-0.04 ± 0.008
		Timing (%)	54 ± 1	70 ± 1
	Second Peak	Magnitude (m)	-0.057 ± 0.009	NA
		Timing (%)	75 ± 1	NA
Knee Brace	First peak	Magnitude (m)	0.023 ± 0.005	-0.04 ± 0.01
		Timing (%)	60 ± 2	70 ± 1
	Second Peak	Magnitude (m)	-0.066 ± 0.01	NA
		Timing (%)	78 ± 3	NA

7.6.1 Input 1

In **Table 7.3**, the CSROD results before and after DTW alignment has insignificant difference for ankle braced walking experiment but significant difference for knee braced walking experiment in term of peaks magnitude and timing. For ankle bracing, affected lower limb does not have dorsi-plantar flexion and there are no amplitude observed in the ankle angle graph in before and after DTW alignment. Therefore, alignment between affected and unaffected lower limbs was not significant and it does not affected the results significantly after DTW alignment.

Meanwhile, for knee bracing, the ankle angle before DTW alignment shows both gait data from affected and unaffected limb were out of phase. They were in phase after DTW alignment. Therefore, there was a significant difference in term of CSROD results after the alignment.

7.6.2 Input 2

There was only one peak observed in CSROD after alignment. This is because the swing phase is now aligned for both affected and unaffected lower limb. After alignment, the maximum vertical movement during swing phase for both lower limbs can be compared directly.

7.6.3 Discussion

7.6.3.1 Ankle bracing

For Input 1, there was a negative peak observed at 54% gait cycle timing. This peak happened between the terminal stance and the transition to swing. The negative peak indicated a smaller joint angle on the affected side. During the toe-off event, the ankle plantarflexion occurs to propel the foot to mid-air. Since ankle brace restricted the ankle movement, the affected lower limb does not have any ankle joint movement and hence asymmetry happens. The second peak was a positive peak and it was smaller compared to the first peak. This peak happened at 77%, which was during mid-swing to terminal-swing. During this duration, ankle dorsiflexion happened to prepare for the next heel strike. The movement of ankle from plantar-flex to dorsi-flex at this moment appeared on the negative part of ankle angle graph for unaffected side.

For Input 2, the only peak was observed at 70% and it was a negative peak. This was during mid-swing. Negative peak indicated smaller vertical movement on affected limb. Since there are insufficient plantar-flexion on ankle joint, there is not enough propulsion to lift the foot to mid-air. This vertical movement on affected limb was compensated by other joint to avoid foot drag.

7.6.3.2 Knee bracing

For Input 1, the first peak was observed at 47% gait cycle time. This peak happened at terminal stance when the heel prepared to leave the ground (heel-off). With knee locked by the brace, ankle joint will reduce its range of motion. The foot lifting movement was compensated by the hip joint in this event. The second peak happened approximately at 91% gait cycle time, which was during terminal-swing.

For Input 2, one peak was observed at 70% gait cycle time. This was during mid-swing. With knee restricted, it reduced the ankle joint propulsion. The flexion of ankle joint movement only associated with hip joint movement only. Without knee flexion, it will reduce the vertical displacement on affected leg as well.

7.7 Gait asymmetry among stroke (Experiment 2, DTW alignment)

Fig 7.13 and **Fig 7.14** present the mean and standard deviation of ankle angle and heel vertical displacement from three different groups (based on classification Approach 2) and their corresponding CSROD results. **Table 7.5** shows the CSROD normalise peaks magnitude and timing from these three groups and their mean gait cycle time.

7.7.1 Input 1

For Group I patients, the first peak happened at 44% ± 2%, which is the transition from mid-stance to the heel-off timing. This event is to move the upper body forward. Lack of ankle movement on the affected leg reduced the step length on the unaffected leg. The asymmetry on this period occurred due to better ankle angle movement on the unaffected leg to compensate the affected leg to move the upper body forward. Meanwhile, unlike Group I patients, there were no obvious peaks during the transition from mid-stance to heel-off timing for Group II patients. This is because Group II patients lacked of dorsi-flexion during stance time for both lower limbs. This will greatly reduce the patients step length. The first peak for Group II occurred at 71% ± 4%, which was during mid-swing. The lack of ankle movement during mid-swing for affected leg indicated insufficient propulsion to create foot clearance. In contrast, patients from Group III had prolong stance phase. Group III patients had the slowest gait speed and they were considered to have the most severe gait abnormality. Therefore, they often tried to reduce the swing time and increased the stance time to balance themselves. The first peak at 77% ± 5% is at terminal stance. Similar to Group I patients, this event is to move upper body forward. Lack of ankle movement in affected leg decreased the patients step length.

The second peak for Group I patients is located at 84% ± 1% gait cycle time. This duration is the transition from mid-swing to terminal swing. The positive peak on this event suggests a smaller ankle angle on unaffected lower limb. This smaller angle was due to the plantar-flexion of ankle joint on unaffected side. Similar phenomenon is observed in Group II patients where the second peak is at 89% ±

1%. Meanwhile, the second peak on Group III patients happened at 94% ± 1% gait cycle timing. This duration was where mid-swing happen for this group since they had shorter swing time. This positive peak implied no ankle movement on affected lower limb.

7.7.2Input 2

Generally, there is only one peak observed for all three groups of stroke patients when applying Input 2 on CSROD. This is because only the maximum vertical displacement for both affected and unaffected lower limbs were compared. This peak appear during mid-swing for all groups (76% ± 2%, 79% ± 1% and 94% ± 1%) for Group I, II and III respectively). The normalised peak magnitude in Table 6.3 shows greatest asymmetry in Group III, moderate in Group II and lowest in Group I. Heel vertical displacement only captures the foot clearance during swing phase. Therefore, once the gait data from both lower limbs were aligned using DTW, CSROD only compared the peaks during swing phase.

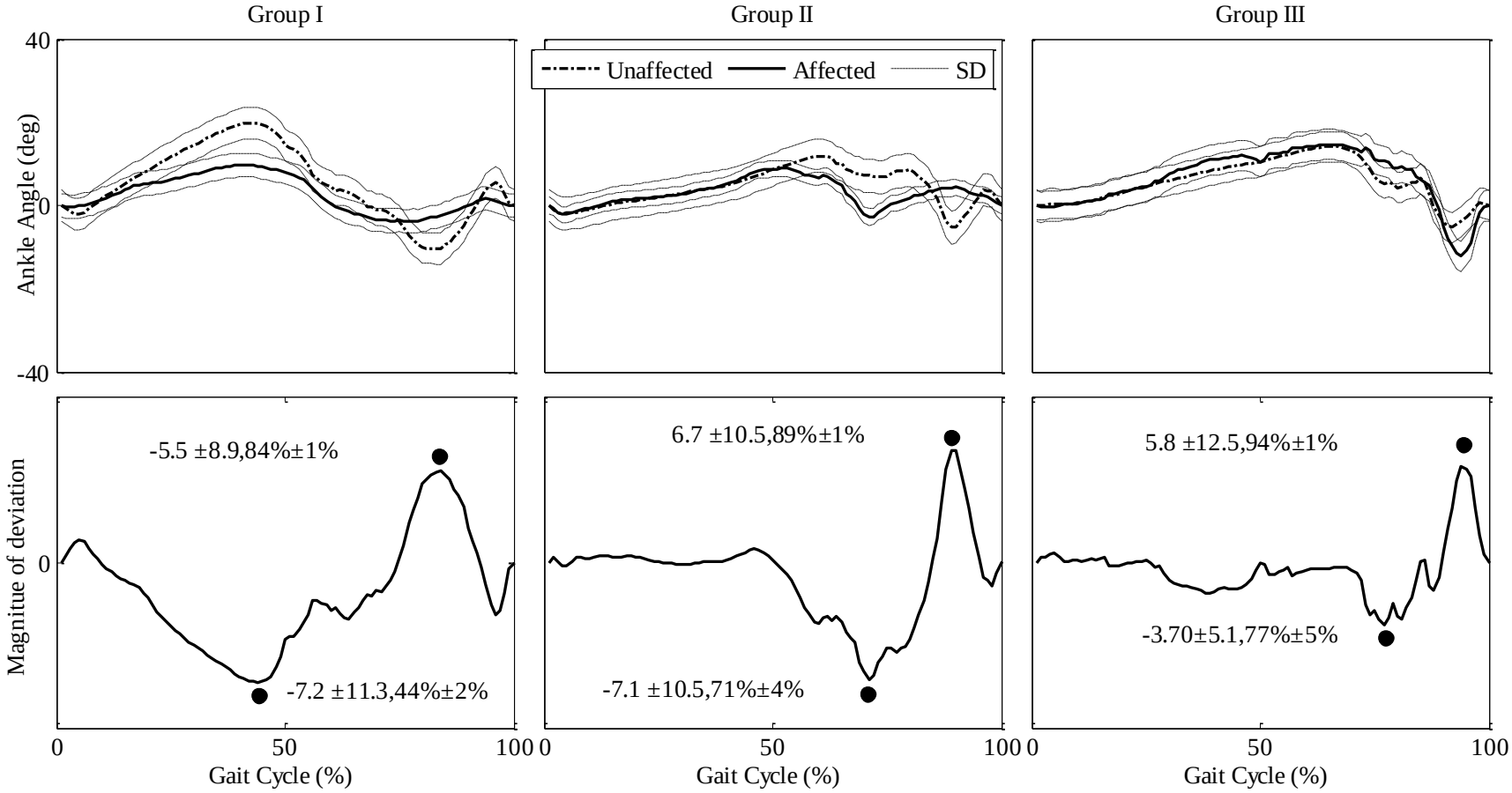

Fig 7.13. (Top) Mean and standard deviation of ankle angle from 60 stroke patients categorised into three groups with 29 on Group I (Left), 17 on Group II (Middle), 14 on Group III (Right); (Bottom) Their corresponding CSROD results.

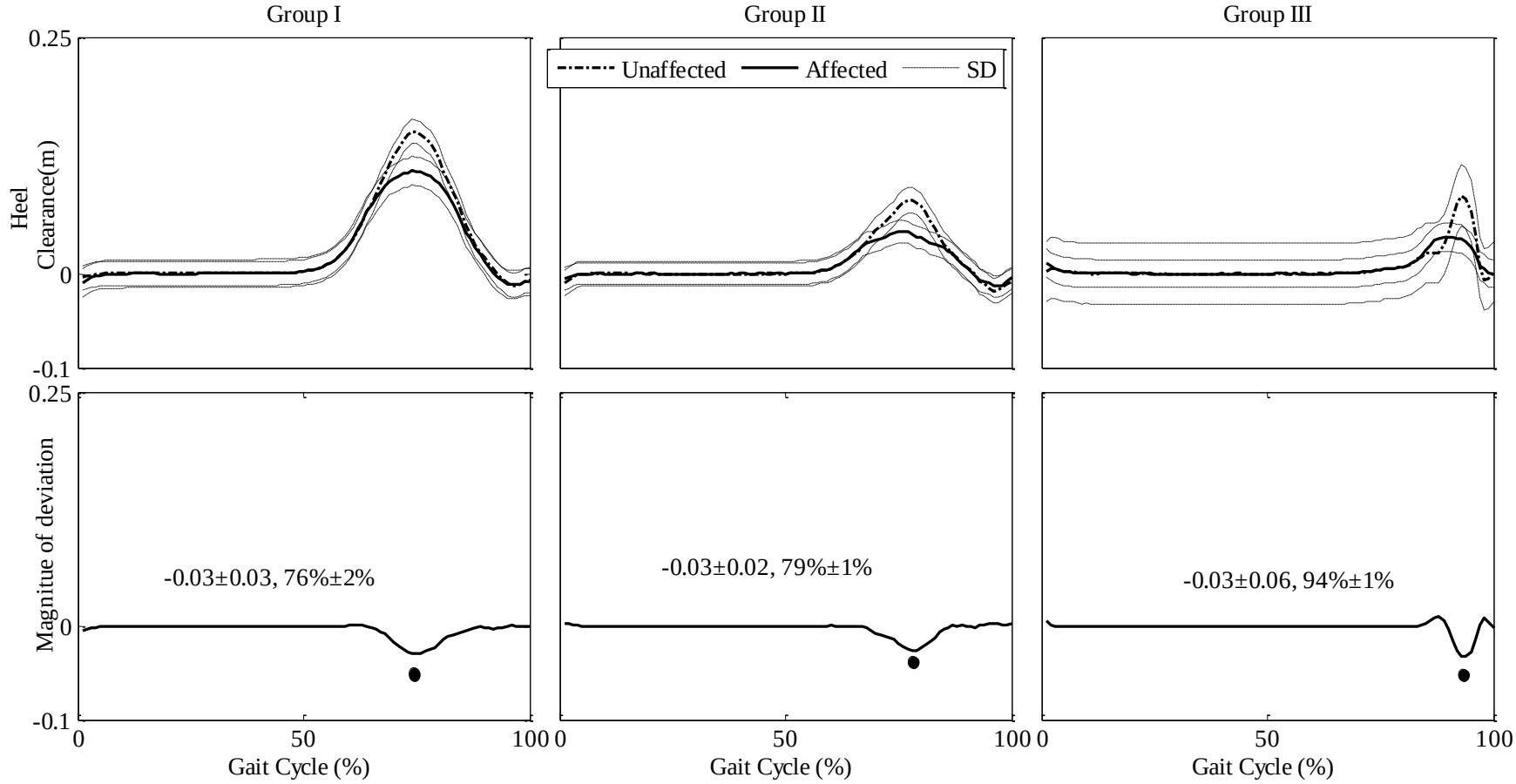

Fig 7.14. (Top) Mean and standard deviation of heel vertical displacement from 60 stroke patients categorised into three groups with 29 on Group I (Left), 17 on Group II (Middle), 14 on Group III (Right); (Bottom) Their corresponding CSROD results.

Table 7.5. CSROD results using Input 1 and Input 2 from three different group of stroke patients.

			Group I	Group II	Group III
Number of Patients			29	17	14
Average Gait Cycle Time (s)			1.68	2.64	3.32
			CSROD	CSROD	CSROD
Input 1	First Peak	PM_{norm}	-0.37 ± 0.57	-1.00 ± 1.48	-0.35 ± 0.48
		Timing (%)	44 ± 2	71 ± 4	77 ± 5
	Second Peak	PM_{norm}	2.23 ± 3.60	1.27 ± 1.99	0.48 ± 1.03
		Timing (%)	84 ± 1	89 ± 1	94 ± 1
Input 2	First Peak	PM_{norm}	0.20 ± 0.20	0.39 ± 0.25	0.36 ± 0.72
		Timing (%)	76 ± 2	79 ± 1	94 ± 1
	Second Peak	PM_{norm}	NA	NA	NA
		Timing (%)	NA	NA	NA

7.7.3 Case study

In this section, three individuals stroke patients from each subgroup were selected and studied. The selection of these three individuals was randomized. **Fig 7.15** and **Fig 7.16** display the mean and standard deviation of ankle angle and heel vertical displacement of three different stroke individuals and their corresponding CSROD results. The gait cycle time, stance time, swing time, Robinson Index (with stance and swing time as variables) and CSROD normalised peaks magnitude and timing of these three stroke individuals are shown in **Table 7.6**.

For stroke individual from Group I, the CSROD results from Input 1had first peak at 50% gait cycle timing and second peak at 75% (normalised peak magnitude 0.183 and 0.143 respectively), Input 2 had one peak at 72% gait cycle timing (normalised peak magnitude 0.069). Stroke individual from Group II had first peak at 74% and second peak at 89% using Input 1 (normalised peak magnitude 0.259 and 0.549 respectively) and one peak at 78% using Input 2 (normalised peak magnitude 0.289). Lastly, stroke individual from Group III had first and second peak at 64% and 76% respectively using Input 1 (normalised peak magnitude 0.426 and 0.521 respectively) and one peak at 94% using Input 2 (normalised peak magnitude 0.519).

Generally, the normalised peak magnitude shows greater asymmetry on the second peak using Input 1. As mentioned earlier, the moment during second peak often took place within swing phase. Lack of ankle movement always causes poor foot clearance and it reflected on the Input 2 normalised peak magnitude. Moreover, Robinson Index with swing time as variable also showed greater asymmetry compare to stance time as variable. The Robinson Index with both swing and stance time as variables show increasing asymmetry from stroke individual from Group I to Group III, which correlate to normalised peak magnitude.

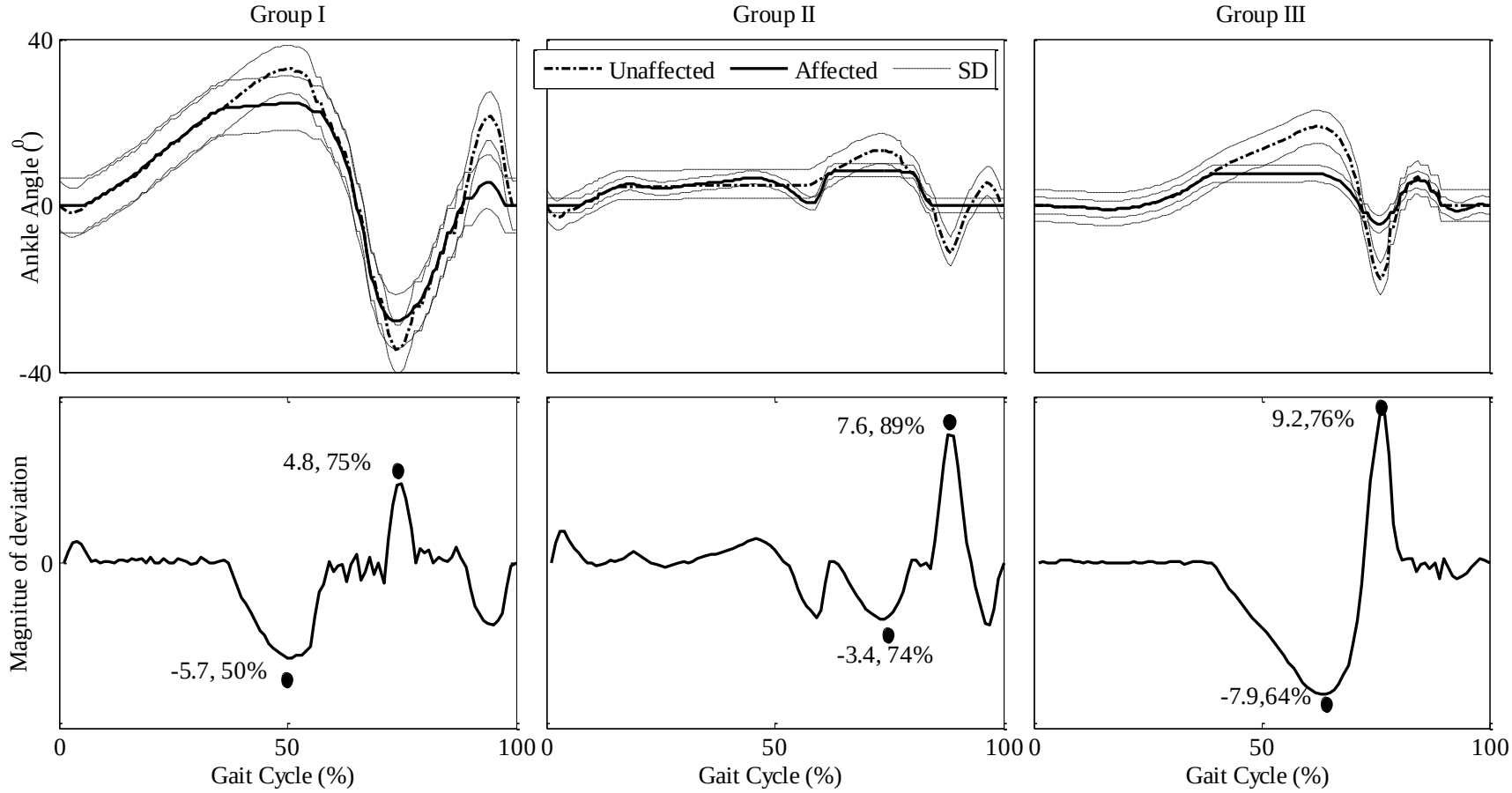

Fig 7.15. (Top) Mean and standard deviation of ankle angle from stroke patients on Group I (Left), Group II (Middle), Group III (Right); (Bottom) Their corresponding CSROD results.

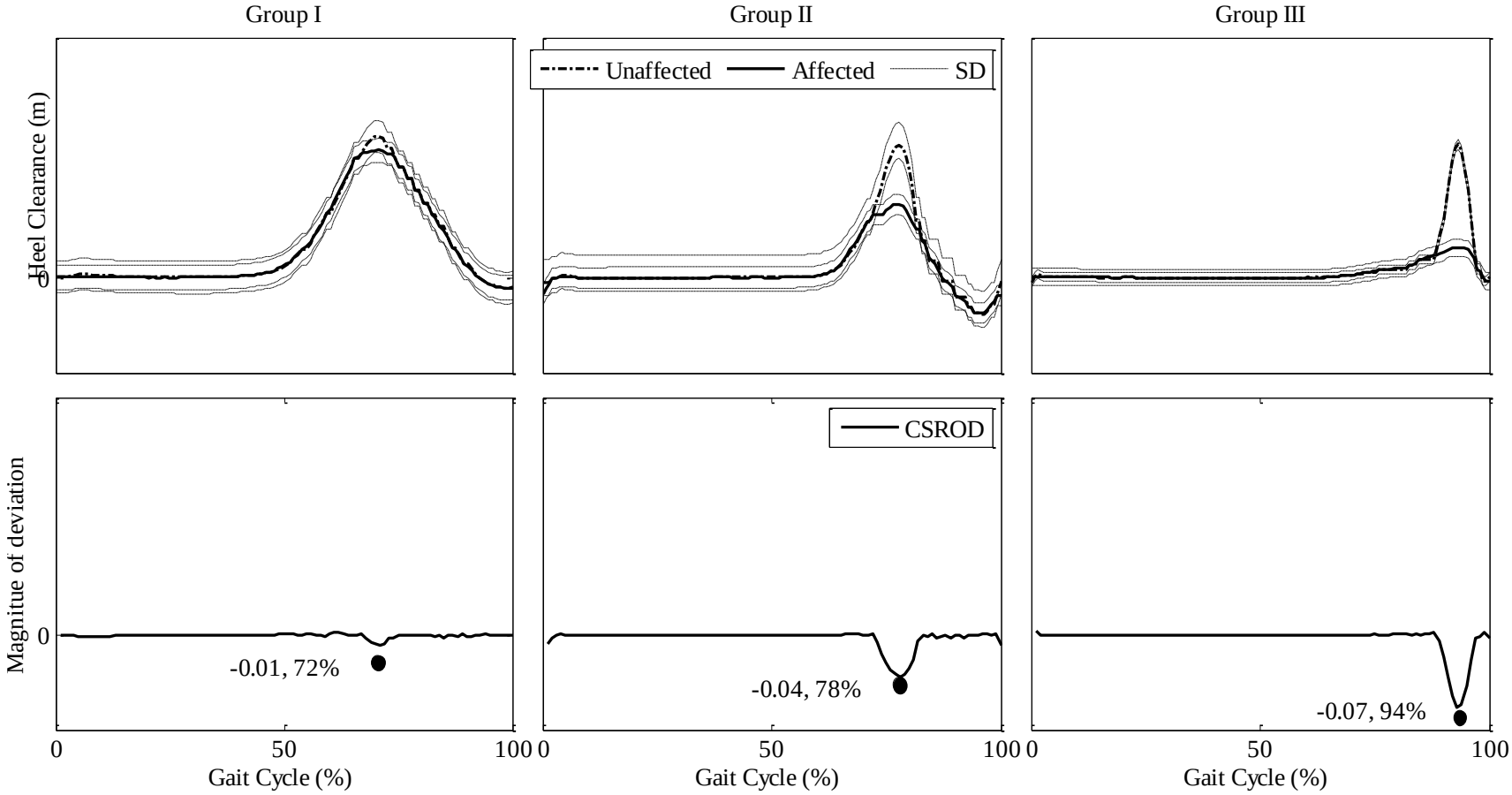

Fig 7.16. (Top) Mean and standard deviation of heel vertical displacement from stroke patients on Group I (Left), Group II (Middle), Group III (Right); (Bottom) Their corresponding CSROD results.

Table 7.6. CSROD results using Input 1 and Input 2 from three stroke patients from different groups.

			Individual I	**Individual II**	**Individual III**
Hemiplegia Side			Left	Left	Right
Gait Cycle Time (s)			1.61	2.10	3.37
Stance Time (%)		Unaffected leg	62.3	73.3	63.9
		Affected leg	67.5	81.9	82.7
Swing Time (%)		Unaffected leg	37.7	26.7	36.1
		Affected leg	32.5	18.0	17.3
Robinson Index		Stance Time	4.02	5.58	12.77
		Swing Time	7.43	19.39	35.08
			CSROD	CSROD	CSROD
Input 1	First Peak	PM_{norm}	0.143	0.259	0.426
		Timing (%)	50	74	64
	Second Peak	PM_{norm}	0.183	0.549	0.521
		Timing (%)	75	89	76
Input 2	First Peak	PM_{norm}	0.069	0.289	0.519
		Timing (%)	72	78	94
	Second Peak	PM_{norm}	NA	NA	NA
		Timing (%)	NA	NA	NA

7.8 Chapter Summary

In this chapter, a new gait asymmetry quantification method was proposed similar to the SROD algorithm. This new CSROD method is easier to use since it does not require to collect extra healthy walking data by introducing a symmetry line in cyclogram. The results from CSROD were being compared to the SROD results from this study and Shorter's experiment. The outcome shows that both CSROD and SROD were capable in tracking the asymmetry in joint angle during joint restricted walking. Linear length normalisation technique to align affected and unaffected lower limb gait data had demonstrated certain limitation and it cannot align gait events. This misalignment leads to false CSROD results. Therefore, DTW as used to replace it. Furthermore, it is necessary to normalise the peaks observed in CSROD results to provide consistent asymmetry information. CSROD was used to analyse the gait characteristic of stroke patients. Most of these stroke patients had problem to perform ankle dorsiflexion to move upper body forward, minimal to none plantar-flexed movement to provide foot clearance on the affected lower limb. The advantages of using CSROD and their normalised peak magnitude are they can provide timing information which traditional symmetry indices such as Robinson Index failed to deliver (as observed in Chapter 5), and the direction of these asymmetry can be easily studied among the normalised peak magnitude.

Chapter 8 Development of mathematical gait prediction models in stroke rehabilitation

8.1 Introduction

In the previous chapters, we have focused on extracting and analysing the gait characteristics from a large group of stroke patients (kinesiology and kinematic based gait analysis). In Chapter 6 we proposed a new K.I., which has good correlation to TUG score, and it can classify stroke subjects into different homogeneous subgroups. In Chapter 7, a new CSROD is introduced to characterise the complex gait asymmetry among stroke. These two features are very important in gait analysis and they can help physiotherapist or clinicians to comprehend the gait pattern of stroke subjects better and able to arrange suitable rehabilitation strategies. During stroke rehabilitation, it is very crucial to monitor the gait characteristics of stroke subjects at all time. This is to make sure they are receiving the proper rehabilitation treatments. Therefore, there is a growing interest in conducting longitudinal study after stroke to formulate a gait recovery prediction model. This model is able to help physiotherapists or clinicians to predict the gait recovery status after certain periods. If the actual gait pattern is not the same as the predicted gait, it is necessary for the physiotherapists or clinicians to reorganise the rehabilitation strategies.

In this chapter, we are going to develop two models to predict the gait functionality of stroke patients. We defined two new gait functionality indices in terms of gait trajectory performance and time delay between gait events. The aims of this chapter are:

1. To introduce two new gait functionality indices.

2. To examine the correlation between independent variables (spatial-temporal gait parameters, K.I., CSROD), dummy variables (type of strokes, age) and gait functionality indices.
3. To propose multivariate regression models to predict the gait functionality indices.
4. To validate these prediction models.

8.2 Overview of gait parameters in different recovery stages

In this chapter, the stroke patients from Experiment 3 (procedures were described in Chapter 3) are analysed. The demographic of these 15 stroke patients from this experiment are shown in **Table 8.1**.

In **Fig 8.1**, the stage 1, stage 2 and stage 3 of spatial-temporal parameters (stance and swing time percentage, gait cycle time, gait velocity, stride length, heel clearance), K.I. and CSROD of these 15 stroke patients are shown (bar from left to right). The stance time percentage, gait cycle time, K.I. and CSROD values were decreasing when stroke subjects were recovering. Meanwhile, swing time percentage, gait velocity, stride length, and heel clearance were increasing when stroke patients were recovering.

During stroke patients recovery period, they will walk in a faster manner to achieve healthier gait parameters. They will decrease their stance time, which will also decrease the double limb support time and increase swing time. The gait cycle time decreases due to the shorter stance time. The K.I. values decrease because the sEMG signal from these stroke subjects were more towards healthy manners, and a lower K.I. values indicates lesser TUG scores. Furthermore, the decrease in CSROD discrete values indicates less gait asymmetry. Meanwhile, the gait velocity increases due to the longer stride length and shorter gait cycle time. The heel clearance during swing time increases to help the stroke patients to lift the foot from the ground and prevent fall (hence lower K.I. values indicates lower TUG score).

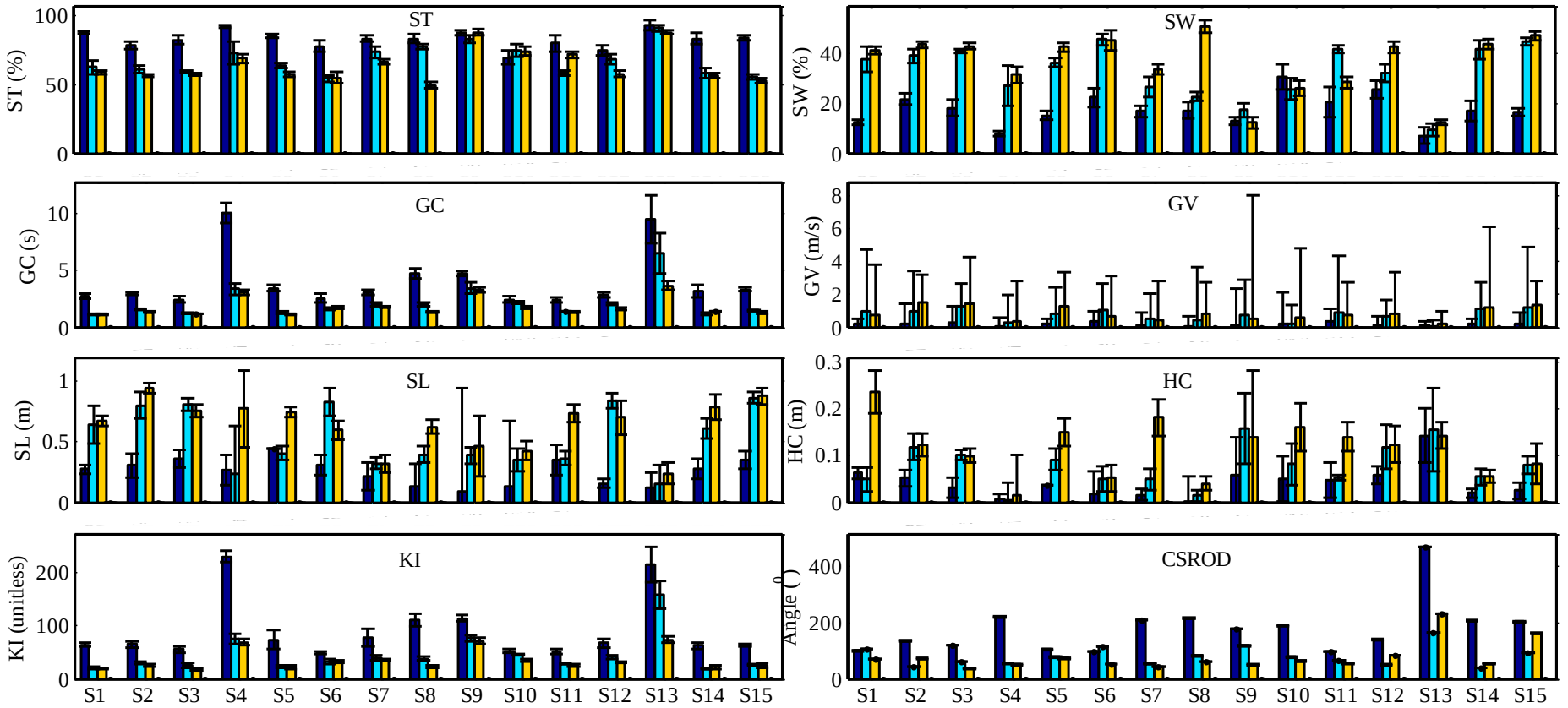

Fig 8.1. Spatial-temporal parameters, K.I. CSROD and gait velocity from 15 different stroke subjects throughout three different stages during their recovery period. ST-stance time percentage, SW-swing time percentage, GC-gait cycle time, GV-gait velocity, SL-stride length, HC-heel clearance, KI-Kinetic Index, CSROD-Cyclogram Symmetry Region of Deviation. Stage 1 to stage 3 were the bar chart from left to right for each subject.

Table 8.1. Demographic of stroke patients from Experiment 3.

	Age	Gender	Hemiplegia Side	Type of Stroke
S1	51	M	L	Ischemia
S2	68	M	L	Ischemia
S3	69	M	L	Ischemia
S4	47	M	L	Hemorrhage
S5	70	M	L	Ischemia
S6	57	M	L	Ischemia
S7	65	M	L	Ischemia
S8	69	M	L	Ischemia
S9	55	M	L	Hemorrhage
S10	46	M	L	Hemorrhage
S11	48	F	L	Ischemia
S12	57	F	R	Ischemia
S13	60	F	R	Hemorrhage
S14	70	M	L	Hemorrhage
S15	56	F	L	Ischemia

8.3 Gait functionality

In this section, we are going to introduce two new gait functionality indices to assess the walking ability of stroke subjects. The details descriptions of these indices are stated in the following sections.

8.3.1 Gait functionality based on gait trajectory, G_Funct_{GT}

The first gait functionality is based on deviation of gait trajectory, G_Funct_{GT}. This gait functionality is to find the difference of gait trajectory between the normal healthy subjects and stroke patients. The procedures G_Funct_{GT} are as shown as the following:

1. Gait alignment between the gait trajectory from stroke patient's paretic lower limb and normal healthy subjects.
2. Find the Euclidean distance between gait trajectory from stroke and healthy subjects.
3. Formulate G_Funct_{GT}.

8.3.1.1 Gait alignment using Piecewise Linear Length Normalisation (PLLN)

In Chapter 7, different gait alignment methods (DTW, PLLN, PDTW) were introduced in details. The gait alignment results show that DTW and PDTW are the better alignment methods to compare the two different lower limbs within the same subject. This is because the temporal information from both lower limbs are very similar. However, the temporal information of stroke gait trajectory and healthy normal gait trajectory are significant difference most of the time. This caused poor temporal alignment between the trajectories. **Fig 8.2** (a) presents the healthy and stroke vertical displacements. **Fig 8.2** (b), (c) and (d) displays the alignment results from DTW, PLLN and PDTW respectively. As shown in **Fig 8.2** (b) and (d), the distortion area was caused by poor temporal alignment. Therefore, the PLLN method [252] is used to align stroke gait data from paretic lower limb to normal gait data.

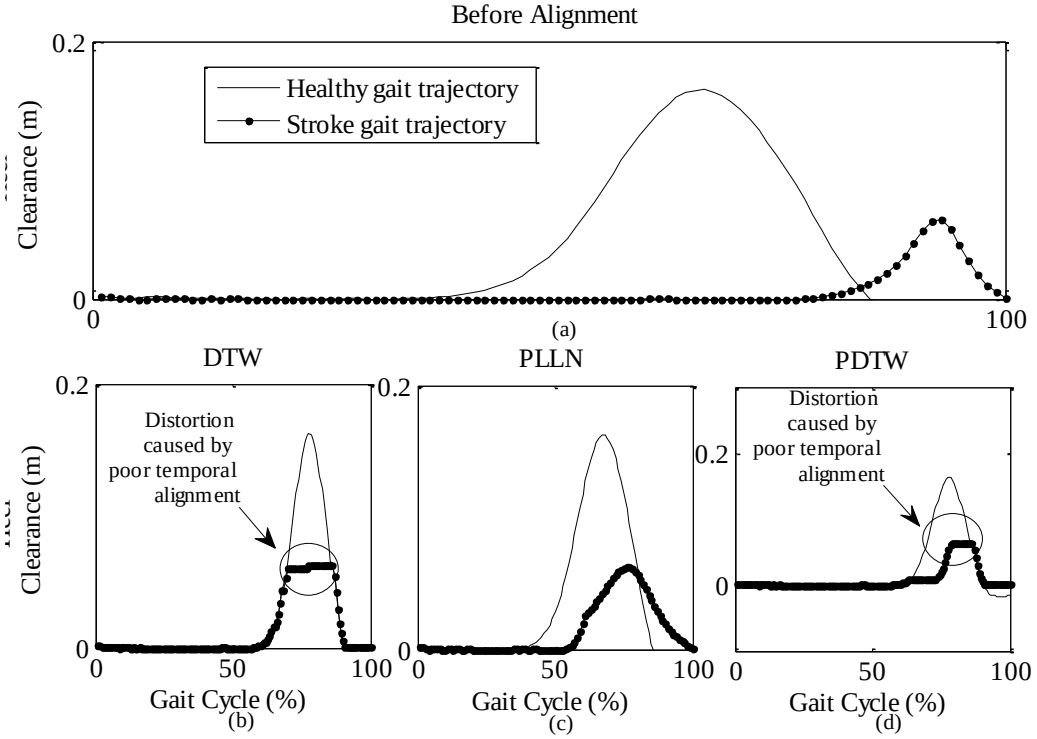

Fig 8.2. Vertical displacements from healthy and stroke subjects (a) before any alignment, (b) after DTW alignment, (c) after PLLN alignment. (d) after PDTW alignment. The highlighted area indicates poor temporal alignment by DTW and PDTW, which caused distortion at that area.

To form a complete gait trajectory, both the vertical and horizontal displacements were aligned between stroke and healthy subjects. A complete gait trajectory is computed by plotting vertical displacement against horizontal displacement as shown in **Fig 8.3**.

8.3.1.2 Determine Euclidean Distance between gait trajectory of stroke and healthy subjects

Let $X_h = [x_{h,1}, x_{h,2}, x_{h,3}, \dots, x_{h,N}]$, $Y_h = [y_{h,1}, y_{h,2}, y_{h,3}, \dots, y_{h,N}]$, $X_s = [x_{s,1}, x_{s,2}, x_{s,3}, \dots, x_{s,N}]$, and $Y_s = [y_{s,1}, y_{s,2}, y_{s,3}, \dots, y_{s,N}]$ to be the horizontal (X) and vertical (Y) displacements for both healthy (h) and stroke (s) respectively, N is the total number of data points after alignment. The Euclidean distance between two points from both healthy and stroke patient's gait trajectories is:

$$ED_1 = \sqrt{(x_{h,1} - x_{s,1})^2 + (y_{h,1} - y_{s,1})^2} \tag{8.1}$$

where ED_1 is the first Euclidean distance between the first point of gait trajectory from healthy and stroke patients. Repeat Eq (8.1) from point one to point N to form a vector $ED(N) = [ED_1, ED_2, ED_3, \dots, ED_N]$. **Fig 8.3** shows the gait trajectories between healthy and stroke subjects. The straight lines in this figure illustrated the Euclidean Distance between two points.

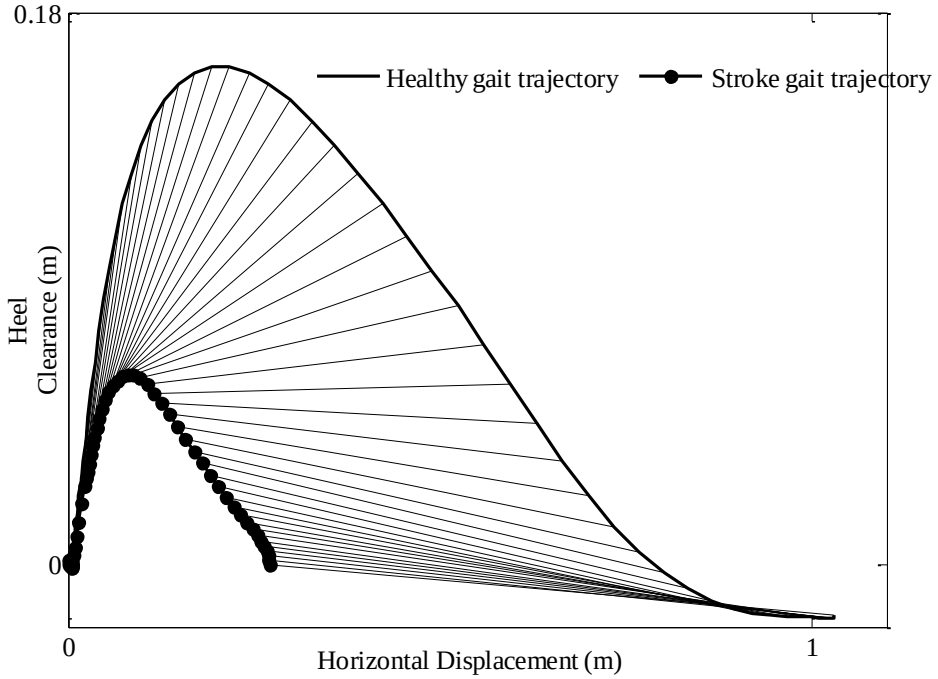

Fig 8.3. Gait trajectories from healthy and stroke subjects formed by plotting vertical displacement against horizontal displacement. The straight lines illustrated the Euclidean distance between each points.

8.3.1.3 Formulate gait functionality based on gait trajectory, G_Funct_{GT}

After the Euclidean distance for *N* data points are determined, each *ED*(*N*) gait cycle is plotted. **Fig 8.4** displays the *ED*(*N*) plotted against one gait cycle time from one stroke patient. These graphs represent the gait functionality based on gait trajectory over time in three different stage of recovery period. The results from this figure stated few key features from this stroke patient; (i) the gait trajectories between this stroke and healthy subjects started to deviate severely from each other after 50% gait cycle time; (ii) the final deviation between two trajectories were 0.758, 0.393 and 0.362m for stages 1, 2 and 3 respectively.

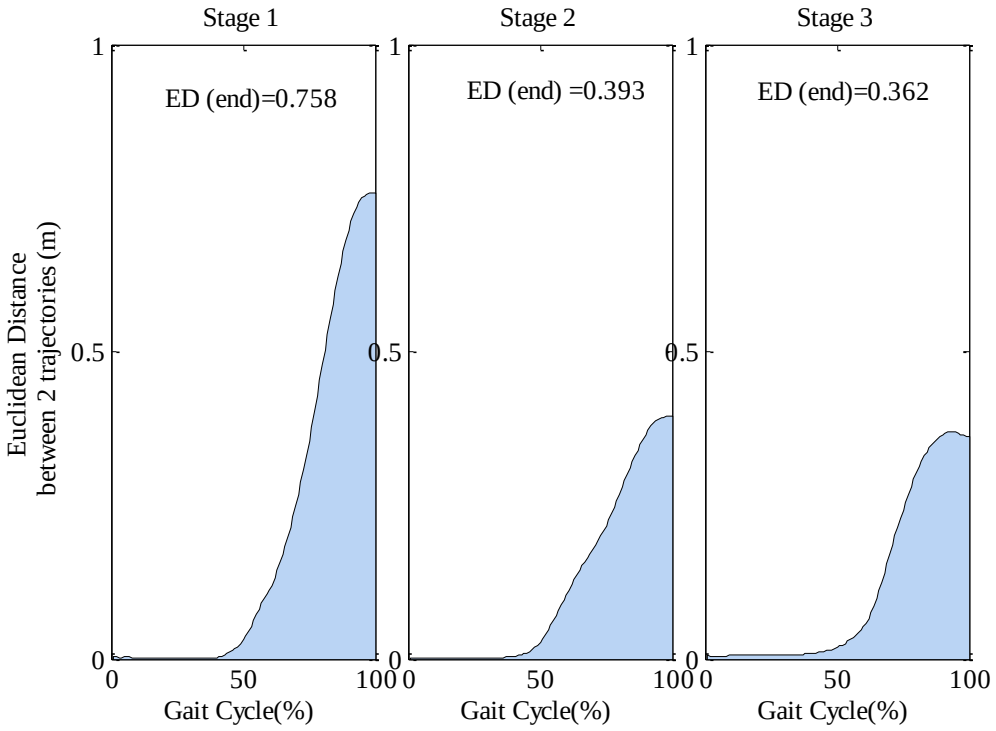

Fig 8.4. *ED(N)* plotted over one gait cycle time from one stroke subject in three different recovery stages.

Based on the results from **Fig 8.4**, we can further develop a gait functionality index based on gait trajectory.

$$G\_Funct_{GT} = \frac{A_{ED} * ED(end)}{A_{GT,h} * 100} \tag{8.2}$$

where A_{ED} is area under the curve for $ED(N)$ against gait cycle time, $ED(end)$ is the last point on this curve and $A_{GT,h}$ is area under the curve for healthy gait trajectory. As observed in stage 3 from **Fig 8.4**, the Euclidean distance between healthy and stroke gait trajectory is reducing. This form the reason to choose $ED(end)$ (last point of $ED(N)$) in this function, i.e. to detect the final deviation of $ED(N)$ curve. Both $A_{GT,h}$ and 100 are served as the normalisation factor. The value 100 is selected based on the maximum gait cycle time, which is 100%.

8.3.2 Gait functionality based on time delay, G_Funct_{TD}

The second gait functionality is based on gait events time delay. After the heel-strike and toe-off events are determined using gyroscope [19], mid-stance and mid-swing events can be estimated as follow:

$$midstance = \frac{toeoff_t - heelstrike_t}{2} \tag{8.3}$$

$$midswing = \frac{heelstrike_{t+1} - toeoff_t}{2} \tag{8.4}$$

where $toeoff_t$ is the current toe-off, $heelstrike_t$ is the current heel-strike and $heelstrike_{t+1}$ is the next heel-strike. Once these two gait events are determined, a gait event vector, G is formed where G=[$heelstrike_t$, *midstance,* $toeoff_t$, *midswing,* $heelstrike_{t+1}$].

The average vector G for healthy is determined using the 10 healthy subjects from Experiment 1, and it is G_h=[1, 30, 60, 80, 100] after converted in term of gait cycle percentage. This vector G_h demonstrates that the gait for healthy subjects started at 1% gait cycle time, mid-stance happened around 30% gait cycle time, toe-off at 60% gait cycle time, mid-swing at 80% gait cycle time and the gait cycle ended at 100% gait cycle time (next heel-strike). By using this standard healthy gait event as comparison, the time delay between stroke and healthy subjects can be determined using this equation:

$$TD(i) = |G_s(i) - G_h(i)| \tag{8.5}$$

where *TD(i)* is the time delay function, *i* is the number of gait event (*i*=5) and G_s is the gait event vector from stroke, $|\cdot|$ bracket indicates absolute number. Once *TD(i)* is constructed, it is being interpolated using spline-fit to 100 data points to form a time delay function with time history.

Fig 8.5 displays the *TD(i)* plotted in one gait cycle from one stroke patient in three different recovery stages. The black dots in this figure represent gait events in different phases. This figure provides information such as the time delay at each gait event between stroke and healthy subjects. For instance, in stage 1, the mid-

stance, toe-off and mid-swing of this stroke patient were slower than healthy by 13.83, 18.95 and 9.00% respectively. Based on this result, the gait event that caused the maximum time delay in stage 1 for this particular stroke patient was toe-off. This subject was later trying to speed up the swing time and it reduced the mid-swing time delay to complete the gait cycle.

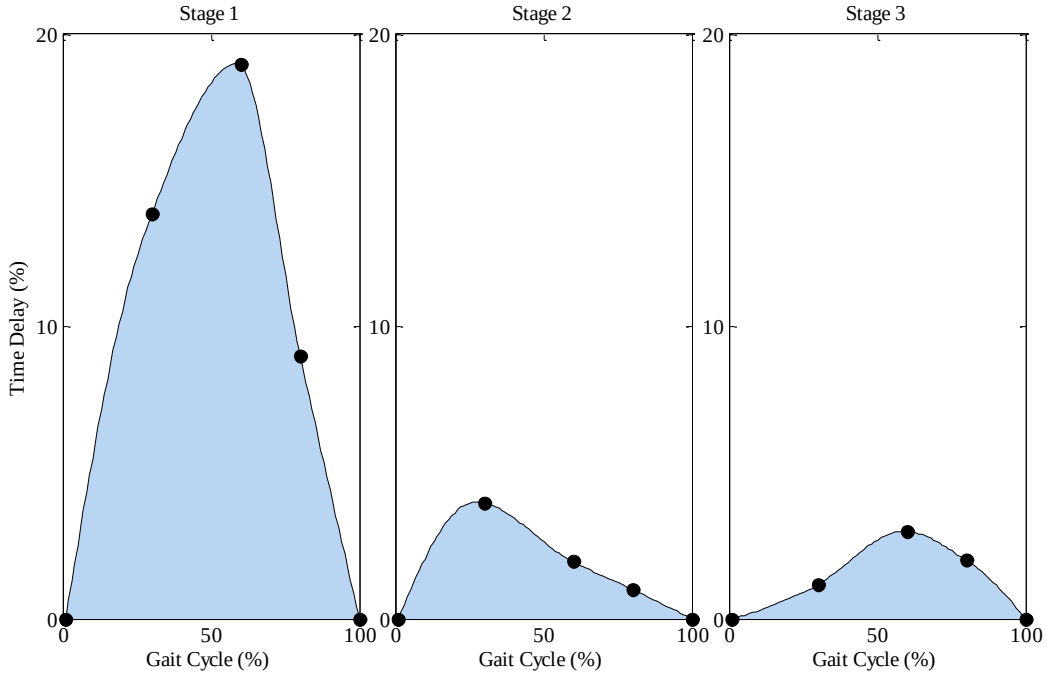

Fig 8.5. *TD(i)* plotted over one gait cycle time from one stroke subject in three different recovery stages.

Since Stage 1 had the highest and stage 3 had the lowest area under the curve, we can compute the gait functionality index based on time delay:

$$G\_Funct_{TD} = \frac{A_{TD}}{100} \tag{8.6}$$

where A_{TD} is the area under the curve for *TD(i)* plotted, and the value 100 is chosen as normalisation factor based on maximum gait cycle percentage (100%).

8.3.3 Results from gait functionality indices

Fig 8.6 displays the results of gait functionality indices based on gait trajectory and time delay, G_Funct_{GT} and G_Funct_{TD} respectively. As expected, both indices have

highest value in stage 1 and the value decreases throughout the recovery period for all stroke patients. These two indices describe the walking ability of stroke patients throughout their recovery period in term of their trajectories pattern and time delay on gait events. Since the healthy subject's gait trajectory and gait events are used as a standard comparison to compute these two indices, the values on these indices indicates the deviation of gait trajectories and delay in gait events between healthy and stroke patients.

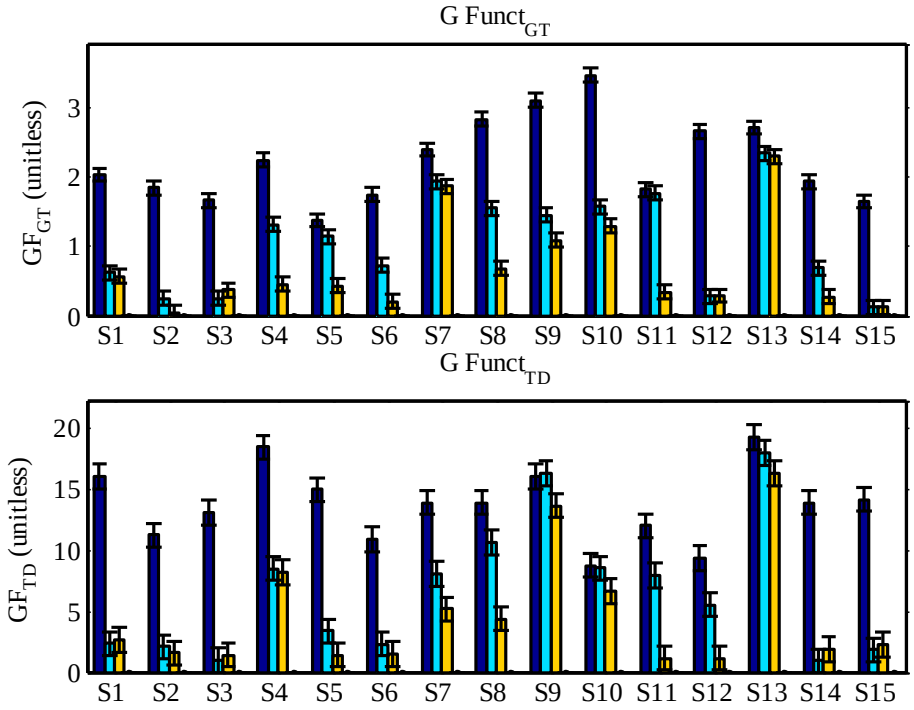

Fig 8.6. Gait functionality indices based on both gait trajectory and time delay from 15 different stroke subjects throughout three different stages during their recovery period.

8.4 Multivariate Linear Regression Model

In this section, multivariate linear regression models are developed to predict the gait functionality indices described in earlier section based on several dependent variables (gait parameters and stroke demographic). Two models are formulated based on two different approaches:

i. Regression Model Approach 1- Prediction of Outcome Based on Baseline Strokes Characteristics. This model is used to predict:
   - Gait functionality based on gait trajectory index, G_Funct_{GT} in stage 2.
   - Gait functionality based on gait trajectory index, G_Funct_{GT} in stage 3.
   - Gait functionality based on time delay index, G_Funct_{TD} in stage 2.
   - Gait functionality based on time delay index, G_Funct_{TD} in stage 3.

ii. Regression Model Approach 2- Prediction of Outcome based on Recovery History. This model is used to predict:
   - Gait functionality based on gait trajectory index, G_Funct_{GT} in stage 3.
   - Gait functionality based on time delay index, G_Funct_{TD} in stage 3.

Based on the total number of stroke patients participated in this longitudinal study (n=15), the data from 12 subjects were used as the training data for regression model and the data from three subjects were being used to validate the model.

8.4.1 Model Description

Multivariate linear regression model is described in the following equation:

$$y = \beta_c + \beta_1 x_1 + \beta_2 x_2 + \cdots + \beta_p x_p + \epsilon \quad (8.7)$$

where y is the true dependent variable, β_c is the constant intercept, x_p is the independent variables with total p variables, β_p is the regression coefficient for independent variables x_p, and ϵ is the error term. Assuming the error term ϵ to be zero, the estimate multivariate linear regression equations are stated in the following sections.

8.4.1.1 Regression Model Approach 1

Regression Model Approach 1 is a prediction model to predict the gait functionality indices (G_Funct_{GT} and G_Funct_{TD}) at stage 2 and stage 3 based on stroke patients baseline characteristics. It can be modelled as:

$$\hat{y}^{(i)} = \beta_{c,Approach1} + \sum_{o=1}^{p} \beta_o x_o \quad (8.8)$$

where $\hat{y}^{(i)}$ is the predicted value of the dependent variable based on baseline stroke characteristics (*i*= stage 2, stage 3), $\beta_{c,Approach1}$ reflects the random intercept and β_o the selected regression coefficient for the stroke patients baseline gait data x_o. Eq (8.8) can be rewritten in the form of matrix:

$$\hat{\boldsymbol{y}} = \boldsymbol{X}\boldsymbol{\beta} \tag{8.9}$$

$$\hat{\boldsymbol{y}} = \begin{bmatrix} \hat{y}_1^{(i)} \\ \hat{y}_2^{(i)} \\ \hat{y}_3^{(i)} \\ \vdots \\ \hat{y}_n^{(i)} \end{bmatrix} \tag{8.10}$$

$$\boldsymbol{\beta} = \begin{bmatrix} \beta_{c,Approach1} \\ \beta_{\mathbf{1}} \\ \beta_{\mathbf{2}} \\ \vdots \\ \beta_{\boldsymbol{p}} \end{bmatrix} \tag{8.11}$$

$$\boldsymbol{X} = \begin{bmatrix} 1 & x_{1,1} & x_{1,2} & x_{1,3} & \dots & x_{1,p} \\ 1 & x_{2,1} & x_{2,2} & x_{2,3} & \dots & x_{2,p} \\ 1 & x_{3,1} & x_{3,2} & x_{3,3} & \dots & x_{3,p} \\ 1 & x_{4,1} & x_{4,2} & x_{4,3} & \dots & x_{4,p} \\ \vdots & \vdots & \vdots & \vdots & \dots & \vdots \\ 1 & x_{n,1} & x_{n,2} & x_{n,3} & \dots & x_{n,p} \end{bmatrix} \tag{8.12}$$

where *n* is the number of training samples (in our study *n*=12), *p* is the total number of variables. $\hat{\boldsymbol{y}}$ is a *n*x1 matrix, $\boldsymbol{\beta}$ is a (p+1) x 1 matrix, and $\boldsymbol{X}$ is a *n* x (*p*+1) matrix. Using this matrix form, the $\beta_{c,Approach1}$ intercept is assigned with an independent variable x_0 with x_0=1. To determine the coefficient $\boldsymbol{\beta}$, the sum of squared residuals (RSS) between the predicted and the exact dependent variable need to be minimised. The scalar form of RSS is as shown below.

$$RSS = \sum_{j=1}^{n} (y_j - \hat{y}^{(i)}{}_j)^2 \tag{8.13}$$

Eq (8.13) can be rewritten in the form of matrix:

$$RSS = (\boldsymbol{y} - \hat{\boldsymbol{y}})^{\boldsymbol{T}} (\boldsymbol{y} - \hat{\boldsymbol{y}}) \tag{8.14}$$

$$RSS = (\boldsymbol{y} - \boldsymbol{\beta^T X^T})^T(\boldsymbol{y} - \boldsymbol{X\beta}) \tag{8.15}$$

where $\boldsymbol{y}$ is the experimental training data. The matrix $\boldsymbol{\beta}$ can be determined by taking the partial derivative of *RSS* with respect to $\boldsymbol{\beta}$.

$$\frac{\delta(RSS)}{\delta(\boldsymbol{\beta})} = \frac{\delta\Big((\boldsymbol{y} - \boldsymbol{\beta^T X^T})^T(\boldsymbol{y} - \boldsymbol{X\beta})\Big)}{\delta(\boldsymbol{\beta})} = 0 \tag{8.16}$$

By expanding the term$(\boldsymbol{y} - \boldsymbol{\beta^T X^T})^T(\boldsymbol{y} - \boldsymbol{X\beta})$, we can obtain:

$$\frac{\delta(\boldsymbol{y^T y})}{\delta(\boldsymbol{\beta})} - \frac{\delta(\boldsymbol{y^T X\beta})}{\delta(\boldsymbol{\beta})} - \frac{\delta(\boldsymbol{\beta X^T y})}{\delta(\boldsymbol{\beta})} + \frac{\delta(\boldsymbol{\beta^T X^T X\beta})}{\delta(\boldsymbol{\beta})} = 0 \tag{8.17}$$

$$0 - \boldsymbol{y^T X} - (\boldsymbol{X^T y})^T + \boldsymbol{2\beta^T X^T X} = \boldsymbol{0} \tag{8.18}$$

$$\boldsymbol{\beta^T} = \boldsymbol{y^T X}(\boldsymbol{X^T X})^{-\boldsymbol{1}} \tag{8.19}$$

$$\boldsymbol{\beta} = (\boldsymbol{X^T X})^{-\boldsymbol{1}}\boldsymbol{X^T y} \tag{8.20}$$

By using simple matrix multiplication, the regression coefficient in $\boldsymbol{\beta}$ can be determined easily using Eq (8.20).

8.4.1.2 Regression Model Approach 2

Regression Model Approach 2 is a prediction model to predict the gait functionality indices (G_Funct_{GT} and G_Funct_{TD}) in stage 3 based on the recovery trajectory from stage 1 to stage 2. It can be modelled as:

$$\hat{z} = \beta_{c,Approach2} + \sum_{o=1}^{p} \beta_o({x_o}^{(1)} - {x_o}^{(2)}) \tag{8.21}$$

where $\hat{z}$ is the recovery trajectory from stage 1 to stage 3.

$$\hat{z} = \hat{y}^{(1)} - \hat{y}^{(3)} \tag{8.22}$$

In this model, the recovery trajectory from stage 1 to stage 2 is the different between gait data from stage 1 and stage 2. This recovery trajectory is a useful indicator to predict stage 3 gait performance as most of the stroke patients will followed this trajectory trend. Eq (8.21) can also be rewritten as matrix form:

$$\hat{\boldsymbol{z}} = \Delta \boldsymbol{X}\boldsymbol{\beta} \tag{8.23}$$

$$\hat{\boldsymbol{z}} = \begin{bmatrix} \hat{y}_1^{(1)} - \hat{y}_1^{(3)} \\ \hat{y}_2^{(1)} - \hat{y}_2^{(3)} \\ \hat{y}_3^{(1)} - \hat{y}_3^{(3)} \\ \vdots \\ \hat{y}_n^{(1)} - \hat{y}_n^{(3)} \end{bmatrix} \tag{8.24}$$

$$\boldsymbol{\beta} = \begin{bmatrix} \beta_{c,Approach2} \\ \beta_{\mathbf{1}} \\ \beta_{\mathbf{2}} \\ \vdots \\ \beta_{\boldsymbol{p}} \end{bmatrix} \tag{8.25}$$

$$\Delta \boldsymbol{X} = \begin{bmatrix} 1 & {x_{1,1}}^{(1)} - {x_{1,1}}^{(2)} & \cdots & {x_{1,p}}^{(1)} - {x_{1,p}}^{(2)} \\ 1 & {x_{2,1}}^{(1)} - {x_{2,1}}^{(2)} & \cdots & {x_{2,p}}^{(1)} - {x_{2,p}}^{(2)} \\ 1 & {x_{3,1}}^{(1)} - {x_{3,1}}^{(2)} & \cdots & {x_{3,p}}^{(1)} - {x_{3,p}}^{(2)} \\ 1 & {x_{4,1}}^{(1)} - {x_{4,1}}^{(2)} & \cdots & {x_{4,p}}^{(1)} - {x_{4,p}}^{(2)} \\ \vdots & \vdots & \vdots\ \vdots\ \vdots & \vdots \\ 1 & {x_{n,1}}^{(1)} - {x_{n,1}}^{(2)} & \cdots & {x_{n,p}}^{(1)} - {x_{n,p}}^{(2)} \end{bmatrix} \tag{8.26}$$

Similar to previous section, the sum of squared residuals (RSS) between the predicted and the exact dependent variable need to be minimised in order to determine regression coefficient for model 2. Following the same procedures from Eq (8.13) to (8.20), the regression coefficient for this model is:

$$\boldsymbol{\beta} = \left((\boldsymbol{X}^{(\mathbf{1})} - \boldsymbol{X}^{(\mathbf{2})})^{\boldsymbol{T}}(\boldsymbol{X}^{(\mathbf{1})} - \boldsymbol{X}^{(\mathbf{2})})\right)^{-\mathbf{1}}(\boldsymbol{X}^{(\mathbf{1})} - \boldsymbol{X}^{(\mathbf{2})})^{\boldsymbol{T}}(\boldsymbol{y}^{(\mathbf{1})} - \boldsymbol{y}^{(\mathbf{3})}) \tag{8.27}$$

where $\boldsymbol{X^{(1)}}$ and $\boldsymbol{X^{(2)}}$ are the independent variable matrices at stage 1 and stage 2 respectively, $\boldsymbol{y^{(1)}}$ and $\boldsymbol{y^{(2)}}$ are the experimental dependent variable matrices at stage 1 and stage 3 respectively.

8.4.1.3 Procedure to select independent variables

There are two predicted dependent variables, G_Funct_{GT} and G_Funct_{TD}. Meanwhile, there are plenty of independent variables to be selected from gait parameters or the demographic of the subject. If there are not enough independent variables, it will affect the accuracy of the predicted model; however if there are

too many independent variables, it will lead to multicollinearity [255]. Multicollinearity happens when the independent variables were highly related to each other.

The procedures to select independent variables as the model training inputs are described as follow:

i. Find the correlations between independent variables and dependent variable. Only include independent variables which are highly correlated to the dependent variable.
ii. Find the correlation among independent variables. Remove variables that are highly correlate to each other to avoid multicollinearity.

8.4.2 Statistical analysis

Pearson correlation coefficient, *r* was used to determine the correlation between variables. The values *r* between -1 to -0.5 and 0.5 to 1 are considered as strong correlation. Student paired t-test were used to determine the statistical significant between variables with *p*-value < 0.05 as threshold.

The mean absolute percentage error was applied to determine the prediction accuracy between the predicted gait functionality indices and the actual indices. The formula to compute this mean absolute percentage is:

$$Error = \frac{Y_{actual} - Y_{predicted}}{Y_{actual}} * 100\% \quad (8.28)$$

8.4.3 Results from regression model approach 1

8.4.3.1 Selection of independent variables

Initially, the independent variables that were considered as the training input for regression model were stroke subjects' demography (type of stroke, hemiplegia side, gender), baseline conventional gait parameters (stride length, heel clearance, stance and swing time percentage, gait velocity), baseline K.I., baseline CSROD and baseline gait functionality indices. To select the proper independent variables, the procedures explained in section 8.4.1.3 were executed. The results were shown

in **Table 8.2** and **Table 8.3**. In **Table 8.2**, it clearly shows that none of the dummy variables were highly correlate to the predicted variables. This means that the predicted stage 2 and 3 gait functionality indices were not affected by the demographic of stroke patients.

8.4.3.2 Prediction of G_Funct$_{GT}$ in stage 2

In **Table 8.2**, only baseline heel clearance, baseline gait velocity, baseline K.I., baseline CSROD and baseline *G_Funct$_{GT}$* are highly correlated to *G_Funct$_{GT}$* at stage 2. To avoid multicollinearity, the correlation coefficient of these five variables are determined in **Table 8.3**. Baseline heel clearance is highly correlate to baseline K.I. and CSROD values. Since baseline heel clearance has lower correlation to predicted variable compared to other independent variables, therefore baseline gait velocity, baseline K.I., baseline CSROD and baseline G_Funct_{GT} are selected as the independent variables to predict *G_Funct$_{GT}$* at stage 2.

8.4.3.3 Prediction of G_Funct$_{GT}$ in stage 3

The baseline stride length, baseline gait velocity, baseline K.I, baseline CSROD values and baseline *G_Funct$_{GT}$* are highly correlated to *G_Funct$_{GT}$* at stage 3 according to **Table 8.2**. From **Table 8.3**, baseline stride length is highly correlate to baseline *G_Funct$_{GT}$*. Since baseline stride length has weaker correlation compared to baseline *G_Funct$_{GT}$*, therefore the independent variables selected to predict *G_Funct$_{GT}$* at stage 3 are baseline gait velocity, baseline K.I., baseline CSROD and baseline *G_Funct$_{GT}$*.

8.4.3.4 Prediction of G_Funct$_{TD}$ in stage 2

The baseline heel clearance, baseline gait velocity, baseline K.I, baseline CSORD values and baseline *G_Funct$_{TD}$* from **Table 8.2** are highly correlated *G_Funct$_{TD}$* at stage 3. After the filtering process based on result from **Table 8.3**, the independent variables to predict *G_Funct$_{TD}$* at stage 3 are baseline K.I, baseline CSORD values and baseline *G_Funct$_{TD}$*.

8.4.3.5 Prediction of G_Funct$_{TD}$ in stage 3

In **Table 8.2**, type of stroke, baseline heel clearance, baseline stance and swing time, baseline gait velocity, baseline K.I., baseline CSORD values and baseline *G_Funct$_{TD}$* are highly correlate to dependent variable *G_Funct$_{TD}$* at stage 3. Similar to the previous process, the final independent variables are baseline K.I, baseline CSORD values and baseline *G_Funct$_{TD}$*.

8.4.3.6 Validation of regression model approach 1

In **Table 8.4** and **Table 8.5**, the regression coefficient for each independent variable and constant intercept were presented for predicted stage 2 and stage 3 G*_Funct$_{GT}$* and *G_Funct$_{TD}$* respectively. The baseline independent variables that were selected for prediction are shown in **Table 8.6**. The predicted gait functionality indices are determined by substituting the regression coefficient and baseline independent variables into Eq (8.8).

To validate these prediction models, the mean absolute percentage error between the predicted values and actual values were determine. **Table 8.7** and **Table 8.8** present the predicted results, actual values and their error for *G_Funct$_{GT}$* and *G_Funct$_{TD}$* at stage 2 and stage 3 of three stroke patients respectively. The results illustrate that S13 had high accuracy with less than 10% error in all predicted indices; S14 had high error in all indices beside *G_Funct$_{GT}$* at stage 2; S15 had very high accuracy in all indices with less than 10% error beside *G_Funct$_{GT}$* at stage 2.

Table 8.2. Correlation coefficient and *p*-values between independent variables and predicted gait functionality indices at state 2 and stage 3.

Independent Variables	Predicted Stage 2 G_Funct_{GT}		Predicted Stage 3 G_Funct_{GT}		Predicted Stage 2 G_Funct_{TD}		Predicted Stage 3 G_Funct_{TD}	
	r	*p*-value	*r*	*p*-value	*r*	*p*-value	*r*	*p*-value
	Stroke Demographic							
Gender (m/f)	-0.0555	0.160	-0.0695	0.818	-0.213	<0.01	-0.078	<0.01
Type of stroke (I/H)	-0.424	0.152	-0.431	0.949	-0.439	<0.01	-0.496	<0.01
Hemiplegia Side (L/R)	-0.143	0.377	-0.369	0.420	0.397	<0.01	-0.351	<0.05
	Conventional Spatial-Temporal Parameters							
Baseline Stride Length	-0.269	<0.01	-0.512	0.0530	0.469	<0.01	-0.356	<0.01
Baseline Heel Clearance	0.504	<0.01	0.355	<0.01	0.557	<0.01	0.667	<0.01
Baseline Stance Time	0.302	<0.01	0.291	<0.01	0.367	<0.01	0.532	<0.01
Baseline Swing Length	-0.302	<0.01	-0.291	<0.01	-0.367	<0.01	-0.532	<0.01
Baseline Gait Velocity	-0.593	<0.01	-0.507	<0.05	-0.575	<0.01	-0.571	<0.01
	Proposed Gait Assessment Indices							
Baseline K.I.	0.504	<0.01	0.557	<0.01	0.653	<0.01	0.753	<0.01
Baseline CSROD	0.560	<0.01	0.731	<0.01	0.678	<0.01	0.778	<0.01
	Proposed Gait Functionality Indices							
Baseline G_Funct_{GT}	0.508	<0.01	0.600	<0.01	-	-	-	-
Baseline G_Funct_{TD}	-	-	-	-	0.723	<0.01	0.638	0.053

m=male; f=female; I=Ischemia; H=Haemorrhage; L=left; R=right; *r*=Pearson Correlation Coefficient

Table 8.3. Correlation coefficient between baseline independent variables.

	ST	**SW**	**SL**	**HC**	**GV**	**KI**	**CSROD**	***G_Funct$_{GT}$***	***G_Funct$_{TD}$***
ST	NA	-1	0.295	0.392	-0.424	0.742	0.489	-0.156	0.988
SW		NA	-0.295	-0.392	0.424	-0.742	-0.489	0.156	-0.988
SL			NA	-0.157	0.310	0.182	-0.307	-0.683	0.253
HC				NA	-0.185	0.598	0.611	0.284	0.443
GV					NA	-0.493	-0.475	-0.470	-0.567
KI						NA	0.429	0.296	0.477
CSROD							NA	0.432	0.457
G_Funct$_{GT}$								NA	NA
G_Funct$_{TD}$								NA	NA

ST= Stance time percentage; SW=Swing time percentage; SL=Stride length; HC=Heel Clearance; GV=Gait Velocity.

Table 8.4. Multivariate Linear Regression Model to predict gait functionality index *G_Funct$_{GT}$* at stage 2 and stage 3.

	Predicted Stage 2 *G_Funct$_{GT}$*		**Predicted Stage 3 *G_Funct$_{GT}$***	
	b coefficient	Standard error	*b* coefficient	Standard error
Baseline Gait Velocity	1.3355	0.958	-0.01731	0.220
Baseline K.I.	0.0033	0.0004	-0.00171	0.003
Baseline CSROD	0.0021	0.0002	0.00492	0.002
Baseline *G_Funct$_{GT}$*	0.4564	0.245	0.3784	0.250
Intercept	-0.86399	0.125	-0.87348	0.094

Table 8.5. Multivariate Linear Regression Model to predict gait functionality index *G_Funct$_{TD}$* at stage 2 and stage 3.

	Predicted Stage 2 *G_Funct$_{TD}$*		**Predicted Stage 3 *G_Funct$_{TD}$***	
	b coefficient	Standard error	*b* coefficient	Standard error
Baseline K.I.	0.0463	0.03	0.0276	0.02
Baseline CSROD	0.0236	0.01	0.0251	0.01
Baseline *G_Funct$_{TD}$*	-0.316	0.05	0.125	0.04
Intercept	2.471	1.49	-4.045	2.66

Table 8.6. Baseline independent variables values for three patients for validation.

	Baseline Gait Velocity (m/s)	Baseline K.I. (unitless)	Baseline CSROD (unitless)	Baseline G_Funct_{GT} (unitless)	Baseline G_Funct_{TD} (unitless)
S13	0.095	215.684	465.572	2.704	19.29
S14	0.165	62.734	204.767	1.525	15.90
S15	0.200	63.165	190.518	0.440	18.16

Table 8.7. Comparison between predicted and actual G_Funct_{GT} values and the error percentage.

	Stage 2 G_Funct_{GT} (unitless)			Stage 3 G_Funct_{GT} (unitless)		
	Predicted	Actual	Error (%)	Predicted	Actual	Error (%)
S13	2.203	2.337	5.73	2.069	2.189	5.48
S14	0.694	0.683	1.61	0.501	0.366	36.8
S15	0.217	0.122	77.8	0.118	0.121	2.48

Table 8.8. Comparison between predicted and actual G_Funct_{TD} values and the error percentage.

	Stage 2 G_Funct_{TD} (unitless)			Stage 3 G_Funct_{TD} (unitless)		
	Predicted	Actual	Error (%)	Predicted	Actual	Error (%)
S13	17.375	17.977	3.35	16.031	16.317	1.75
S14	1.433	0.934	53.4	1.484	1.896	21.72
S15	1.912	1.820	5.05	2.443	2.261	8.05

8.4.4 Results from regression model approach 2

8.4.4.1 Selection of independent variables

In this section, the gait functionality indices at stage 3 are predicted based on the recovery history from stage 1 to stage 2. Following the same procedure as in Section 8.4.3, the selected independent variables for each gait functionality indices at stage 3 are:

i. Gait functionality based on gait trajectory index, G_Funct_{GT} in stage 3.
   - Difference of K.I. value between stage 1 to stage 2.
   - Difference of CSROD value between stage 1 to stage 2.
   - Difference of G_Funct_{GT} between stage 1 to stage 2.

ii. Gait functionality based on time delay index, G_Funct_{TD} in stage 3.
   - Difference of gait velocity between stage 1 to stage 2.
   - Difference of K.I. value between stage 1 to stage 2.
   - Difference of CSROD value between stage 1 to stage 2.
   - Difference of G_Funct_{TD} from between 1 to stage 2.

8.4.4.2 Validation of regression model approach 1

Based on the selected independent variables, a multivariate linear regression model to predict the gait functionality indices based on recovery history at stage 3 is developed. **Table 8.9** displays the regression coefficient for both predicted indices, which to be substituted to Eq. (8.21). **Table 8.10** shows the difference of independent variables between stage 1 and 2. **Table 8.11** presents the predicted results, actual values and their error for G_Funct_{GT} and G_Funct_{TD} at stage 2 and stage 3 of three stroke patients respectively. The results in this table demonstrats that this model can accurately predict stage 3 indices using this model besides G_Funct_{GT} from S14 and S15.

Table 8.9. Multivariate Linear Regression Model to predict gait functionality index G_Funct_{GT} and G_Funct_{TD} at stage 3.

	Predicted Stage 3 G_Funct_{GT}		**Predicted Stage 3 G_Funct_{TD}**	
	b coefficient	Standard error	*b* coefficient	Standard error
Δ Gait Velocity	-	-	-0.6447	0.298
Δ K.I.	0.0043	0.003	0.0144	0.020
Δ CSROD	-0.0021	0.001	-0.0098	0.008
Δ G_Funct_{GT}	0.6756	0.154	-	-
Δ G_Funct_{TD}	-	-	0.5778	0.1799
Intercept	0.7633	0.175	4.895	1.886

Table 8.10. Baseline independent variables values for three subjects for validation.

	Δ Gait Velocity (m/s)	**Δ K.I. (unitless)**	**Δ CSROD (unitless)**	**Δ G_Funct_{GT} (unitless)**	**Δ G_Funct_{TD} (unitless)**
S13	0.07	58.16	302.80	0.37	1.31
S14	-0.91	43.96	166.75	1.24	12.9
S15	-0.94	37.04	109.45	1.52	12.3

Table 8.11. Comparison between predicted and actual $\hat{y}_{s3}$ values and the error percentage.

	Stage 3 G_Funct_{GT} (unitless)			**Stage 3 G_Funct_{TD} (unitless)**		
	Predicted	Actual	Error (%)	Predicted	Actual	Error (%)
S13	2.066	2.189	9.75	15.82	16.317	3.04
S14	0.475	0.366	79.1	1.93	1.896	1.88
S15	0.084	0.121	30.5	2.07	2.261	8.27

8.5 Discussion

8.5.1 Changes of spatial-temporal parameters during recovery

Fig 8.1 shows the spatial-temporal parameters, K.I. and CSROD values throughout the sixth month recovery period. Generally, stroke patients are expected to improve their gait pattern and walk better by: i) increase stride length and heel clearance; ii) decrease gait cycle time to increase gait velocity; iii) decrease stance time and increase swing time; and iv) increase joint angle range of motion on both paretic and non-paretic lower limbs. Moreover, it is to believe that stroke patients have improved in term of gait symmetry when recovered. The decreased in gait asymmetry will improve the balancing, and hence reduce the risk of falling down. This can be reflected in the K.I. value since it is highly associate with TUG score. The K.I. values decrease from the stage 1 to stage 3 of recovery and it indicates a lower TUG score.

8.5.2 Gait Functionality Indices

The gait functionality indices proposed in this chapter, G_Funct_{GT} and G_Funct_{TD} are very important to assess the walking ability of stroke subjects. Since the ultimate rehabilitation goal is to help the stroke patients to achieve the normal healthy gait as close as possible, these two indices are formulated by finding the deviation between stroke and healthy subjects' gait trajectory and time delay among gait events. The time history of these two indices are *ED(N)* and *TD(i)* respectively. For *ED(N)*, it provides information such as gait trajectory deviation between healthy and stroke subjects at any gait events. For *TD(i),* it is able to notify which gait events among stroke patients have the highest delay compared to healthy.

8.5.3 Comparison between two prediction models

In this chapter, two new prognostic models for gait functionality recovery after stroke was developed. It is generally accepted that the stroke patients improved the most during the first sixth month after diagnosed with stroke. Therefore,

longitudinal study during first month (stage 1), third month (stage 2) and sixth month (stage 3) of stroke patients were analysed. Noted that all these stroke patients that were recruited for this study only received the normal rehabilitation treatment from physiotherapist without any additional intervention.

The first model is computed based on stroke patients' baseline gait data only. It can be used to predict the gait functionality indices at stage 2 and stage 3. Meanwhile, the second model uses the changes of gait data from stage 1 to stage 2 as independent variables and to predict the gait functionality indices at stage 3.

The application of these two models are very crucial for clinicians and physiotherapist. For the first model, initial predictions of recovery can be used to set rehabilitation targets. The predicted gait performance at stage 2 and stage 3 can be used as a comparison to the actual gait performance at stage 2 and stage 3. The second model is based on the recovery pattern from stage 1 to stage 2. Since every stroke patients have different recovery trajectory compare to each other, it is very important to use recovery history as independent variables.

Actual recovery for each stroke patients could be compared with the predicted values using these models. This information can help to adjust the type and amount of rehabilitation treatment received by each stroke patients. For those stroke patients who are not recovering as expected using the prediction model, additional intervention may be warranted. This can help to reduce the amount of time physiotherapist spent on stroke subjects and improve the workload efficiency.

The errors by the difference between actual and predicted indices in **Table 8.7**, **Table 8.8** and **Table 8.11** are mainly caused by the assumption that all stroke patients follow linear recovery curve. While it is true for most subjects, some patients had rapid recovery at the beginning and slow recovery at the later stage. For example, **Table 8.12** shows the classification result by using the Hierarchical Cluster Analysis with K.I. as single input as shown in Chapter 6. These results suggested that most of the stroke subjects started as the most severe gait performance group (Group 3 KI3), and had very different recovery trajectories

between different patients. Different subgroups of stroke patients should received different type of rehabilitation. However, since all recruited stroke patients received same amount and same type of rehabilitation from physiotherapist, some patients were not recovering better at the sixth month period. This can be caused by the lack of motivation from patients or improper rehabilitation strategy planned by physiotherapist.

Table 8.12. Classification outcome for three different recovery stages from 15 stroke patients.

Subject	Stage 1	Stage 2	Stage 3
S1	Group 3 (KI 3)	Group 1 (KI 1)	Group 1 (KI 1)
S2	Group 3 (KI 3)	Group 1 (KI 1)	Group 1 (KI 1)
S3	Group 3 (KI 3)	Group 1 (KI 1)	Group 1 (KI 1)
S4	Group 3 (KI 3)	Group 3 (KI 3)	Group 3 (KI 3)
S5	Group 3 (KI 3)	Group 1 (KI 1)	Group 1 (KI 1)
S6	Group 2 (KI 2)	Group 1 (KI 1)	Group 1 (KI 1)
S7	Group 3 (KI 3)	Group 1 (KI 1)	Group 1 (KI 1)
S8	Group 3 (KI 3)	Group 1 (KI 1)	Group 1 (KI 1)
S9	Group 3 (KI 3)	Group 3 (KI 3)	Group 3 (KI 3)
S10	Group 2 (KI 2)	Group 2 (KI 2)	Group 1 (KI 1)
S11	Group 2 (KI 2)	Group 1 (KI 1)	Group 1 (KI 1)
S12	Group 3 (KI 3)	Group 2 (KI 2)	Group 1 (KI 1)
S13	Group 3 (KI 3)	Group 3 (KI 3)	Group 3 (KI 3)
S14	Group 3 (KI 3)	Group 1 (KI 1)	Group 1 (KI 1)
S15	Group 3 (KI 3)	Group 1 (KI 1)	Group 1 (KI 1)

8.6 Chapter summary

In this chapter, the recovery of stroke patients in different period were studied and analysed. There are clear pattern and behaviour of spatial-temporal parameters over the recovery period. Stroke patients were expected to: i) increase stride length and heel clearance; ii) decrease gait cycle time to increase gait velocity; iii) decrease stance time and increase swing time; iv) increase joint angle range of motion on both paretic and non-paretic lower limbs; v) decrease in gait asymmetry (CSROD); and vi) decrease in K.I. value (decrease in TUG score).

The gait functionality indices introduced in this chapter are based on the deviation of gait trajectory and time delay in gait event between stroke and healthy subjects (G_Funct_{GT} and G_Funct_{TD} respectively). These two indices are able to assess the walking ability of stroke patients and provide the time history with details deviation.

Multivariate linear regression models were developed to predict the two gait functionality indices at different recovery stages. Two regression models were computed: the first was the prediction model based on stroke subjects' baseline gait data and the second was the prediction model based on the recovery history from stage 1 to stage 2. The validation results show that these two models can predict gait functionality indices accurately with few exceptions. The error between the predicted value and actual value is caused by two factors:

i. Assumption of linear recovery trajectory among stroke.
ii. Stroke patients were not recovering better in stage 3.

The reasons patients had no recovery in stage 3 can be due to lack of motivation during rehabilitation process and improper rehabilitation strategy from physiotherapist. Therefore, it is very important to predict subjects walking ability from the beginning to prevent them from derailing from the correct recovery trajectory.

Chapter 9 Determine the fundamental principles of gait recovery through sEMG decomposition

9.1 Introduction

In Chapter 8, the behaviour of gait parameters such as stride length, heel clearance, stance time, swing time, gait velocity, K.I. value, CSROD value and gait functionality indices during recovery were well explained. However, most of these parameters and indices only described the recovery of a patient physically (besides K.I.). While K.I. can determined the weaker muscles in hemiparetic leg (as shown in Section 6.5.3) by studying the fractal features among each muscle, it still cannot provide information such as time history and duration of activated muscle. It remains uncertain regarding the kinesiology status throughout the whole recovery period. Therefore, it is important to study the skeleton muscle condition of stroke subjects during their recovery. This leads to the study of motor unit recruitment and its firing pattern during recovery period. Hence, EMG decomposition has attracted our attention to reveal the motor unit information [215,256,257]. Noted most of the EMG decomposition methods focus on decomposed needle EMG and high-density arrays EMG into MUAP. It is very challenging to accurately decompose sEMG due to its low spatial selectivity [216]. All the MUAPs from sEMG tend to look alike and they overlap with each other. It is very hard to extract useful information of MUAP on stroke subjects using existing EMG decomposition methods. Therefore, partial sEMG decomposition method such as Emperical Mode Decomposition (EMD) and Ensemble Emperical Mode Decomposition (EEMD) served as a substitute to decompose sEMG signal partially.

The aims of this chapter are:

1. To study and analyse the decomposed sEMG signal using EEMD on healthy subjects.
2. To study and analyse the decomposed sEMG signal using EEMD on stroke patients.
3. To study the motor impairment among stroke patients.
4. To study the motor recovery after stroke.

9.2 Theory

9.2.1 Model description

In 1998, Huang *et al* [217] proposed a new technique for analysing non-linear and non-stationary data and the key part of the method is the Empirical Mode Decomposition (EMD). EMD can decompose a complicated signal into finite and small number of intrinsic mode functions (IMF). These IMFs yield instantaneous frequencies as functions of time. One of the problem arises in cases of EMD is mode mixing. Mode mixing is defined as single IMF consists of signals of widely disparate scales, or a signal of similar scare residing in different IMF components [222]. This issue can cause failure to decompose the signal accurately. To overcome this issue, Wu and Huang [222] proposed a noise-assisted EMD algorithm called Ensemble Empirical Mode Decomposition (EEMD) in 2005.

9.2.1.1 Empirical Mode Decomposition (EMD)

By applying EMD, the sEMG signal $x(t)$ is decomposed into different finite of intrinsic mode function IMFs, c_j where an IMF represents a simple oscillatory function satisfying two conditions:

1. The number of zero crossings and the number of local extrema are either equal or differ by one. Local extrema are either local minima or local maxima.
2. The mean value of the envelopes from local maxima and local minima should be zero.

The sEMG signal *x(t)* can be represented in the form of IMFs and residual as:

$$x(t) = \sum_{j=1}^{n} c_j + r_n \quad (9.1)$$

where $r_n$is the residue of sEMG signal $x(t)$, and *n* is the number of IMFs extracted from the original data. The EMD method is a sifting process that estimates IMFs by using only local extrema. The procedure is as follows:

1. Identify all local extrema (both local maxima and local minima). Connect all these local maxima (minima) with a cubic spline as upper (lower) envelope (UE- upper envelope; LE- lower envelope).
2. Determine the average envelope *m* by calculating the mean between UE and LE.
3. Obtain the first IMF, *h* by taking the difference between the data and *m*.
4. Treat *h* as the data and repeat steps 1 to 3 as many times as required until *h* meet the two conditions stated above.
5. Save the final *h* (the real IMF) as c_j. This sifting process stops when the residue, r_n becomes a monotonic function where no more IMF can be extracted.

9.2.1.2 Ensemble Empirical Mode Decomposition (EEMD)

Mode mixing is a problem arises from EMD decomposition. Mode mixing is caused by overlapping of different IMFs [220] and this affects the accuracy of the decomposed signal. To solve this problem, Ensemble EMD (EEMD) is proposed by Wu *et al* [222]. This EEMD method is a noise-assisted EMD algorithm. It works by following the below procedure:

1. Add white noise into the signal in i^{th} trials.

   $$x_i(t) = x(t) + w_i(t), i = 1, 2, \ldots, N \quad (9.2)$$

   where $x_i(t)$ is the i^{th} trials of signal by adding $w_i(t)$ of white noise to the original data $x(t)$ and *N* is the ensemble number.
2. The new noise-contaminated signal, $x_i(t)$ is decomposed into finite set of IMFs using the EMD procedure described earlier.

$$x_i(t) = \sum_{j=1}^{n} c_j^{(i)} + r_j^{(i)} \tag{9.3}$$

where $c_j^{(i)}$ is the IMF and $r_j^{(i)}$ is the residual obtained in the i^{th} trials.

3. Repeat step 1 and step 2 with different white noise series $w_i(t)$.
4. Obtain the final IMF, $c_j(t)$ of EEMD by averaging the total j IMFs related to i^{th} trials.

$$C_j(t) = \frac{1}{i}\sum_{i=1}^{N} c_j^{(i)} \tag{9.4}$$

The final decomposed signal is highly affected by the choice of ensemble number N and the amplitude of noise, ε

$$\varepsilon_n = \frac{\varepsilon}{\sqrt{N}} \tag{9.5}$$

where ε_n is the final standard deviation of error, which calculated as the difference between original signal and the sum of the IMDs resulting from the EEMD. In our study, the standard deviation of the added noise is 0.2 and the ensemble number is set to N = 500.

9.2.2 Experiment protocol

The sEMG signal from healthy subjects (in Experiment 1) are analysed during walking. Besides that, the sEMG signal from stroke sEMG signal in prospective cohort study (Experiment 3) are also analysed. All sEMG signals were processed with EEMD to obtain IMFs as described in Section 9.2.1. Fast Fourier Transform (FFT) was applied to each IMF component to show the corresponding frequency spectrum.

9.3 Decomposed sEMG from healthy subjects

There are two agonist and antagonist muscles (GL and TA) tested in this study. For a normal gait, GL muscle activates during the mid-stance to toe-off and TA muscle activates during the swing phase to heel-strike [248]. This means that the GL

muscle mainly contributes to move the upper body forward during the stance phase (plantarflexion) while the TA muscle is to provide foot clearance during the swing phase (dorsiflexion).

In this section, the sEMG of GL and TA muscles from healthy subjects were decomposed by the EEMD method. **Fig 9.1** and **Fig 9.2** show the sEMG signal and its decomposition from the tested muscles. On the left side of the figures, it is the sEMG signal and its decomposed IMF signal; on the right side, it is the corresponding frequency computed by FFT. From the EEMD results, it can clearly see that the frequency is the highest in the first IMF (c_1), and it slowly decreases to the following IMF components. Noted that after the fifth IMF component, the amplitude of the IMF is not clear in the same scale as the previous IMF component. Besides that, the Fourier analysis shows that the frequency after the fifth IMF component are very low. Therefore, it is suggested that only the first to fifth IMFs components would be analysed. Similar to Chang *et al* [258], EEMD has more concentrated and band limited components and therefore, high frequency noises are more localised in the low IMF level (for example c_1). Each of these IMFs indicates the superimposed of MUAPs at that particular frequency range as shown in their FFT. For example, the median frequency of each FFT of healthy's decomposed GL muscle sEMG are 94, 57, 30, 15 and 6 Hz (c_1, c_2, c_3, c_4 and c_5 respectively). This means that the first IMF component, c_1, contains superimposed of motor unit firing frequency at around 94Hz. It is similar for the rest of IMF components. Meanwhile, the median frequency of each FFT of healthy's decomposed TA muscle's sEMG are 109, 54, 29, 15 and 8 Hz (c_1, c_2, c_3, c_4 and c_5 respectively). Therefore, the information that can be extracted from the decomposed sEMG are: i) the range of frequency of different MUs group in each IMF component; ii) the temporal information of these different MUs group in each IMF component; iii) the amplitude of these different MUs group compared to other IMF components.

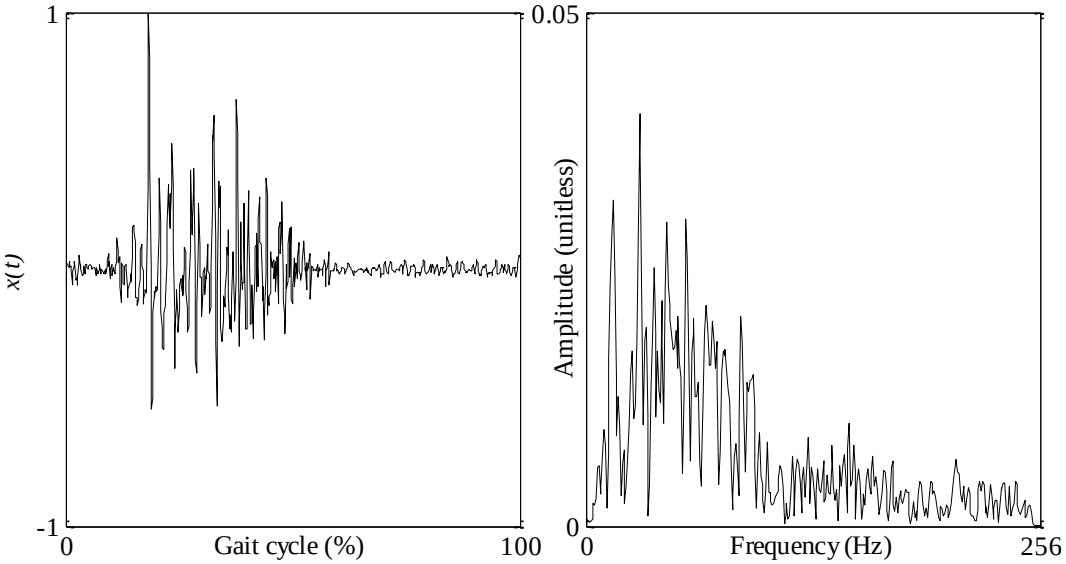

(a)

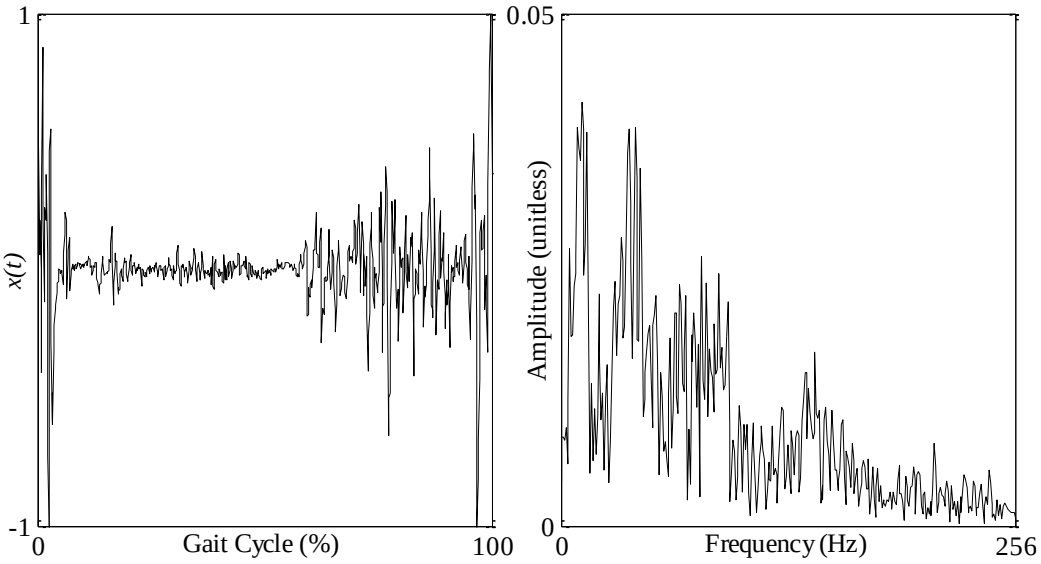

(b)

Fig 9.1. Typical healthy gait sEMG (left) and the corresponding FFT (right) from (a) GL muscle, (b) TA muscle.

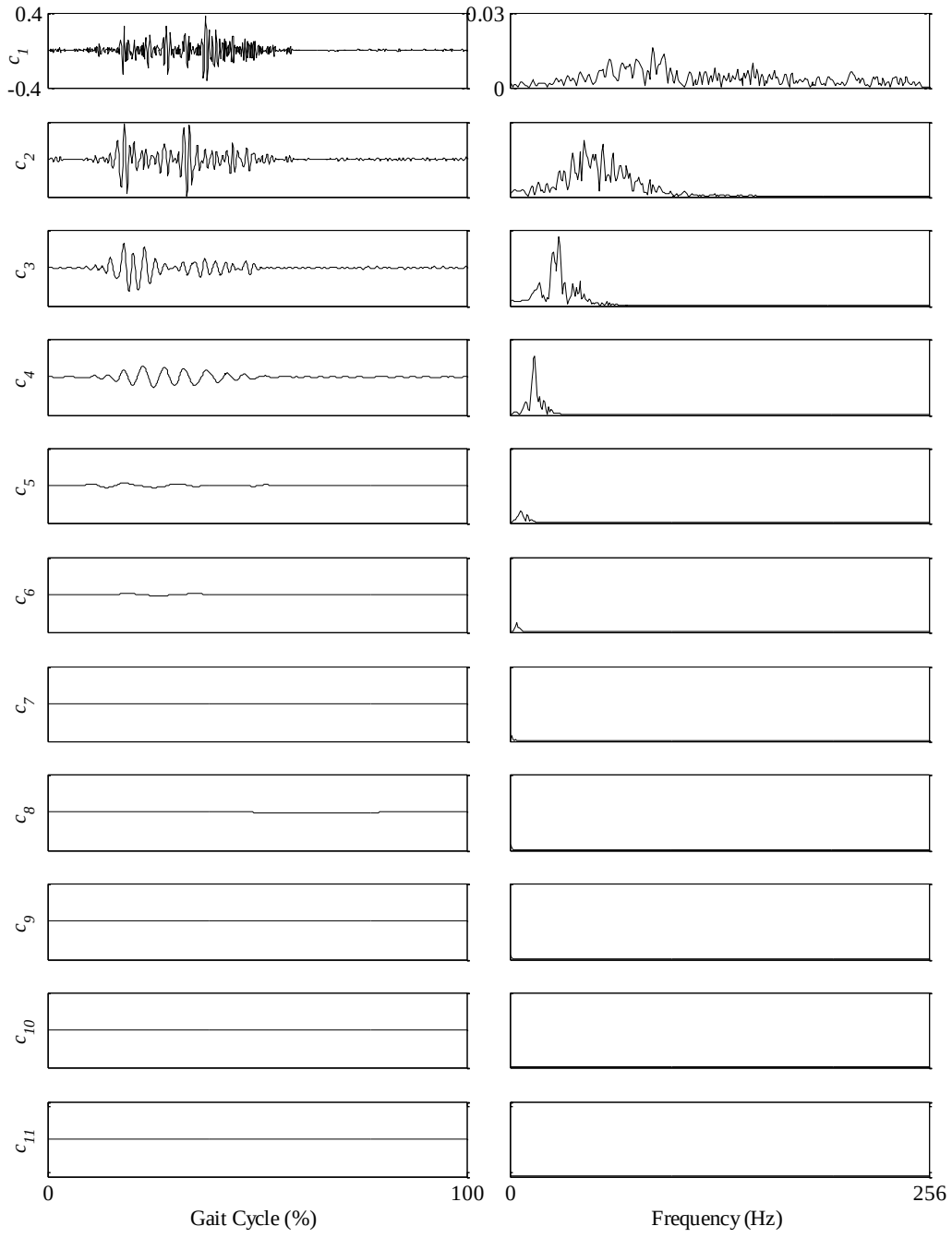
0.4
-0.4
0.03
0
c_1
c_2
c_3
c_4
c_5
c_6
c_7
c_8
c_9
c_{10}
c_{11}
0
100
Gait Cycle (%)
0
256
Frequency (Hz)

(a)

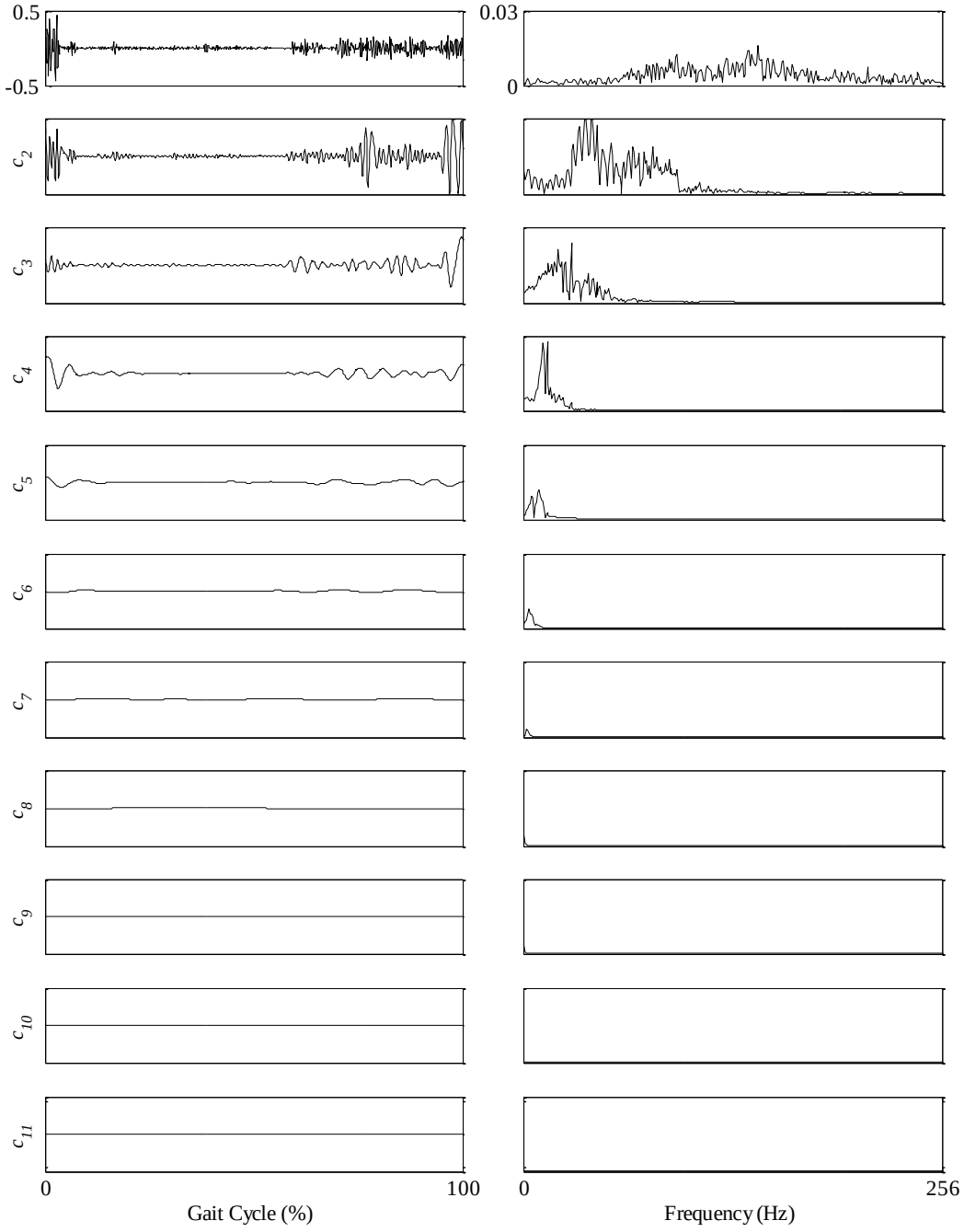

(b)

Fig 9.2. Typical decomposed healthy gait sEMG from (a) GL muscle. (b) TA muscle. On the left side are the IMFs (c_1, c_2,…, c_{11}). Their respective frequency range derived from FFT is shown on the right side. All y-axis has the same scale as the first IMF component and its corresponding FFT.

9.4 Decomposed sEMG from stroke subjects

Before we study the behaviour of decomposed sEMG signals throughout the stroke patients recovery period, it is necessary to understand the features that can be extracted using EEMD to decompose stroke patients sEMG signal.

9.4.1 Foot drop

Foot drop is one of the gait abnormality observed among stroke patients. Foot drop is mainly caused by inactive dorsiflexion from ankle during the swing phase [259], which leads to subject unable to lift the foot and clear the floor. In this study, the maximum vertical foot displacement during the swing phase is taken as a standard measurement. For healthy subjects, the vertical foot displacement is in the range of 0.10-0.15m. To analyse stroke subjects foot drop phenomenon, their decomposed sEMG signal during gait were analysed. Two different subjects were selected due to their severe foot drop conditions. The first and second subjects had a vertical heel clearance during the swing phase of 0.005m and 0.0015m respectively. Compared to healthy data, these two subjects had very minimum to none vertical clearance during the swing phase.

Fig 9.3 shows an example of foot drop phenomenon caused by spasticity of GL muscle from one patients. **Fig 9.3** (a) is the GL sEMG signal and its corresponding FFT results and **Fig 9.3** (b) is the decomposed IMFs from GL sEMG. In this figure, there is a consistent activation from the beginning to the end of gait cycle from GL muscles. This is caused by the spasticity of that particular muscle. Spasticity is a symptom where the muscle is continuously contracting and the subject has no control over it. In this example, spasticity in GL muscles causes the muscle to be very stiff, which counteracting the TA muscle [260]. The median frequency of each IMF components were 105, 71, 42, 22 and 12Hz (c_1, c_2, c_3, c_4 and c_5 respectively). These frequencies were higher compared to the healthy one. There was no activation during swing phase for this low frequency motor unit. Spasticity happened when the subject tried to recruit more motor units and it caused GL muscle contracting at swing phase as well, leading to foot drop.

Fig 9.4 shows another example of foot drop phenomenon caused by lack of TA muscle activation from another patient. **Fig 9.4** (a) is the TA sEMG signal and its corresponding FFT results and **Fig 9.4** (b) is the decomposed IMFs from TA sEMG. TA muscle is primary contributing for foot clearance during the swing phase; therefore, there should be activities during the swing phase. However, it is observed that there were not many high frequency activities in the EEMD results. There are only some muscle activities on lower frequency range. This showed that the motor units did not activate at a higher frequency for "heavier" load. The "heavier" load indicates ankle dorsiflexion, which is to push the foot from the ground. There is one activation happened at the end of the gait cycle, which is the beginning of another heel strike. This is a very common phenomenon, as the stroke patients will need more support during heel strike for balancing and prepare for the next step. The median frequencies of each IMF component were 100, 34, 20, 11 and 6 Hz (c_1, c_2, c_3, c_4 and c_5 respectively). They were slightly lower than the healthy one for comparison.

9.4.2 Prolong stance time

For healthy subjects, the typical stance time is around 60% of the gait cycle time [70]. However, most of the stroke patients have longer stance time [70]. Although longer stance time will lead to slower gait velocity, it is necessary for some stroke patients with walking difficulty. It allows stroke patients to have more time to balance their upper body and reposition themselves for the next gait cycle to prevent falling. Nonetheless, improvement of stance time is necessary to increase the gait velocity as a sign of recovery. Plantarflexion happened during the stance phase to propel the upper body forward. To analyse stroke patients prolong stance time phenomenon, their decomposed sEMG signal during gait were analysed. Two different patients were selected due to their long stance time condition. The first and second patients had a stance time of 85% and 82% respectively. Compared to healthy data, these two patients had very long stance phase during gait.

Fig 9.5 shows an example of prolong stance time due to lack of GL muscle activation. **Fig 9.5** (a) is the GL sEMG signal and its corresponding FFT results and **Fig 9.5** (b) is the decomposed IMFs from GL sEMG. There were not many activities from low IMF to high IMF. The lack of motor unit recruitment, especially high frequency contraction, suggested that the GL muscle did not recruit more motor unit to perform the complete plantarflexion. The median frequencies of each IMF component were 96, 58, 13, 7 and 5 Hz (c_1, c_2, c_3, c_4 and c_5 respectively). These frequency ranges were much lower than the healthy one. There were more motor unit activities in the low frequency range compared to other IMF components. The activation timing of these low frequency motor units were at the end of gait cycle, which was to support for the next heel-strike.

Meanwhile, **Fig 9.6** shows another example of prolong stance time due to coactivation from TA muscle, which will counteracting with GL. **Fig 9.6** (a) is the GL sEMG signal and its corresponding FFT results and **Fig 9.6** (b) is the decomposed IMFs from GL sEMG. The TA muscle from this patient had activation during stance phase. This activation of TA on stance phase can be explained by compensation of TA on other muscles. According to Krogt *et al* [261], the weakness in gluteus medius and iliopsoas muscles will lead to increased activations in TA muscles during the stance phase. Both gluteus medius and iliopsoas muscles are for hip flexion and extension. As stated earlier, the main function of the stance phase is to propel the upper body forward, and it requires extensive hip movements. Weakness in the gluteus medius and iliopsoas muscles will only lead to increase in stance time. The median frequencies of each IMF component were 97, 58, 32, 15 and 8 Hz (c_1, c_2, c_3, c_4 and c_5 respectively). These frequencies were very similar to the healthy one. At low frequency motor units, there were no motor unit recruitment during the stance phase. The CNS started to recruit more motor units at higher frequency range during the stance phase to compensate other joints.

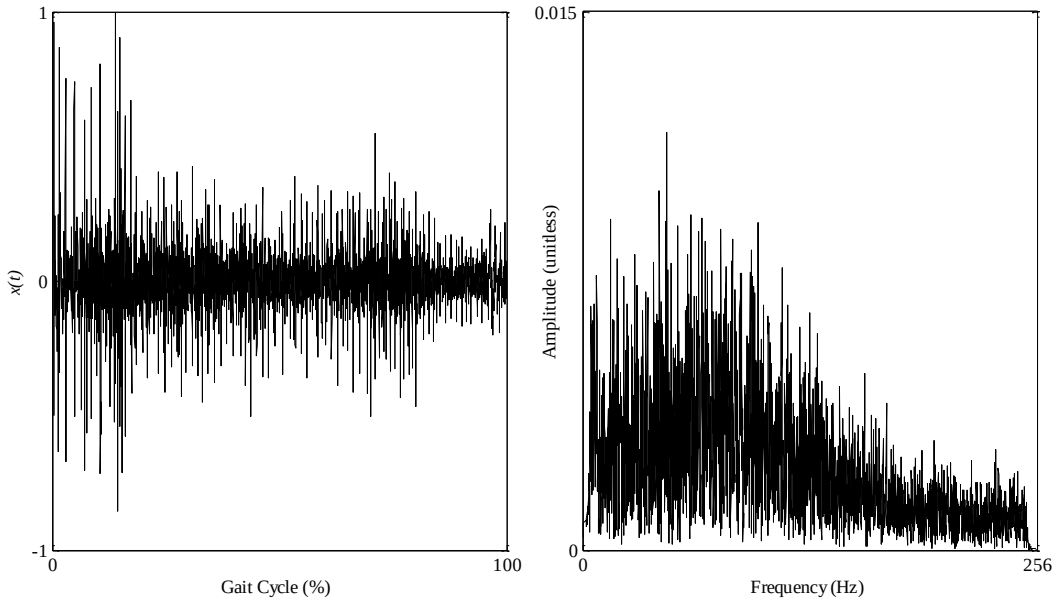

(a)

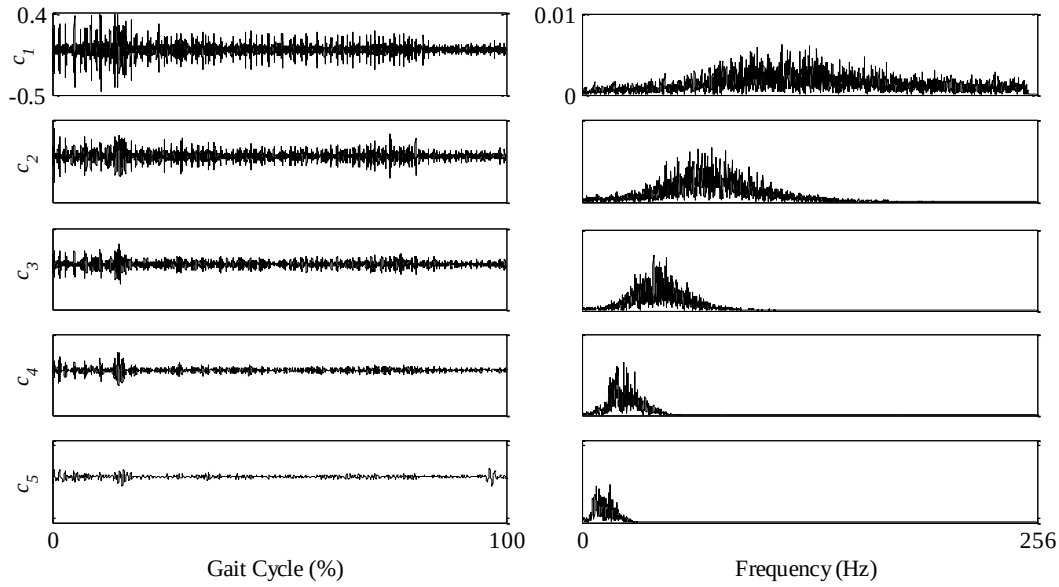

(b)

Fig 9.3. An example of foot drop caused by spasticity of GL muscle from one subject, which counteracting the TA muscle [260]**. (a) GL sEMG signal with its corresponding FFT result, (b) IMFs from decomposed GL muscle. Maximum foot clearance from this subject is 0.005m. All y-axis has the same scale as the first IMF component and its corresponding FFT.**

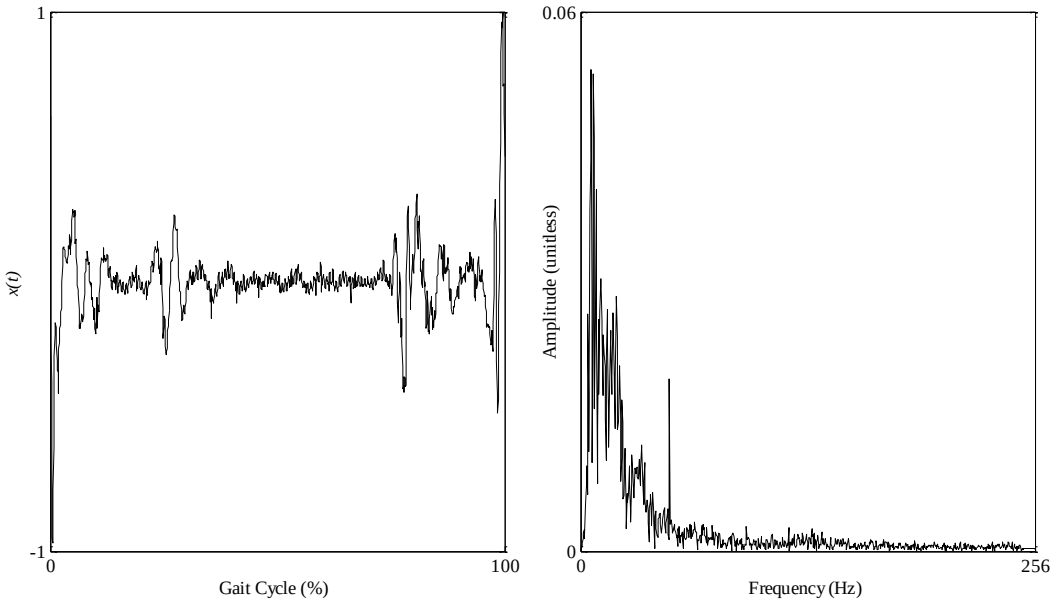

(a)

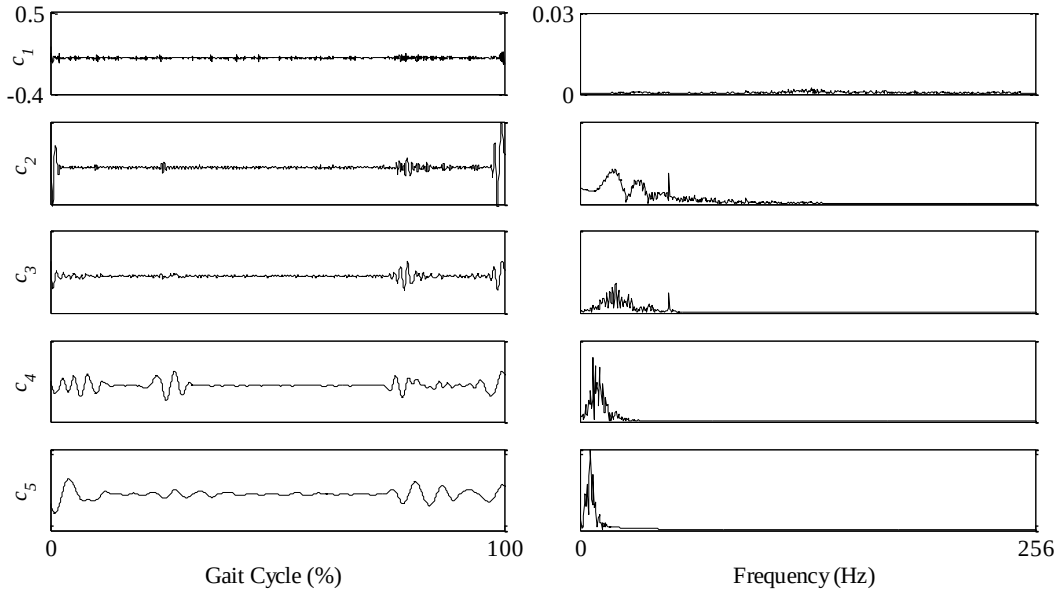

(b)

Fig 9.4. An example of foot drop caused by lack of TA muscle activation from one subject. (a) TA sEMG signal with its corresponding FFT result, (b) IMFs from decomposed TA muscle. Maximum foot clearance from this subject is 0.0015m. All y-axis has the same scale as the first IMF component and its corresponding FFT.

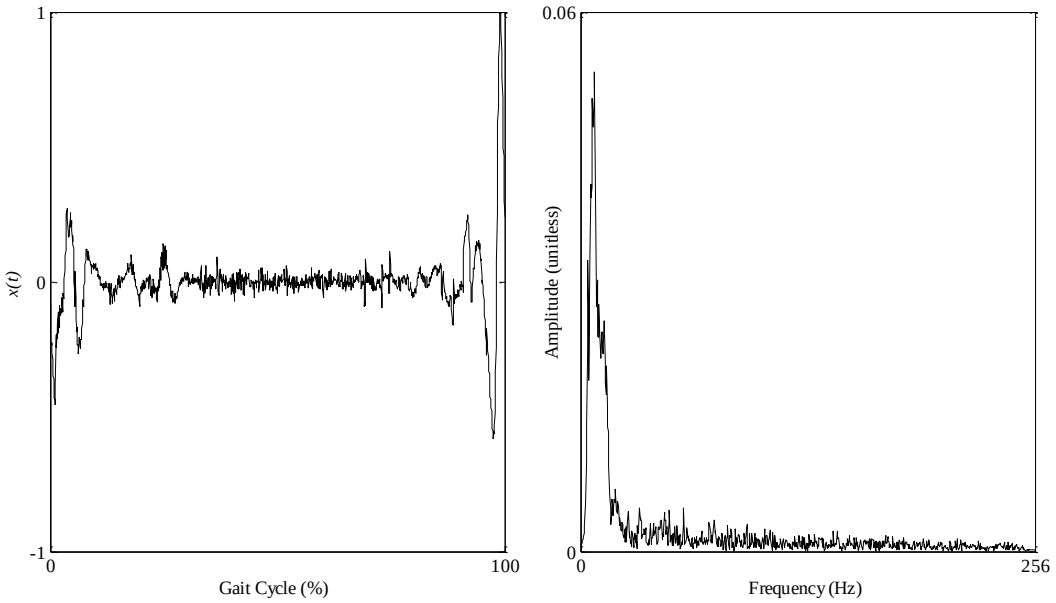

(a)

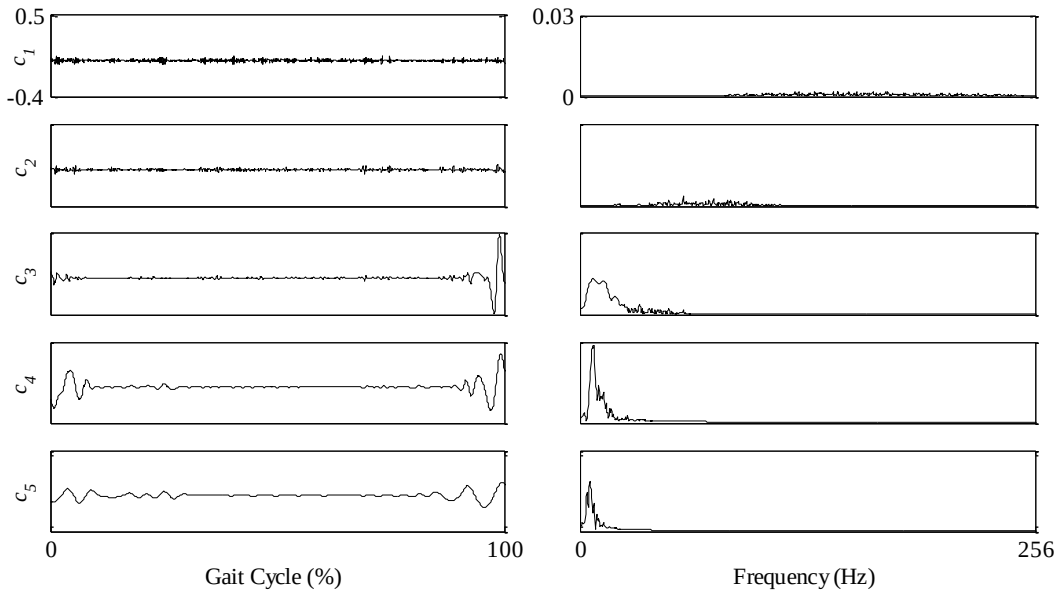

(b)

Fig 9.5. An example of prolong stance time caused by lack of GL muscle activation from one subject. (a) GL sEMG signal with its corresponding FFT result, (b) IMFs from decomposed GL muscle. Stance time percentage from this subject is 85%. All y-axis has the same scale as the first IMF component and its corresponding FFT.

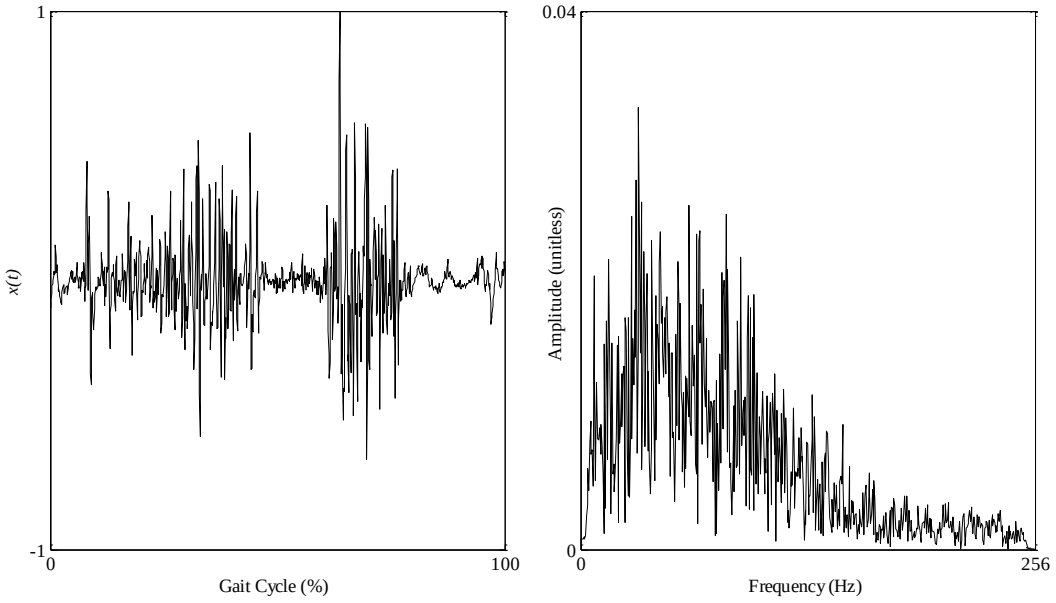

(a)

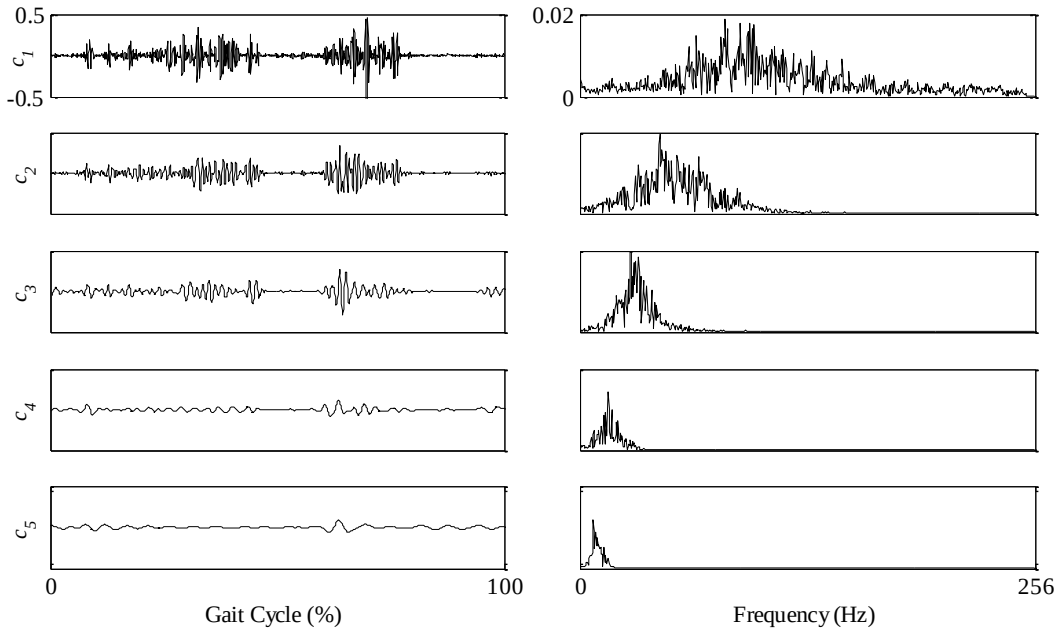

(b)

Fig 9.6. An example of prolong stance time caused by abnormal activation of TA muscle from one subject. (a) TA sEMG signal with its corresponding FFT result, (b) IMFs from decomposed TA muscle. Stance time percentage from this subject is 82%. All y-axis has the same scale as the first IMF component and its corresponding FFT.

9.5 Recovery after stroke

9.5.1 Decomposed sEMG from three different stages

Proper rehabilitation after stroke is crucial to improve the gait quality. For perfect recovery, improvement in joint kinematics should be associated with the improvement of muscle kinesiology. However, some of the stroke patients recruited in this study only recovered physically, i.e. improvement in the stance time and foot clearance. This is due to the muscle compensation. A detailed study of how lower limb muscles compensating each other is given in Krogt *et al* [261]. Long-term muscle compensation can lead to muscle injury. Therefore, during the rehabilitation, observation from both spatial-temporal parameters and muscle conditions must be evaluated properly.

Appendix D shows all the decomposed sEMG (GL and TA muscles from both lower limbs) from 15 stroke patients for three different stages. The details of recovery in term of kinematics (G_Funct_{GT} and G_Funct_{TD}) and kinesiology are described in **Table 9.1**. Most of the stroke patients had very regular recovery in term of their gait functionality indices. This means that their gait trajectory and time delay between each gait events were very similar to the healthy one. However, the recovery in term of their muscle status stated otherwise. The physical recovery achievements detected by the gait functionality indices were mostly a form of compensation. For example, according to the previous section, lack of activation (especially high frequency MUs) of the tested muscle (GL and TA) normally leads to longer stance phase and insufficient foot clearance during swing phase respectively. For certain stroke patients, the GL and TA muscles were still considering as weaker muscles from **Table 9.1** and other muscles increased activation to assist GA and TA muscles to accomplish the tasks (shorter stance phase and greater foot clearance).

Table 9.1. Detail comparison between kinematics (*G_Funct*$_{GT}$ and *G_Funct*$_{TD}$) and kinesiology.

Subject	*G_Funct*$_{GT}$		*G_Funct*$_{TD}$		Kinesiology Changes	
	Stage 1 to Stage 2	Stage 2 to Stage 3	Stage 1 to Stage 2	Stage 2 to Stage 3	Stage 1 to Stage 2	Stage 2 to Stage 3
1	Normal Recovery	Normal Recovery	Normal Recovery	Normal Recovery	**GL** - Abnormal activation of high frequencies MUs (C_1 and C_2) at swing phase. - Lack of activation at stance phase for all frequency ranges. **TA** - Abnormal activation of high frequencies MUs (C_1 and C_2) at stance phase. - Lack of activation at swing phase.	**GL** - Abnormal activation of high frequencies MUs (C_1 and C_2) at swing phase. - Lack of activation at stance phase for low frequency ranges (C_4 and C_5). **TA** - Abnormal activation of high frequencies MUs (C_1 and C_2) at stance phase. - Normal activation at stance phase.
2	Normal Recovery	Normal Recovery	Normal Recovery	Normal Recovery	**GL** - Abnormal activation of high frequencies MUs (C_1 and C_2) at swing phase. - Lack of activation at stance phase for low frequency ranges (C_4 and C_5). **TA** - Abnormal activation of high frequencies MUs (C_1 and C_2) at stance phase. - Lack of activation at swing phase.	**GL** - Abnormal activation at swing phase for all frequency ranges. **TA** - Abnormal activation of high frequencies MUs (C_1 and C_2) at stance phase. - Lack of activation at swing phase.
3	Normal Recovery	No Recovery	Normal Recovery	No Recovery	**GL** - Hyperactive stretch reflexes at frequencies MUs (C_1 and C_2). **TA**	**GL** - Hyperactive stretch reflexes at frequencies MUs (C_1 and C_2). **TA** - Lack of activation of high frequencies MUs (C_1 and C_2) at swing phase.

					- Abnormal activation of high frequencies MUs (C_1 and C_2) at stance phase. - Lack of activation at swing phase.	- Normal activation at swing phase.
4	Normal Recovery	Normal Recovery	Normal Recovery	Normal Recovery	**GL** - Abnormal activation of low frequency MUs (C_4) at swing phase. - Lack of activation at stance phase for all frequency ranges **TA** - Abnormal activation of high frequencies MUs (C_1 and C_2) at stance phase. - Lack of activation at swing phase.	**GL** - Abnormal activation of high frequencies MUs (C_1 and C_2) at swing phase. - Lack of activation at stance phase for low frequency ranges (C_4 and C_5). **TA** - Abnormal activation of high frequencies MUs (C_1 and C_2) at stance phase. - Lack of activation at swing phase.
5	Normal Recovery	Normal Recovery	Normal Recovery	Normal Recovery	**GL** - Abnormal activation of low frequency MUs (C_4) at swing phase. - Normal activation at stance phase. **TA** - Abnormal activation of high frequencies MUs (C_1 and C_2) at stance phase. - Normal activation at swing phase.	**GL** - Abnormal activation of high frequencies MUs (C_1 and C_2) at early heel strike. - Lack of activation at stance phase for low frequency ranges (C_4 and C_5). **TA** - Abnormal activation of high frequencies MUs (C_1 and C_2) at stance phase. - Normal activation at swing phase.
6	Normal Recovery	Normal Recovery	Normal Recovery	Normal Recovery	**GL** - Hyperactive stretch reflexes at frequencies MUs (C_1 and C_2). **TA** - Abnormal activation of high frequencies MUs (C_1 and C_2) at stance phase.	**GL** - Hyperactive stretch reflexes at frequencies MUs (C_1 and C_2). **TA** - Abnormal activation of high frequencies MUs (C_1 and C_2) at stance phase.

					- Normal activation at swing phase.	- Normal activation at swing phase.
7	Normal Recovery	Normal Recovery	Normal Recovery	Normal Recovery	**GL** - Abnormal activation of high frequencies MUs (C_1 and C_2) at swing phase. - Lack of activation at stance phase for low frequency ranges (C_4 and C_5). **TA** - Abnormal activation of high frequencies MUs (C_1 and C_2) at stance phase. - Lack of activation at swing phase.	**GL** - Lack of activation at stance phase for low frequency ranges (C_4 and C_5). **TA** - Abnormal activation of high frequencies MUs (C_1 and C_2) at stance phase. - Normal activation at swing phase.
8	Normal Recovery	Normal Recovery	Normal Recovery	Normal Recovery	**GL** - Hyperactive stretch reflexes at frequencies MUs (C_1 and C_2). **TA** - Abnormal activation of high frequencies MUs (C_1 and C_2) at stance phase. - Normal activation at swing phase.	**GL** - Abnormal activation of high frequencies MUs (C_1 and C_2) at swing phase. - Lack of activation at stance phase for all frequency ranges **TA** - Abnormal activation of high frequencies MUs (C_1 and C_2) at stance phase. - Normal activation at swing phase.
9	Normal Recovery	Normal Recovery	Normal Recovery	Normal Recovery	**GL** - Hyperactive stretch reflexes at frequencies MUs (C_1 and C_2). **TA** - Abnormal activation of high frequencies MUs (C_1 and C_2) at stance phase. - Lack of activation at swing phase.	**GL** - Hyperactive stretch reflexes at frequencies MUs (C_1 and C_2). **TA** - Abnormal activation of high frequencies MUs (C_1 and C_2) at stance phase.
10	Normal Recovery	Normal Recovery	Normal Recovery	Normal Recovery	**GL** - Hyperactive stretch reflexes at frequencies MUs (C_1 and C_2).	**GL** - Hyperactive stretch reflexes at frequencies MUs (C_1 and C_2).

					TA - Abnormal activation of high frequencies MUs (C_1 and C_2) at stance phase. - Lack of activation at swing phase.	**TA** - Abnormal activation of high frequencies MUs (C_1 and C_2) at stance phase. - Lack of activation at swing phase.
11	Normal Recovery	Normal Recovery	Normal Recovery	Normal Recovery	**GL** - Abnormal activation of high frequencies MUs (C_1 and C_2) at swing phase. - Lack of activation at stance phase for low frequency ranges (C_4 and C_5). **TA** - Abnormal activation of high frequencies MUs (C_1 and C_2) at stance phase. - Normal activation at swing phase.	**GL** - Abnormal activation of high frequencies MUs (C_1 and C_2) at swing phase. - Lack of activation at stance phase for low frequency ranges (C_4 and C_5). **TA** - Normal activation.
12	Normal Recovery	No Recovery	Normal Recovery	Normal Recovery	**GL** - Abnormal activation of high frequencies MUs (C_1 and C_2) at swing phase. - Lack of activation at stance phase for low frequency ranges (C_4 and C_5). **TA** - Lack of activation of high frequencies MUs (C_1 and C_2) at swing phase.	**GL** - Abnormal activation of low frequencies MUs (C_4 and C_5) at swing phase. **TA** - Abnormal activation of high frequencies MUs (C_1 and C_2) at stance phase.
13	Normal Recovery	Normal Recovery	Normal Recovery	Normal Recovery	**GL** - Hyperactive stretch reflexes at frequencies MUs (C_1 and C_2). **TA** - Hyperactive stretch reflexes at frequencies MUs (C_1 and C_2).	**GL** - Lack of activation of high frequencies MUs (C_1 and C_2) at stance phase. **TA** - Normal activation.

14	Normal Recovery	Normal Recovery	Normal Recovery	No Recovery	**GL** - Lack of activation of high frequencies MUs (C_1 and C_2) at stance phase. **TA** - Lack of activation for all frequency ranges.	**GL** - Abnormal activation of low frequencies MUs (C_4 and C_5) at swing phase. **TA** - Lack of activation of high frequencies MUs (C_1 and C_2) at swing phase.
15	Normal Recovery	Normal Recovery	Normal Recovery	No Recovery	**GL** - Normal activation. **TA** - Normal activation.	**GL** - Normal activation. **TA** - Normal activation.

9.5.2 Case study

In this section, two stroke patients were selected as the individual case studies. **Table 9.2** shows spatial-temporal parameters and gait functionality indices from two different stroke patients during their six-month recovery period. These two stroke patients had recovered in a similar fashion. Both of them had increased the vertical foot clearance during the swing phase and decrease the stance time and gait cycle time from stage 1 to stage 3. **Fig 9.7** and **Fig 9.8** demonstrate the IMF results from stage 1 to stage 3 for both subject 1 and 2 respectively.

For subject 1, the GL muscle at stage 1 showed activation on the swing phase on low frequency range, meaning GL muscle is compensating hamstring muscle [261]. At stage 2 to stage 3, there is not much compensation happening and the GL muscle activated in the correct timing. There were high frequency IMFs shown in both stages, indicating proper plantarflexion. However, there were still lack of low frequency activation in higher IMGs. It means that this subject still not fully recovered. Nonetheless, this subject still considered as good recovery compared to other subjects.

As for the subject 2, there was no activation in all frequency ranges during stage 1. At stage 2, there are some activities during the swing phase in low frequency range but not during the stance phase. Finally, at stage 3, high frequency range muscle activities observed during the stance phase and low frequency range of muscle activities were still observed during the swing phase. This means that GL muscle from this subject was still compensating the weaker muscle at stage 3.

The TA muscle for subject 1 was compensating the weaker muscle during stage 1 and stage 2. In stage 1, high frequency range of activity can be observed during the stance phase and only low frequency range of activities observed during the swing phase. High frequency range of activity can be observed during both stance and swing phases for stage 2. The subject further improved to stage 3 where no compensation for weaker muscle observed during the stance phase. Meanwhile for subject 2, the subject experienced lack of activation during stage 1. The subject

slowly recovered to have high frequency of activation during the swing phase in stage 2. However, the TA muscle from this subject stated that there were compensate other weaker muscle during stage 3.

Table 9.2. Spatial-temporal parameters of two stroke subjects from their hemiplegia lower limb during three different stages.

	Stage 1	Stage 2	Stage 3
Subject 1 (good recovery EMG)			
Heel Clearance (m)	0.002	0.07	0.08
Stance Time Percentage (%)	88	62	60
Gait Cycle Time (s)	3.1	1.4	1.3
$\boldsymbol{G\_Funct_{GT}}$	1.64	0.122	0.121
$\boldsymbol{G\_Funct_{TD}}$	14.2	2.26	1.82
Subject 2 (bad recovery EMG)			
Heel Clearance (m)	0.015	0.050	0.057
Stance Time Percentage (%)	85	64	61
Gait Cycle Time (s)	3.2	1.25	1.20
$\boldsymbol{G\_Funct_{GT}}$	1.925	0.683	0.265
$\boldsymbol{G\_Funct_{TD}}$	13.90	0.934	1.898

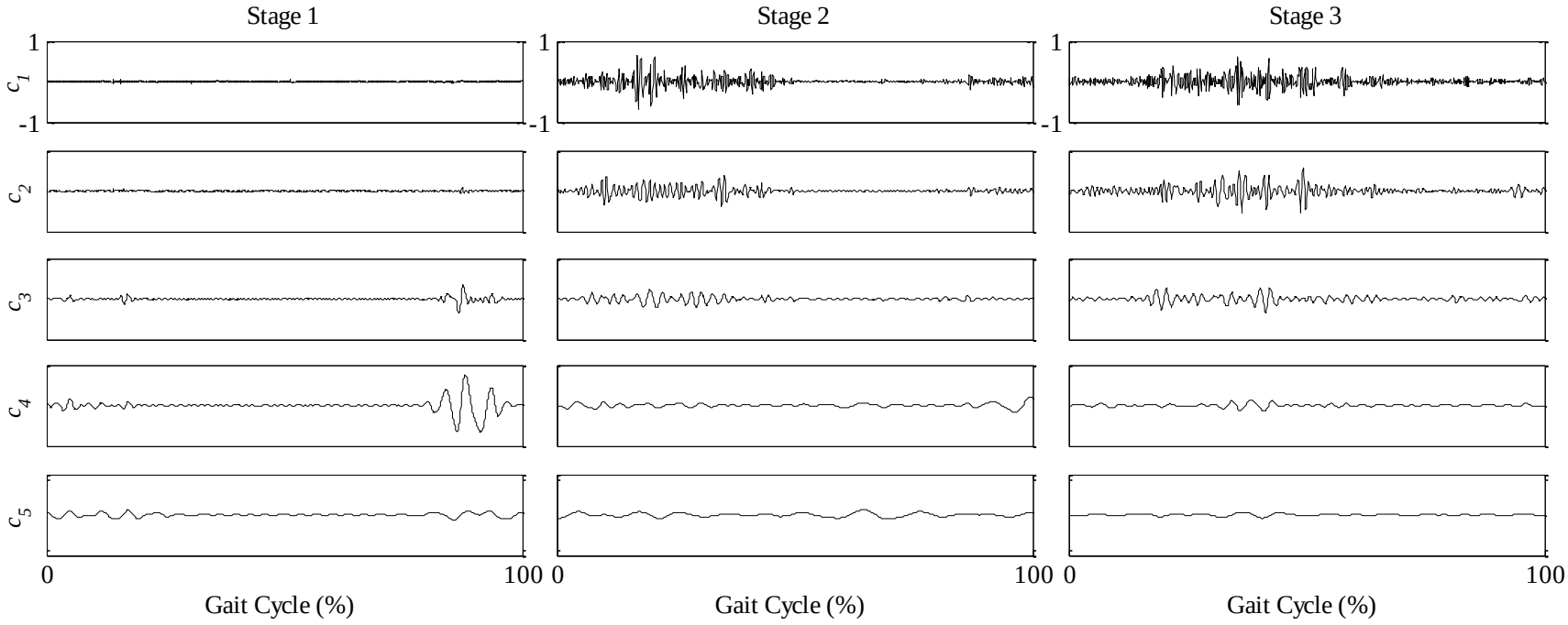

(a)

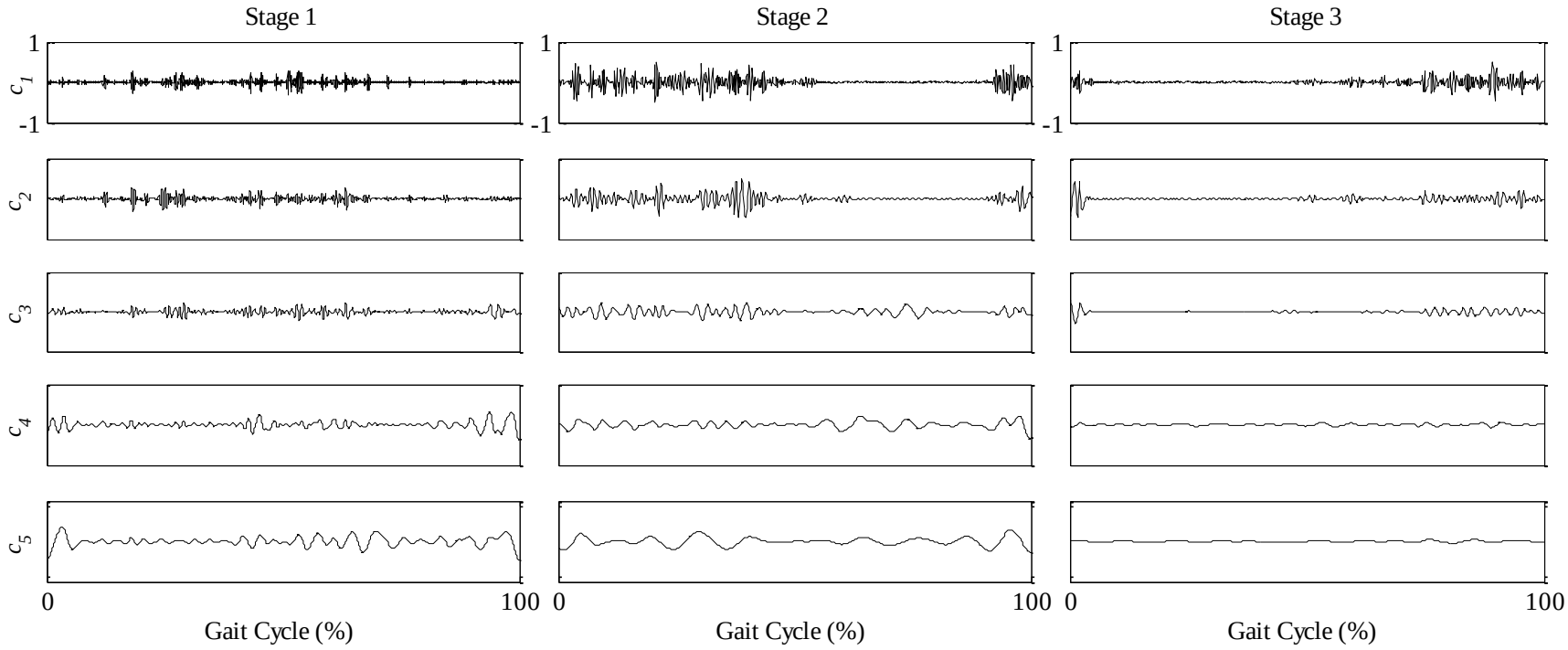

(b)

Fig 9.7. Stage 1, stage 2 and stage 3 IMFs from decomposition of gait sEMG from subject 1, (a) GL muscle, (b) TA muscle. The IMFs show a good recovery in term of muscle condition from beginning to stage 3.

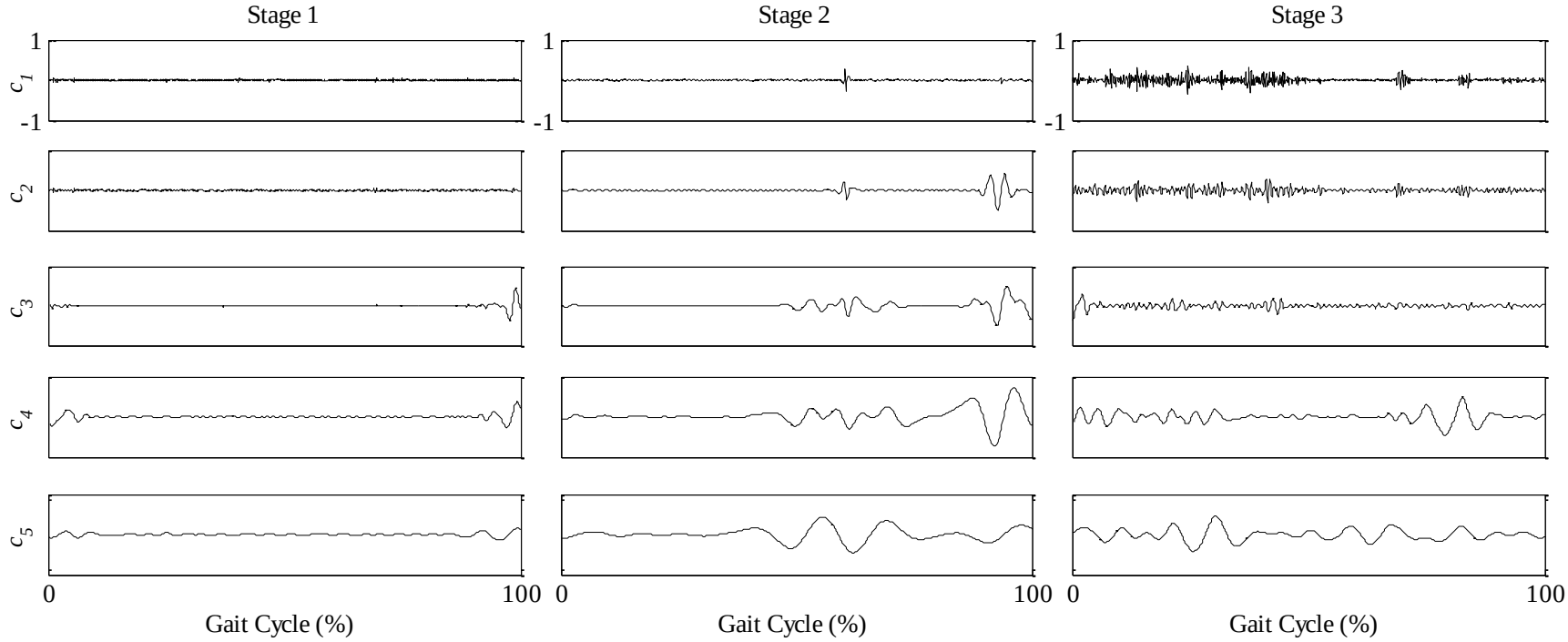

(a)

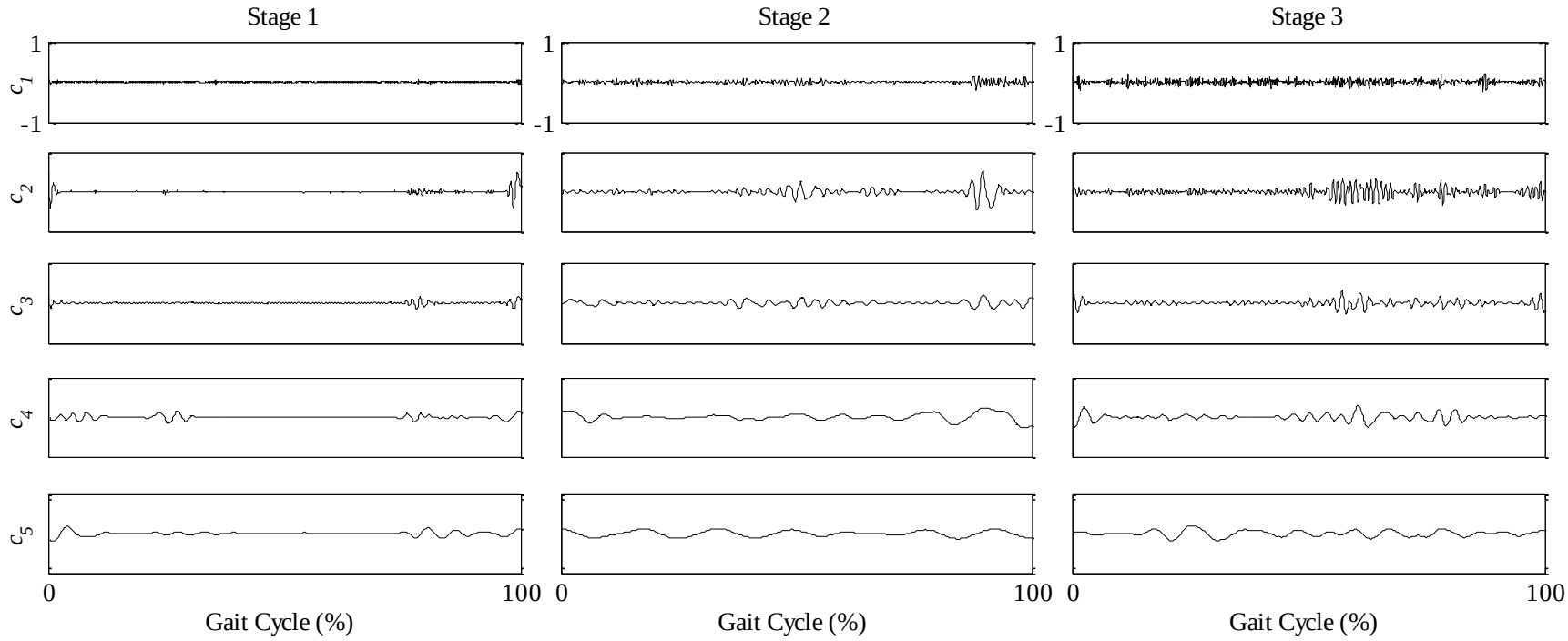

(b)

Fig 9.8. Stage 1, stage 2 and stage 3 IMFs from decomposition of gait sEMG from subject 2, (a) GL muscle, (b) TA muscle. The IMFs show a bad recovery in term of muscle condition from beginning to stage 3.

9.6 Chapter Summary

In this chapter, the gait sEMG from stroke patients were decomposed into different frequency components called IMFs. The decomposition method used is EEMD. Each IMFs decomposed from gait sEMG contained few information such as:

i. The frequency range of motor unit recruited at particular IMF component (median frequency obtained from FFT).
ii. The range of motor unit temporal information at particular IMF component.
iii. The amplitude of the range of motor unit at particular IMF component.

The abnormal gait pattern such as foot drop and prolong stance time can be explained using the temporal information provided by IMFs. The features that can be extracted from IMFs for each abnormal gait are described below:

i. Foot drop
   - Spasticity of GL muscle especially in higher IMF frequency.
   - Lack of TA muscle activation especially in higher IMF frequency.
ii. Prolong Stance Time
   - Lack of GL muscle activation especially in higher IMF frequency.
   - Coactivation of TA muscle especially in higher IMF frequency.

While these IMF features can used to explain the abnormal gait (foot drop and prolong stance time), the same features can be observed among stroke patients without these abnormal gait symptom as well. During recovery, some stroke patients had recovered well as observed by their spatial-temporal parameters (sufficient heel clearance and shorter stance time). However, they still possessed similar IMF features as those with the abnormal gait. This recovery can be due to compensation from other muscles. Long-term compensation can cause injury in the compensating muscle. Therefore, it is very important for physiotherapist to make sure subjects had recovered without any kind of muscle compensation.

Chapter 10 Conclusion and Future Work

10.1 Conclusion

This chapter concludes the key findings obtained in this research study. A sophisticated inertia based gait sensor system (IGS) with a commercial sEMG system and an inertia based gait integration algorithm were developed in Chapter 3. Three different type of experiments were conducted. The first experiment (Experiment 1, n=10) was designed to obtain gait data from the healthy subjects, with three different walking conditions (normal walking, knee braced walking and ankle braced walking). The second experiment (Experiment 2, n=60) was a cross sectional study of stroke patients. Meanwhile, the third experiment (Experiment 3, n=15) was a prospective cohort longitudinal study of stroke patients. The gait data during first month after admitted to hospital (stage 1), third month after stroke (stage 2) and sixth month after stroke (stage 3) were monitored.

Each of these experiments were designed to develop a sophisticated gait analysis system. This system will help clinician to assess the gait characteristics of stroke patients throughout their recovery period more accurately. After the development of gait sensor system (IGS), two important gait features were extracted (K.I. (Chapter 7) and CSROD (Chapter 8)). In Chapter 7, the results showed that K.I. is highly correlated to TUG score. Furthermore, it can be used to classify a large group of stroke patients into homogeneous subgroup accurately. This feature can help clinician to identify the type of stroke patients in particular subgroup and provide necessary rehabilitation methods. In Chapter 8, CSROD was derived from a Cyclogram. This gait feature can distinguish the gait asymmetry on certain gait events. While these gait features can provide meaningful information regarding stroke patients gait characteristics, they are still restricted to unveil the information on certain area (kinesiology and kinematics). This means that K.I. and CSROD provide detail information on kinesiology and kinematics area only, and they still cannot describe deviation between stroke patients and normal human. Therefore,

the gait functionality G_Funct_{GT} and G_Funct_{TD} were introduced. These indices were derived from gait trajectory deviation and time delay between stroke and healthy subjects. Noted these two indices tell how much the stroke patient's gait deviated from the healthy subjects (which served as a standard comparison), while K.I. and CSROD reveal why these deviations occurred. These gait features were later adopted in the development of stroke recovery prediction models (Chapter 8). These models can help clinicians to predict the gait status in stage 2 (third month) and stage 3 (sixth month) time. If the stroke patients do not follow the recovery pattern, it means the rehabilitation treatments may not suitable for those particular stroke patients. Therefore, clinicians can reorganise a proper strategy in the future. Certain stroke patients rely on muscle compensation to complete the gait. This will reduce the gait deviation between them and healthy subjects, hence improving the gait functionality G_Funct_{GT} and $G\_Funct_{TD.}$ However, long-term muscle compensation will caused muscle fatigue, which leads to muscle impairment. Therefore, the muscle status changes across stroke recovery period were studied carefully by using the EEMG method (Chapter 9). This is to make sure that stroke patients recovery does not heavily rely on compensation.

10.1.1 Development of an accurate low cost gait sensor system

- MPU-6050, Arduino Pro Mini and a micro SD shield module were embedded to form one IGS system. Each of this system was mounted on shank and ankle on both lower limbs.
- A new inertial based integration algorithm was proposed to obtain gait trajectory. This algorithm is based on Zero Velocity Update (ZUPT) to reset and update the gait trajectory at heel-strike event to zero.
- The results from this algorithm was validated using the gait data from recruited healthy subjects in Experiment 1. The gait trajectory results obtained from this gait sensor system have high accuracy compared to video regardless of different walking conditions.

10.1.2 Limitation of conventional gait analysis

- The conventional gait analysis on stroke patients (spatial-temporal parameters, traditional gait asymmetry index, clinical assessment score such

as TUG score) are not sufficient to provide a detail assessment on stroke patients. For example, the gait parameters and TUG score (in Section 5.4.4) shows poor correlation between each other. Furthermore, the traditional gait asymmetry index (Robinson Index) also poorly correlated to TUG score and gait velocity. This means lack of sensitivity in conventional gait parameters and gait asymmetry index to detect the gait deficits among stroke subjects. Therefore, new gait analysis methods were proposed to obtain kinesiology and kinematic features in Chapter 6 and Chapter 7 respectively.

- The gait features obtained from conventional gait analysis (spatial-temporal parameters) can used to classify stroke subjects into three different homogeneous subgroups (in Section 5.4.2) using Hierarchical Cluster Analysis. However, this classification method requires multiple gait parameters as inputs, which are very subjective and generally based on observation by visual inspection from researchers. Therefore, the kinesiology feature proposed in Chapter 6 was adopted as a single input to this Hierarchical Cluster Analysis classification methods.

10.1.3 Kinesiology based gait analysis

- In Chapter 6, a new Kinetic Index (K.I.) was proposed to characterise stroke patients gait performance in term of their muscle status. This K.I. was derived from the fractal analysis on sEMG from TA and GL muscles.
- The results from K.I. showed strong correlation to the TUG scores ($r = 0.9222$, $p<0.05$). This suggested that K.I. value could assess the risk of fall among stroke subjects.
- Furthermore, this K.I. value can be used as a single input to Hierarchical Cluster Analysis gait classification. The results of classification (in Section 6.4.2) using K.I. as single input were similar to the results of classification using traditional gait parameters as multiple input (in Section 5.4.2).

10.1.4 Kinematic based gait analysis

- In Chapter 7, a new gait asymmetry quantification method was proposed similar to SROD algorithm. This new algorithm adopted the idea of cyclogram, therefore, we named it Cyclogram SROD (CSROD). This new

CSROD is able to provide temporal and direction information regarding gait asymmetry among stroke.

- The results from CSROD were being compared to the SROD results from original paper (in Section 6.3). The statistic results showed that both CSROD and SROD were capable in tracking the asymmetry in joint angle during gait.
- Previous CSROD and SROD computation used LLN to align left and right lower limbs gait data. However, this alignment led to false peaks in CSROD and SROD results. Therefore, DTW was used to align gait data.
- The CSROD with the ankle joint angle (Input 1) and the vertical heel clearance (Input 2) as inputs revealed detail gait asymmetry among stroke. Most of the stroke subjects had problem in dorsiflexion of ankle joint to move upper body forward, and minimal to no plantarflexion to provide foot clearance on the hemiplegia lower limb. This caused huge gait asymmetry among two lower limbs. The temporal and direction information from CSROD method can help physiotherapist to focus gait training on specific gait events in specific lower limb.

10.1.5 Multivariate linear regression recovery model

- In Chapter 8, two new gait functionality indices (G_Funct_{GT} and G_Funct_{TD}) were proposed to monitor the walking ability of stroke patients throughout their recovery period.
- Two recovery models were developed based on multivariate linear regression model. The first recovery model used stroke patients baseline (stage 1) gait data to predict the gait functionality indices at stage 2 and stage 3. Meanwhile, the second recovery model used the recovery history from stage 1 to stage 2 to predict the gait functionality indices at stage 3.
- The application of these two models are very crucial for researchers. For the first model, initial predictions of recovery could be used to set rehabilitation targets based on stroke subject baseline gait performance. The predicted indices at stage 2 and stage 3 can be compared with actual gait indices later. This information can help to adjust the type and amount of rehabilitation

treatment received by each stroke subjects. For the second model, final state gait indices (at stage 3) can be predicted by using the recovery pattern from stage 1 to stage 2. Since every stroke subjects had different recovery trajectory, it is therefore very important to use recovery history as prediction.

10.1.6 Fundamental principles of gait recovery through sEMG decomposition

- The sEMG signals from stroke patients were decomposed into different frequency components called Intrinsic Mode Functions (IMFs) by Ensemble Empirical Mode Decomposition (EEMD) method. Each decomposed IMFs contained information such as : (i) frequency range of the motor units (MUs) group recruited at particular IMF component; (ii) the temporal information of the MUs group at particular IMF component (i.e. activation timing of the MUs group); and (iii) the amplitude of the MUs group at particular IMF component.
- The abnormal gait pattern such as foot drop and prolong stance time can be observed in the decomposed sEMG signal. Foot drop can be caused by (i) lack of high frequency range of MUs group in GL muscle; (ii) abnormal activation of TA muscle. Meanwhile, prolong stance time can be caused by (i) lack of high frequency range of MUs group in TA muscle; (ii) abnormal activation of GL muscle.
- The recovery of muscle from stroke patients were studied using these decomposed information. Stroke patients may have similar baseline gait data with similar recovery trajectory physically (analysed using kinematic data). However, they may have different kinesiology recovery status, i.e. recovery of muscle may not reflect recovery of gait trajectory. This can be due to compensation from other muscles to achieve the physical tasks. The study of decomposed sEMG can show which MUs group responsible for the compensation of GL and TA muscles.

10.2 Limitation and Future work

The main limitation of this current study is lack of number of sample in Experiment 3 for multivariate linear regression model. As mentioned in Chapter 8, the recovery trajectory is different from each stroke subject. By using Hierarchical Cluster Analysis with K.I. as single input, the classified subgroups of each stroke subjects in three different recovery stages were different (see **Table 8.12**). Therefore, future work can focus on developing multivariate non-linear regression model with different classified subgroups as input (since recovery trajectory is non-linear).

Furthermore, different stroke patients employed different kind of assistive devices (such as cane, ankle foot orthosis etc.) during the experiment. This was to ensure the safety of the stroke patients. However, it also introduced inconsistency to the modelling, which affected the results from the recovery models. The age differences between young adult in Experiment 1 and elder stroke patients in Experiment 2 and 3 also caused improper comparison for the modelling of gait functionality indices, G_Funct_{GT} and G_Funct_{TD}. The future work can focus on recruiting similar age between control group and stroke patients.

The analysed muscles in this study are GL and TA muscles only. This is not sufficient to study the compensation between each lower limbs muscles. As mentioned in Chapter 9, some stroke patients without foot drop or prolong stance time possessed similar IMF features with those patients with these abnormal gait symptoms. This is due to compensation from other muscles. In this study, we adopted the findings from Krogt *et al* [261] as comparison. However, the decomposed sEMG from other muscles cannot be performed. The future work can be extended to collect sEMG signal from all lower limbs muscles and decompose them to obtain the information of MUs group.

Reference

[1] How Stroke Is Diagnosed? | Stroke Prevention | National Stroke Association of Malaysia | NASAM, (n.d.). http://www.nasam.org/

[2] L. Nilsson, J. Carlsson, A. Danielsson, A. Fugl-Meyer, K. Hellström, L. Kristensen, B. Sjölund, K.S. Sunnerhagen, G. Grimby, Walking training of patients with hemiparesis at an early stage after stroke: a comparison of walking training on a treadmill with body weight support and walking training on the ground., Clin. Rehabil. 15 (2001) 515–527.

[3] C. Vaughan, B. Davis, J. O'connor, Dynamics of human gait., Human Kinetics Publishers, 1999.

[4] J.B. Saunders, V.T. Inman, H.D. Eberhart, The major determinants in normal and pathological gait., J. Bone Joint. Surg. Am. 35–A (1953) 543–558.

[5] S. Schmid, K. Schweizer, J. Romkes, S. Lorenzetti, R. Brunner, Secondary gait deviations in patients with and without neurological involvement: A systematic review., Gait Posture. 37 (2013) 480–493.

[6] S. Olney, C. Richards, Hemiparetic gait following stroke. Part I: Characteristics., Gait Posture. 4 (1996) 136–148.

[7] R.W. Bohannon, Comfortable and maximum walking speed of adults aged 20-79 years: reference values and determinants., Age Ageing. 26 (1997) 15–9.

[8] D. Podsiadlo, S. Richardson, The timed "Up & Go": a test of basic functional mobility for frail elderly persons., J. Am. Geriatr. Soc. 39 (1991) 142–148.

[9] M. Akay, M. Sekine, T. Tamura, Y. Higashi, T. Fujimoto, Fractal dynamics of body motion in post-stroke hemiplegic patients during walking., J. Neural Eng. 1 (2004) 111–116.

[10] C. Redd, S. Bamberg, A wireless sensory feedback device for real-time gait feedback and training, Mechatronics, {IEEE/ASME} Trans. Mechatronics. 17 (2012) 425–433.

[11] K. Aminian, B. Najafi, C. Büla, P.-F. Leyvraz, P. Robert, Spatio-temporal parameters of gait measured by an ambulatory system using miniature gyroscopes., J. Biomech. 35 (2002) 689–99.

[12] C. Senanayake, S. Senanayake, Human assisted tools for gait analysis and intelligent gait phase detection, in: Conf. Innov. Technol. Intell. Syst. Ind. Appl. (CITISIA 2009), 2009: 230–235.

[13] N. Mijailović, M. Gavrilović, S. Rafajlović, Gait phases recognition from accelerations and ground reaction forces: Application of neural networks, Telfor J. 1 (2009) 34–36.

[14] J. Pawin, T. Khaorapapong, S. Chawalit, Neural-based human's abnormal gait detection using force sensitive resistors, Fourth Int. Work. Adv. Comput. Intell. (2011) 224–229.

[15] S.O.H. Madgwick, A.J.L. Harrison, A. Vaidyanathan, Estimation of IMU and MARG orientation using a gradient descent algorithm., IEEE Int. Conf. Rehabil. Robot. 2011.

[16] K. Abdulrahim, C. Hide, T. Moore, C. Hill, Integrating low cost IMU with building heading in indoor pedestrian navigation, J. Glob. Position. Syst. 10 (2011) 30–38.

[17] A.M. Sabatini, Quaternion-based extended Kalman filter for determining orientation by inertial and magnetic sensing, IEEE Trans. Biomed. Eng. 53 (2006) 1346–1356.

[18] G. Cooper, I. Sheret, L. McMillan, L. McMillian, K. Siliverdis, N. Sha, D. Hodgins, L. Kenney, D. Howard, Inertial sensor-based knee flexion/extension angle estimation., J. Biomech. 42 (2009) 2678–2685.

[19] A.M. Sabatini, C. Martelloni, S. Scapellato, F. Cavallo, Assessment of walking features from foot inertial sensing., IEEE Trans. Biomed. Eng. 52 (2005) 486–494.

[20] K.P. Westlake, C. Patten, Pilot study of Lokomat versus manual-assisted treadmill training for locomotor recovery post-stroke., J. Neuroeng. Rehabil. 6 (2009) 18.

[21] M. Franceschini, S. Carda, M. Agosti, R. Antenucci, D. Malgrati, C. Cisari, Walking after stroke: what does treadmill training with body weight support add to overground gait training in patients early after stroke?: a single-blind, randomized, controlled trial., Stroke. 40 (2009) 3079–85.

[22] B. Brouwer, K. Parvataneni, S.J. Olney, A comparison of gait biomechanics and metabolic requirements of overground and treadmill walking in people with stroke., Clin. Biomech. (Bristol, Avon). 24 (2009) 729–734.

[23] S. Hesse, C. Werner, T. Paul, a Bardeleben, J. Chaler, Influence of walking speed on lower limb muscle activity and energy consumption during treadmill walking of hemiparetic patients., Arch. Phys. Med. Rehabil. 82 (2001) 1547–1550.

[24] K. Kaczmarczyk, A. Wit, M. Krawczyk, J. Zaborski, Gait classification in post-stroke patients using artificial neural networks., Gait Posture. 30 (2009) 207–210.

[25] J. Wikströ, G. Georgoulas, T. Moutsopoulos, A. Seferiadis, Intelligent data analysis of instrumented gait data in stroke patients-A systematic review, Comput. Biol. Med. 51 (2014) 61–72.

[26] S. Kinsella, K. Moran, Gait pattern categorization of stroke participants with equinus deformity of the foot, Gait Posture. 27(2008) 144-151.

[27] S. Mulroy, J.J.J. Gronley, W. Weiss, C. Newsam, J. Perry, Use of cluster analysis for gait pattern classification of patients in the early and late recovery phases following stroke, Gait Posture. 18 (2003) 114–125.

[28] K. Kaczmarczyk, A. Wit, M. Krawczyk, J. Zaborski, J. Gajewski, Associations between gait patterns, brain lesion factors and functional recovery in stroke patients., Gait Posture. 35 (2012) 214–217.

[29] C. Hodt-Billington, J.L. Helbostad, R. Moe-Nilssen, Should trunk movement or footfall parameters quantify gait asymmetry in chronic stroke patients?, Gait Posture. 27 (2008) 552–558.

[30] S. Hesse, F. Reiter, M. Jahnke, M. Dawson, Asymmetry of gait initiation in hemiparetic stroke, Phys Med Rehabil. 78 (1997) 718–724.

[31] H. Sadeghi, P. Allard, F. Prince, H. Labelle, Symmetry and limb dominance in able-bodied gait: a review., Gait Posture. 12 (2000) 34–45.

[32] H. Sadeghi, P. Allard, M. Duhaime, Functional gait asymmetry in able-bodied subjects, Hum. Mov. Sci. 16 (1997) 243–258.

[33] J.C. Echeverria, E. Rodriguez, A. Velasco, J. Alvarez-Ramirez, Limb dominance changes in walking evolution explored by asymmetric correlations in gait dynamics, Phys. A Stat. Mech. Its Appl. 389 (2010) 1625–1634.

[34] C.M. Kim, J.J. Eng, Symmetry in vertical ground reaction force is accompanied by symmetry in temporal but not distance variables of gait in persons with stroke, Gait Posture. 18 (2003) 23–28.

[35] S. Durham, L. Eve, C. Stevens, D. Ewins, Effect of Functional Electrical Stimulation on asymmetries in gait of children with hemiplegic cerebral palsy, Physiotherapy. 90 (2004) 82–90.

[36] S. Winiarski, A. Czamara, Evaluation of gait kinematics and symmetry during the first two stages of physiotherapy after anterior cruciate ligament reconstruction, Acta Bioeng Biomech. 14 (2012), 91-100.

[37] L. Sörnmo, P. Laguna, Bioelectrical signal processing in cardiac and neurological applications, Elsevier Academic, New York, 2005.

[38] P. Wang, K.H. Low, Qualitative evaluations of gait rehabilitation via EMG muscle activation pattern: Repetition, symmetry, and smoothness, in: IEEE Int. Conf. Robot. Biomimetics., 2009: 215–220.

[39] R. Brunner, J. Romkes, Abnormal EMG muscle activity during gait in patients without neurological disorders., Gait Posture. 27 (2008) 399–407.

[40] E.C. Wentink, V.G.H. Schut, E.C. Prinsen, J.S. Rietman, P.H. Veltink, Detection of the onset of gait initiation using kinematic sensors and EMG in transfemoral amputees., Gait Posture. 39 (2014) 391–396.

[41] M.L. Harris-Love, L.W. Forrester, R.F. Macko, K.H.C. Silver, G. V. Smith, Hemiparetic Gait Parameters in Overground Versus Treadmill Walking, Neurorehabil. Neural Repair. 15 (2001) 105–112.

[42] I. Khanna, A. Roy, M.M. Rodgers, H.I. Krebs, R.M. Macko, L.W. Forrester, Effects of unilateral robotic limb loading on gait characteristics in subjects with chronic stroke., J. Neuroeng. Rehabil. 7 (2010).

[43] G. Chen, C. Patten, D.H. Kothari, F.E. Zajac, Gait deviations associated with post-stroke hemiparesis: improvement during treadmill walking using weight support, speed, support stiffness, and handrail hold., Gait Posture. 22 (2005) 57–62.

[44] C.-L. Hsieh, C.-F. Sheu, I.-P. Hsueh, C.-H. Wang, Trunk Control as an Early Predictor of Comprehensive Activities of Daily Living Function in Stroke Patients, Stroke. 33 (2002) 2626-2630.

[45] B. Kollen, I. Van De Port, E. Lindeman, J. Twisk, G. Kwakkel, Predicting Improvement in Gait After Stroke A Longitudinal Prospective Study, Stroke. 36 (2005) 2676-2680.

[46] K. Tilling, J.A. Sterne, A.G. Rudd, T.A. Glass, , R.J. Wityk, C. D Wolfe, A New Method for Predicting Recovery After Stroke, Stroke. 32 (2001) 2867–2873.

[47] I.G. van de Port, G. Kwakkel, V.P. Schepers, E. Lindeman, Predicting mobility outcome one year after stroke: a prospective cohort study, J Rehabil Med. 38 (2006) 218–223.

[48] S. Masiero, R. Avesani, M. Armani, P. Verena, M. Ermani, Predictive factors for ambulation in stroke patients in the rehabilitation setting: A multivariate analysis, Clin. Neurol. Neurosurg. 109 (2007) 736–769.

[49] R.W. Teasell, S.K. Bhogal, N.C. Foley, M.R. Speechley, Gait retraining post stroke., Top. Stroke Rehabil. 10 (2003) 34–65.

[50] Rancho Los Amigos Medical Centre, Observational gait analysis handbook, Development Medical Child Neurology. 14:332-335

[51] S. Cuccurullo, Physical medicine and rehabilitation board review, Springer. 2004.

[52] F. Bugané, M.G. Benedetti, G. Casadio, S. Attala, F. Biagi, M. Manca, A Leardini, Estimation of spatial-temporal gait parameters in level walking based on

a single accelerometer: validation on normal subjects by standard gait analysis., Comput. Methods Programs Biomed. 108 (2012) 129–137.

[53] C. Lee, J. Lee, Estimation of walking behavior using accelerometers in gait rehabilitation, Int. J. Human-Friendly Welf. Robot. Syst. (2002) 1–4.

[54] G.I. Zdragkas, J.N. Avaritsiotis, Gait analysis and automatic gait event identification using accelerometers, in: 2008 8th IEEE Int. Conf. Bioinforma. Bioeng., Ieee, 2008: 1–6.

[55] A. Salarian, H. Russmann, F.J.G. Vingerhoets, C. Dehollain, Y. Blanc, P.R. Burkhard, K. Aminian, Gait assessment in Parkinson's disease: toward an ambulatory system for long-term monitoring., IEEE Trans. Biomed. Eng. 51 (2004) 1434–1443.

[56] J.P. Giuffrida, A. Lerner, R. Steiner, J. Daly, Upper-extremity stroke therapy task discrimination using motion sensors and electromyography., IEEE Trans. Neural Syst. Rehabil. Eng. 16 (2008) 82–90.

[57] P.T. Wang, C.E. King, A.H. Do, Z. Nenadic, A durable, low-cost electrogoniometer for dynamic measurement of joint trajectories., Med. Eng. Phys. 33 (2011) 546–552.

[58] F. Grenez, M. Viqueira Villarejo, B. García Zapirain, A. Méndez Zorrilla, Wireless prototype based on pressure and bending sensors for measuring gate quality., Sensors (Basel). 13 (2013) 9679–9703.

[59] M. Hanlon, R. Anderson, Real-time gait event detection using wearable sensors., Gait Posture. 30 (2009) 523–527.

[60] J. Garza-Ulloa, H. Yu, T. Sarkodie-Gyan, A mathematical model for the validation of the ground reaction force sensor in human gait analysis, Measurement. 45 (2012) 755–762.

[61] A.M. Howell, T. Kobayashi, T.R. Chou, W. Daly, M. Orendurff, S.J.M. Bamberg, A laboratory insole for analysis of sensor placement to determine ground reaction force and ankle moment in patients with stroke., IEEE Eng. Med. Biol. Soc. 2012 (2012) 6394–7.

[62] G. Courtine, M. Schieppati, Human walking along a curved path. II. Gait features and EMG patterns, Eur. J. Neurosci. 18 (2003) 191–205.

[63] J. Jonsdottir, D. Cattaneo, M. Recalcati, A. Regola, M. Rabuffetti, M. Ferrarin, A. Casiraghi, Task-oriented biofeedback to improve gait in individuals with chronic stroke: motor learning approach., Neurorehabil. Neural Repair. 24 (2010) 478–485.

[64] S.J. Morris, A Shoe-Integrated Sensor System for Wireless Gait Analysis and Real-Time Therapeutic Feedback., 2004.

[65] P. Lereim, F.S.- Hanssen, A method of recording pressure distribution under the sole of the foot, Bull. Pros. Res. 20 (1973) 118–125.

[66] H. Zhu, N. Maalej, J. Webster, An umbilical data-acquisition system for measuring pressure between the foot and show, IEEE Trans. Biomed. Eng. 37 (1990) 908–911.

[67] J.M. Hausdorff, Z. Ladin, J.Y. Wei, Footswitch system for measurement of the temporal parameters of gait., J. Biomech. 28 (1995) 347–351.

[68] A. Howell, T. Kobayashi, H. Hayes, K. Foreman, S. Bamberg, Kinetic gait analysis using a low-cost insole., IEEE Trans. Biomed. Eng. 60 (2013) 3284-3290.

[69] I.P. Pappas, M.R. Popovic, T. Keller, V. Dietz, M. Morari, A reliable gait phase detection system., IEEE Trans. Neural Syst. Rehabil. Eng. 9 (2001) 113–125.

[70] P. Lopez-Meyer, G.D. Fulk, E.S. Sazonov, Automatic detection of temporal gait parameters in poststroke individuals., IEEE Trans. Inf. Technol. Biomed. 15 (2011) 594–601.

[71] B. Mariani, H. Rouhani, X. Crevoisier, K. Aminian, Quantitative estimation of foot-flat and stance phase of gait using foot-worn inertial sensors., Gait Posture. 37 (2013) 229–234.

[72] T. Liu, Y. Inoue, K. Shibata, Development of a wearable sensor system for quantitative gait analysis, Measurement. 42 (2009) 978–988.

[73] S.J.M. Bamberg, A.Y. Benbasat, D.M. Scarborough, D.E. Krebs, J.A Paradiso, Gait analysis using a shoe-integrated wireless sensor system., IEEE Trans. Inf. Technol. Biomed. 12 (2008) 413–423.

[74] G. Welch, G. Bishop, An introduction to the Kalman filter, (2001). http://www.cs.unc.edu/

[75] Y. Teruyama, T. Watanabe, Effectiveness of variable-gain Kalman filter based on angle error calculated from acceleration signals in lower limb angle measurement with inertial sensors., Comput. Math. Methods Med. 2013 (2013).

[76] A.M. Sabatini, Kalman-filter-based orientation determination using inertial/magnetic sensors: observability analysis and performance evaluation., Sensors (Basel). 11 (2011) 9182–9206.

[77] C. Mazzà, M. Donati, J. McCamley, P. Picerno, A. Cappozzo, An optimized Kalman filter for the estimate of trunk orientation from inertial sensors data during treadmill walking., Gait Posture. 35 (2012) 138–142.

[78] H. Tan, A.M. Wilson, J. Lowe, Measurement of stride parameters using a wearable GPS and inertial measurement unit., J. Biomech. 41 (2008) 1398–1406.

[79] F. Caron, E. Duflos, D. Pomorski, P. Vanheeghe, GPS/IMU data fusion using multisensor Kalman filtering: introduction of contextual aspects, Inf. Fusion. 7 (2006) 221–230.

[80] S. Godha, G. Lachapelle, Foot mounted inertial system for pedestrian navigation, Meas. Sci. Technol. 19 (2008).

[81] J. A. Corrales, F. A. Candelas, F. Torres, Sensor data integration for indoor human tracking, Rob. Auton. Syst. 58 (2010) 931–939.

[82] R. Takeda, S. Tadano, A. Natorigawa, M. Todoh, S. Yoshinari, Gait posture estimation using wearable acceleration and gyro sensors., J. Biomech. 42 (2009) 2486–2494.

[83] T. Sayeed, A. Sama, A. Catala, J. Cabestany, Comparison and adaptation of step length and gait speed estimators from single belt worn accelerometer positioned on lateral side of the body, 2013 IEEE 8th Int. Symp. Intell. Signal Process. (2013) 14–20.

[84] S. Ganguli, P. Mukherji, K.S. Bose, Gait evaluation of unilateral below-knee amputees fitted with patellar-tendon-bearing prostheses., J. Indian Med. Assoc. 63 (1974) 256–259.

[85] M. Kljajić, T. Bajd, U. Stanic, Quantitative gait evaluation of hemiplegic patients using electrical stimulation orthoses., IEEE Trans. Biomed. Eng. 22 (1975) 438–41.

[86] R.O. Andres, S.K. Stimmel, Prosthetic alignment effects on gait symmetry: a case study., Clin. Biomech. (Bristol, Avon). 5 (1990) 88–96.

[87] R.O. Robinson, W. Herzog, B.M. Nigg, Use of force platform variables to quantify the effects of chiropractic manipulation on gait symmetry., J. Manipulative Physiol. Ther. 10 (1987) 172–176.

[88] R. Huiskes, D.H. Campen, J.R. Wijn, Biomechanics: Principles and Applications, Springer Netherlands, Dordrecht, 1982.

[89] M. Plotnik, N. Giladi, J.M. Hausdorff, A new measure for quantifying the bilateral coordination of human gait: effects of aging and Parkinson's disease., Exp. Brain Res. 181 (2007) 561–570.

[90] R.A. Zifchock, I. Davis, J. Higginson, T. Royer, The symmetry angle: a novel, robust method of quantifying asymmetry., Gait Posture. 27 (2008) 622–627.

[91] D.A. Winter, H.J. Yack, EMG profiles during normal human walking: stride-to-stride and inter-subject variability, Electroencephalogr. Clin. Neurophysiol. 67 (1987) 402–411.

[92] C. Hershler, M. Milner, An optimality criterion for processing electromyographic (EMG) signals relating to human locomotion, Biomed. Eng. IEEE Trans. Biomed. Eng. 25(1978) 413–420.

[93] J.M. Haddad, R.E. a van Emmerik, S.N. Whittlesey, J. Hamill, Adaptations in interlimb and intralimb coordination to asymmetrical loading in human walking., Gait Posture. 23 (2006) 429–434.

[94] F. Liao, J. Wang, P. He, Multi-resolution entropy analysis of gait symmetry in neurological degenerative diseases and amyotrophic lateral sclerosis., Med. Eng. Phys. 30 (2008) 299–310.

[95] I. Milovanović, D.B. Popović, Principal component analysis of gait kinematics data in acute and chronic stroke patients., Comput. Math. Methods Med. 2012 (2012).

[96] H. Sadeghi, F. Prince, S. Sadeghi, H. Labelle, Principal component analysis of the power developed in the flexion/extension muscles of the hip in able-bodied gait, Med. Eng. Phys. 22 (2000) 703–710.

[97] H. Sadeghi, P. Allard, F. Barbier, S. Sadeghi, Main functional roles of knee flexors/extensors in able-bodied gait using principal component analysis (I), Knee. 9 (2002) 47–53.

[98] S. Olney, M. Griffin, I. McBride, Multivariate examination of data from gait analysis of persons with stroke, Phys. Ther. 78 (1998) 814–828.

[99] N.E. Helwig, S. Hong, J.D. Polk, Parallel Factor Analysis of gait waveform data: A multimode extension of Principal Component Analysis., Hum. Mov. Sci. 31 (2012) 630–648.

[100] C. Nüesch, V. Valderrabano, C. Huber, V. von Tscharner, G. Pagenstert, Gait patterns of asymmetric ankle osteoarthritis patients., Clin. Biomech. (Bristol, Avon). 27 (2012) 613–618.

[101] K.A. Shorter, J.D. Polk, K.S. Rosengren, E.T. Hsiao-Wecksler, A new approach to detecting asymmetries in gait., Clin. Biomech. (Bristol, Avon). 23 (2008) 459–467.

[102] E.T. Hsiao-Wecksler, J.D. Polk, K.S. Rosengren, J.J. Sosnoff, S. Hong, A Review of New Analytic Techniques for Quantifying Symmetry in Locomotion, Symmetry (Basel). 2 (2010) 1135–1155.

[103] A. Goswami, A new gait parameterization technique by means of cyclogram moments: Application to human slope walking., Gait Posture. 8 (1998) 15–36.

[104] A. Goswami, Kinematic quantification of gait asymmetry based on bilateral cyclograms, New Zealand, Dunedin, 2003.

[105] P. Kutilek, S. Viteckova, Z. Svoboda, P. Smrcka, Kinematic quantification of gait asymmetry in patients with peroneal nerve palsy based on bilateral cyclograms, J. Musculoskelet. Neuronal. Interact. 13 (2013) 244–250.

[106] P. Kutilek, S. Viteckova, Z. Svoboda, Kinematic quantification of gait asymmetry based on characteristics of angle-angle diagrams, Acta Polytech.Hungarica. 11 (2014) 25–38.

[107] P. Kutilek, V. Socha, S. Viteckova, Z. Svoboda, Quantification of gait asymmetry in patients with ankle foot orthoses based on hip–hip cyclograms, Biocybern. Biomed. Eng. 34 (2014) 46–52.

[108] P. Kutilek, P. Smrcka, Z. Svoboda, Evaluation of muscle length asymmetry using OpenSim SW and bilateral cyclograms, Int. Conf. Applied. Electronics. (2013) 165-168.

[109] O. Hajný, B. Farkašová, A Study of Gait and Posture with the Use of Cyclograms, Acta Polytechnica. 50 (2010) 48-51.

[110] N. Stergiou, J.L. Jensen, B.T. Bates, S.D. Scholten, G. Tzetzis, A dynamical systems investigation of lower extremity coordination during running over obstacles, Clin. Biomech. 16 (2001) 213–221.

[111] L. Li, E.C.H. Bogert, G.E. Caldwell, R.E. Emmerik, J. Hamill, Coordination patterns of walking and running at similar speed and stride frequency, Hum. Mov. Sci. 18 (1999) 67–85.

[112] J. Hamill, R.E. Emmerik, B.C. Heiderscheit, L. Li, A dynamical systems approach to lower extremity running injuries, Clin. Biomech. 14 (1999) 297–308.

[113] J.D. Polk, J. Spencer-Smith, L. DiBerardino, D. Ellis, M. Downen, K.S. Rosengren, Quantifying variability in phase portraits: application to gait ontogeny., Infant Behav. Dev. 31 (2008) 302–306.

[114] L. A DiBerardino, J.D. Polk, K.S. Rosengren, J.B. Spencer-Smith, E.T. Hsiao-Wecksler, Quantifying complexity and variability in phase portraits of gait., Clin. Biomech. (Bristol, Avon). 25 (2010) 552–556.

[115] J. Longworth, Kinematic variability of wheelchair propulsion, The effects of speed and exercise, (2014).

[116] K.S. Rosengren, F.J. Deconinck, L.A Diberardino, J.D. Polk, J. Spencer-Smith, D. De Clercq, M. Lenoir, Differences in gait complexity and variability between children with and without developmental coordination disorder., Gait Posture. 29 (2009) 225–229.

[117] K. Manal, S.J. Stanhope, A novel method for displaying gait and clinical movement analysis data., Gait Posture. 20 (2004) 222–226.

[118] K. Manal, C.C. Chang, J. Hamill, S.J. Stanhope, A three-dimensional data visualization technique for reporting movement pattern deviations., J. Biomech. 38 (2005) 2151–2156.

[119] D.E. Turner, P.S. Helliwell, K.L. Siegel, J. Woodburn, Biomechanics of the foot in rheumatoid arthritis: identifying abnormal function and the factors associated with localised disease "impact"., Clin. Biomech. (Bristol, Avon). 23 (2008) 93–100.

[120] D.E. Turner, J. Woodburn, Characterising the clinical and biomechanical features of severely deformed feet in rheumatoid arthritis., Gait Posture. 28 (2008) 574–580.

[121] S.J. Crenshaw, J.G. Richards, A method for analyzing joint symmetry and normalcy, with an application to analyzing gait., Gait Posture. 24 (2006) 515–521.

[122] R. Fellin, K. Manal, I. Davis, Comparison of lower extremity kinematic curves during overground and treadmill running, J. Appl. Biomech. 26 (2010) 407–414.

[123] C. Doherty, C. Bleakley, J. Hertel, K. Sweeney, B. Caulfield, J. Ryan, E. Delahunt, Lower extremity coordination and symmetry patterns during a drop vertical jump task following acute ankle sprain., Hum. Mov. Sci. 38C (2014) 34–46.

[124] K.R. Kaufman, S. Frittoli, C.A Frigo, Gait asymmetry of transfemoral amputees using mechanical and microprocessor-controlled prosthetic knees., Clin. Biomech. (Bristol, Avon). 27 (2012) 460–465.

[125] T.A Exell, M.J.R. Gittoes, G. Irwin, D.G. Kerwin, Gait asymmetry: composite scores for mechanical analyses of sprint running., J. Biomech. 45 (2012) 1108–1111.

[126] R.R. Caron, R.C. Wagenaar, C.L. Lewis, E. Saltzman, K.G. Holt, Center of mass trajectory and orientation to ankle and knee in sagittal plane is maintained with forward lean when backpack load changes during treadmill walking., J. Biomech. 46 (2013) 70–76.

[127] V.L. Roger, A.S. Go, D.M. Lloyd-Jones, R.J. Adams, J.D. Berry, T.M. Brown, M.R. Carnethon, S. Dai, G. de Simone, E.S. Ford, C.S. Fox, H.J. Fullerton, C. Gillespie, K.J. Greenlund, S.M. Hailpern, J. a Heit, P.M. Ho, V.J. Howard, B.M. Kissela, S.J. Kittner, D.T. Lackland, J.H. Lichtman, L.D. Lisabeth, D.M. Makuc, G.M. Marcus, A. Marelli, D.B. Matchar, M.M. McDermott, J.B. Meigs, C.S. Moy, D. Mozaffarian, M.E. Mussolino, G. Nichol, N.P. Paynter, W.D. Rosamond, P.D. Sorlie, R.S. Stafford, T.N. Turan, M.B. Turner, N.D. Wong, J. Wylie-Rosett, Heart disease and stroke statistics--2011 update: a report from the American Heart Association., Circulation. 123 (2011) 18–209.

[128] WHO Global InfoBase, (2004). https://apps.who.int/infobase

[129] PDP Ferreora, Development of functional numerical scores improving the diagnostic of motion impairment of stroke patients using non-traditional gait parameters, (2016).

[130] G.J. Rinkel, J. van Gijn, E.F. Wijdicks, M. Lewis, N. Beauchamp, D. O'Leary, J. Carr, C. Furberg, S. Schwartz, C. Blum, S. Coutts, F. Purroy, J. Alvarez-Sabin, D. Sander, K. Sander, L. Restrepo, R. Wityk, J. Marx, J. Easton, H. V. Vinters, Subarachnoid hemorrhage without detectable aneurysm. A review of the causes., Stroke. 24 (1993) 1403–1409.

[131] G. Chen, C. Patten, D.H. Kothari, F.E. Zajac, Gait differences between individuals with post-stroke hemiparesis and non-disabled controls at matched speeds, Gait Posture. 22 (2005) 51–56.

[132] J.J. Chen, T.Y. Sun, T.H. Lin, T.S. Lin, Spatio-temporal representation of multichannel EMG firing patterns and its clinical applications., Med. Eng. Phys. 19 (1997) 420–340.

[133] J. Hendrickson, K.K. Patterson, E.L. Inness, W.E. McIlroy, A. Mansfield, Relationship between asymmetry of quiet standing balance control and walking post-stroke., Gait Posture. 39 (2014) 177–181.

[134] A. Lamontagne, F. Malouin, C. Richards, F. Dumas, Mechanisms of disturbed motor control in ankle weakness during gait after stroke, Gait Posture. 15 (2002) 244–255.

[135] A. Pizzi, G. Carlucci, C. Falsini, F. Lunghi, S. Verdesca, A. Grippo, Gait in hemiplegia: evaluation of clinical features with the Wisconsin Gait Scale., J. Rehabil. Med. 39 (2007) 170–174.

[136] R. Verma, Understanding gait control in post-stroke: Implications for management, J. Bodyw. Mov. Ther. 16 (2012) 14–21.

[137] K.M. Sibley, A. Tang, K.K. Patterson, D. Brooks, W.E. McIlroy, Changes in spatiotemporal gait variables over time during a test of functional capacity after stroke., J. Neuroeng. Rehabil. 6 (2009).

[138] J. Moreland, C. Goldsmith, Progressive resistance strengthening exercises after stroke: a single-blind randomized controlled trial, Arch. Phys. Med. Rehabi. 84 (2003) 1433–1440.

[139] A. Weiss, T. Suzuki, J. Bean, R.A. Fielding, High intensity strength training improves strength and functional performance after stroke., Am. J. Phys. Med. Rehabil. 79 (2000) 369-376.

[140] A.M. Roy, Functional Electrical Stimulation Information for Patients and Families, Stroke Engine. 1–5.

[141] P.N. Taylor, J.H. Burridge, A.L. Dunkerley, D.E. Wood, J.A. Norton, C. Singleton, I.D. Swain, Clinical use of the odstock dropped foot stimulator: its effect

on the speed and effort of walking., Arch. Phys. Med. Rehabil. 80 (1999) 1577–1583.

[142] C. Richards, S. Olney, Hemiparetic gait following stroke. Part II: Recovery and physical therapy, Gait Posture. 4 (1996) 149–162.

[143] A.R. Den Otter, A.C.H. Geurts, T. Mulder, J. Duysens, Gait recovery is not associated with changes in the temporal patterning of muscle activity during treadmill walking in patients with post-stroke hemiparesis., Clin. Neurophysiol. 117 (2006) 4–15.

[144] S. Hesse, M. Konrad, D. Uhlenbrock, Treadmill walking with partial body weight support versus floor walking in hemiparetic subjects, Arch. Phys. Med. Rehab. 80 (1999) 421–427.

[145] C. Geroin, A. Picelli, D. Munari, A. Waldner, C. Tomelleri, N. Smania, Combined transcranial direct current stimulation and robot-assisted gait training in patients with chronic stroke: a preliminary comparison., Clin. Rehabil. 25 (2011) 537–548.

[146] M. Roerdink, C.J.C. Lamoth, G. Kwakkel, P.C.W. Wieringen, P.J. Beek, Gait coordination after stroke: benefits of acoustically paced treadmill walking., Phys. Ther. 87 (2007) 1009–1022.

[147] M.H. Thaut, a K. Leins, R.R. Rice, H. Argstatter, G.P. Kenyon, G.C. McIntosh, H. V Bolay, M. Fetter, Rhythmic auditory stimulation improves gait more than NDT/Bobath training in near-ambulatory patients early poststroke: a single-blind, randomized trial., Neurorehabil. Neural Repair. 21 (2007) 455–459.

[148] J.H. Kahn, T.G. Hornby, Rapid and long-term adaptations in gait symmetry following unilateral step training in people with hemiparesis., Phys. Ther. 89 (2009) 474–483.

[149] S. Karthikbabu, Role of Trunk Rehabilitation on Trunk Control, Balance and Gait in Patients with Chronic Stroke: A Pre-Post Design, Neurosci. Med. 2 (2011) 61–67.

[150] M. Pohl, J. Mehrholz, Immediate effects of an individually designed functional ankle-foot orthosis on stance and gait in hemiparetic patients, Clin. Rehabil. 20 (2006) 324–330.

[151] A. Esquenazi, D. Ofluoglu, B. Hirai, S. Kim, The effect of an ankle-foot orthosis on temporal spatial parameters and asymmetry of gait in hemiparetic patients., PM R. 1 (2009) 1014–1018.

[152] R. Swigchem, V. Weerdesteyn, H.J. Duijnhoven, J. Boer, T. Beems, A.C. Geurts, Near-normal gait pattern with peroneal electrical stimulation as a neuroprosthesis in the chronic phase of stroke: a case report., Arch. Phys. Med. Rehabil. 92 (2011) 320–324.

[153] J.-H. Kim, Y. Chung, Y. Kim, S. Hwang, Functional electrical stimulation applied to gluteus medius and tibialis anterior corresponding gait cycle for stroke., Gait Posture. 36 (2012) 65–67.

[154] G. Yavuzer, F. Eser, D. Karakus, B. Karaoglan, H.J. Stam, The effects of balance training on gait late after stroke: a randomized controlled trial., Clin. Rehabil. 20 (2006) 960–969.

[155] Y.-R. Yang, J.-G. Yen, R.-Y. Wang, L.-L. Yen, F.-K. Lieu, Gait outcomes after additional backward walking training in patients with stroke: a randomized controlled trial, Clin. Rehabil. 19 (2005) 264–273.

[156] K.H.C. Silver, R.F. Macko, L.W. Forrester, A.P. Goldberg, G.V. Smith, Effects of Aerobic Treadmill Training on Gait Velocity, Cadence, and Gait Symmetry in Chronic Hemiparetic Stroke: A Preliminary Report, Neurorehabil. Neural Repair. 14 (2000) 65–71.

[157] C.M. Tyrell, M. a Roos, K.S. Rudolph, D.S. Reisman, Influence of systematic increases in treadmill walking speed on gait kinematics after stroke., Phys. Ther. 91 (2011) 392–403.

[158] T.M. Kesar, S.A. Binder-Macleod, G.E. Hicks, D.S. Reisman, Minimal detectable change for gait variables collected during treadmill walking in individuals post-stroke., Gait Posture. 33 (2011) 314–317.

[159] R. Stock, P.J. Mork, The effect of an intensive exercise programme on leg function in chronic stroke patients: a pilot study with one-year follow-up., Clin. Rehabil. 23 (2009) 790–799.

[160] V.M. Pomeroy, B. Evans, M. Falconer, D. Jones, E. Hill, G. Giakas, An exploration of the effects of weighted garments on balance and gait of stroke patients with residual disability, Clin. Rehabil. 15 (2001) 390–397.

[161] S. Ferrante, E. Ambrosini, P. Ravelli, E. Guanziroli, F. Molteni, G. Ferrigno, A. Pedrocchi, A biofeedback cycling training to improve locomotion: a case series study based on gait pattern classification of 153 chronic stroke patients., J. Neuroeng. Rehabil. 8 (2011).

[162] L. Teixeira-Salmela, Effects of muscle strengthening and physical conditioning training on temporal, kinematic and kinetic variables during gait in chronic stroke survivors, J. Rehabil. Med. 33(2001) 53–60.

[163] Y.-R. Yang, Y.-C. Chen, C.-S. Lee, S.-J. Cheng, R.-Y. Wang, Dual-task-related gait changes in individuals with stroke., Gait Posture. 25 (2007) 185–190.

[164] A.-L. Hsu, P.-F. Tang, M.-H. Jan, Analysis of impairments influencing gait velocity and asymmetry of hemiplegic patients after mild to moderate stroke, Arch. Phys. Med. Rehabil. 84 (2003) 1185–1193.

[165] C.K. Balasubramanian, M.G. Bowden, R.R. Neptune, S.A. Kautz, Relationship between step length asymmetry and walking performance in subjects with chronic hemiparesis., Arch. Phys. Med. Rehabil. 88 (2007) 43–49.

[166] M.A. Dettmann, M.T. Linder, S.B. Sepic, Relationships among walking performance, postural stability, and functional assessments of the hemiplegic patient., Am. J. Phys. Med. 66 (1987) 77–90.

[167] V.S. Mercer, J.K. Freburger, Z. Yin, J.S. Preisser, Recovery of paretic lower extremity loading ability and physical function in the first six months after stroke., Arch. Phys. Med. Rehabil. 95 (2014) 1547–1555.

[168] J.C. Wall, G.I. Turnbull, Gait asymmetries in residual hemiplegia., Arch. Phys. Med. Rehabil. 67 (1986) 550–553.

[169] R. Bayat, H. Barbeau, A. Lamontagne, Speed and temporal-distance adaptations during treadmill and overground walking following stroke., Neurorehabil. Neural Repair. 19 (2005) 115–124.

[170] N. Goodwin, A. Sunderland, Intensive, time-series measurement of upper limb recovery in the subacute phase following stroke, Clin. Rehabil. 17 (2003) 69–82.

[171] J.P. Clarys, Electrology and localized electrization revisited, J. Electromyogr. Kinesiol. 4 (1994) 5–14.

[172] R.F.M. Kleissen, J.H. Buurke, J. Harlaar, G. Zilvold, Electromyography in the biomechanical analysis of human movement and its clinical application, Gait Posture. 8 (1998) 143–158.

[173] L.H. Lindstrom, R.I. Magnusson, Interpretation of myoelectric power spectra: A model and its applications, Proc. IEEE. 65 (1977) 653–662.

[174] C. Miller, Real-time feature extraction and classification of prehensile EMG signals, San Diego State University, 2008.

[175] C. De Luca, L.D. Gilmore, M. Kuznetsov, S.H. Roy, Filtering the surface EMG signal: Movement artifact and baseline noise contamination., J. Biomech. 43 (2010) 1573–1579.

[176] C. De Luca, Surface electromyography: Detection and recording, DelSys Inc. (2002) 1–10.

[177] SENIAM. http://seniam.org.

[178] Lower Limb Articulations/Movements. http://anatomyuniverse.com/reviews/movements/limbs/lower.

[179] Muscle Anatomy, Pearson Educ. Inc. (2009). http://droualb.faculty.mjc.edu/Course Materials/Elementary Anatomy and Physiology 50/Lecture outlines/muscle_anatomy.htm

[180] C.J. Miller, Real Time Feature Extraction And Classification of Prehensile EMG Signals, San Diego State University, (2013).

[181] S. Du, Feature Extraction For Classification Of Perhensile Electromyographyc Patterns, San Diego State Univeristy, (2003).

[182] G. Staude, Onset Detection in Surface Electromyographic Signals : A systematic comparison of methods, J. Applied Sig. Process. 2(2001) 67–81.

[183] C. Lee, D. Landgrebe, Feature extraction and classification algorithms for high dimensional data, University West Lafayette, 1993.

[184] K. Englehart, B. Hudgins, P. a Parker, M. Stevenson, Classification of the myoelectric signal using time-frequency based representations., Med. Eng. Phys. 21 (1999) 431–438.

[185] S. Du, Temporal vs. spectral approach to feature extraction from prehensile EMG signals, IEEE Int. Conf. Info. Reuse. Integration. (2004) 344–350.

[186] M.B.I. Raez, M.S. Hussain, F. Mohd-Yasin, Techniques of EMG signal analysis: detection, processing, classification and applications., Biol. Proced. Online. 8 (2006) 11–35.

[187] B.S. Day, Important Factors in Surface EMG Measurement, Bortec Biomedical LTD Publisher. (2002) 1–17.

[188] G.G. Hirschberg, M. Nathanson, Electromyographic recording of muscular activity in normal and spastic gaits., Arch. Phys. Med. Rehabil. 33 (1952) 217–225.

[189] J.H. Buurke, A. V. Nene, G. Kwakkel, V. Erren-Wolters, M.J. IJzerman, H.J. Hermens, Recovery of Gait After Stroke: What Changes?, Neurorehabil. Neural Repair. 22 (2008) 676–683.

[190] M. Talebinejad, A.D.C. Chan, A. Miri, R.M. Dansereau, Fractal analysis of surface electromyography signals: a novel power spectrum-based method., J. Electromyogr. Kinesiol. 19 (2009) 840–850.

[191] G. Fele-Zorz, G. Kavsek, Z. Novak-Antolic, F. Jager, A comparison of various linear and non-linear signal processing techniques to separate uterine EMG records of term and pre-term delivery groups., Med. Biol. Eng. Comput. 46 (2008) 911–922.

[192] J.-P. Eckmann, S.O. Kamphorst, D. Ruelle, Recurrence Plots of Dynamical Systems, Europhys. Lett. 4 (1987) 973–977.

[193] D. Rodrick, W. Karwowski, Nonlinear dynamical behavior of surface electromyographical signals of biceps muscle under two simulated static work postures., Nonlinear Dynamics. Psychol. Life Sci. 10 (2006) 21–35.

[194] G. Ouyang, X. Zhu, Z. Ju, H. Liu, Dynamical Characteristics of Surface EMG Signals of Hand Grasps via Recurrence Plot, IEEE J. Biomed. Heal. Informatics. 18 (2014) 257–265.

[195] N. Marwan, M. Carmenromano, M. Thiel, J. Kurths, Recurrence plots for the analysis of complex systems, Phys. Rep. 438 (2007) 237–329.

[196] C. Morana, S. Ramdani, S. Perrey, A. Varray, Recurrence quantification analysis of surface electromyographic signal: Sensitivity to potentiation and neuromuscular fatigue, J. Neurosci. Methods. 177 (2009) 73–79.

[197] C.L. Webber, J.P. Zbilut, Dynamical assessment of physiological systems and states using recurrence plot strategies., J. Appl. Physiol. 76 (1994) 965–973.

[198] Y. Liu, M. Kankaanpaa, J.P. Zbilut, C.L. Webber, EMG recurrence quantifications in dynamic exercise, Biol. Cybern. 90 (2004) 337–348.

[199] C. Morana, S. Ramdani, S. Perrey, A. Varray, Recurrence quantification analysis of surface electromyographic signal: sensitivity to potentiation and neuromuscular fatigue., J. Neurosci. Methods. 177 (2009) 73–79.

[200] F. Felici, A. Rosponi, P. Sbriccoli, G.C. Filligoi, L. Fattorini, M. Marchetti, Linear and non-linear analysis of surface electromyograms in weightlifters, Eur. J. Appl. Physiol. 84 (2001) 337–342.

[201] D. Farina, L. Fattorini, F. Felici, G. Filligoi, Nonlinear surface EMG analysis to detect changes of motor unit conduction velocity and synchronization., J. Appl. Physiol. 93 (2002) 1753–1763.

[202] G. Filligoi, F. Felici, Detection of hidden rhythms in surface EMG signals with a non-linear time-series tool., Med. Eng. Phys. 21 (1999) 439–448.

[203] P. Faure, H. Korn, A new method to estimate the Kolmogorov entropy from recurrence plots: its application to neuronal signals, Phys. D Nonlinear Phenom. 122 (1998) 265–279.

[204] B.B. Mandelbrot, The Fractal Geometry of Nature, American J. Physics. 51 (1983).

[205] C.K. Peng, S. V. Buldyrev, S. Havlin, M. Simons, H.E. Stanley, A.L. Goldberger, Mosaic organization of DNA nucleotides, Phys. Rev. E. 49 (1994) 1685–1689.

[206] M.J. Katz, Fractals and the analysis of waveforms., Comput. Biol. Med. 18 (1988) 145–156.

[207] T. Higuchi, Approach to an irregular time-series on the basis of the fractal theory, Phys. D. 31 (1988) 277–283

[208] V. Gupta, Fractal analysis of surface EMG signals from the biceps, Int. J. Med. Informatics 45. (1997) 185–192.

[209] X. Hu, Z. Wang, X. Ren, Classification of surface EMG signal with fractal dimension., J. Zhejiang Univ. Sci. B. 6 (2005) 844–848.

[210] A. Phinyomark, P. Phukpattaranont, C. Limsakul, Fractal analysis features for weak and single-channel upper-limb EMG signals, Expert Syst. Appl. 39 (2012) 11156–11163.

[211] A. Ancillao, M. Galli, C. Rigoldi, G. Albertini, Linear correlation between fractal dimension of surface EMG signal from Rectus Femoris and height of vertical jump, Chaos, Solitons Fractals Interdiscip. J. Nonlinear Sci. Nonequilibrium Complex Phenom. 66 (2014) 120–126.

[212] S.P. Arjunan, D.K. Kumar, G. Naik, Computation and evaluation of features of surface electromyogram to identify the force of muscle contraction and muscle fatigue., Biomed Res. Int. 2014 (2014).

[213] M. Beretta-Piccoli, G. D'Antona, M. Barbero, B. Fisher, C.M. Dieli-Conwright, R. Clijsen, C. Cescon, Evaluation of Central and Peripheral Fatigue in the Quadriceps Using Fractal Dimension and Conduction Velocity in Young Females, PLoS One. 10 (2015).

[214] G. Boccia, D. Dardanello, M. Beretta-Piccoli, C. Cescon, G. Coratella, N. Rinaldo, M. Barbero, M. Lanza, F. Schena, A. Rainoldi, Muscle fiber conduction velocity and fractal dimension of EMG during fatiguing contraction of young and elderly active men, Physiol. Meas. 37 (2016) 162–174.

[215] C.J. De Luca, Decomposition of Surface EMG Signals, J. Neurophysiol. 96 (2006) 1646–1657.

[216] G. Biagetti, P. Crippa, S. Orcioni, C. Turchetti, Homomorphic Deconvolution for MUAP Estimation from Surface EMG Signals, IEEE J. Biomed. Heal. Informatics. 21 (2017) 328–338.

[217] N. Huang, Z. Shen, S. Long, M. Wu, H. Shih, Q. Zheng, N. Yen, C. Tung, H. Liu, The empirical mode decomposition and the Hilbert spectrum for nonlinear and non-stationary time series analysis, Proc. R. Soc. A Math. Phys. Eng. Sci. 454 (1998).

[218] A.O. Andrade, S. Nasuto, P. Kyberd, C.M. Sweeney-Reed, F.R. Van Kanijn, EMG signal filtering based on Empirical Mode Decomposition, Biomed. Signal Process. Control. 1 (2006) 44–55.

[219] B. Mijović, M. De Vos, I. Gligorijević, J. Taelman, S. Van Huffel, Source separation from single-channel recordings by combining empirical-mode

decomposition and independent component analysis, IEEE Trans. Biomed. Eng. 57 (2010) 2188–2196.

[220] V.K. Mishra, V. Bajaj, A. Kumar, D. Sharma, G.K. Singh, An efficient method for analysis of EMG signals using improved empirical mode decomposition, AEU - Int. J. Electron. Commun. 72 (2017) 200–209.

[221] Y. Zhi-Guo, W. Zhi-Zhong, R. Xiao-Mei, Joint application of feature extraction based on EMD-AR strategy and multi-class classifier based on LS-SVM in EMG motion classification, J Zhejiang Univ Sci A. 8 (2007) 1246–1255.

[222] Z. Wu, N.E. Huang, Ensemble Empirical Mode Decomposition: A Noise Assisted Data Analysis Method, Adv. Adaptive Data Analysis. 1 (2005) 1-41.

[223] A.M. Sabatini, Quaternion-based strap-down integration method for applications of inertial sensing to gait analysis, Med. Biol. Eng. Comput. 43 (2005) 94–101.

[224] AN-1005 Understanding Euler Angles, 2013. http://www.chrobotics.com/docs/AN-1005-UnderstandingEulerAngles.pdf

[225] R. Baker, Gait analysis methods in rehabilitation, J. Neuroeng. Rehabil. 3 (2006) 4.

[226] D.L. Skaggs, S.A. Rethlefsen, R.M. Kay, S.W. Dennis, R.A. Reynolds, V.T. Tolo, Variability in gait analysis interpretation., J. Pediatr. Orthop. 20 (2000) 759–764.

[227] R. Senden, B. Grimm, I.C. Heyligers, H.H.C.M. Savelberg, K. Meijer, Acceleration-based gait test for healthy subjects: Reliability and reference data, Gait Posture. 30(2009) 192-196.

[228] B. Auvinet, G. Berrut, C. Touzard, L. Moutel, N. Collet, D. Chaleil, E. Barrey, Reference data for normal subjects obtained with an accelerometric device, Gait Posture. 16 (2002) 124–134.

[229] S.H. Cho, J.M. Park, O.Y. Kwon, Gender differences in three dimensional gait analysis data from 98 healthy Korean adults, Clin. Biomech. 19 (2004) 145-152.

[230] H.B. Menz, M.D. Latt, A. Tiedemann, M. Mun, S. Kwan, S.R. Lord, Reliability of the GAITRite walkway system for the quantification of temporo-spatial parameters of gait in young and older people, Gait Posture. 20 (2004) 20–25.

[231] S. Kinsella, K. Moran, Gait pattern categorization of stroke participants with equinus deformity of the foot, Gait Posture. 27(2008) 144-151.

[232] B. Balaban, F. Tok, Gait Disturbances in Patients With Stroke., PM R. 6 (2014) 635-642.

[233] J. Perry, M. Garrett, J.K. Gronley, S.J. Mulroy, Classification of walking handicap in the stroke population, Stroke. 26 (1995) 982–989.

[234] S.M. Woolley, Characteristics of Gait in Hemiplegia, Top. Stroke Rehabil. 7 (2001) 1–18.

[235] M. Gaviria, P. Chaveta, J. Pelissierb, E. Peruchona, P. Rabischong, Plantar dynamics of hemiplegic gait: a methodological approach, Gait Posture. 4 (1996) 297–305.

[236] K.K. Patterson, I. Parafianowicz, C.J. Danells, V. Closson, M.C. Verrier, W.R. Staines, S.E. Black, W.E. McIlroy, Gait asymmetry in community-ambulating stroke survivors., Arch. Phys. Med. Rehabil. 89 (2008) 304–310.

[237] G. Williams, B. Galna, M.E. Morris, J. Olver, Spatiotemporal deficits and kinematic classification of gait following a traumatic brain injury: a systematic review., J. Head Trauma Rehabil. 25 (2010) 366–374.

[238] K.K. Patterson, W.H. Gage, D. Brooks, S.E. Black, W.E. McIlroy, Evaluation of gait symmetry after stroke: a comparison of current methods and recommendations for standardization., Gait Posture. 31 (2010) 241–246.

[239] K.K. Patterson, W.H. Gage, D. Brooks, S.E. Black, W.E. McIlroy, Changes in gait symmetry and velocity after stroke: a cross-sectional study from weeks to years after stroke., Neurorehabil. Neural Repair. 24 (2010) 783–790.

[240] E.J. Roth, C. Merbitz, K. Mroczek, S.A. Dugan, W.W. Suh, Hemiplegic gait. Relationships between walking speed and other temporal parameters., Am. J. Phys. Med. Rehabil. 76 (1997) 128–133.

[241] M. Akay, Nonlinear biomedical signal processing, Dynamic analysis and modeling, Wiley-IEEE, (2001).

[242] B.J. West, L. Griffin, Allometric Control\ Inverse Power Laws and Human Gait, Chaos. Solitons. Fractals. 10(1999) 1519-1527.

[243] J.M. Hausdorff, S.L. Mitchell, R.E. Firtion, C.K. Peng, M.E. Cudkowicz, J.Y. Wei, A.L. Goldberger, R. Firtion, Altered fractal dynamics of gait: reduced stride-interval correlations with aging and Huntington's disease, J. Appl. Physiol (1985). 82 (1997) 262-269.

[244] C. Gómez, Á. Mediavilla, R. Hornero, D. Abásolo, A. Fernández, Use of the Higuchi's fractal dimension for the analysis of MEG recordings from Alzheimer's disease patients, Med. Eng. Phys. 31 (2009) 306–313.

[245] T.L.A. Doyle, E.L. Dugan, B. Humphries, R.U. Newton, Discriminating between elderly and young using a fractal dimension analysis of centre of pressure., Int. J. Med. Sci. 1 (2004) 11–20.

[246] L.J. Hadjileontiadis, I.T. Rekanos, Detection of explosive lung and bowel sounds by means of fractal dimension, IEEE Signal Process. Lett. 10 (2003) 311–314.

[247] L.J. Hadjileontiadis, E. Douka, A. Trochidis, Fractal dimension analysis for crack identification in beam structures, Mech. Syst. Signal Process. 19 (2005) 659–674.

[248] A.L. Hof, H. Elzinga, W. Grimmius, J.P.K. Halbertsma, Speed dependence of averaged EMG profiles in walking, Gait Posture. 16 (2002) 78–86.

[249] S.J. Olney, M.P. Griffin, T.N. Monga, I.D. McBride, Work and power in gait of stroke patients., Arch. Phys. Med. Rehabil. 72 (1991) 309–314.

[250] T. Seel, J. Raisch, T. Schauer, IMU-Based Joint Angle Measurement for Gait Analysis, Sensors. 14 (2014) 6891–6909.

[251] U. Puh, G.D. Baer, A comparison of treadmill walking and overground walking in independently ambulant stroke patients: A pilot study, Disabil. Rehabil. 31 (2009) 202–210.

[252] N.E. Helwig, S. Hong, E.T. Hsiao-Wecksler, J.D. Polk, Methods to temporally align gait cycle data., J. Biomech. 44 (2011) 561–566.

[253] S. Hong, Warped Image Factor Analysis, 1st IEEE Int. Work. Comput. Adv. Multi-Sensor Adapt. Process. (2005) 121–124.

[254] H. Sakoe, S. Chiba, Dynamic Programming Algorithm Optimization for Spoken Word Recognition, Readings Speech Recognit. (1990) 159–165.

[255] F.E. Harrell, K.L. Lee, D.B. Matchar, T.A. Reichert, Regression models for prognostic prediction: advantages, problems, and suggested solutions., Cancer Treat. Rep. 69 (1985) 1071–1077.

[256] K.R. Wheeler, M.H. Chang, K.H. Knuth, Gesture-Based Control and EMG Decomposition, Appl. Rev. 36 (2006).

[257] S.H. Nawab, S.-S. Chang, C.J. De Luca, High-yield decomposition of surface EMG signals., Clin. Neurophysiol. 121 (2010) 1602–1615.

[258] K.-M. Chang, Kang-Ming, Arrhythmia ECG noise reduction by ensemble empirical mode decomposition, Sensors. 10 (2010) 6063–6080.

[259] P.M. Kluding, K. Dunning, M.W. O'Dell, S.S. Wu, J. Ginosian, J. Feld, K. McBride, Foot drop stimulation versus ankle foot orthosis after stroke: 30-week outcomes, Stroke. 44 (2013) 1660–1669.

[260] D. Intiso, V. Santilli, M.G. Grasso, R Rossi, I. Caruso, Rehabilitation of walking with electromyographic biofeedback in foot-drop after stroke, Stroke. 25 (1994) 1189-1192.

[261] M.M. Van Der Krogt, S.L. Delp, M.H. Schwartz, How robust is human gait to muscle weakness?, Gait Posture. 36 (2012).

[262] A.L. Whitehead, S.A. Julious, C.L. Cooper, M.J. Campbell, Estimating the sample size for a pilot randomised trial to minimise the overall trial sample size for the external pilot and main trial for a continuous outcome variable., Stat Methods Med Res. 25 (2016).

[263] A.B. Anand (2010), Tracking red color objects using matlab(Version 1.1.0.0.
[Source code]. https://www.mathworks.com/matlabcentral/fileexchange/28757-tracking-red-color-objects-using-matlab

[263] R. Williamson, B.J. Andrews, Detecting absolute human knee angle and angular velocity using accelerometers and rate gyroscopes., Med. Biol. Eng. Comput. 39 (2001).

[264] K.T. Ozgunen, C. Umut, S.S. Kurdak, Determination of an optimal threshold value for muscle activity detection in EMG analysis. J. Sport. Sci. Med., 9(2010).

Appendix A Derivation of Numerical Integration Algorithm

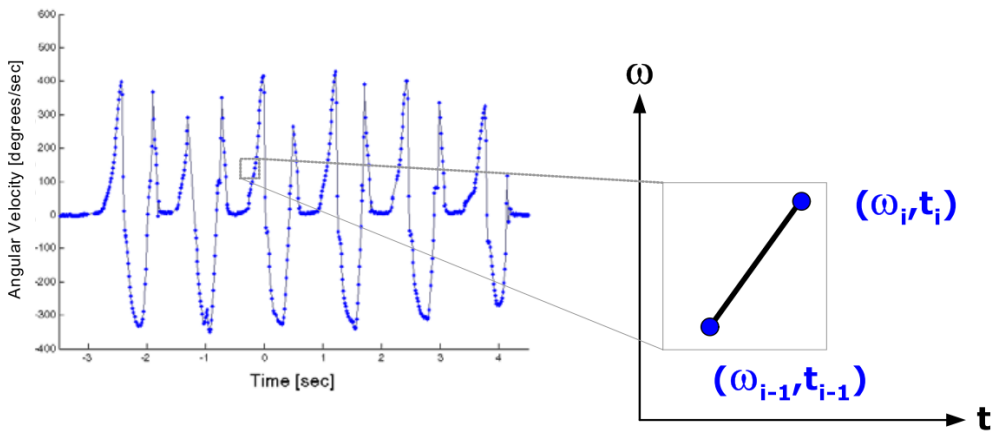

Fig A.1. Illustratuib for linear integration [64].

The linear integrator used the assumption that the interval between each data is a small interval that the change of signal can be considered as linear between two points as shown in Fig A.1. This numerical algorithm is inspired by Stacy [64].

The equation of the line between two points can be defined by its gradient, m.

$$m = \frac{(\omega_i - \omega_{i-1})}{(t_i - t_{i-1})} \tag{A.1}$$

And its y-intercept, b

$$b = \omega_{i-1} - m \cdot t_{i-1} \tag{A.2}$$

The integral of the signal between time point is

$$\theta_i - \theta_{i-1} = \int_{t_{i-1}}^{t_i} (m \cdot \tau + b) d\tau \tag{A.3}$$

which reduces to

$$\theta_i = \frac{1}{2} \cdot m \cdot (t_i^2 - t_{i-1}^2) + b \cdot (t_i - t_{i-1}) + \theta_{i-1} \quad \text{(A.4)}$$

The Matlab code for this equation is as followed:

```
function int_data=linear_integrator(data,time,initialvalue)

% LINEAR_INTEGRATOR(data,time,initialvalue) integrates the data function v. time, % with the assumption that DelT is small enough theat the data function is linear % between each DelT. It returns the integrated function. % %

 (c)2003 Stacy J. Morris ~ sjm@alum.mit.edu

time_end=length(time);

int_data(1,1)=initialvalue;

 for i=2:time_end

        m=(data(i)-data(i-1))/(time(i)-time(i-1));

        b=data(i-1)-m*time(i-1);

        int_data(i,1)=(1/2)*m*(time(i)^2 - time(i-1)^2) + b*(time(i)-time(i-1)) +

        int_data(i-1,1);

end
```

Appendix B Tracking Red Colour Objects Matlab Code

```
a = imaqhwinfo;
[camera_name, camera_id, format] = getCameraInfo(a);
% Capture the video frames using the videoinput function
% You have to replace the resolution & your installed adaptor name.
vid = videoinput(camera_name, camera_id, format);
% Set the properties of the video object
set(vid, 'FramesPerTrigger', Inf);
set(vid, 'ReturnedColorspace', 'rgb')
vid.FrameGrabInterval = 5;
%start the video aquisition here
start(vid)
% Set a loop that stop after 100 frames of aquisition
while(vid.FramesAcquired<=200)

    % Get the snapshot of the current frame
    data = getsnapshot(vid);

    % Now to track red objects in real time
    % we have to subtract the red component
    % from the grayscale image to extract the red components in the image.
    diff_im = imsubtract(data(:,:,1), rgb2gray(data));
    %Use a median filter to filter out noise
    diff_im = medfilt2(diff_im, [3 3]);
    % Convert the resulting grayscale image into a binary image.
    diff_im = im2bw(diff_im,0.18);

    % Remove all those pixels less than 300px
    diff_im = bwareaopen(diff_im,300);

    % Label all the connected components in the image.
    bw = bwlabel(diff_im, 8);

    % Here we do the image blob analysis.
    % We get a set of properties for each labeled region.
    stats = regionprops(bw, 'BoundingBox', 'Centroid');

    % Display the image
    imshow(data)

    hold on

    %This is a loop to bound the red objects in a rectangular box.
    for object = 1:length(stats)
        bb = stats(object).BoundingBox;
        bc = stats(object).Centroid;
        rectangle('Position',bb,'EdgeColor','r','LineWidth',2)
        plot(bc(1),bc(2), '-m+')
        a=text(bc(1)+15,bc(2), strcat('X: ', num2str(round(bc(1))), '    Y:
', num2str(round(bc(2)))));
        set(a, 'FontName', 'Arial', 'FontWeight', 'bold', 'FontSize', 12,
'Color', 'yellow');
```

```
    end

    hold off
end
% Both the loops end here.
% Stop the video aquisition.
stop(vid);
% Flush all the image data stored in the memory buffer.
flushdata(vid);
% Clear all variables
clear all
sprintf('%s','That was all about Image tracking, Guess that was pretty
easy :) ')
```

Appendix C Derivation of CSROD

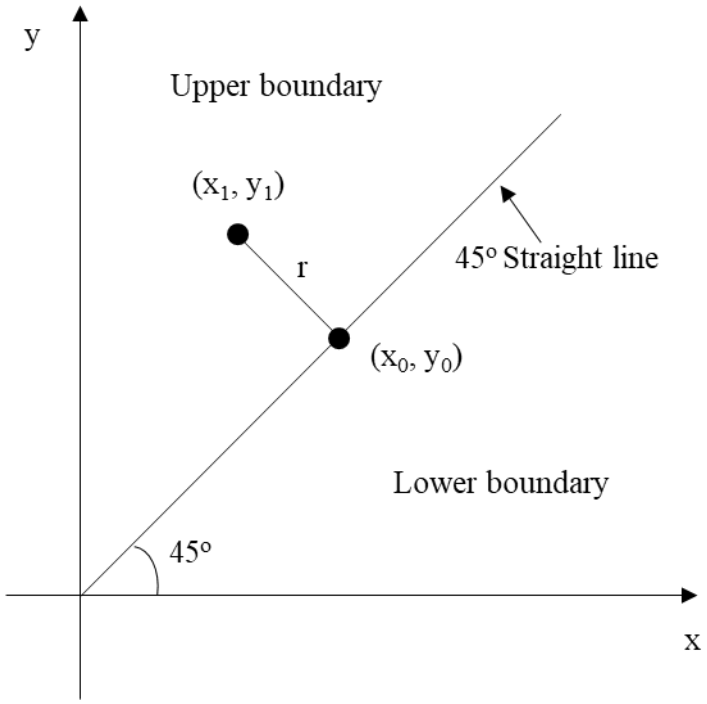

Fig C.1 The distance between the left and right gait data and the 45° symmetry straight line on a Cyclogram.

The line formed using points from (x_0, y_0) to (x_1, y_1) has a straight-line equation:

$$Y = MX + C \tag{C.2}$$

To determine the slope of *M*, we must first find the slope of the 45° symmetry straight line, M_{45}.

$$M_{45} = \tan(45) = 1 \tag{C.3}$$

The straight line from Eqn (C.2) is perpendicular to 45° symmetry straight line. Therefore, we can determine *M* by taking the negative reciprocal of M_{45}.

$$M = -\frac{1}{M_{45}} = -1 \tag{C.4}$$

To determine the intercept *C*, simply substitute (x_1, y_1):

$$\begin{aligned} y_1 &= -x_1 + C \\ C &= y_1 + x_1 \end{aligned} \tag{C.5}$$

Therefore, the equation of straight-line (x_0, y_0) to (x_1, y_1) is

$$Y = -X + y_1 + x_1 \tag{C.6}$$

On the 45° symmetry straight line, $x_0 = y_0$. Substitute them into Eqn (C.6) and we will obtain x_0 and y_0 points in term of x_1 and y_1:

$$\begin{aligned} y_0 &= -x_0 + y_1 + x_1 \\ 2x_0 &= y_1 + x_1 \\ x_0 &= \frac{y_1 + x_1}{2} = y_0 \end{aligned} \tag{C.7}$$

To determine the perpendicular distance between the cyclogram trajectory and the 45° symmetry straight line, the distance of r is computed:

$$r = \sqrt{(x_1 - x_0)^2 + (y_1 - y_0)^2} \tag{C.8}$$

Substituting the x_0 and y_0 values into Eqn (C.8):

$$\begin{aligned} r &= \sqrt{\left(x_1 - \frac{y_1 + x_1}{2}\right)^2 + \left(y_1 - \frac{y_1 + x_1}{2}\right)^2} \\ r &= \sqrt{\left(x_1 - \left(\frac{y_1 + x_1}{2}\right)\right)^2 + \left(y_1 - \left(\frac{y_1 + x_1}{2}\right)\right)^2} \\ r &= \frac{1}{\sqrt{2}}\sqrt{{x_1}^2 - 2x_1y_1 + {y_1}^2} \\ r &= \frac{1}{\sqrt{2}}\sqrt{(x_1 - y_1)^2} \end{aligned} \tag{C.9}$$

And therefore

$$r = |x_1 - y_1|\sin(45°) \tag{C.10}$$

For those points lying at upper boundary $(X < Y)$ of the cyclogram, we define them as negative CSROD magnitude. For those points lying at lower boundary $(Y < X)$ of the cyclogram, we define them as positive CSROD magnitude. Therefore, it leads to final CSROD equation:

$$CSROD = \begin{cases} |\mathrm{X} - \mathrm{Y}| * \sin(45°), & Y < X \\ -|\mathrm{X} - \mathrm{Y}| * \sin(45°), & X < Y \end{cases} \tag{C.11}$$

Since the cyclogram is plotted using the joint angle from unaffected lower limb against affected lower limbs, the points on upper boundary indicates a bigger angle magnitude on unaffected lower limb (since $X < Y$), and vice versa for those points lying at lower boundary. Therefore, a negative CSROD value indicates asymmetry on joint angle due to smaller magnitude of angle on affected lower limb and vice versa.

Appendix D Decomposed sEMG from 15 stroke patients

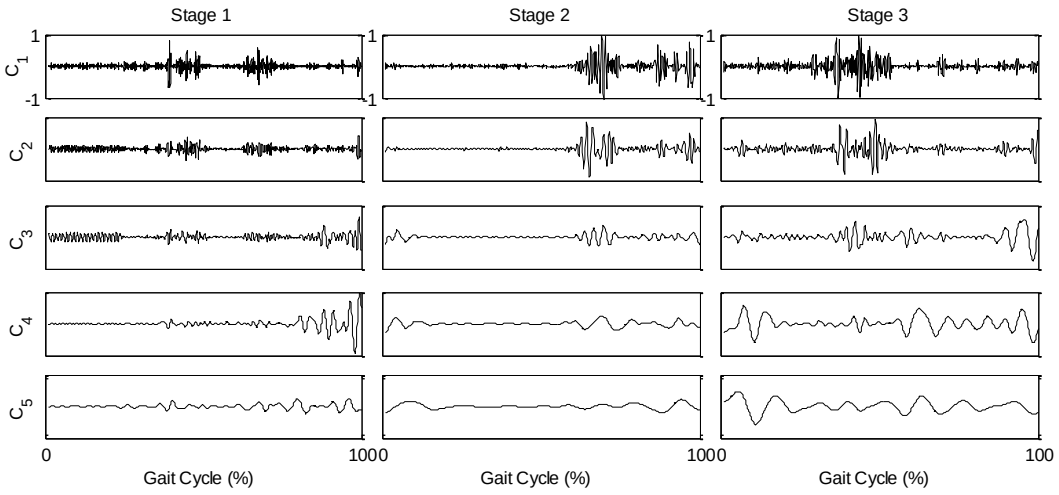

(a)

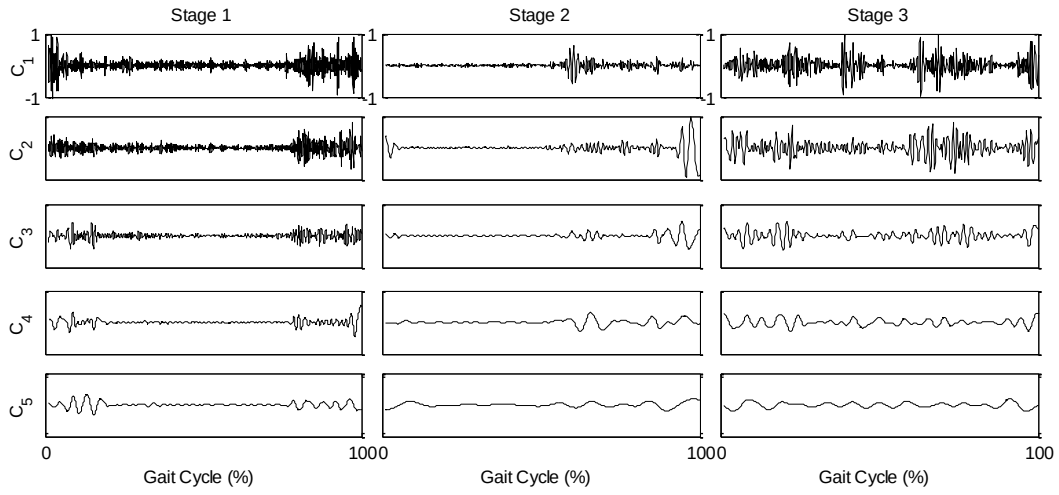

(b)

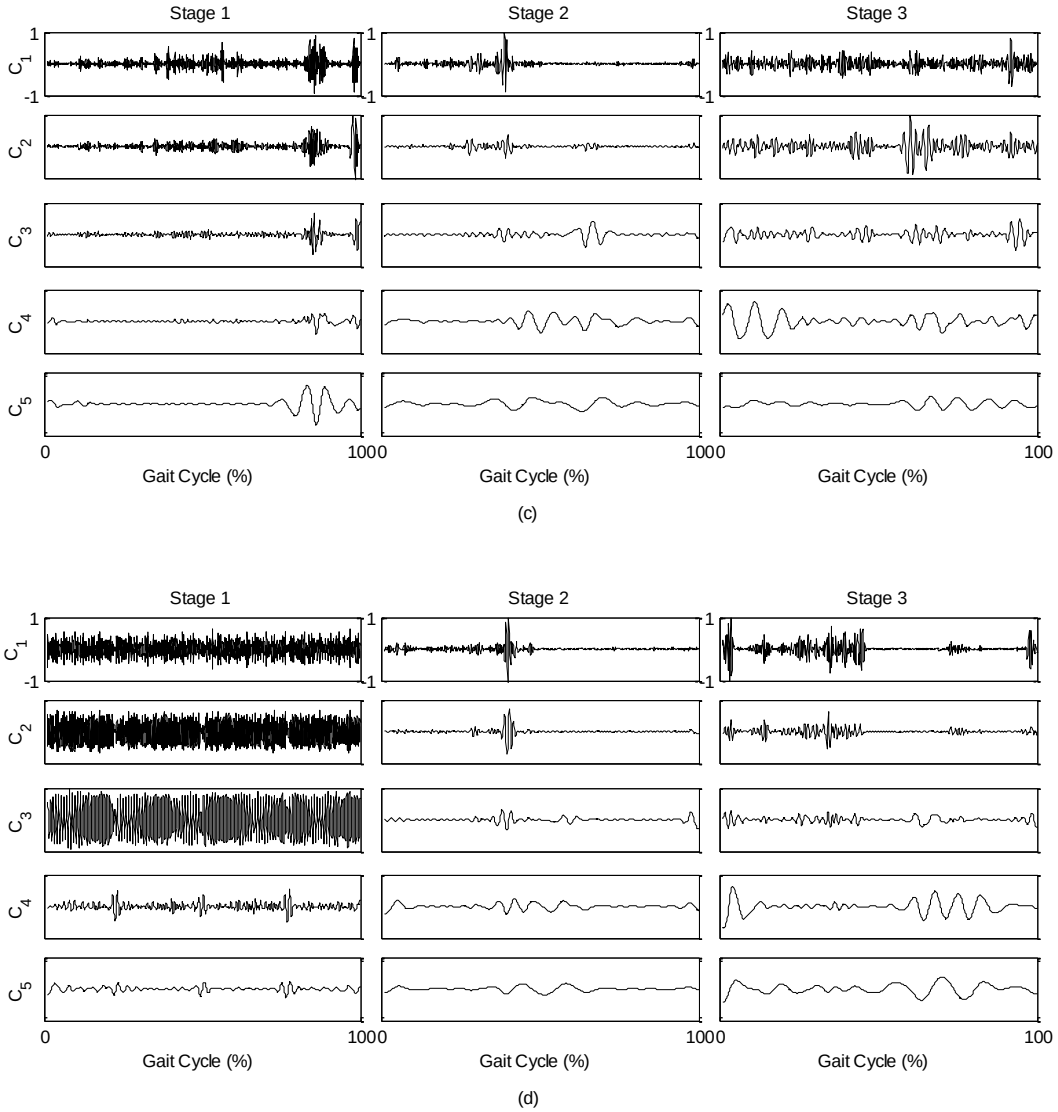

Fig D.1. Stage 1, stage 2 and stage 3 IMFs from decomposition of gait sEMG from subject 1, (a) GL left muscle, (b) GL right muscle, (c) TA left muscle, (d) TA right muscle.

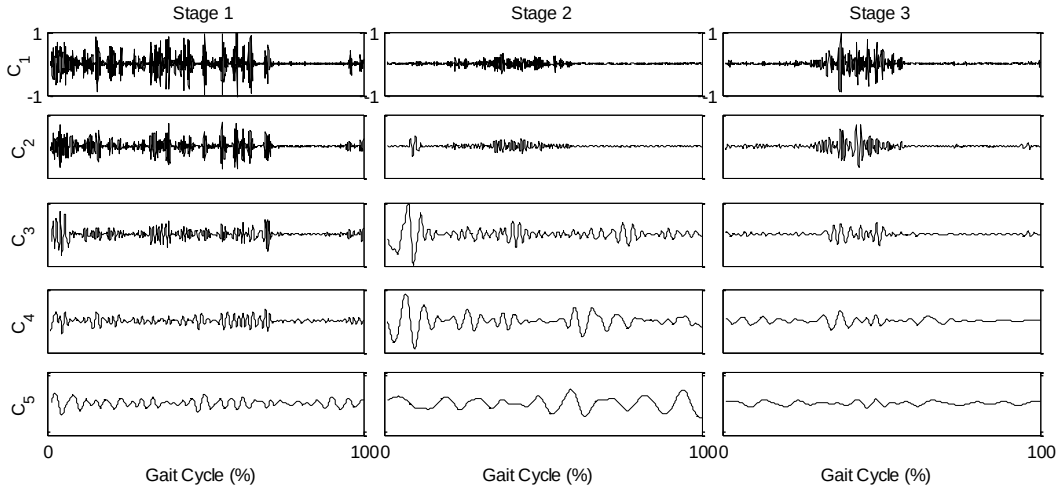
Stage 1
Stage 2
Stage 3
C1
C2
C3
C4
C5
1
-1
0
1000
Gait Cycle (%)

(a)

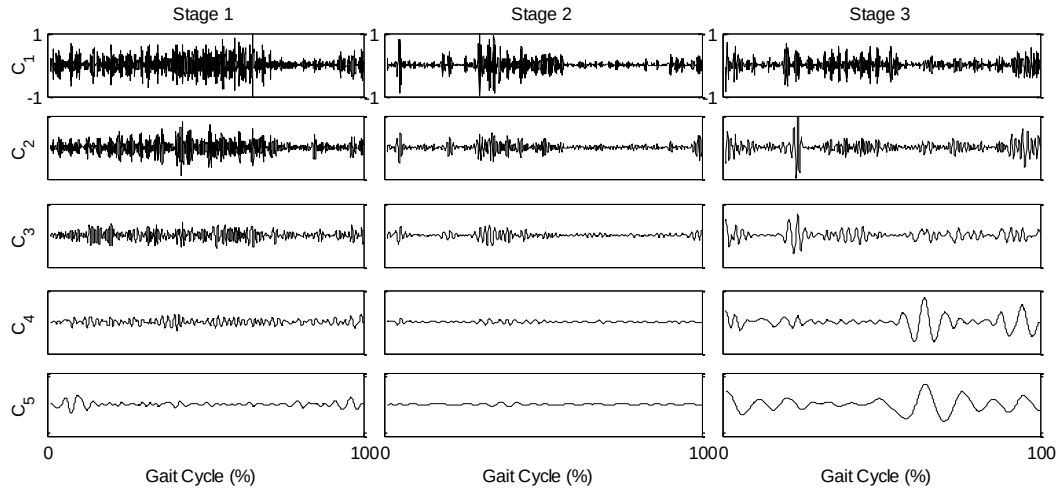
Stage 1
Stage 2
Stage 3
C1
C2
C3
C4
C5
1
-1
0
1000
Gait Cycle (%)

(b)

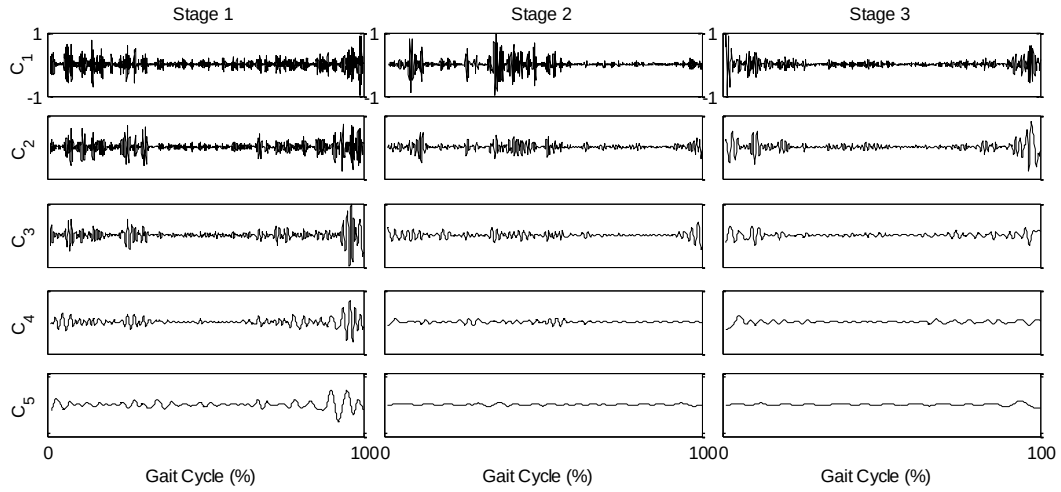
Stage 1
Stage 2
Stage 3
C1
C2
C3
C4
C5
1
-1
0
1000
Gait Cycle (%)

(c)

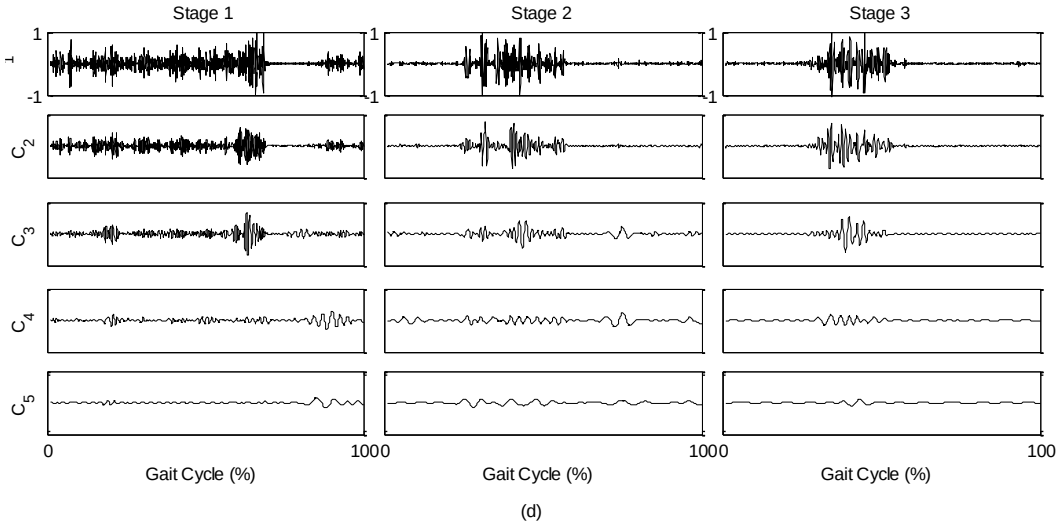

Fig D.2. Stage 1, stage 2 and stage 3 IMFs from decomposition of gait sEMG from subject 2, (a) GL left muscle, (b) GL right muscle, (c) TA left muscle, (d) TA right muscle.

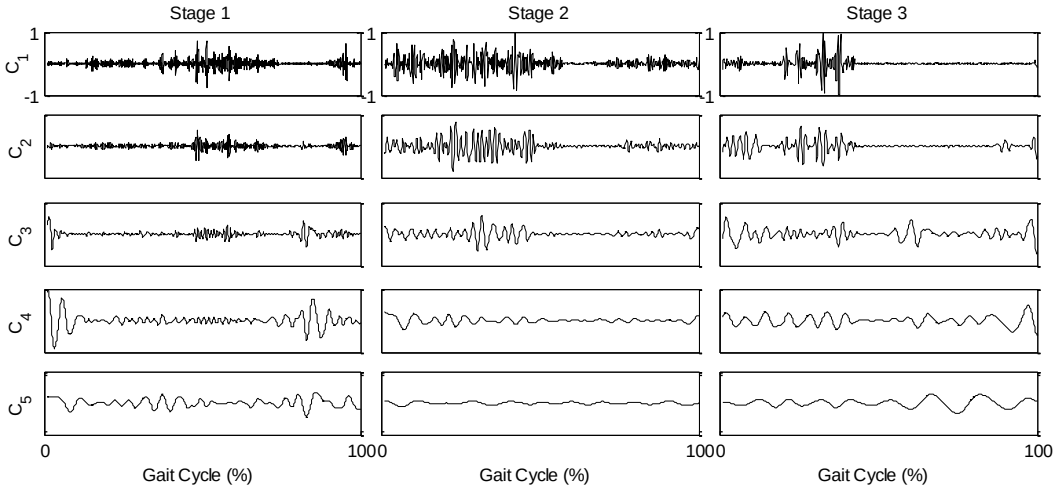
Stage 1
Stage 2
Stage 3
c1
c2
c3
c4
c5
1
-1
0
1000
100
Gait Cycle (%)

(a)

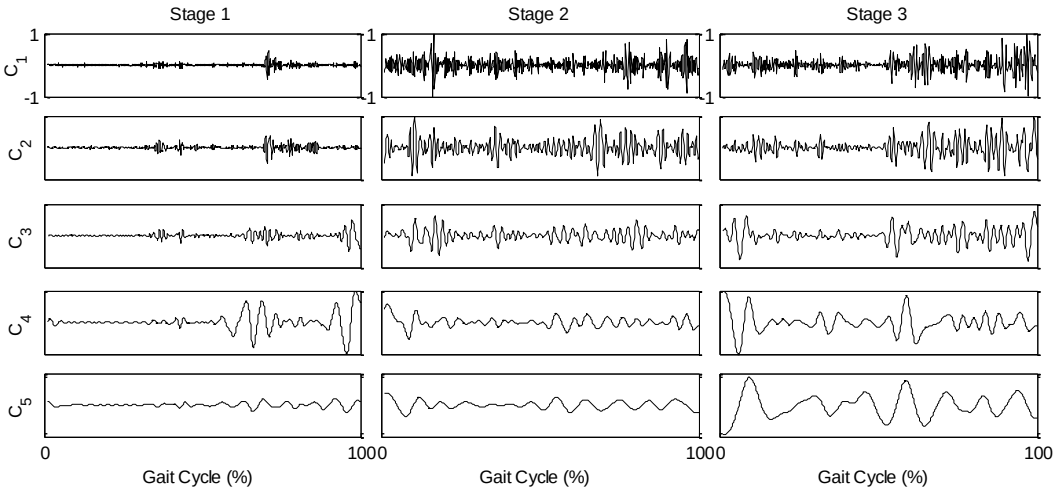
Stage 1
Stage 2
Stage 3
c1
c2
c3
c4
c5
1
-1
0
1000
100
Gait Cycle (%)

(b)

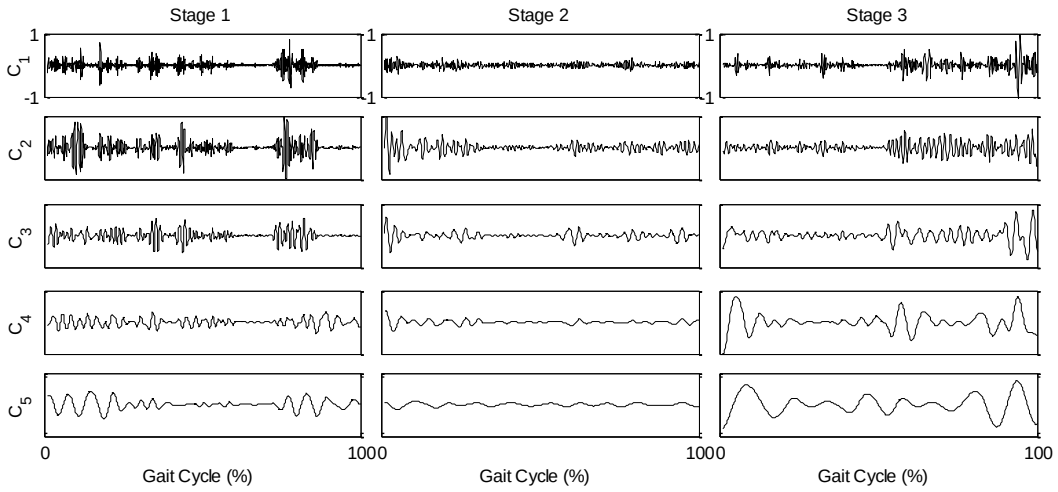
Stage 1
Stage 2
Stage 3
c1
c2
c3
c4
c5
1
-1
0
1000
100
Gait Cycle (%)

(c)

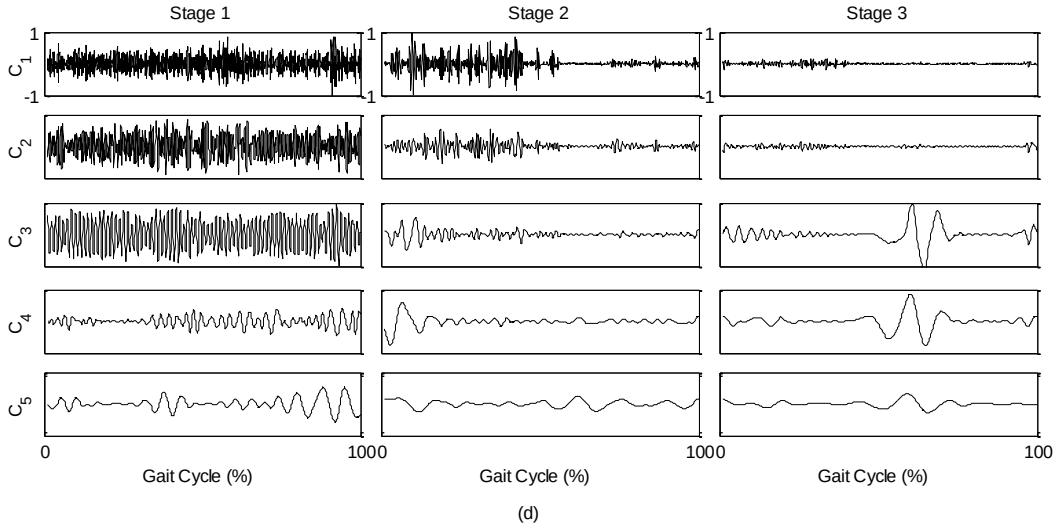

Fig D.3. Stage 1, stage 2 and stage 3 IMFs from decomposition of gait sEMG from subject 3, (a) GL left muscle, (b) GL right muscle, (c) TA left muscle, (d) TA right muscle.

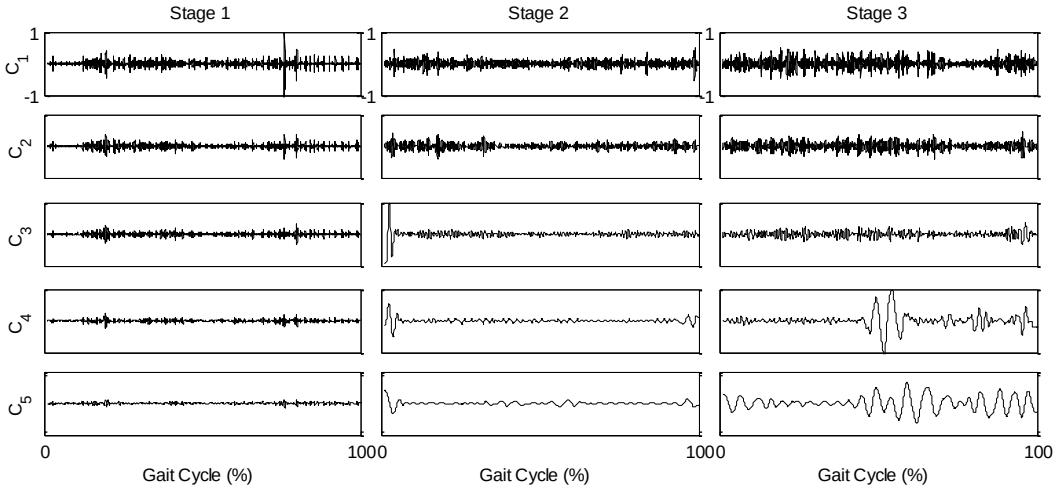
Stage 1
Stage 2
Stage 3
C1
C2
C3
C4
C5
1
-1
0
1000
100
Gait Cycle (%)

(a)

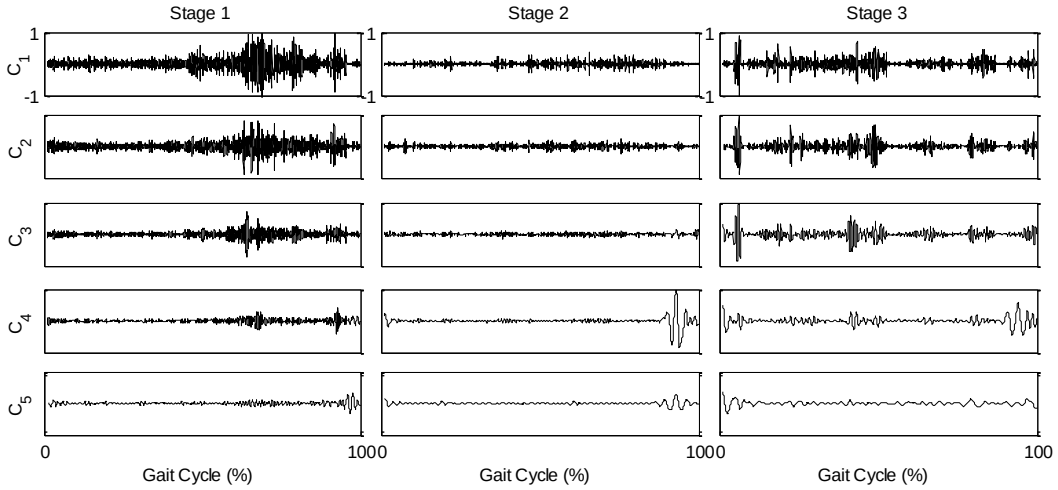
Stage 1
Stage 2
Stage 3
C1
C2
C3
C4
C5
1
-1
0
1000
100
Gait Cycle (%)

(b)

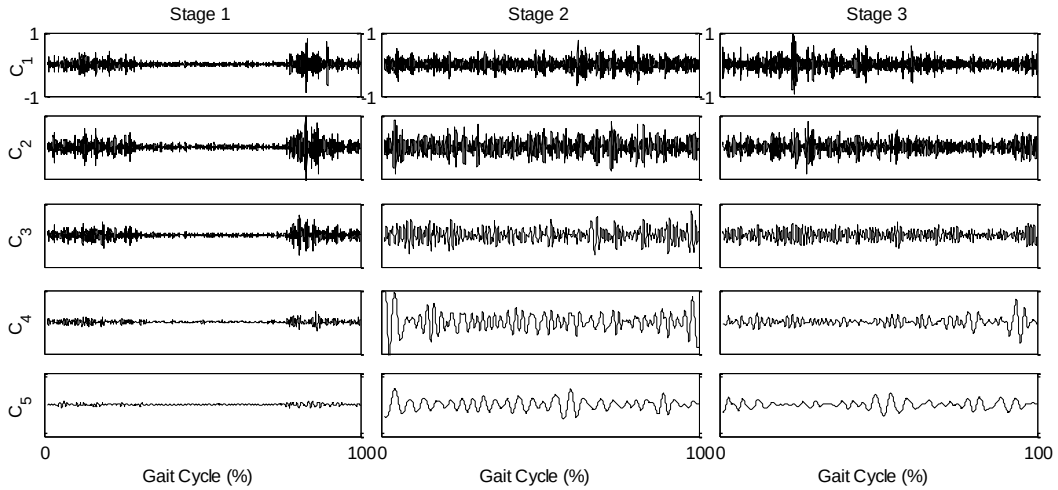
Stage 1
Stage 2
Stage 3
C1
C2
C3
C4
C5
1
-1
0
1000
100
Gait Cycle (%)

(c)

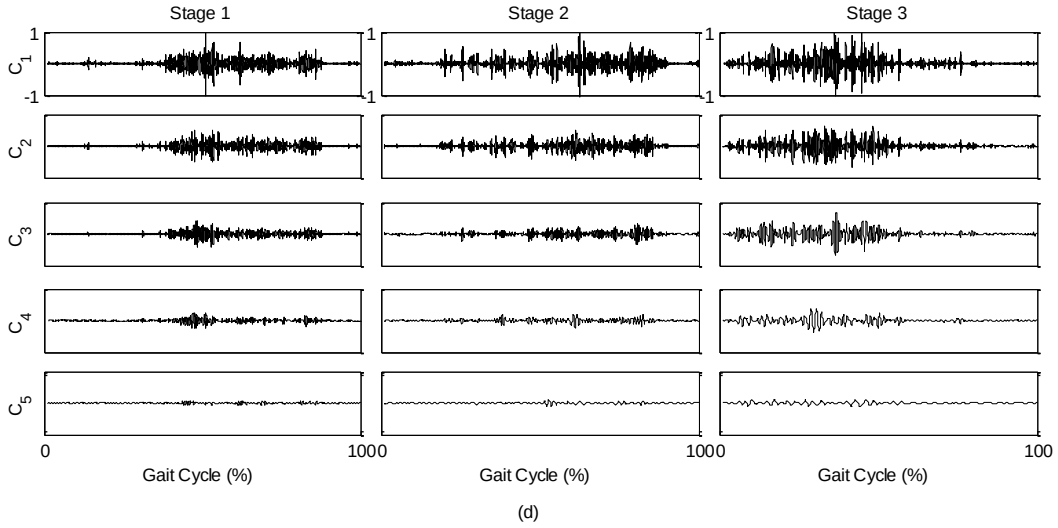

Fig D.4. Stage 1, stage 2 and stage 3 IMFs from decomposition of gait sEMG from subject 4, (a) GL left muscle, (b) GL right muscle, (c) TA left muscle, (d) TA right muscle.

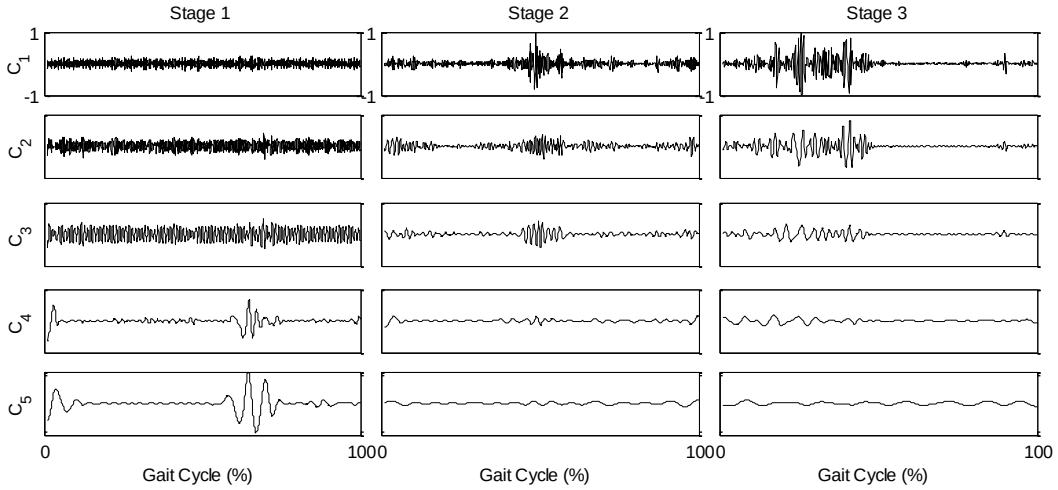
Stage 1
Stage 2
Stage 3
c1
c2
c3
c4
c5
1
-1
0
1000
100
Gait Cycle (%)

(a)

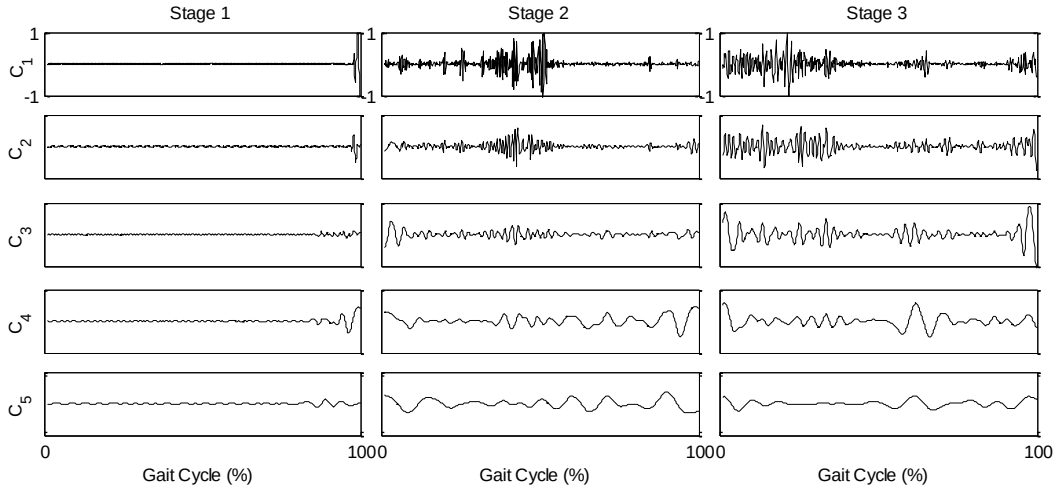
Stage 1
Stage 2
Stage 3
c1
c2
c3
c4
c5
1
-1
0
1000
100
Gait Cycle (%)

(b)

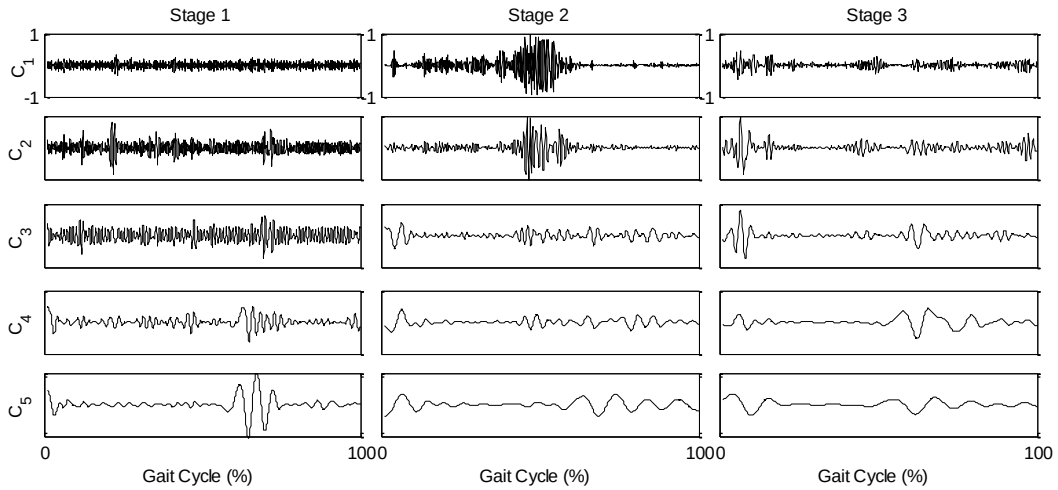
Stage 1
Stage 2
Stage 3
c1
c2
c3
c4
c5
1
-1
0
1000
100
Gait Cycle (%)

(c)

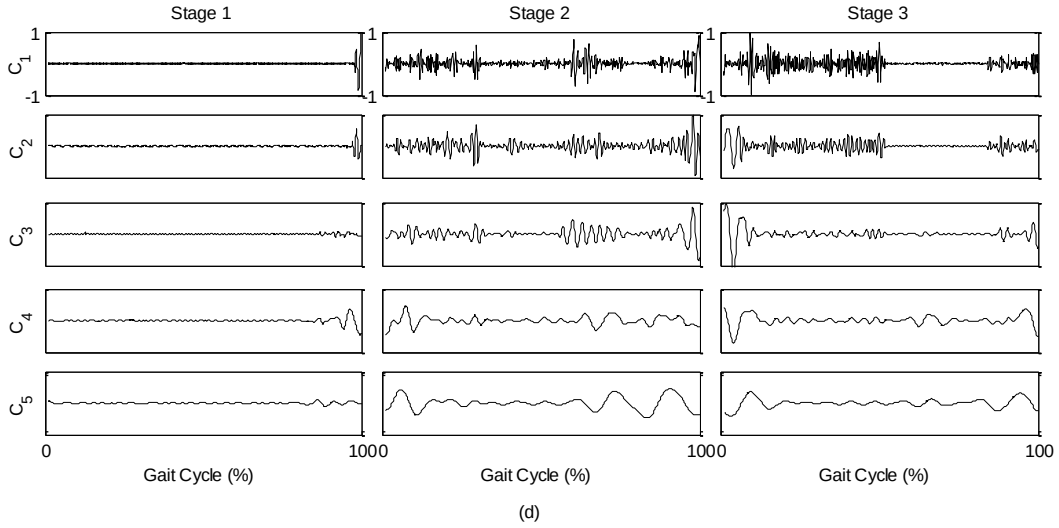

Fig D.5. Stage 1, stage 2 and stage 3 IMFs from decomposition of gait sEMG from subject 5, (a) GL left muscle, (b) GL right muscle, (c) TA left muscle, (d) TA right muscle.

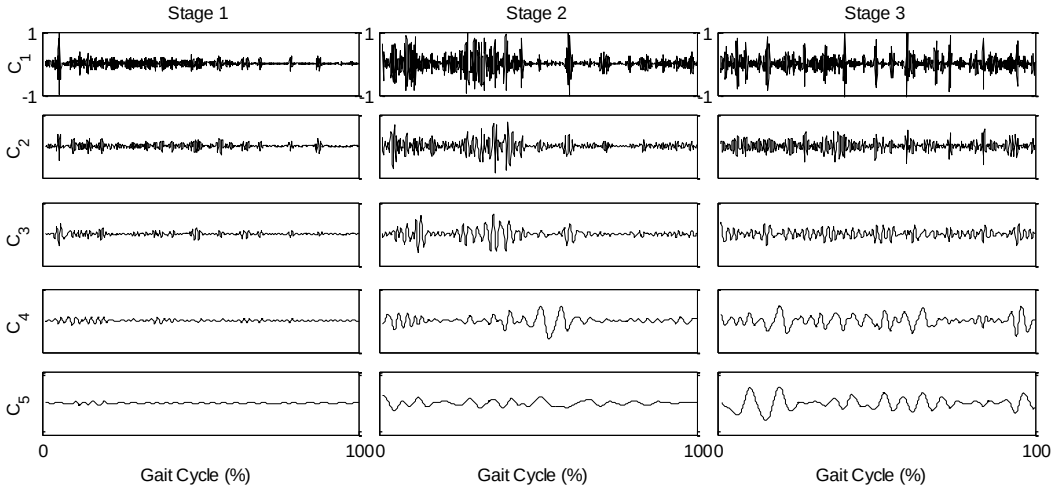
Stage 1
Stage 2
Stage 3
C1
C2
C3
C4
C5
1
-1
0
1000
Gait Cycle (%)

(a)

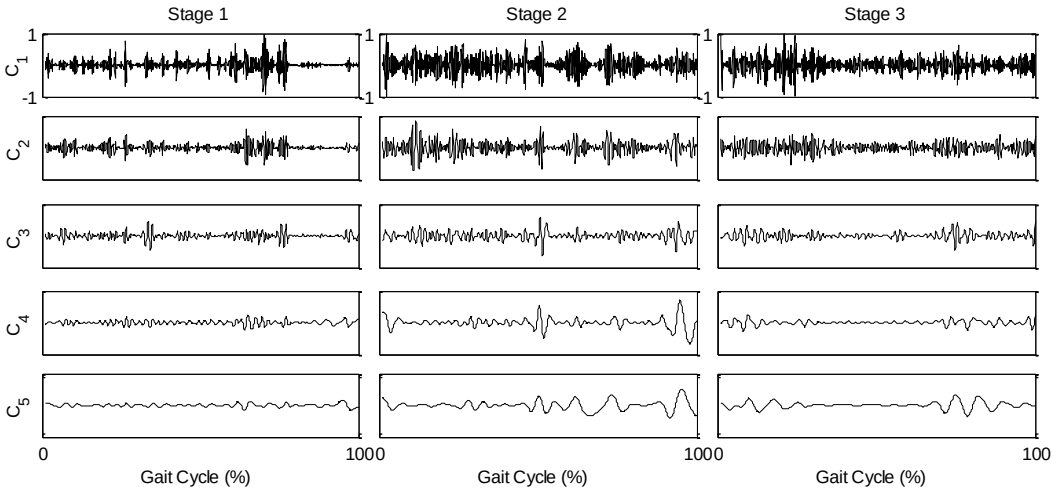
Stage 1
Stage 2
Stage 3
C1
C2
C3
C4
C5
1
-1
0
1000
Gait Cycle (%)

(b)

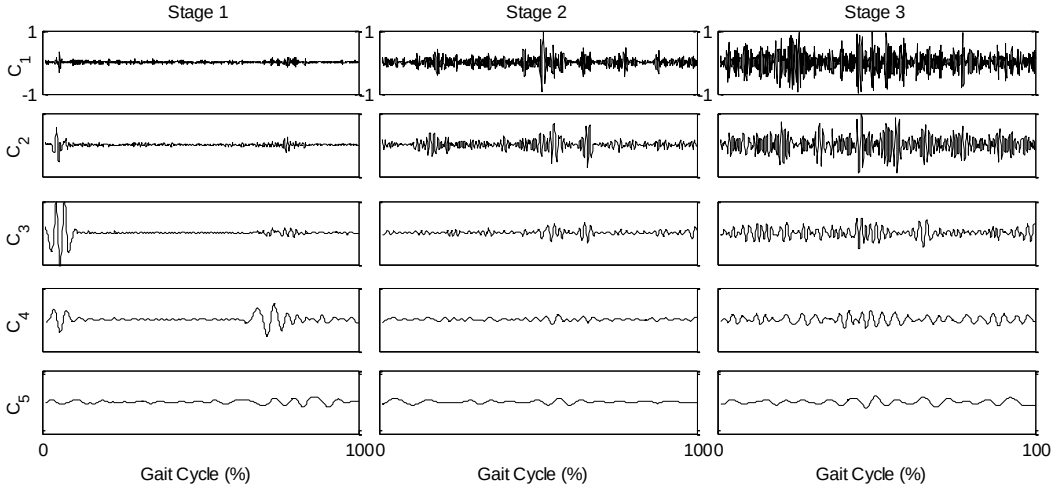
Stage 1
Stage 2
Stage 3
C1
C2
C3
C4
C5
1
-1
0
1000
Gait Cycle (%)

(c)

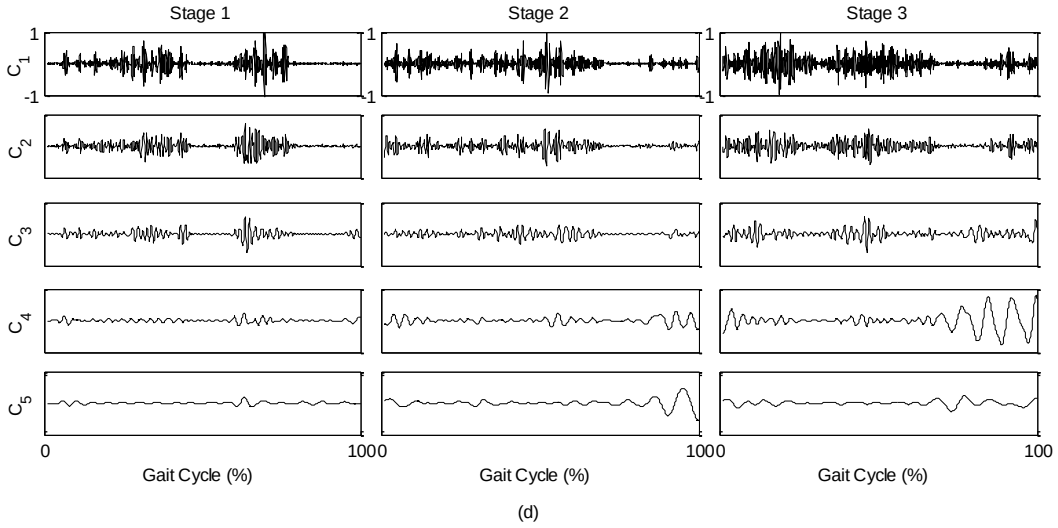

Fig D.6. Stage 1, stage 2 and stage 3 IMFs from decomposition of gait sEMG from subject 6, (a) GL left muscle, (b) GL right muscle, (c) TA left muscle, (d) TA right muscle.

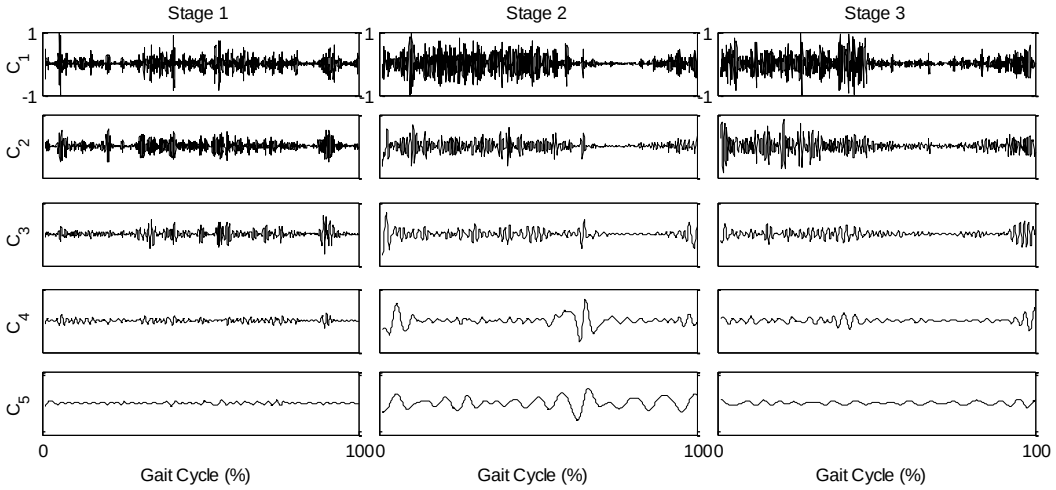
Stage 1
Stage 2
Stage 3
C1
C2
C3
C4
C5
1
-1
0
1000
100
Gait Cycle (%)

(a)

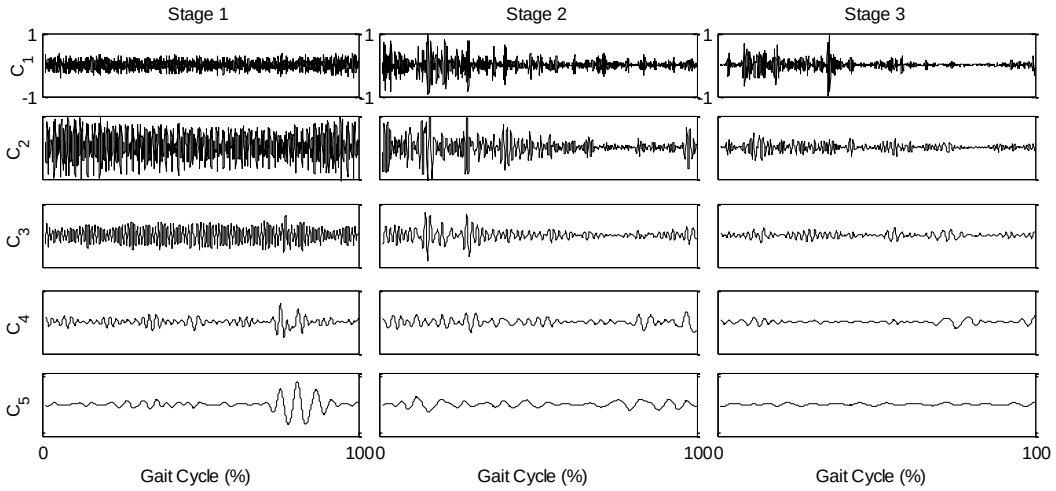
Stage 1
Stage 2
Stage 3
C1
C2
C3
C4
C5
1
-1
0
1000
100
Gait Cycle (%)

(b)

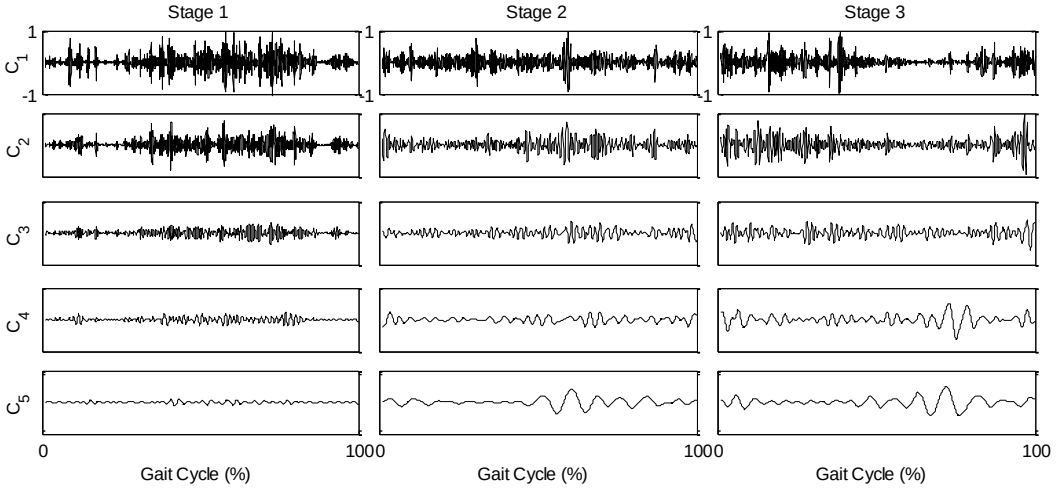
Stage 1
Stage 2
Stage 3
C1
C2
C3
C4
C5
1
-1
0
1000
100
Gait Cycle (%)

(c)

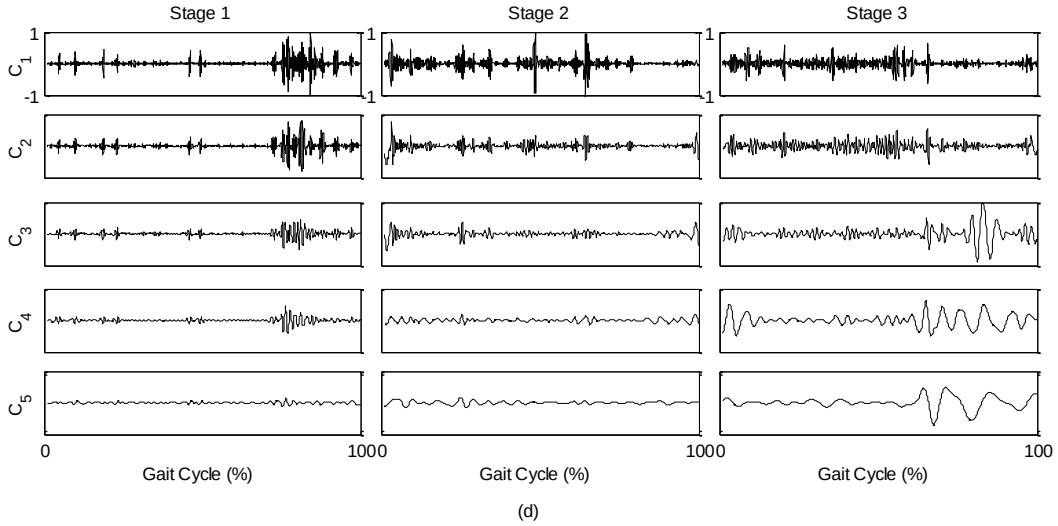

Fig D.7. Stage 1, stage 2 and stage 3 IMFs from decomposition of gait sEMG from subject 7, (a) GL left muscle, (b) GL right muscle, (c) TA left muscle, (d) TA right muscle.

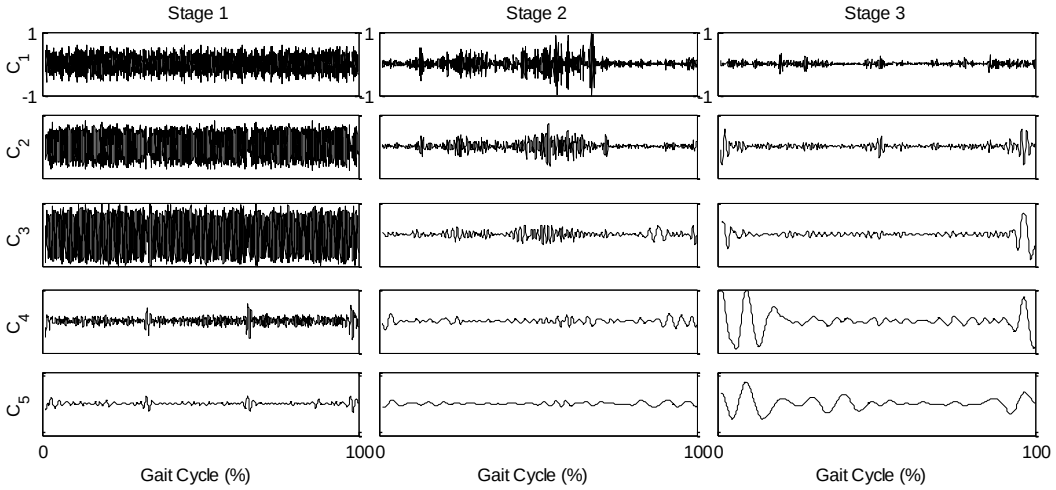
Stage 1
Stage 2
Stage 3
C1
C2
C3
C4
C5
1
-1
0
1000
100
Gait Cycle (%)

(a)

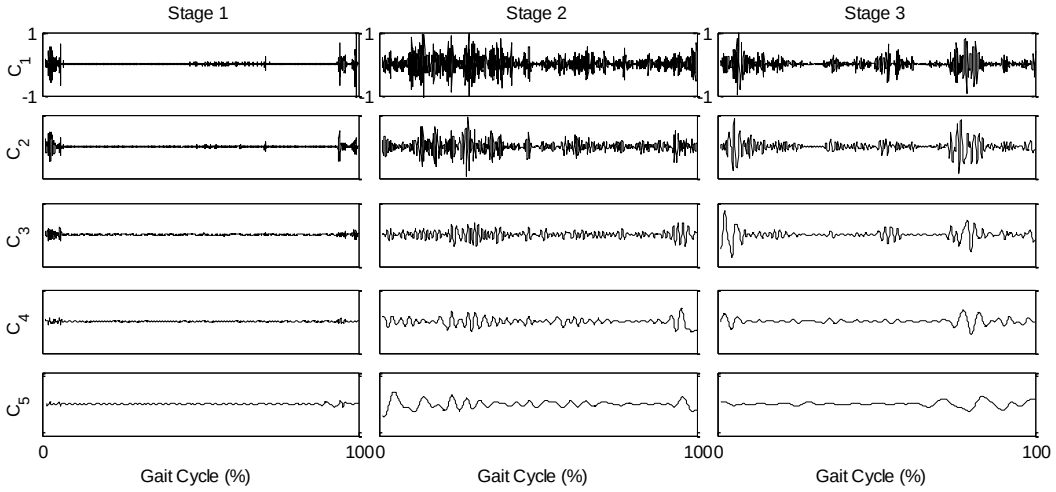
Stage 1
Stage 2
Stage 3
C1
C2
C3
C4
C5
1
-1
0
1000
100
Gait Cycle (%)

(b)

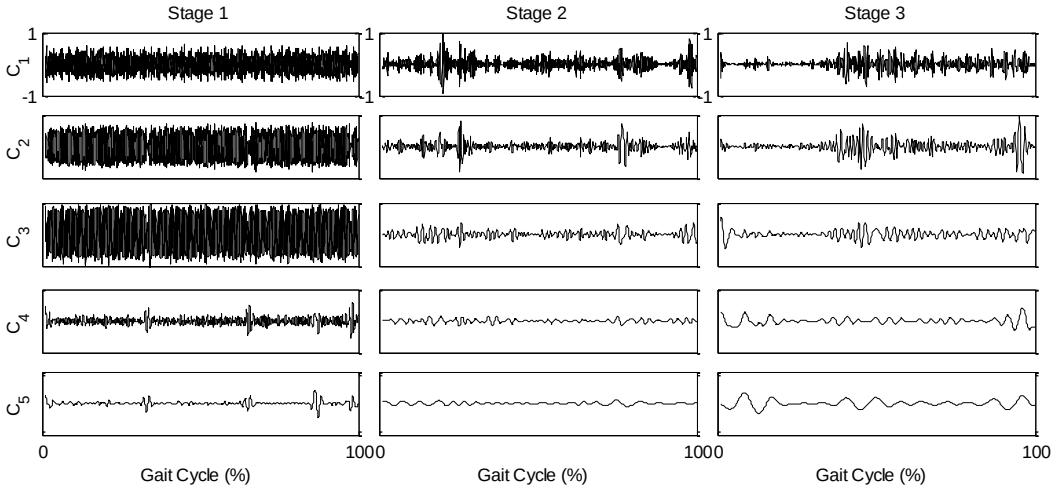
Stage 1
Stage 2
Stage 3
C1
C2
C3
C4
C5
1
-1
0
1000
100
Gait Cycle (%)

(c)

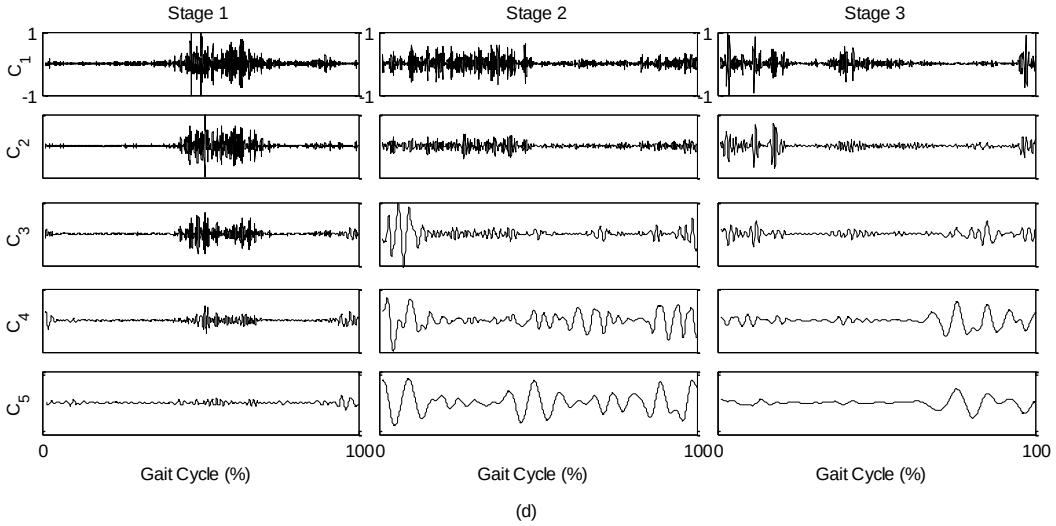

Fig D.8. Stage 1, stage 2 and stage 3 IMFs from decomposition of gait sEMG from subject 8, (a) GL left muscle, (b) GL right muscle, (c) TA left muscle, (d) TA right muscle.

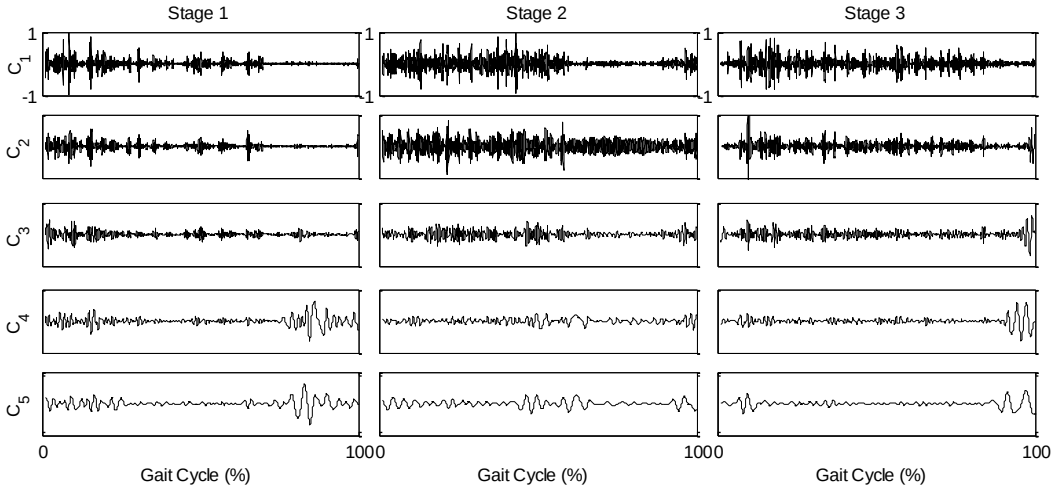
Stage 1
Stage 2
Stage 3
C1
C2
C3
C4
C5
1
-1
0
1000
100
Gait Cycle (%)

(a)

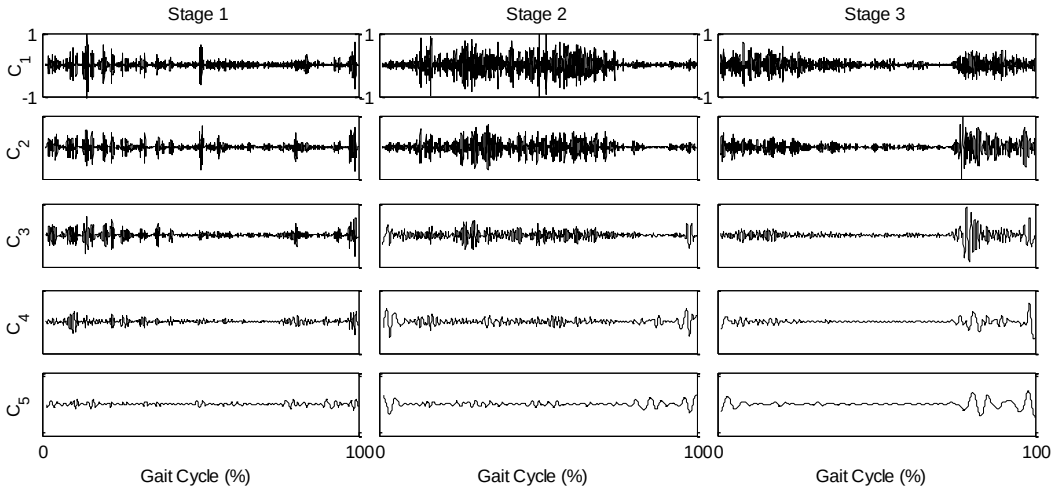
Stage 1
Stage 2
Stage 3
C1
C2
C3
C4
C5
1
-1
0
1000
100
Gait Cycle (%)

(b)

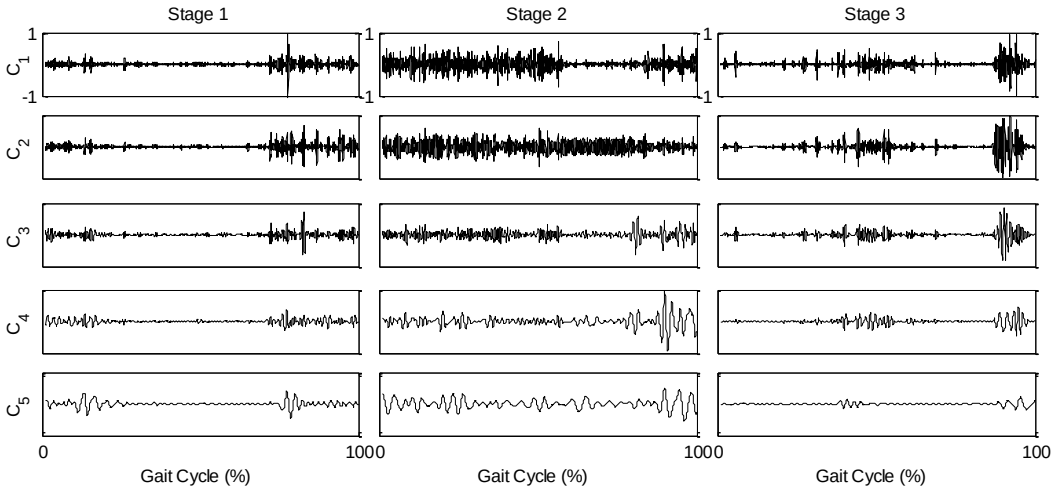
Stage 1
Stage 2
Stage 3
C1
C2
C3
C4
C5
1
-1
0
1000
100
Gait Cycle (%)

(c)

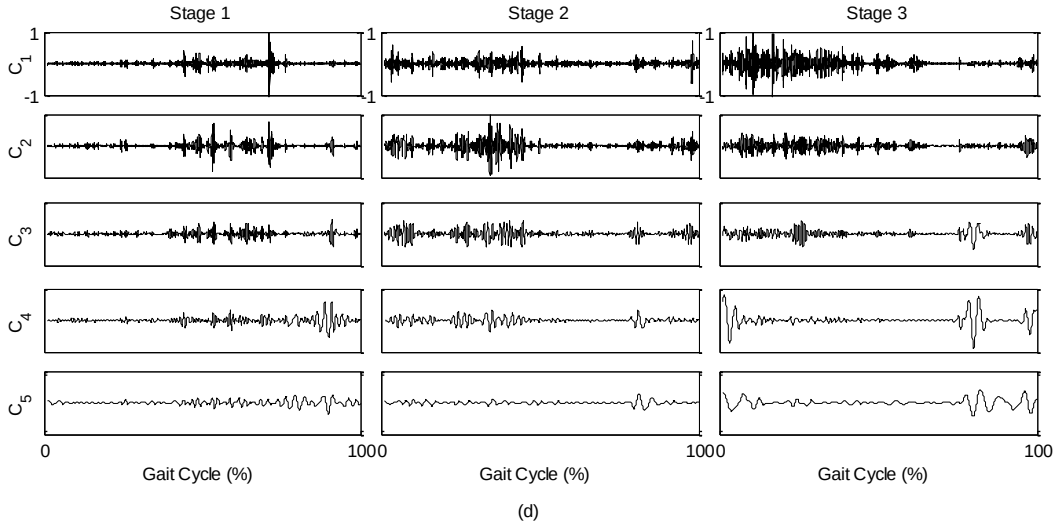

Fig D.9. Stage 1, stage 2 and stage 3 IMFs from decomposition of gait sEMG from subject 9, (a) GL left muscle, (b) GL right muscle, (c) TA left muscle, (d) TA right muscle.

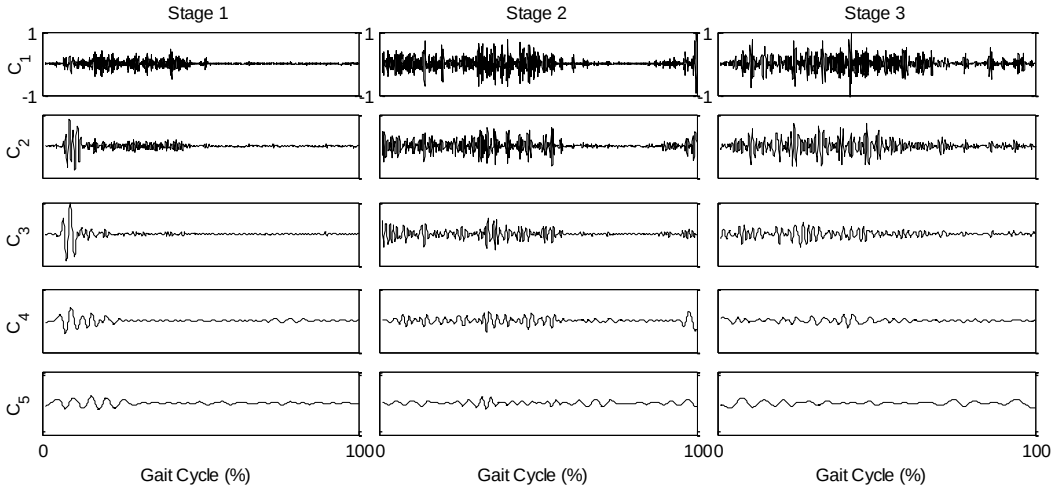
Stage 1
Stage 2
Stage 3
C1
C2
C3
C4
C5
1
-1
0
1000
100
Gait Cycle (%)

(a)

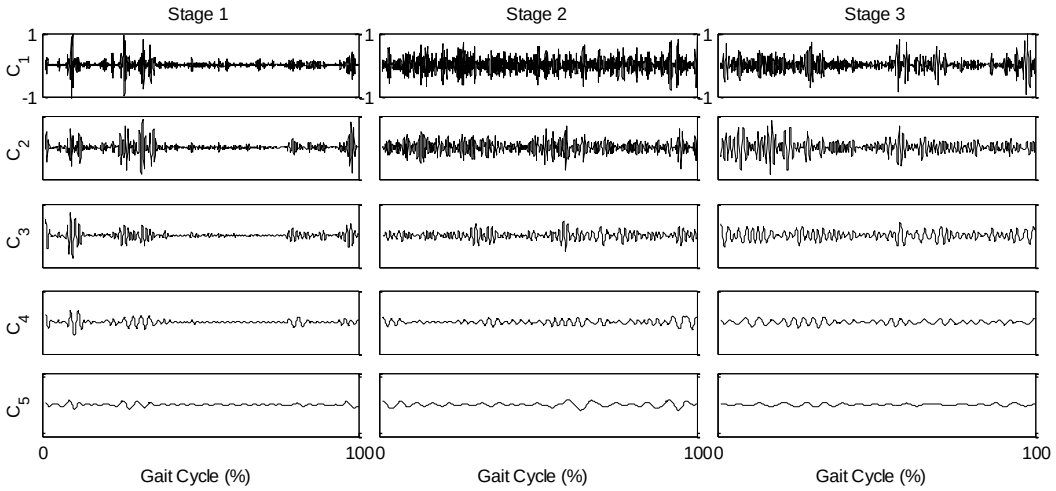
Stage 1
Stage 2
Stage 3
C1
C2
C3
C4
C5
1
-1
0
1000
100
Gait Cycle (%)

(b)

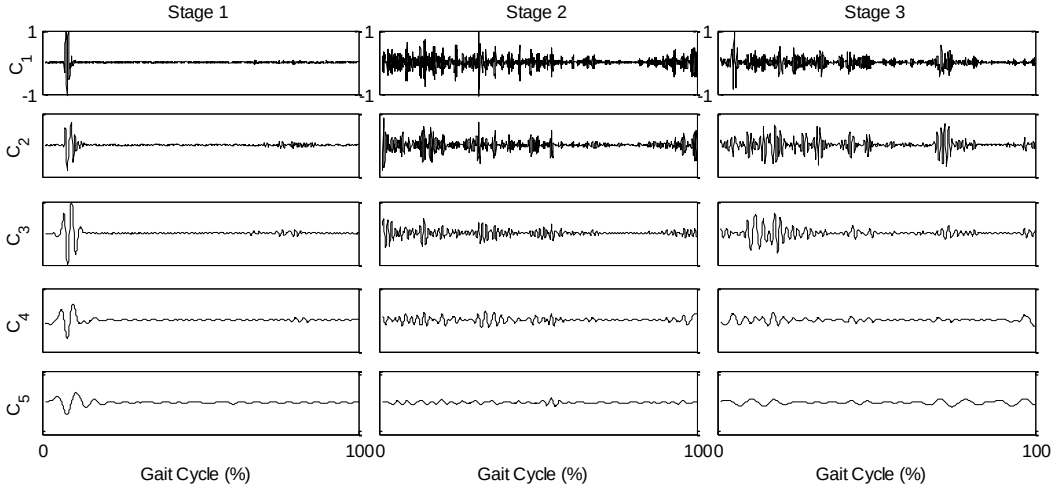
Stage 1
Stage 2
Stage 3
C1
C2
C3
C4
C5
1
-1
0
1000
100
Gait Cycle (%)

(c)

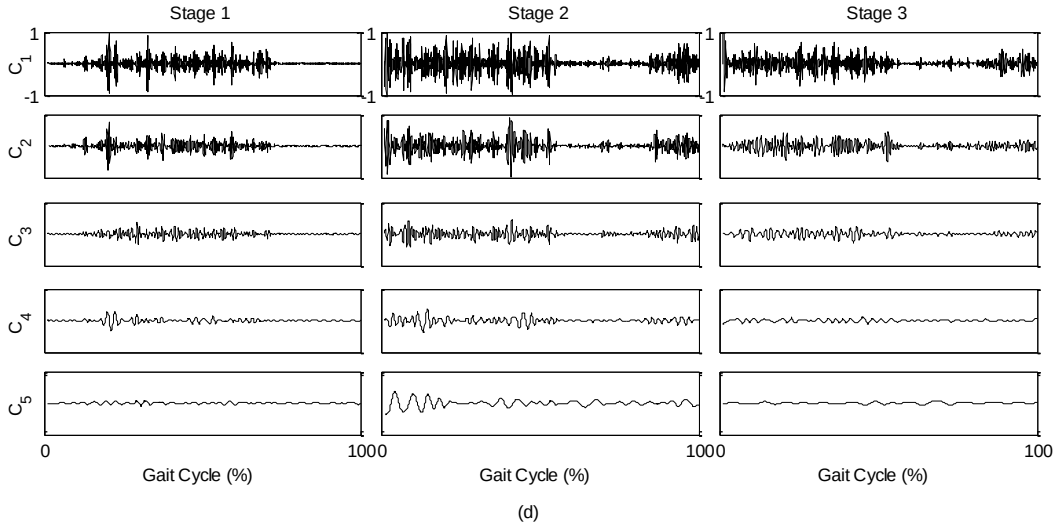

Fig D.10. Stage 1, stage 2 and stage 3 IMFs from decomposition of gait sEMG from subject 10, (a) GL left muscle, (b) GL right muscle, (c) TA left muscle, (d) TA right muscle.

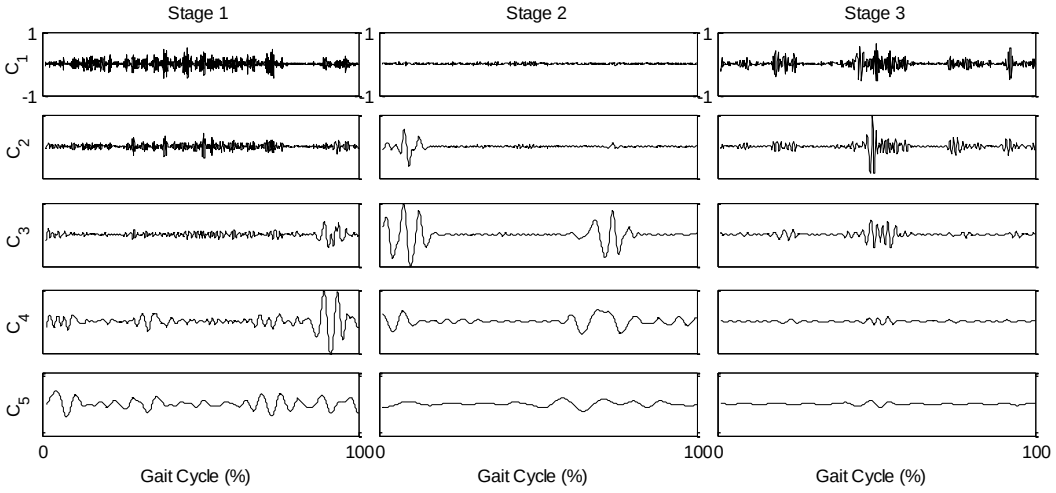
Stage 1
Stage 2
Stage 3
C1
C2
C3
C4
C5
1
-1
0
1000
100
Gait Cycle (%)

(a)

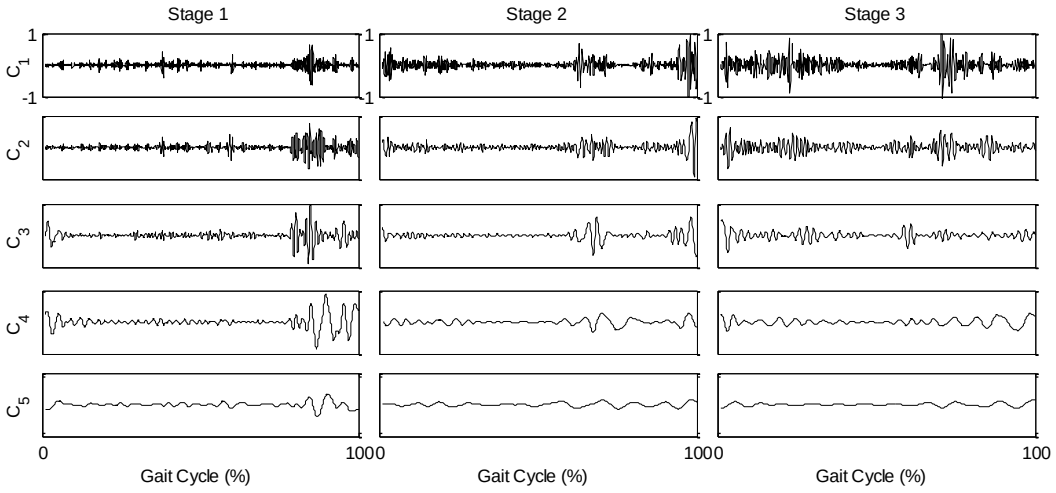
Stage 1
Stage 2
Stage 3
C1
C2
C3
C4
C5
1
-1
0
1000
100
Gait Cycle (%)

(b)

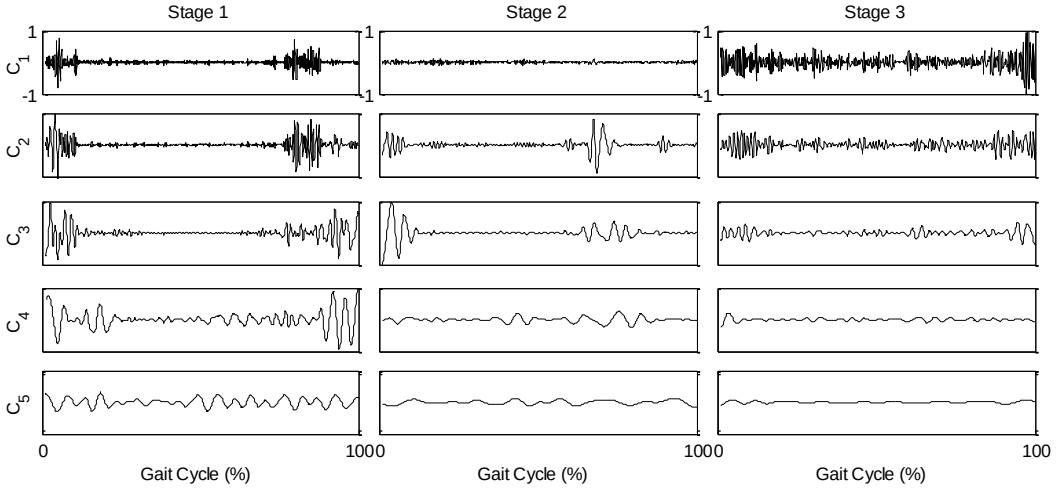
Stage 1
Stage 2
Stage 3
C1
C2
C3
C4
C5
1
-1
0
1000
100
Gait Cycle (%)

(c)

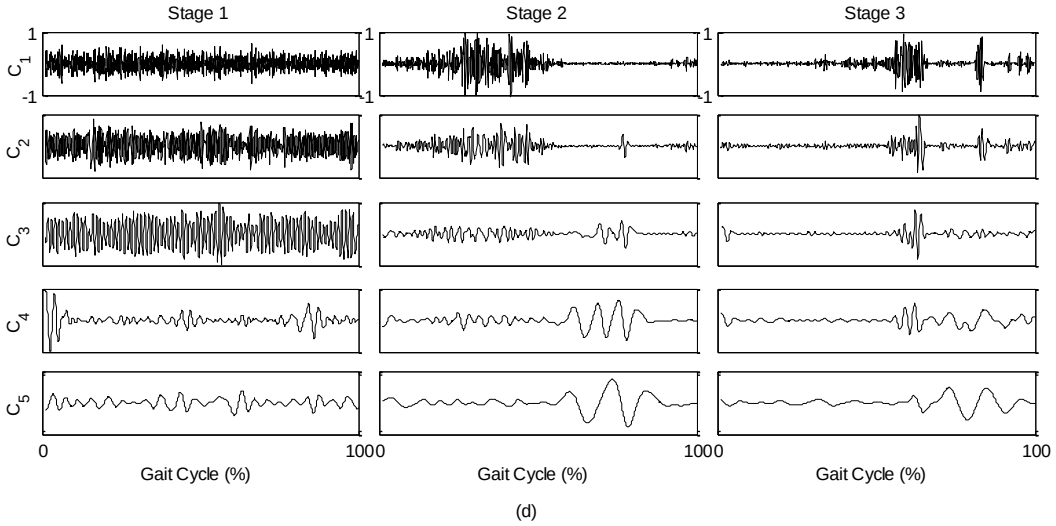

Fig D.11. Stage 1, stage 2 and stage 3 IMFs from decomposition of gait sEMG from subject 11, (a) GL left muscle, (b) GL right muscle, (c) TA left muscle, (d) TA right muscle.

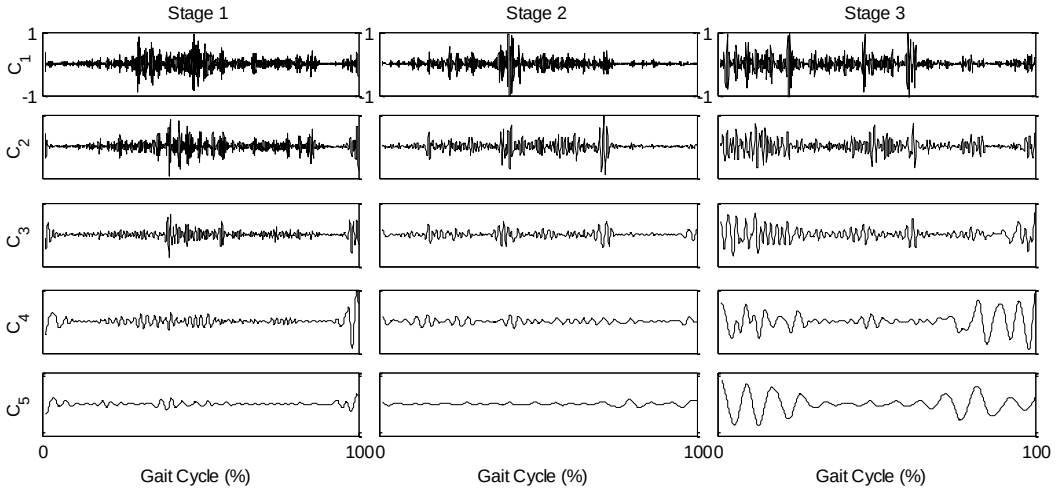
Stage 1
Stage 2
Stage 3
C1
C2
C3
C4
C5
1
-1
0
1000
Gait Cycle (%)

(a)

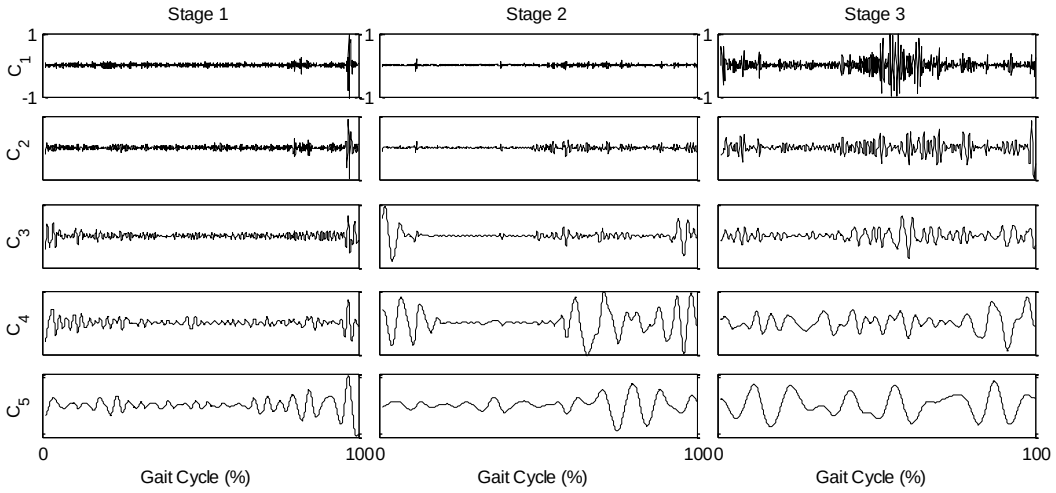
Stage 1
Stage 2
Stage 3
C1
C2
C3
C4
C5
1
-1
0
1000
Gait Cycle (%)

(b)

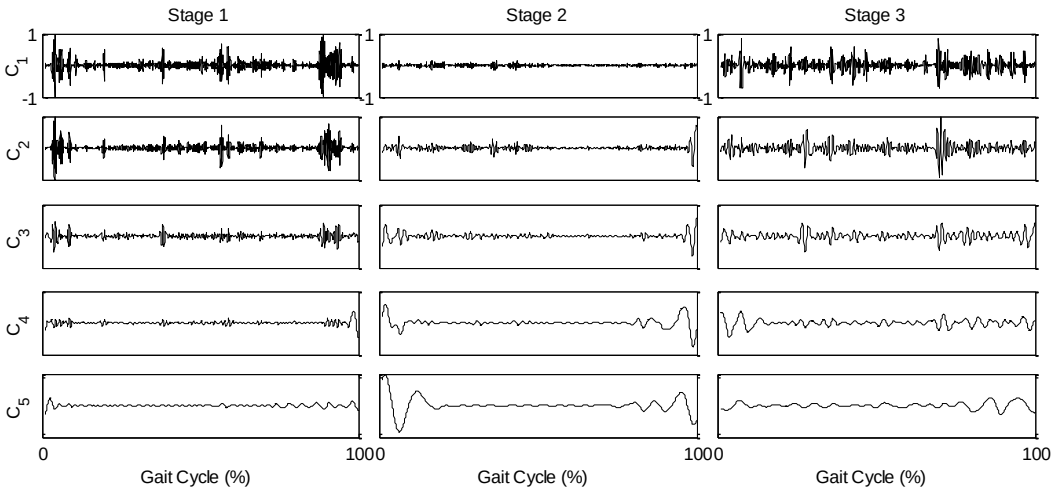
Stage 1
Stage 2
Stage 3
C1
C2
C3
C4
C5
1
-1
0
1000
Gait Cycle (%)

(c)

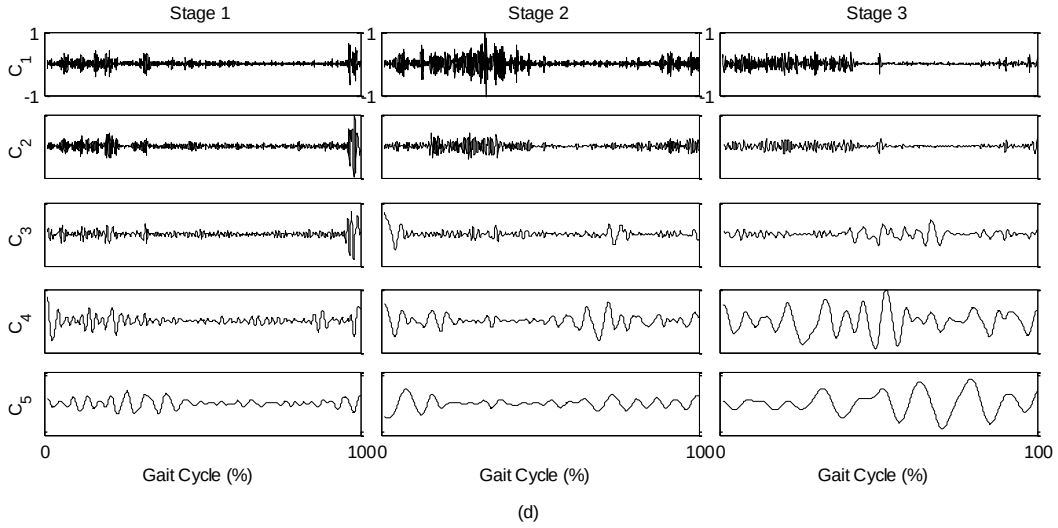

Fig D.12. Stage 1, stage 2 and stage 3 IMFs from decomposition of gait sEMG from subject 12, (a) GL left muscle, (b) GL right muscle, (c) TA left muscle, (d) TA right muscle.

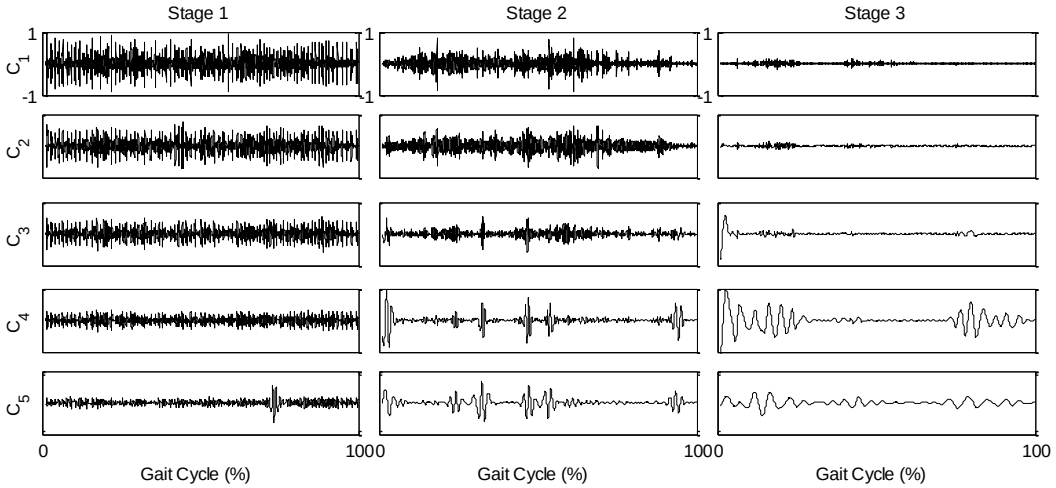
Stage 1
Stage 2
Stage 3
C1
C2
C3
C4
C5
1
-1
0
1000
Gait Cycle (%)

(a)

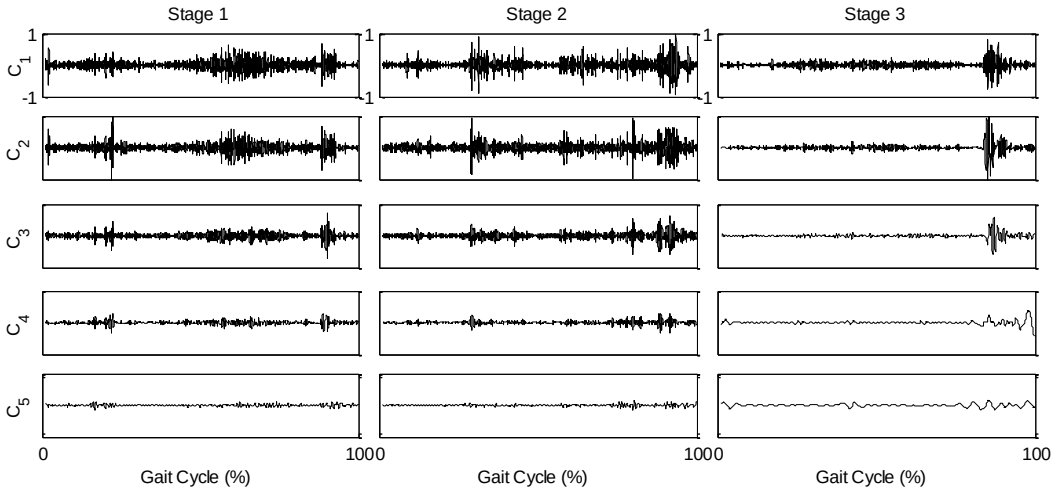
Stage 1
Stage 2
Stage 3
C1
C2
C3
C4
C5
1
-1
0
1000
Gait Cycle (%)

(b)

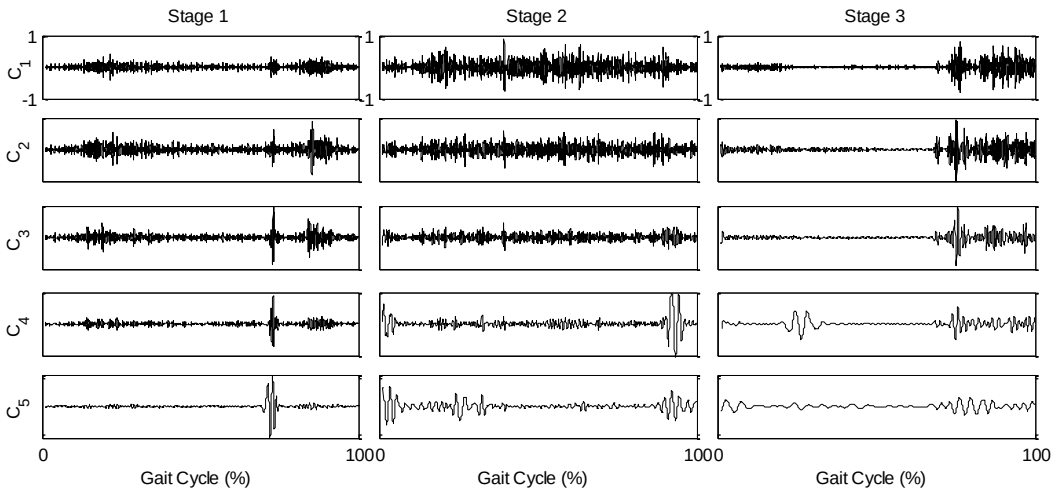
Stage 1
Stage 2
Stage 3
C1
C2
C3
C4
C5
1
-1
0
1000
Gait Cycle (%)

(c)

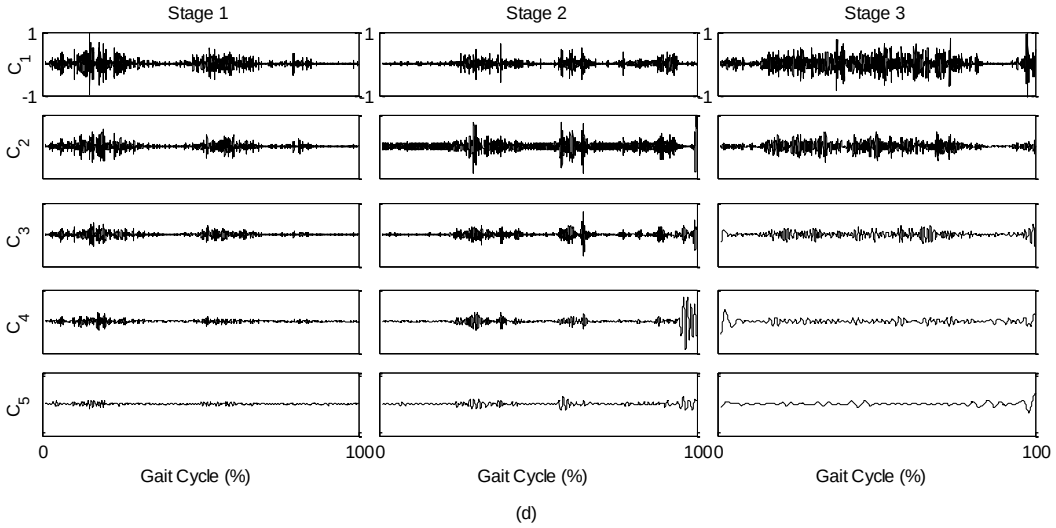

Fig D.13. Stage 1, stage 2 and stage 3 IMFs from decomposition of gait sEMG from subject 13, (a) GL left muscle, (b) GL right muscle, (c) TA left muscle, (d) TA right muscle.

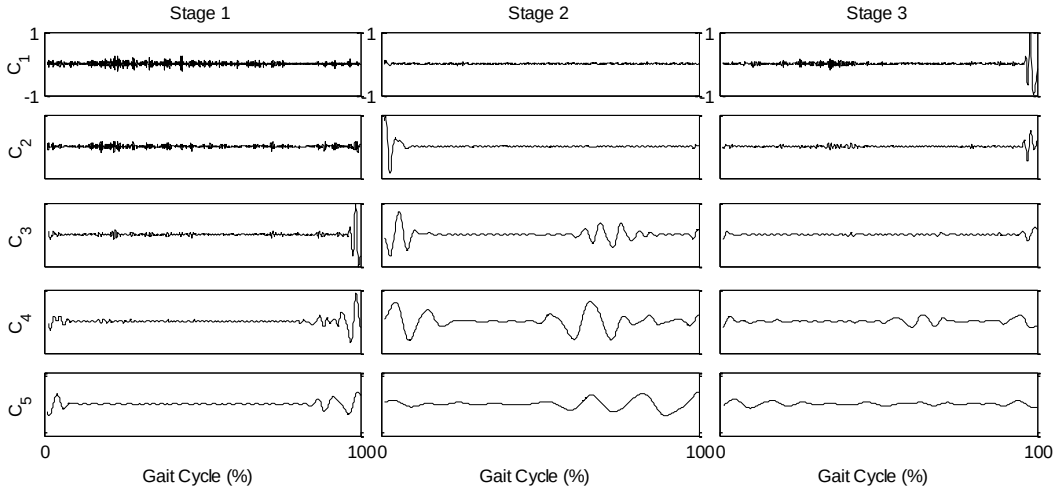
Stage 1
Stage 2
Stage 3
C1
C2
C3
C4
C5
1
-1
0
1000
100
Gait Cycle (%)

(a)

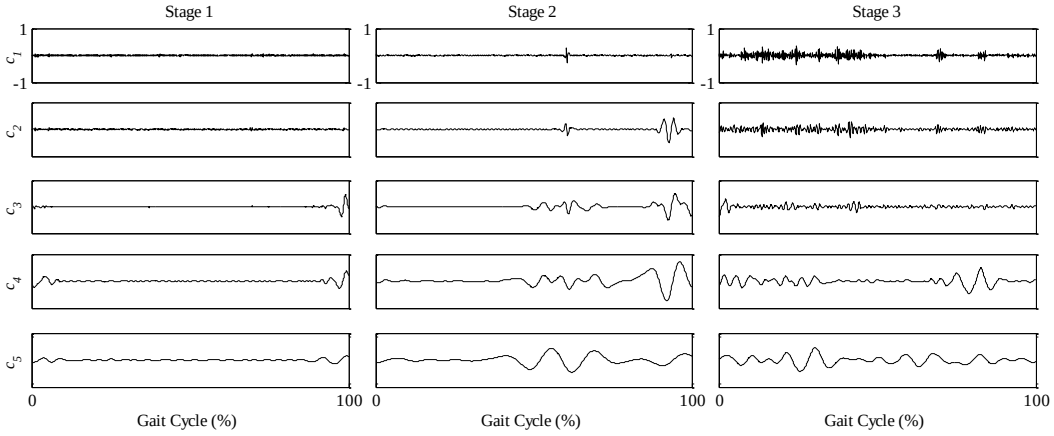
Stage 1
Stage 2
Stage 3
c1
c2
c3
c4
c5
1
-1
0
100
Gait Cycle (%)

(b)

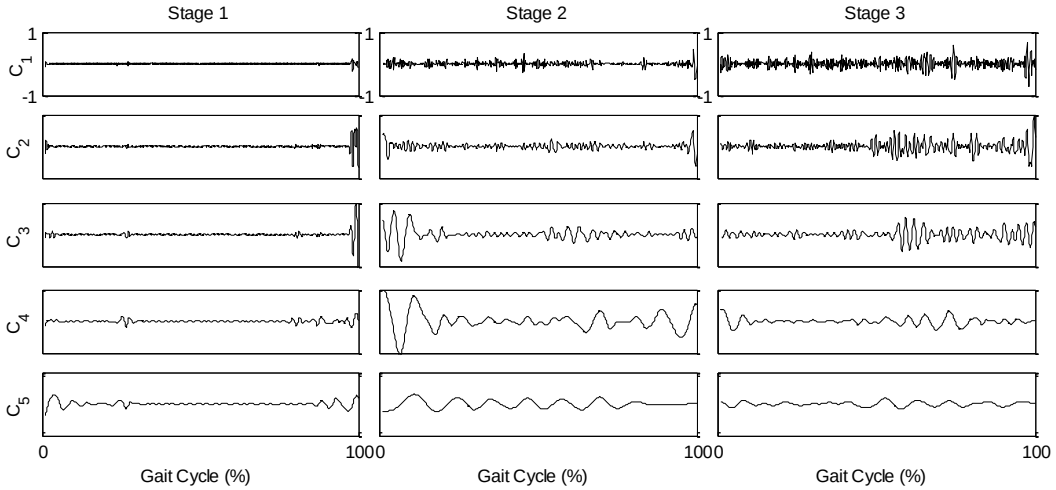

(c)

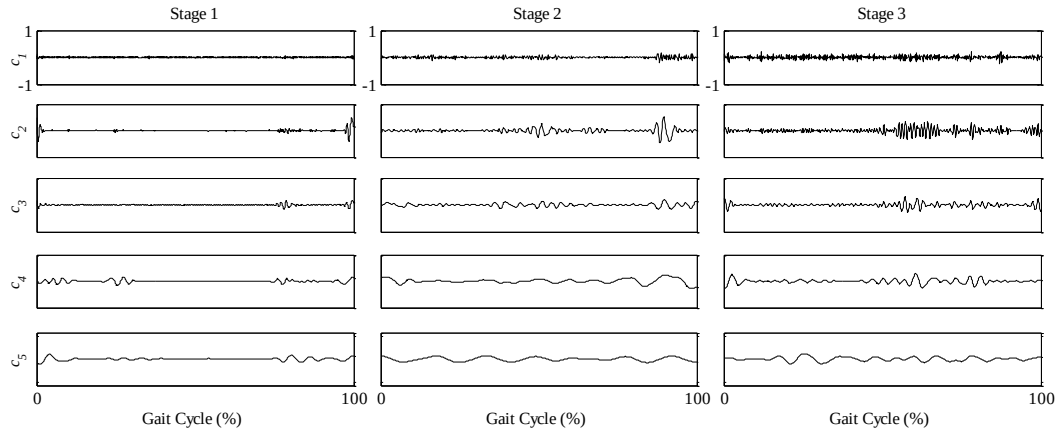

(d)

Fig D.14. Stage 1, stage 2 and stage 3 IMFs from decomposition of gait sEMG from subject 14, (a) GL left muscle, (b) GL right muscle, (c) TA left muscle, (d) TA right muscle.

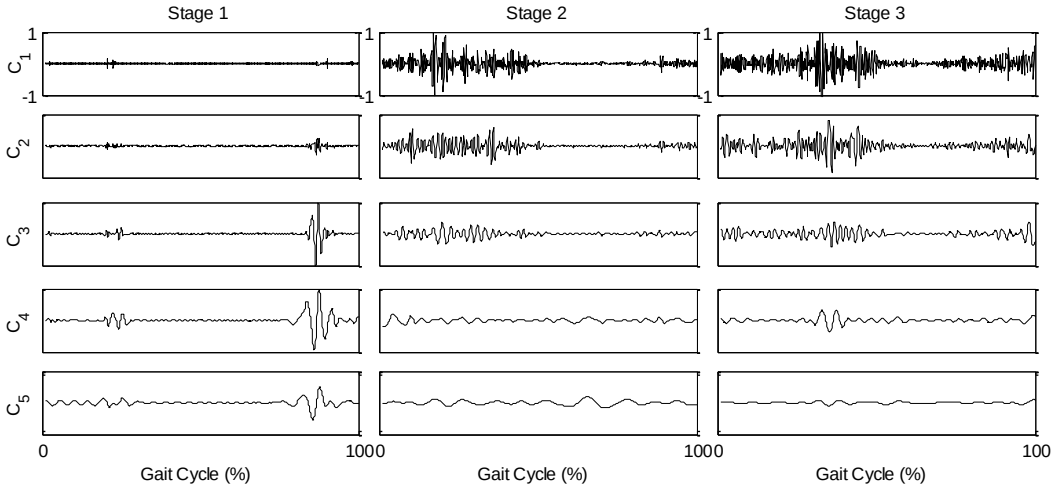
Stage 1
Stage 2
Stage 3
C1
C2
C3
C4
C5
1
-1
0
1000
100
Gait Cycle (%)

(a)

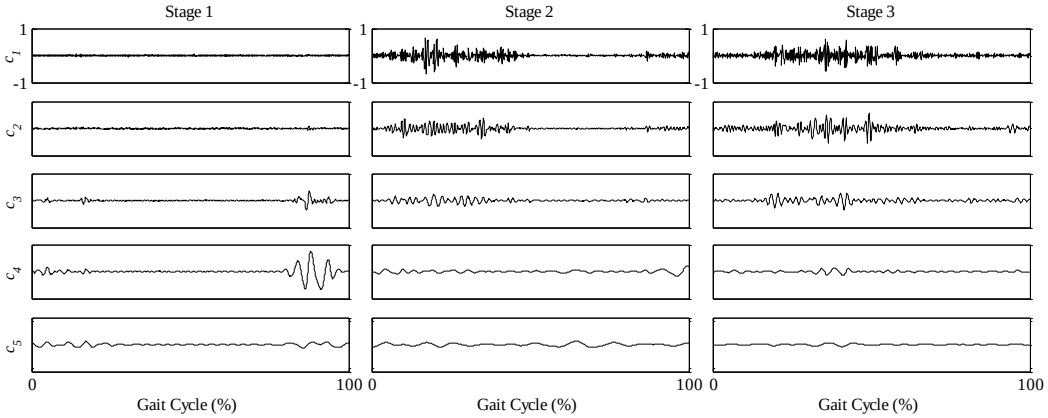
Stage 1
Stage 2
Stage 3
c1
c2
c3
c4
c5
1
-1
0
100
Gait Cycle (%)

(b)

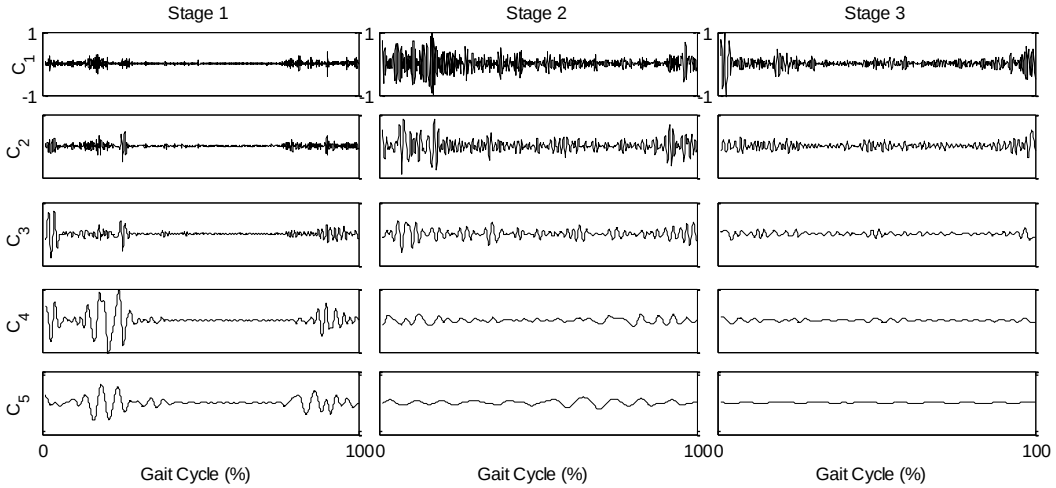

(c)

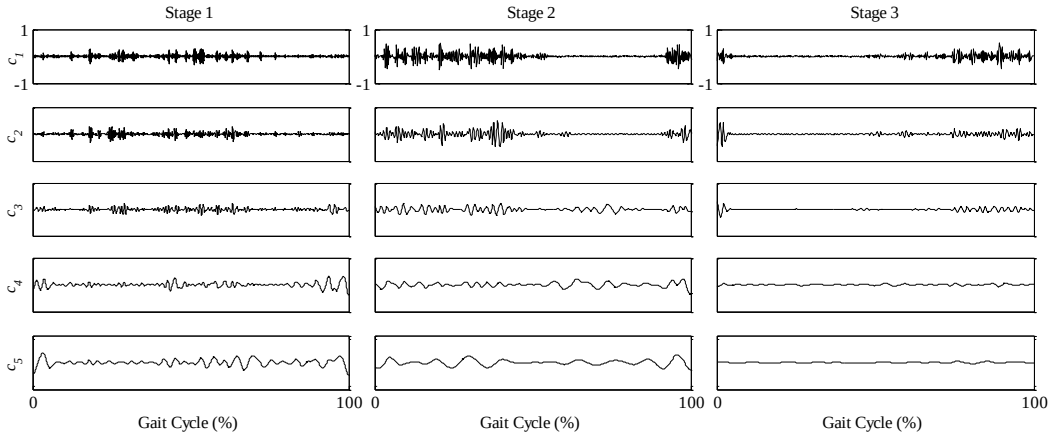

(d)

Fig D.15. Stage 1, stage 2 and stage 3 IMFs from decomposition of gait sEMG from subject 15, (a) GL left muscle, (b) GL right muscle, (c) TA left muscle, (d) TA right muscle.